

Can Tissue-On-Chip Technology provide a platform for
investigating differences in Extracellular Vesicle miRNA
content between Thyroid Pathologies?

Volume 1 (a)

Thomas Haigh

MBChB BSc(Hons) MRCS DOHNS

MD Research Thesis

The University of Hull and the University of York

Hull York Medical School

June 2024

Abstract

This study uses an established method to maintain human thyroid tissue *ex vivo* on a tissue-on-chip device, allowing for the collection, isolation and interrogation of the small extracellular vesicles (sEVs) released directly from thyroid tissue. The size and concentration of the sEVs from the thyroid tissue on chip effluent was analysed using nanoparticle tracking analysis (NTA) ($n=11$) along with histoarchitectural integrity following both pre and post incubation on chip ($n=16$). sEVs were analysed for differences in miRNA levels released from euthyroid multinodular goitre (EMG), Graves' disease (GD) and papillary thyroid cancer (PTC), using miRNA sequencing (miRNASeq) and quantitative reverse transcriptase polymerase chain reaction (RT-qPCR) to identify potential biomarkers of disease. Thyroid biopsies from patients with EMG ($n = 5$), GD ($n = 5$) and PTC ($n = 5$) were perfused with medium containing sEV-depleted serum for 6 days on the tissue-on-chip device. All the effluents were collected and ultracentrifuged to isolate sEVs; miRNA was extracted and sequenced. Out of the 15 samples, 14 passed the quality control and miRNASeq analysis detected significantly higher expression of miR-375-3p, miR-7-5p, miR-382-5p and miR-127-3p in the sEVs isolated from GD tissue compared to those from EMG (false discovery rate; FDR < 0.05). Similarly, miR-375-3p and miR-7-5p were also detected at a higher level in the GD tissue sEVs compared to the PTC tissue sEVs (FDR < 0.05). No significant differences were observed between sEV miRNA from PTC vs. EMG. These results were supported by RT-qPCR. The novel findings demonstrate that the tissue-on-chip technology is a robust method for isolating sEVs directly from the tissue of interest. This has permitted the identification of four miRNAs, which through further investigation could be used as biomarkers or therapeutic targets within thyroid disease. Further works will look to validate these findings in patient serum samples with the long-term aim of developing a non-invasive liquid biopsy to help diagnose and manage thyroid disease.

List of Contents

Abstract	2
List of Figures	9
List of Tables	13
Thesis associated Grants, Presentations and Publication	14
Acknowledgements	15
Author's declaration	16
List of Abbreviations	17
Chapter 1 - Introduction	19
1.1 - The Thyroid Gland.....	19
1.2 – Hypothalamic-Pituitary-Thyroid Axis	20
1.3 – Thyroid Hormone Synthesis	21
1.4 - Benign Thyroid Disease.....	24
1.4.1 - Hypothyroidism.....	24
1.4.2 - Hyperthyroidism	26
1.5 – Autoimmune Thyroid Disease (AITD).....	26
1.5.1 – Hashimoto's Thyroiditis (HT).....	27
1.5.2 - Graves' Disease.....	27
1.5.2.1 – Graves' Disease Diagnosis	29
1.5.3 – Toxic Multinodular Goitre (TMG).....	30
1.5.4 – Thyrotoxicosis Management.....	30
1.5.4.1 - Thionamide Therapy	30
1.5.4.2 - Surgery	31
1.5.4.3 - Radioactive Iodine Treatment.....	31
1.6 – Thyroid Cancer (TC).....	32
1.6.1 – Differentiated Thyroid Cancer.....	33
1.6.2 – Papillary Thyroid Cancer.....	33
1.6.2.1 - Papillary Thyroid Microcarcinoma	33
1.6.2.2 - Noninvasive Follicular Thyroid Neoplasm with Papillary-Like Nuclear	34
Features	34
1.7 - Undifferentiated Thyroid Cancers or Anaplastic Thyroid Cancer	35
1.7.1 - Medullary Thyroid Cancer.....	36
1.8 – Increasing Incidence of TC	37
1.8.1 – The 'Overdetection' of TC.....	37

1.8.2 - Radiation Induced TC	39
1.9 – The Investigation of TC.....	40
1.9.1 - British Thyroid Association (BTA) - Ultrasound Grading of Thyroid Nodules	40
1.9.2 - BTA – Royal College of Pathologists Thy System - Fine Needle Aspiration	42
Cytology (FNAC) Guidelines.....	42
1.9.3 - American College of Radiology (ACR) - Thyroid Imaging Reporting and Data System (TI- RADS).....	43
1.9.4 - The Bethesda System for Reporting Thyroid Cytopathology	44
1.9.5 – American Joint Committee on Cancer (AJCC) – Thyroid Cancer Staging – 8th.....	44
Edition	44
1.10 – Management of TC.....	44
1.11 – Thyroglobulin as a Tumour Marker.....	47
1.11.1 - Post Operative Thyroglobulin Monitoring	47
1.11.2 – Preoperative Measurement of Thyroglobulin	47
1.12 - Extracellular Vesicles	49
1.12.1 – The Biogenesis of sEV/Exosomes	50
1.12.2 - Exosome Isolation.....	51
1.13 – NTA – Quantification and Analysis of sEVs	53
1.13.1 - NTA Advantages.....	54
1.14 – The Use of NTA in the detection of Exosomes in Thyroid Disease	55
1.14.1 – Thyroid Cancer (TC)	55
1.14.2 - Autoimmune Thyroid Disease (AITD)	56
1.14.3 – Thyroid Cell Lines.....	58
1.15 – Exosomal miRNAs Biomarkers	59
1.15.1 – The Role of Exosomes within Health.....	60
1.15.2 - Exosomes and Cancer	61
1.15.2.1 - Cancer-Associated Fibroblasts-derived Exosomes	61
1.15.2.2 - Exosomes within Angiogenesis and Metastasis	62
1.16 - Exosomes and TC	62
1.16.1 - Exosomes and PTC	65
1.16.2 - Exosomes and GD.....	66
1.16.3 - Exosomes within HT	68
1.17 - The Development of Microfluidics and ‘Tissue-On-Chip’	68
Technology.....	68
1.17.1 – Microfluidics Fluid Dynamics.....	69
1.17.2 - Different Types of Microfluidics	71
1.18 - Microfluidics within Personalised Medicine	71
1.18.1 – Organ-on-Chip/Tissue-on-Chip Technology	72
1.18.2 - Head and Neck Cancer - Tissue-on-Chip Technology	74
1.18.3 – Thyroid - Tissue-on-Chip Technology	75

1.19 – Thesis Aims.....	77
Chapter 2 – Materials and Methods.....	79
2.1. Obtaining Tissue for Tissue-on-Chip Devices	79
2.1.1 - Ethical Considerations.....	79
2.1.2 - Patient Selection	79
2.1.3 - Tissue Sampling.....	81
2.1.4 - Blood Sampling.....	82
2.2 - Fabrication of the microfluidic culture device – Precision Cut Tissue	82
Slices (PCTS) device.....	82
2.2.1 – Tissue Processing and Preparation.....	83
2.3 – PCTS Device Set Up	84
2.3.1 - PCTS Device and Flow Calculations.....	85
2.4 - Histo-Architectural Analysis.....	86
2.5 – Determination of size and concentration of particles using	87
Nanoparticle Tracking Analysis (NTA)	87
2.5.1 - LM10 – Nanosight NTA System	87
2.5.2 - Nanosight LM10 Preparation	88
2.5.3 - Computer Screen and NTA 3.4 Software.....	89
2.6 - NTA - Materials and Methods.....	90
2.7 - Isolation of total EV content from tissue-on-chip effluent using.....	91
differential ultracentrifugation	91
2.7.1 - Bench top centrifugation steps.....	91
2.7.2 - Ultracentrifugation.....	91
2.8 - Western Blotting (WB) Analysis of Exosomal Content.....	92
2.8.1 - Protein Extraction	92
2.8.2 Electrophoresis.....	93
2.8.3 Preparation of Western Blot Reagents.....	93
2.8.4 - Western Transfer using the semi-dry Trans-Blot® Turbo™ transfer system	94
2.8.5 - Membrane Preparation and Blocking	94
2.8.6 - Film Development	96
2.9 - Extraction of RNA from exosomes using the QIAGEN miRNeasy.....	96
microkit.....	96
2.9.1 - RNA Extraction Procedure.....	96
2.10 - RNA quantification using the Biochrom SimpliNano	98
Spectrophotometer	98
2.11 - miRNA sequencing - QIAGEN, Hilden, Germany	98

2.11.1 - QIAGEN Quality Control (QC) – miRNA: Quantative Polymerase Chain.....	99
Reaction Quality Control (qPCR-QC)	99
2.11.2 - Library preparation and sequencing	99
2.12 - RT-qPCR using Individual miRCURY LNA PCR Assays	99
2.12.1 - cDNA synthesis using QIAGEN kit (339340) with UniSp6 spike.....	99
2.12.2 - Polyadenylation and cDNA synthesis	100
2.12.3 - PCR Thermal Cycler	100
2.12.4 - Quantitative, Real Time PCR (RT-qPCR) using Individual miRCURY Locked	101
Nucleic Acid (LNA) PCR assays.....	101
2.13 - Analysis of PCR Data using the Qiagen PCR Analysis Tool	103

Chapter 3 - Histoarchitectural analysis of thyroid tissue, NTA analysis of thyroid

tissue on chip effluent, western blot analysis of thyroid exosomal and tissue lysate

.....	108
3.1 - Histoarchitectural analysis of thyroid tissue.....	108
3.2 - Materials and Methods.....	108
3.3 - Results.....	109
3.4 - Thyroid Tissues Images (Pre-Culture and Post-Culture) at x10 and x40 Magnification	109
3.4.1 - Euthyroid Multinodular Goitre (EMG).....	109
3.4.2 – Graves Disease (GD)	113
3.4.3 – Papillary Thyroid Cancer (PTC)	115
3.8 - The use of Nanosight Tracking Analysis (NTA) to determine the size.....	119
and concentration of small Extracellular Vesicles (sEVs) produced by	119
thyroid tissue maintained on a tissue-on-chip device	119
3.8.2 - The Role of NTA as per the Minimal Information for Studies of.....	119
Extracellular Vesicles (MISEV) Position Paper 2023.....	119
3.9 - Particle Mean Size and Particles/ml	119
3.10 – NTA Results	122
3.10.1 - Optimisation Studies	122
3.10.2 - Use of DMEM as a Dilution Agent rather than Filtered PBS.....	123
3.10.3 – Degradation of Polypropylene into Plastic Nanoparticles.....	125
3.11 – NTA determination of Particle Size (nm) and Concentration in.....	130
Particles/ml/mg in the tissue-on-chip effluent of EMG, GD and TC Tissue	130
maintained on a PEEK <i>ex vivo</i> device	130
3.11.1 – Particle size.....	130
3.12 - Western Blotting Analysis of Thyroid sEVs and Tissue Lysates	132

3.12.1 - The Detection of Exosomal Tetraspanins	133
3.12.2 - WB in Thyroid Exosome Detection.....	134
3.13 - WB Analysis of 'Tissue-on-Chip' Thyroid Exosomal Samples	136
3.13.1 - Exosome Lysate WB - TC - Hürthle Cell Carcinoma (HCC)	136
3.13.2 - Exosome and Tissue Lysate WB - GD	139
3.14 – Discussion	140
3.14.1 - Histo-Architectural Analysis	140
3.14.2 – NTA Discussion	141
3.14.3 - WB Analysis.....	144
13.15 – Conclusion.....	146

Chapter 4 - The use of miRNA sequencing and RT-qPCR in order to identify differences in miRNA expression in sEV released from EMG, Graves' and PTC tissue

.....	148
4.1 - miRNA Sequencing Introduction.....	148
4.1.1 - Preparation of samples for miRNA sequencing	149
4.1.2 - QIAGEN Qubit Quality Control RNA High Sensitivity Assay	150
4.2 - QIAGEN miRNA Sequencing.....	152
4.2.1 - Quality Control (QC) Checks.....	152
4.2.2 - QIAGEN miRNA Sequencing Methodology.....	152
4.3 - Determination of Differential Gene Expression (DGE) between EMG, GD and PTC cohorts.....	153
4.3.1 - DGE miRNA analysis in sEV isolated from PTC tissue vs EMG tissue.....	154
4.3.2 - DGE miRNA analysis in sEV isolated from GD tissue vs EMG tissue	154
4.3.3 - DGE miRNA analysis in sEV isolated from GD tissue compared to PTC-derived sEV.....	155
4.4 – Reverse Transcription Quantitative Real-Time PCR (RT-qPCR) Analysis to validate QIAGEN miRNA sequencing results.....	157
4.4.1 - RT-qPCR Introduction.....	157
4.4.2 - RT-qPCR Methodology	157
4.4.3 - Samples used for RT-qPCR Analysis	158
4.5 - RT-qPCR Results	158
4.5 - Optimisation of RT-qPCR conditions.....	159
4.5.1 - Determination of the Concentration of RNA to be used in RT-qPCR	164
4.5.2 - Assessing the consistency of the “stable” miRNA.....	165
4.5.3 - Assessing differentially expressed hsa-miR-375-3p and hsa-miR-7-5p across the seventeen thyroid samples.....	167
4.6 - GeneGlobe-integrated RNA-seq Analysis Portal.....	169
4.7 - miRNA Analysis Method	169
4.7.1 - Differential expression of hsa-miR-375-3p and hsa-miR-7-5p in sEV isolated from GD tissue vs those from EMG	170
4.7.2 - Differential expression of hsa-miR-375-3p and hsa-miR-7-5p in sEV isolated from PTC vs those from EMG	170
4.8 - Discussion	171

4.8.1 - miR-375-3p.....	171
4.8.1.1 - The role of miR-375-3p within the context of PTC.....	172
4.8.1.2 - The role of miR-375-3p within the context of AITD	173
4.8.2 - miR-7-5p.....	173
4.8.3 – Conclusion.....	174
Chapter 5 - Conclusion and Future Works	176
5.1 - Future Works	177
5.1.1 - Thyroid exosomal miRNAs effect upon gene regulation.....	177
5.1.2 - Blood Serum.....	178
5.1.3 - FNAC - TC Diagnostics	179
5.1.4 - Administration of Therapeutics.....	179
5.2 - Limitations of Study	180
5.2.1 - Patient Selection and Sample Size	180
5.2.2 - Tissue Availability and Sampling	180
5.3 - ‘Tissue-on-chip’ technology and tissue viability	181
5.4 - Pathology	182
5.5 - Flow cytometry and exosomal marker labelling.....	183
5.6 - Microfluidics in the field of sEV Isolation and Detection	184
5.7 - Conclusion.....	184
Reference list / Bibliography	186
Appendices.....	209
Appendix 1 – U Grading of Thyroid Nodules and AJCC – Thyroid Cancer	209
Staging 8 th Edition for Differentiated Thyroid Cancer.....	209
Appendix 2 – Buffers and Solutions	212
Appendix 3 - H&E Staining	213
Appendix 4 – Nanoparticle Tracking Analysis	233
Appendix 5 – RT-qPCR Melt Curves	242
Appendix 6 – Research participant information sheet and study consent form	245

List of Figures

Fig 1.1 - The position of the thyroid gland within the neck	19
Fig 1.2 - A Histopathological Cross Section of the Thyroid Gland	19
Fig 1.3 - Negative feedback loop involved in the production of thyroxine	20
Fig 1.4 – Structural similarities between triiodothyronine (T3) and thyroxine (T4)	22
Fig 1.5 - Thyroid hormone synthesis	22
Fig 1.6 - Sodium iodide symporter	22
Fig 1.7 - The concentration of iodide ions within the thyroid follicular cells	23
Fig 1.8 - The systemic symptoms of hypothyroidism	24
Fig 1.9 – Clinical signs of Graves’ Disease	28
Fig 1.10 – The pathogenesis of Graves’ Disease	29
Fig 1.11 – 2022 WHO classification of thyroid neoplasms	32
Fig 1.12 - H&E staining of a NIFTP	35
Fig 1.13 – Normal thyroid tissue architecture and ATC tissue architecture	36
Fig 1.14 - Age-standardised thyroid cancer incidence and mortality rates per 100,000 males and females in Australia	37
Fig 1.15 - Thyroid nodules and their associated ultrasound features	41
Fig 1.16 – American College of Radiology (ACR) TI-RADS	44
Fig 1.17 – Different types of EV	48
Fig 1.18 - The surface and intracellular content of exosomes	49
Fig 1.19 - The biogenesis of exosomes	50
Fig 1.20 - MISEV 2024 - Different methods of EV separation and concentration	51
Fig 1.21 - Nanosight LM10 laser mode of action	52
Fig 1.22 - NTA 2.4 software enabling the visualisation of sEV	53
Fig 1.23 - NTA graph demonstrating particle size distribution (nm) and respective concentration (particles/ml)	53

Fig 1.24 – a. TEM analysis of EV morphology and size	56
b. NTA – Particle-size distribution of serum exosomes from a patient with HT	
Fig 1.25 – a. NTA was used to measure the diameter of GD-EXO	57
b. TEM was used to observe the size and morphology of GD-EXO	
Fig 1.26 – The average number of EVs released by thyroid cell lines per 100 cells	58
Fig 1.27 – The roles exosomes play within normal health and disease	59
Fig 1.28 - Liquid biopsy alongside other thyroid cancer diagnostic techniques	62
Fig 1.29 - The roles that thyroid cancer-derived exosomes play in cancer progression	63
Fig 1.30 - Timeline demonstrating the development of microfluidic technology	68
Fig 1.31 - A comparison of <i>laminar</i> and <i>turbulent flow</i>	69
Fig 1.32 - Reynolds Number Calculation	70
Fig 1.33 - The far-reaching applications of tissue-on-chip technology	72
Fig 1.34 – PCTS Device developed at the University of Hull	75
Fig 2.1 - PCTS Culture Device	82
Fig 2.2 - Set-up of the PCTS perfusion device	84
Fig 2.3 – PCTS Reynolds Number calculations	85
Fig 2.4 - LM10 Nanosight and the interaction of the nanoparticles held in liquid suspension with the laser beams	87
Fig 2.5 - Representative linear standard curve produced using Pierce BCA assay kit	92
Fig 3.1 – EMG thyroid tissue architecture at x40 magnification following maintenance on the ‘tissue-on-chip’ device for a period of six days	109
Fig 3.2 – EMG thyroid tissue of 5µm thickness pre and post maintenance on a ‘tissue-on-chip’ device (x10 and x40 magnification)	111
Fig 3.3 – GD tissue architecture at x40 magnification following maintenance on a tissue-on-chip device for a total of six days	112
Fig 3.4 - GD tissue 5µm thickness pre and post maintenance on a ‘tissue-on-chip’ device (x10 and x40 magnification)	114

Fig 3.5 – PTC tissue architecture at x40 magnification following maintenance on a tissue-on-chip device for a total of six days	115
Fig 3.6 - PTC tissue 5µm thickness pre and post maintenance on a tissue-on-chip device (x10 and x40)	117
Fig 3.7 - NTA data output of size (nm) vs. concentration (particles/ml) for each sample, and intensity dotplot (a.u.). Data from GD Device 3, Sample I (Appendix 4)	120
Fig 3.8 - Numerical data provided by the NTA software for the GD Sample I, Device 2, Day 3 effluent (Appendix 4)	121
Fig 3.9. A – Sample A (Appendix 4) for Day 3 to Day 6 mean particles/ml at a 1:2 dilution in filtered (20nm) PBS B – Sample B (Appendix 4) for Day 1 to Day 6 mean particles/ml at 1:8 dilution with DMEM	122
Fig 3.10 - NTA output of size (nm) vs. intensity (a.u.) for both filtered PBS (Galluzzi et al.) and DMEM (b.)	123
Fig 3.11 - NTA output of size (nm) vs. intensity (a.u.) for a freshly opened bottle of DMEM (Galluzzi et al.) vs open for a 2-week period (b.)	124
Fig 3.12 - NTA output of size (nm) vs. intensity (a.u.) for DMEM that has been left in the plastic syringe (Galluzzi et al.) vs glass syringe (b.) for 1 week	125
Fig 3.13 - Comparison of particle size (nm) and particles/ml in sample m (Appendix 4) day 4 effluent that has been run through a ‘tissue-on-chip’ device using either plastic vs glass syringes	127
Fig 3.14 - Average particle size (nm) (Galluzzi et al.) average particles/ml (b.) in the glass or plastic syringes	128
Fig 3.15 - Sample I, GD Day 3 - particle mean size (nm) vs. device number (1 to 6)	129
Fig 3.16 - NTA of EVs showing particle mean size (nm) collected from EMG (<i>n</i> = 3), GD (<i>n</i> = 2) and TC (<i>n</i> = 6), tissue maintained for 6 days	130
Fig 3.17 - NTA of EVs showing particle concentration (particles/ml/mg) collected from EMG (<i>n</i> = 3), GD (<i>n</i> = 2) and TC (<i>n</i> = 6) tissue maintained for 6 days	131
Fig 3.18 – A and C . WB validation of differentially expressed proteins in serum-derived exosomes from thyroid cancer patients. B and D . histogram demonstrating optical density of each immunoreactive band	133
Fig 3.19 – Comparative WB data looking at exosomal molecular chaperones for PTC before and after surgery along with goitre	134

Fig 3.20 – WB of TC Hürthle Cell Carcinoma (HCC) and cell line positive control exosomes	138
Fig 3.21 – WB of GD exosomal and tissue lysate and cell line positive control	139
Fig 4.1 - Flow Chart demonstrating the processing of samples through miRNA sequencing and RT-qPCR	148
Fig 4.2 - Median Phred quality score for samples processed	151
Fig 4.3 - MA Plot demonstrating DGE miRNA in sEV isolated from PTC and EMG Thyroid Pathologies	153
Fig 4.4 - MA Plot demonstrating DGE miRNA expression in sEV isolated from GD tissue and EMG	154
Fig 4.5 - MA Plot demonstrating DGE miRNA expression in sEV isolated from GD tissue and PTC	155
Fig 4.6 - Increasing mean C_T with increasing dilution of cDNA using hsa-miR-191-5p and hsa-miR-320c stable miRNA primers	159
Fig 4.7 – (a.) Melt curve analysis demonstrating high affinity binding for has-miR-320c primer (b.) Melt curve analysis demonstrating high affinity binding for has-miR-191-5p primer	160
Fig 4.8 – (a.) Increasing mean C_T using has-let-7c-5p and has-miR-16-5p with increasing dilution of THTHY3 RNA (b.) Increasing mean C_T using hsa-let-7c-5p and hsa-miR-16-5p with increasing dilution of THTHY23 RNA	162
Fig 4.9 - Mean C_T on detecting stable miRNA hsa-let-7c-5p and hsa-miR-16-5p	163
Fig 4.10 - C_T values obtained for hsa-let-7c-5p, hsa-miR-16-5p, hsa-miR-375-3p and hsa-miR-7-5p at a. 50ng Neat and 1:50 dilution b. 200ng Neat and 1:50 dilution	164
Fig 4.11 - C_T values for 50ng samples for detection of SP6, hsa-miR-191-5p and hsa-let-7e-5p “stable” miRNA	165
Fig 4.12 - C_T values for 50ng samples for detection levels of SP6 hsa-miR-16-5p, hsa-miR-320c (“stable” miRNA), and hsa-miR-375-3p and hsa-miR-7-5p (genes of interest)	167

List of Tables

Table 1.1 - RCPATH FNAC Thyroid Classifications - thyroid nodule scoring	42
Table 1.2 - Examples of the use of organ-on-chip technology in a number of different organ environments	72
Table 2.1 – Patient characteristics in study	79-80
Table 2.2 - Preparation of PCR Reaction Mix	101
Table 2.3 - PCR cycling temperatures and times	101
Table 3.1 - Results from three comparative runs of the Filtered (20nm) PBS and the DMEM particles/frame	123
Table 3.2 - The role of CD9, CD63 and CD81 and their respective molecular weights (kDa)	132
Table 4.1 - Breakdown of the EMG, GD and PTC samples with age and gender selected for QIAGEN RNA sequencing	149
Table 4.2 - Qubit determined RNA concentration for the samples sent to QIAGEN	150
Table 4.3 - sEV DGE miRNA expression in GD-derived sEV compared with EMG tissue-derived sEV	154
Table 4.4 - sEV DGE miRNA expression in Graves' tissue-derived sEV compared with PTC tissue-derived sEV	157
Table 4.5 - Samples available for RT-qPCR, EMG, GD and PTC	153
Table 4.6 - RNA concentration of the respective sEV RNA samples measured on the Biochrom SimpliNano Spectrophotometer	158
Table 4.7 - Thyroid pathologies grouping for the GeneGlobe-integrated RNA-seq Analysis Portal	168
Table 4.8 - Fold Regulation changes for GD vs EMG for the differentially expressed hsa-miR-375-3p and hsa-miR-7-5p	169
Table 4.9 - Fold Regulation changes for GD vs EMG for the differentially expressed hsa-miR-375-3p and hsa-miR-7-5p	169

Thesis associated Grants, Presentations and Publication

Research Grants:

Identification of exosomal miRNA biomarkers in thyroid disease using microfluidics
ENT UK Foundation Grant 2021 - £750 - Grant Number [384198]

British Association of Endocrine and Thyroid Surgeons (BAETS) Research Grant 2022 -
£5000 - Grant Number [3853519]

Thesis Associated Publication:

The Use of Tissue-on-Chip Technology to Focus the Search for Extracellular Vesicle miRNA Biomarkers in Thyroid Disease

Thomas Haigh, Hannah Beattie, Mark Wade, James England, Dmitriy Kuvshinov, Laszlo Karsai, John Greenman, Victoria Green

Published in *International Journal of Molecular Sciences*

Int. J. Mol. Sci. 2024, 25(1), 71; <https://doi.org/10.3390/ijms25010071>

PMID: 38203243, PMCID: PMC10778868

Thesis Associated Presentations:

Identification of exosomal miRNA biomarkers in thyroid disease using microfluidics
(Oral Presentation)

British Association of Endocrine and Thyroid Surgeons (BAETS) - Annual Scientific Meeting 2022

Bournemouth International Centre, 7th October 2022

Identification of exosomal miRNA biomarkers in thyroid disease using microfluidics
(Oral Presentation)

North of England Otolaryngology Society Autumn Meeting 2022

The Royal Armouries, Leeds, 14th October 2022

Can microfluidic technology narrow the search for extracellular vesicle miRNA biomarkers in thyroid disease? (Poster)

UK Society for Extracellular Vesicles (UKEV) Meeting 2022

Royal College of Physicians Edinburgh, 1st-2nd December 2022

Can tissue on-chip technology narrow the search for extracellular vesicle miRNA biomarkers in thyroid disease? (Oral Presentation)

British Association of Endocrine and Thyroid Surgeons (BAETS) - Annual Scientific Meeting 2023

Shortlisted for BJS Prize, Eugenides Foundation, Athens, Greece, 12th October 2023

Can tissue on-chip technology narrow the search for extracellular vesicle miRNA biomarkers in thyroid disease? (Oral Presentation)

UK Society for Extracellular Vesicles (UKEV) Meeting 2023

Fitzwilliam College, Cambridge, 7th December 2023

Acknowledgements

First and foremost, I would like to thank my supervisors Professor John Greenman and Dr Victoria Green. Without your full support and guidance, I would not have been submitting this body of work. Your support in the laboratory and in the writing process of the thesis is appreciated immensely. Thank you for the time taken to help me through the writing process, read the many drafts and provide feedback.

I would like to thank Mr James England for providing me with the opportunity in which to undertake a laboratory-based research MD. It was something I never believed I would do and I am incredibly grateful for the chance to broaden my mind. You motivated me to get the job done and I appreciate your guidance and help with presenting the work to a wider audience. I will miss your Wednesday morning motivational text messages! I may still need them.....

A massive thank you goes to the British Association of Endocrine and Thyroid Surgeons (BAETS) and ENT UK for your kind financial support and the wider support and backing provided to scientific research within the field of ENT and thyroid surgery.

I would like to thank Katie for all your support and listening to me whinge about having to get the thesis done! You will not hear the word 'MD' again. Until next time!

Obviously, the most gratitude is towards my parents whos' support and sacrifices have provided me with the opportunities to undertake and achieve this MD.

Author's declaration

I confirm that this work is original and that if any passage(s) or diagram(s) have been copied from academic papers, books, the internet or any other sources these are clearly identified by the use of quotation marks and the reference(s) is fully cited.

I certify that, other than where indicated, this is my own work and does not breach the regulations of HYMS, the University of Hull or the University of York regarding plagiarism or academic conduct in examinations.

I have read the HYMS Code of Practice on Academic Misconduct, and state that this piece of work is my own and does not contain any unacknowledged work from any other sources.

I confirm that any patient information obtained to produce this piece of work has been appropriately anonymised

List of Abbreviations

AITD – autoimmune thyroid disease
AJCC – American Joint Committee on Cancer
APCs – antigen-presenting cells
ATA – American Thyroid Association
ATC – anaplastic thyroid cancer
ATPase - adenosine triphosphatase
BAETS – British Association of Endocrine and Thyroid Surgeons
BTA – British Thyroid Association
C Cells – chief cells
CAF – cancer associated fibroblasts
CAPNS1 - calpain small subunit 1
CDEs - cancer associated fibroblast (CAF) derived exosomes (CDEs)
CEA – carcinoembryonic antigen
CSCs – cancer stem cells
DIT – diiodotyrosine
DMEM – dulbecco’s modified eagle’s medium
EMG – euthyroid multinodular goitre
EMT – epithelial mesenchymal transition
EV – extracellular vesicles
FDR – false discovery rate
FNA – fine needle aspiration
FNAC – fine needle aspiration cytology
FTC – follicular thyroid cancer
G – g Force or RCF – relative centrifugal force
GD – Graves’ disease
H&E – haematoxylin and eosin
HNSCC – head and neck squamous cell carcinoma
Hsp – heat shock protein
HT – hashimoto’s thyroiditis
IGF-1 – insulin-like growth factor 1
IGF1-R – insulin-like growth factor 1 receptor
IHC – immunohistochemistry
ISEV - international society for extracellular vesicles
ITGB2 - integrin beta chain-2
kDa – kil
LNM – lymph node metastasis
LOD – limit of detection
MES - 2-(N-morpholino)ethanesulfonic acid
MHC – major histocompatibility complex
miRNAseq – microRNA sequencing analysis
MISEV – minimal Information for the study of extracellular vesicles
MIT – monoiodotyrosine
mRNA – messenger RNA
MTC – medullary thyroid cancer
MVB – multivesicular body
MVs - microvesicles
n – number

NIFTP – noninvasive follicular thyroid neoplasm with papillary-like features
NSCLC – non small cell lung cancer
NTA – nanoparticle tracking analysis
OSCC – oral squamous cell carcinoma
PTC – papillary thyroid cancer
PTH – parathyroid hormone
PTMC - papillary thyroid microcarcinoma
RAI – radioactive iodine
RNA – ribonucleic acid
RRA – radioactive iodine remnant ablation
RT-qPCR – reverse transcription quantitative polymerase chain reaction
SCC – squamous cell carcinoma
sEV – small extracellular vesicles
SRC - proto-oncogene SRC
STDEV – standard deviation
T3 – triiodothyronine
T4 – thyroxine
TCR – T cell receptor
TEM – transmission electron microscopy
Tg - thyroglobulin
TH – T helper cell
TKIs – tyrosine kinase inhibitors
TLN1 - talin-1
TME – tumour microenvironment
TMG – toxic multinodular goitre
TNM – tumour, node, metastasis
TPO – thyroid peroxidase
TPOAb – thyroid peroxidase antibody
TRAb – thyroid stimulating hormone receptor autoantibodies
Treg – regulatory T cell
TRH – thyrotropin releasing hormone
TSH – thyroid stimulating hormone
TSHR – thyroid-stimulating hormone receptor
USS – ultrasound scan
UTR – untranslated region
WB – western blotting

Chapter 1 - Introduction

1.1 - The Thyroid Gland

The thyroid gland is a bilobate structure, typically weighing between fifteen and twenty-five grams (**Figure 1.1**). The thyroid is composed of lobules of colloid containing follicles lined by a monolayer of follicular epithelial cells which are surrounded by a thin fibrous pseudocapsule (**Figure 1.2**). The parafollicular/C cells are present within the stroma which secrete calcitonin and are involved in calcium regulation (Garrett et al., 1995).

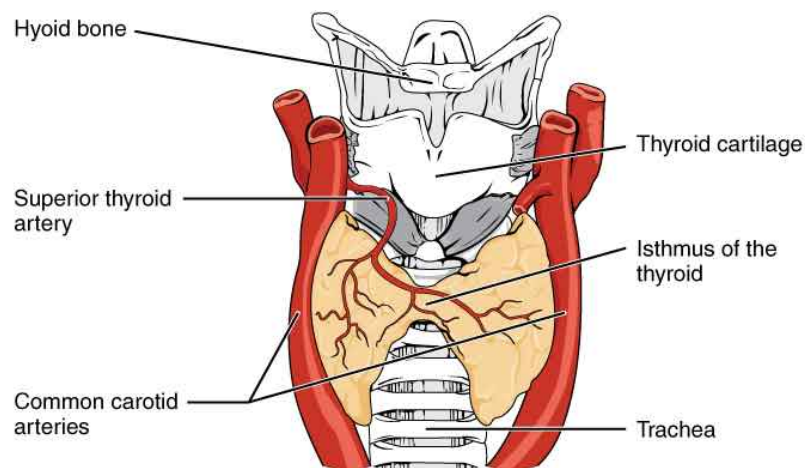


Figure 1.1 - The position of the thyroid gland within the neck (Pund et al., 2022)

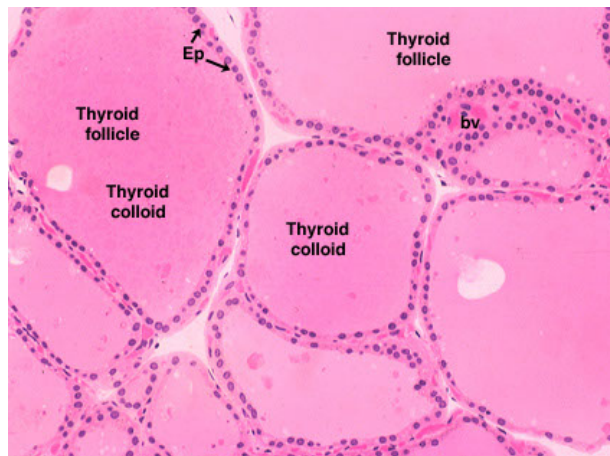


Figure 1.2 - A Histopathological Cross Section of the Thyroid Gland demonstrating thyroid follicles filled with colloid
Taken from (University, 2024)

During the gestation period, the thyroid gland descends from the foramen cecum at the posterior tongue and completes the descent to its expected location by the seventh week of gestation. The thyroid gland is located below the thyroid cartilage at the level

of C5 to T1 vertebral levels in the midline anterior neck. The two lobes are connected by the isthmus at the level of the second and third tracheal rings (Fagman & Nilsson, 2010)

The thyroid gland is attached to the trachea through Berry's ligament and the parathyroid glands and the recurrent laryngeal nerve lie in close proximity to the thyroid gland (Allen & Fingeret, 2023).

1.2 – Hypothalamic-Pituitary-Thyroid Axis

The main function of the thyroid is the production of hormones and control of metabolism (Armstrong et al., 2023). The prohormone, thyroxine (T₄), is secreted from the thyroid gland along with a small amount of the bioactive triiodothyronine (T₃) under the control of a negative feedback mechanism (**Figure 1.3**). Thyroid stimulating hormone (TSH) is released from the anterior pituitary by thyrotropes, in response to the release of thyrotropin releasing hormone (TRH) from the hypothalamus. T₄ is then converted to T₃ within the peripheral circulation via the selenoenzymes deiodinases and concentrated within different parts of the body (Köhrle, 2000; Peeters & Visser, 2017).

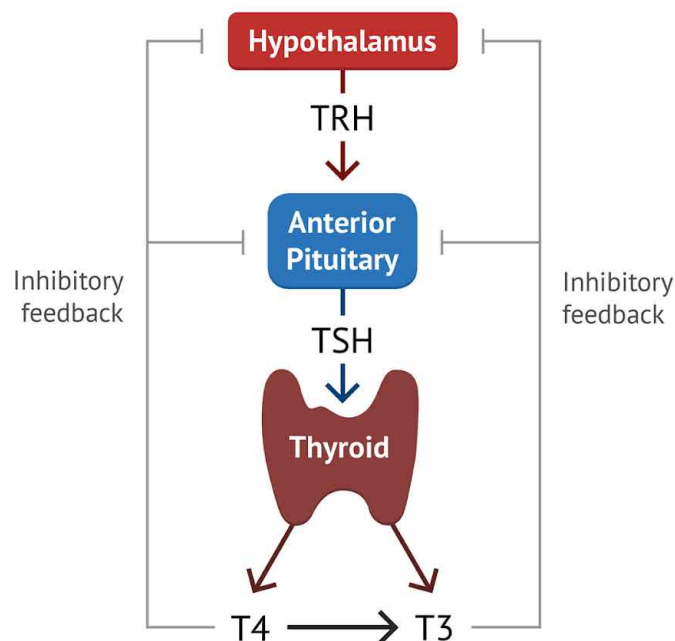


Figure 1.3 - Negative feedback loop involved in the production of thyroxine from the thyroid. **TRH** – thyrotropin releasing hormone, **TSH** – thyroid stimulating hormone, **T₃** – triiodothyronine, **T₄** – thyroxine (Vu, 2024)

Around 80% of T₃ is produced from outside of the thyroid gland through peripheral conversion of T₄, whilst only 20% is secreted from the thyroid itself (Gereben et al.,

2008). In response to a raised metabolic requirement, the peripheral tissues increase their uptake of T4 and its consequent conversion to the bioactive T3 (**Figure 1.4**). This leads to a reduction in the circulating T4 concentration, stimulating further TSH production by the anterior pituitary subsequently causing an increase in further T3 and T4 production.

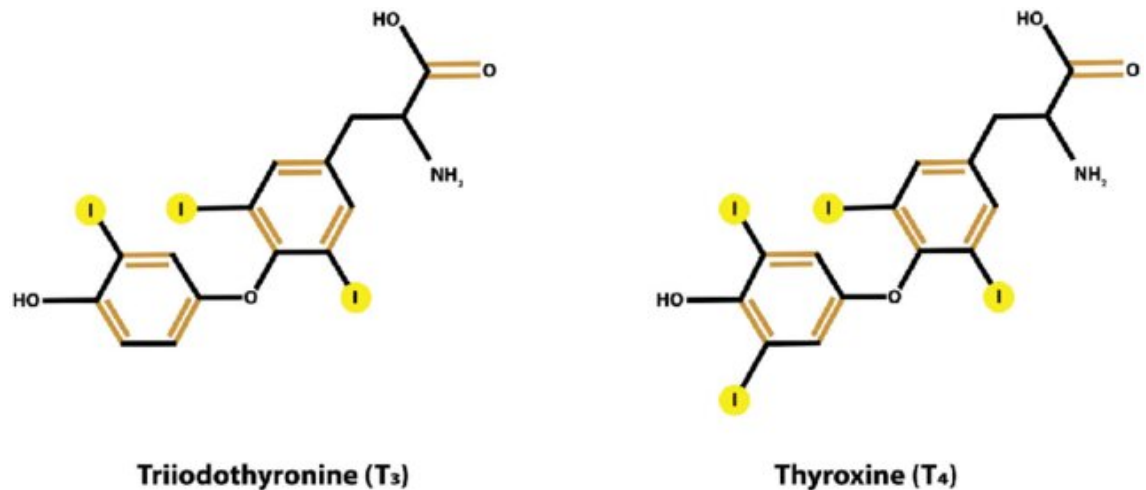


Figure 1.4 – Structural similarities between triiodothyronine (T₃) and thyroxine (T₄) (D'Aurizio et al., 2023)

The thyroid hormones are integral to both the regulation and stimulation of cellular metabolism and are indispensable in development. The hormones induce widespread systemic effects upon bone, the cardiovascular system as well as the central nervous system (Gomberg-Maitland & Frishman, 1998; Bernal, 2005).

1.3 – Thyroid Hormone Synthesis

The thyroid hormones are synthesised through the sequential iodination of the tyrosine phenol rings in thyrocytes (**Figure 1.5**). This process is stimulated through the binding of TSH hormone to TSH receptors on the thyroid follicular cell surface.

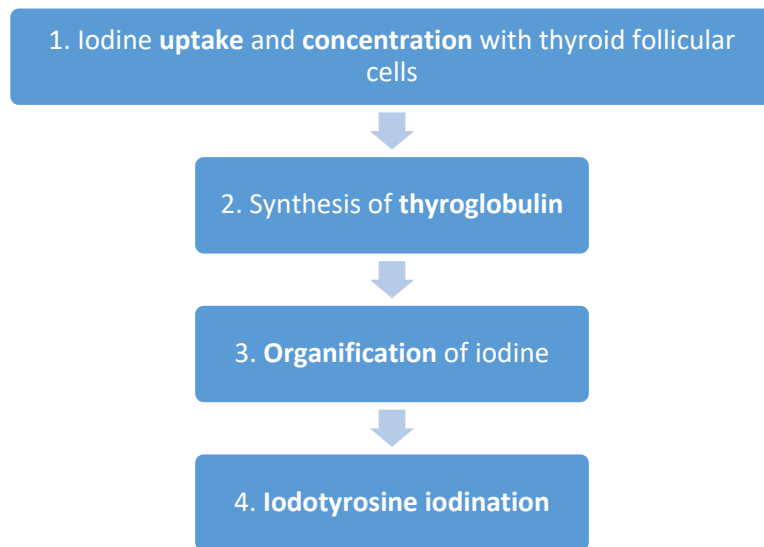


Figure 1.5 - Thyroid hormone synthesis in four sequential steps

Thyroid hormone synthesis is dependent upon iodine which is absorbed in the small intestine from nutrition and then subsequently transported via the bloodstream to the thyroid. The sodium iodide symporter enables the thyroid follicular cells to actively concentrate the iodine at a level that is twenty to fifty times greater than that of the circulating plasma levels (Peeters & Visser, 2017). In the process, one iodide ion is transported across the basement membrane alongside two sodium ions (**Figure 1.6**). The transport of iodide across the cell membrane is driven by the electrochemical gradient of sodium, which is generated through the Na^+/K^+ adenosine triphosphatase (ATPase) pump.

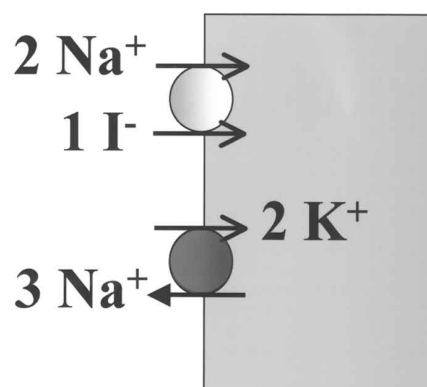


Figure 1.6. Sodium iodide symporter

The sodium iodide symporter cotransports 2 sodium ions (Na^+) and 1 iodide ion (I^-). The sodium gradient provides the energy as generated by the Na^+/K^+ - adenosine triphosphatase (ATPase) pump (Chung, 2012)

Following entry into the follicular cell, the iodide ion is transported out of the cell and into the surrounding colloid by the transporter protein, pendrin (Bizhanova, 2019). Once within the colloid, the iodine is oxidised by the enzyme thyroid peroxidase (TPO). This oxidised iodine is very reactive and iodinates the thyroglobulin. The iodinated thyroglobulin forms the polypeptide framework from which T3 and T4 are then synthesised. Following this process, the complex re-enters the follicular cells through endocytosis (Figure 1.7).

The thyroglobulin tyrosine residue is then broken down into predominantly diiodotyrosine (DIT) and monoiodotyrosine (MIT). The DIT and MIT are oxidized into T3 and T4 through the enzyme, TPO. T4 is formed by the coupling of two diiodinated tyrosines (DIT) whilst the T3 is formed by the coupling of MIT and DIT (Pirahanchi et al., 2023). In the final step, the colloid containing the oxidised thyroglobulin is taken up by the thyroid follicular cells through endocytosis. This uptake is governed through the binding of the TSH with the TSH receptor, a G protein coupled receptor. The colloid then fuses with a lysosome and the thyroglobulin is digested leading to the release of T4, T3, DIT and MIT.

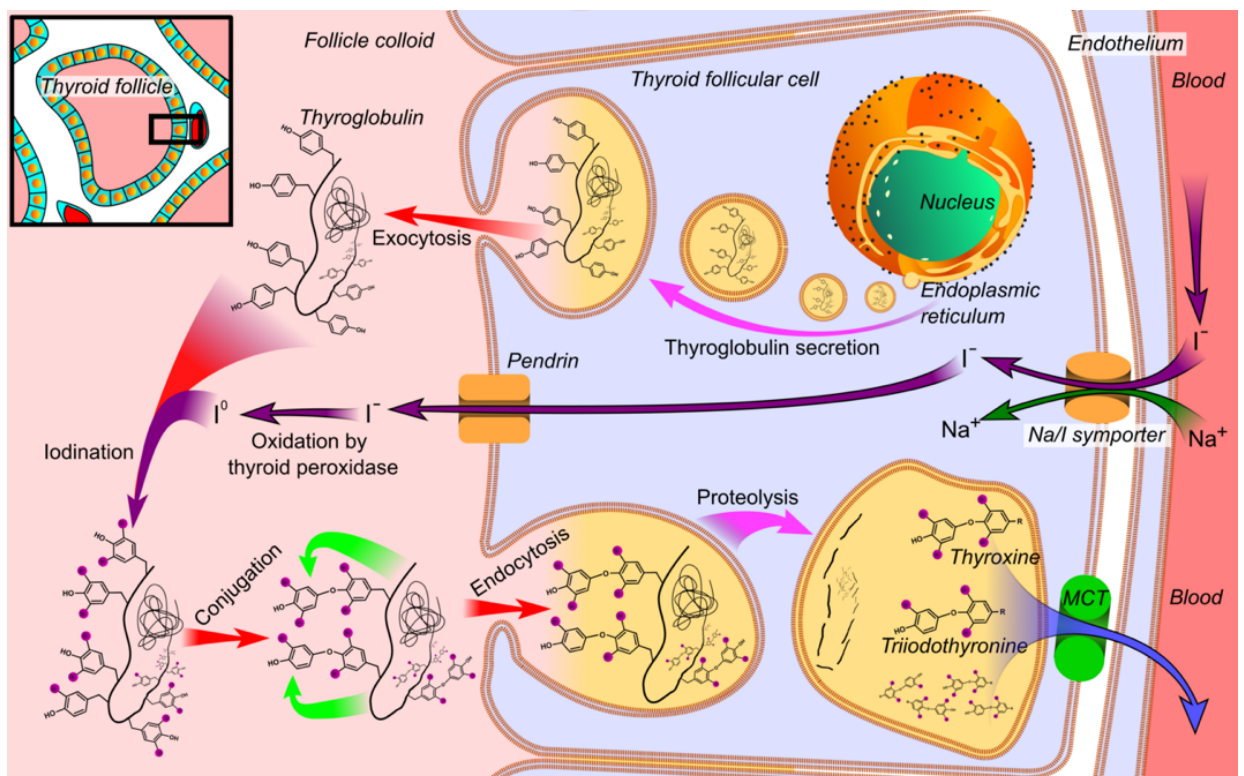


Figure 1.7 - The concentration of iodide ions within the thyroid follicular cells, the subsequent iodination of thyroglobulin and its endocytosis into the thyroid follicular cell

followed by proteolysis into thyroxine (T4) and triiodothyronine (T3) (Boron & Boulpaep, 2024)

1.4 - Benign Thyroid Disease

1.4.1 - Hypothyroidism

Hypothyroidism is a common condition, resulting from a deficiency of T4 and T3 (@NICEcomms, 2023, Hypothyroidism, NICE). Around 5% of the general population have a diagnosis of hypothyroidism, with a further 5% going undiagnosed (Chiovato et al., 2019). The condition is ten times more common in women than in men (Vanderpump et al., 1995; Ingoe et al., 2017). There are a multitude of causes, including insufficient dietary iodine intake and common medications such as amiodarone and lithium (Danzi & Klein, 2015; Shine et al., 2015). Iatrogenic causes such as radioiodine treatment and thyroid surgery can also contribute. Hypothyroidism is classified into either primary, central or peripherally based upon whether the pathology is located within the thyroid, the pituitary or hypothalamus, or peripheral tissues respectively (Chaker et al., 2022).

Hypothyroidism usually has an insidious onset and manifests through a general reduction in physical and mental speed. The classical signs and presenting symptoms include cold intolerance, weight gain, constipation, depression and even hair loss (**Figure 1.8**).

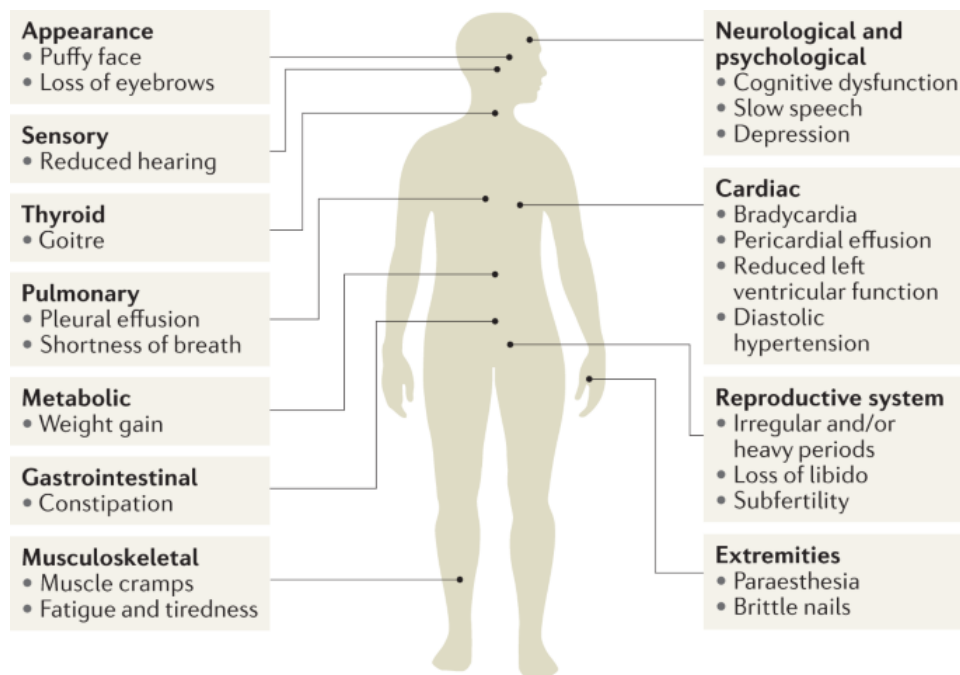


Figure 1.8 - The systemic symptoms of hypothyroidism (Chaker et al., 2022)

Hypothyroidism can result from autoimmune thyroid disease (AITD). However, Hashimoto's thyroiditis (HT) can also present as either hypothyroidism or hyperthyroidism in the form of Hashitoxicosis (Shahbaz et al., 2018). Hypothyroidism can also occur rarely as a consequence of either pituitary or hypothalamic failure. This can be either congenital or acquired as a result of trauma, tumour or cerebrovascular accidents that have affected the hypothalamic-pituitary-thyroid axis (Beck-Peccoz et al., 2017). Iodine deficiency during pregnancy can have a significant impact upon an infant resulting in congenital hypothyroidism and if left untreated will result in cretinism. Untreated hypothyroidism can result in a myxoedematous coma which can be fatal (Gish et al., 2016).

The treatment of hypothyroidism is with T4 replacement in the form of oral levothyroxine. The TSH level needs to be monitored to prevent over treatment, which will result in subclinical thyrotoxicosis. In the UK, the practice is to measure TSH levels three months following the initiation of levothyroxine (@NICEcomms, 2023). Levothyroxine is the second most commonly prescribed medication in the UK in primary care accounting for prescription costs totaling £62 million in 2019 (MacKenna, 2019).

1.4.2 - Hyperthyroidism

Hyperthyroidism is a biochemical diagnosis made through suppressed levels of TSH alongside increased T4 and T3 levels (@NICEcomms, 2023, CKS | NICE). Hyperthyroidism is when there is excessive thyroid hormones production originating from the thyroid gland alone, i.e. exclusively endogenous, whereas thyrotoxicosis is a case of excessive thyroid hormone from any endogenous or exogenous source (Bahn Chair et al., 2011). The two terms of hyperthyroidism and thyrotoxicosis are used interchangeably. The majority of the cases of hyperthyroidism are as a result of Graves' Disease (GD) (80%) and less commonly multinodular goitre (Brent, 2008; Chaker et al., 2024). Rarely, thyrotoxicosis can result from the over ingestion of thyroxine, too much dietary iodine or a pituitary adenoma.

Hyperthyroidism commonly presents with weight loss, nervousness, anxiety, irritability, sweating, palpitations and tremor (Doubleday & Sippel, 2020). Other manifestations include that of thin skin, muscle weakness, gastrointestinal disturbance and menstrual disturbances. Clinical signs that are highly suggestive of a diagnosis of hyperthyroidism include agitation, sinus tachycardia, goitre and the presence of thyroid nodules. In severe, but rare cases, a medical emergency known as a thyroid storm can result, involving tachydysrhythmias, pyrexia, vomiting, diarrhoea and mental agitation. The incidence rate has been reported as between 0.20 to 0.76 per 100,000 hospitalised people per year (Akamizu et al., 2012). The incidence rates are markedly higher in females and three times higher in the over 60 years (Thiyagarajan et al., 2022). Thyroid storm has an associated mortality rate of between 8 and 25% despite the advances in modern medicine (Pokhrel et al., 2022).

1.5 – Autoimmune Thyroid Disease (AITD)

AITDs are thyroid diseases caused by various autoimmune disorders, including Hashimoto's Thyroiditis (HT) and Graves' Disease (GD). The disease processes are manifested through lymphocytic infiltration into the thyroid gland and the subsequent production of autoantibodies. These autoantibodies interfere with normal thyroid function, typically inducing a state of either hypothyroidism in the case of HT or hyperthyroidism in GD (Bogusławska et al., 2022).

The development of these autoimmune conditions are accompanied by the production of thyroid peroxidase antibodies (TPOAb), thyroglobulin antibodies and TSH receptor antibodies (TRAb) (Mikoś et al., 2014). A wide variety of factors combine to result in AITD including genetic predisposition to the disease, environmental factors and immunological factors. Accompanying an increase in AITD has been an increase in papillary thyroid cancer (PTC) which is suggestive of a link between the disease processes (Liang et al., 2017).

1.5.1 – Hashimoto’s Thyroiditis (HT)

HT, also known as chronic lymphocytic thyroiditis or autoimmune thyroiditis is the most common AITD, disproportionately affecting women (17.5% versus 6%) with an estimated total worldwide prevalence of 7.5% (Xiaojie et al., 2022). It was first reported by Japanese physician Hakura Hashimoto in 1912 and accounts for 22.5% of all thyroid disease (Dayan & Daniels, 1996). HT ultimately results in hypothyroidism as a result of the infiltration of thyroid-specific T lymphocytes, followed by goitre enlargement, fibrosis and the destruction of thyrocytes. The disease process is characterized by the TPOAb and anti-thyroglobulin autoantibodies, which mediate complement deposition, bringing about cytotoxicity and ultimately irreversibly damaging thyrocytes (Bogusławska et al., 2022).

1.5.2 - Graves’ Disease

Graves’ disease (GD) is an autoimmune syndrome, and the most common cause of hyperthyroidism in the developed world with an annual incidence of 20 per 100,000 people (Antonelli et al., 2020). The cause is unknown but most frequently affects women of reproductive age and is gender disproportionate with a global percentage rate of 2% for women and 0.2% for men (McLeod & Cooper, 2012). GD has a strong genetic component, but has been postulated to be precipitated by environmental factors like stress, smoking, infection, iodine exposure, postpartum and after highly active antiretroviral therapy (HAART) (Antonelli et al., 2020). The disease is characterized through an enlarged, overactive thyroid gland, Graves’ ophthalmopathy, thyroid acropachy and dermopathy in the form of pretibial myxoedema (Davies et al., 2020) (**Figure 1.9**). The prompt diagnosis and subsequent management of GD can prevent life-threatening cardiac complications (Witczak et al., 2020).

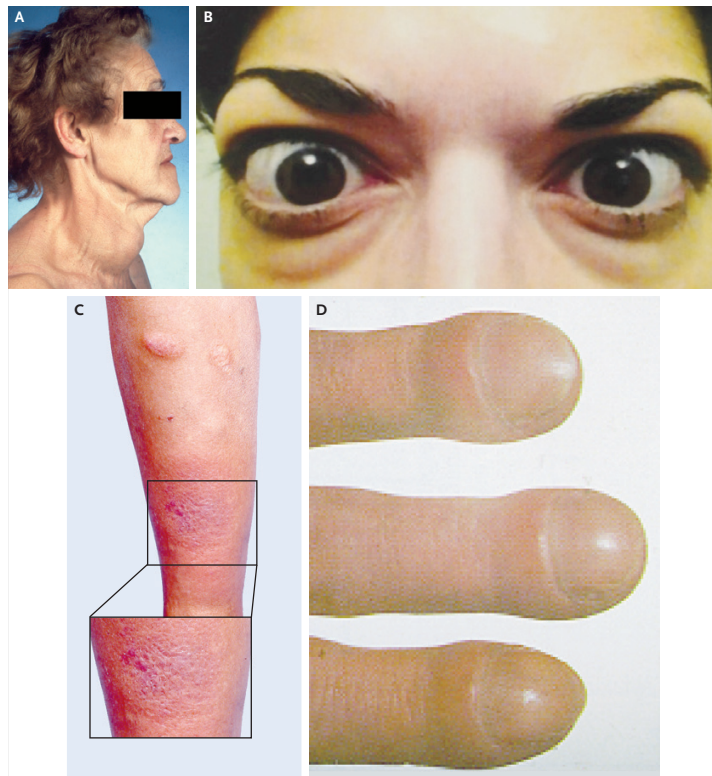


Figure 1.9 - Clinical signs of GD

A – goitre evident in an elderly lady, **B** – thyroid-associated ophthalmopathy, **C** – pretibial myxoedema, **D** – thyroid acropachy (Smith & Hegedüs, 2016)

GD is characterized by elevated circulating thyroid stimulating hormone receptor (TRAb) autoantibodies to the thyrotropin receptor located on the thyroid follicular epithelial cells. Local B cells and plasma cells under the regulation of T cells are involved in the production of these autoantibodies (**Figure 1.10**). TSHR autoantibodies couple to GPCR leading to the activation of a cAMP/Protein Kinase A which culminates in both thyroid growth and thyroid hormone synthesis (Davies et al., 2020).

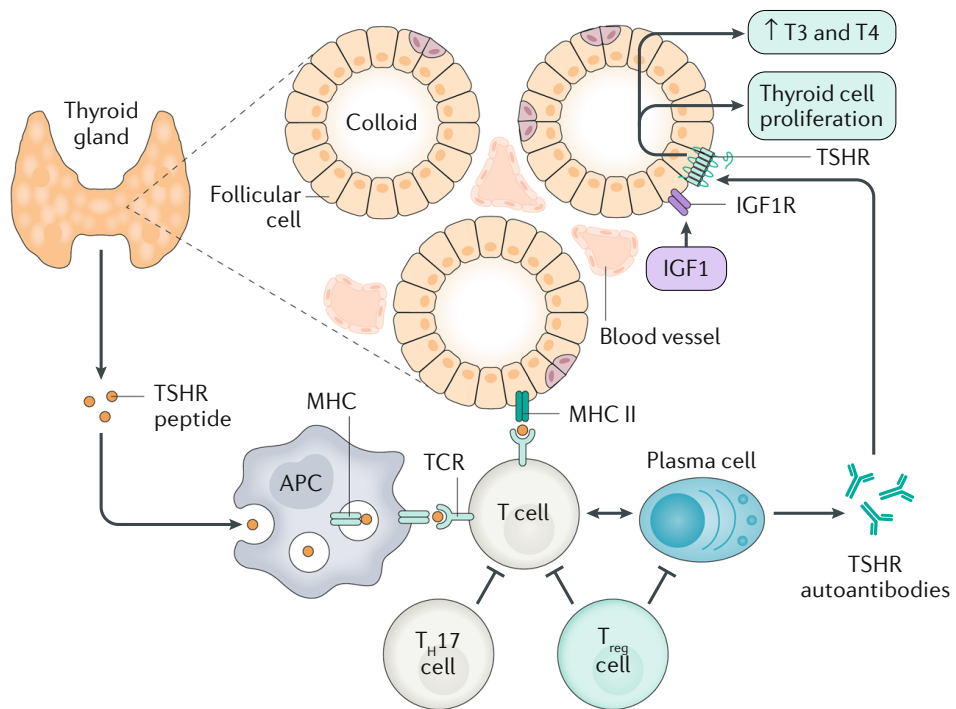


Figure 1.10 - The pathogenesis of GD and the interplay between the TSHR autoantibodies and the thyroid follicular cells

Thyroid follicular cells are stimulated by thyroid-stimulating hormone receptor (TSHR) autoantibodies to secrete thyroid hormones, T3 and T4. The autoantibodies are produced by local B cells and plasma cells controlled by T cells and aided by insulin-like growth factor 1 (IGF-1). The T cells are activated by TSHR peptides on antigen-presenting cells (APCs), which might be the thyroid cells themselves or B cells, macrophages or dendritic cells in the vicinity.

IGF1-R, insulin-like growth factor 1 receptor; **MHC**, major histocompatibility complex; **T_H cell**, T helper cell; **T_{reg} cell**, regulatory T cell; **TCR**, T cell receptor (Davies et al., 2020)

1.5.2.1 – Graves’ Disease Diagnosis

The presenting symptoms of GD vary from patient to patient, and can vary depending upon patient age. In patients presenting under fifty years of age, neurogenic symptomology such as tremor and anxiety are more common, whilst in the elderly it tends to be more cardiovascular symptoms such as sinus tachycardia, atrial fibrillation and heart failure (Boelaert et al., 2010). The diagnosis of GD is made in the hyperthyroid patient through the measurement of the gold standard test of TSH receptor autoantibodies (TRAb) in the serum (Ross, 2016; Bell, 2018). A TRAb > 1.8 IU/L serum is considered to be a positive test. The current ‘third generation’ TRAb assay has a sensitivity and specificity of 97% and 99% for the diagnosis (Kotwal & Stan, 2018). If the

TRAb returns negative and suspicion of GD remains, then a radioiodine uptake test and a thyroid scan are performed (Altayeb et al., 2022).

1.5.3 – Toxic Multinodular Goitre (TMG)

Toxic Multinodular Goitre (TMG) or Plummer's Disease, is a common cause of hyperthyroidism first described by American physician Henry Plummer in 1913 (Kopp, 2023). It is most common in the elderly who reside in iodine deficient areas (Laurberg et al., 2010). The UK is the seventh most iodine deficient country in the world (Davies, 2016). The excess production of thyroid hormones results from functionally autonomous thyroid nodules which no longer require stimulation from TSH. The pathogenesis of the disease is that iodine deficiency results in reduced T4 production. The low levels of T4 culminates in thyroid cell hyperplasia and a multinodular appearance to the gland. This increased cell replication predisposes to a mutation in the TSH receptor, which can then result in the multinodular goitre itself becoming 'toxic' and producing excess T3 and T4. Treatment of TMG, usually involves radioiodine (RAI), which ablates the thyroid gland, and almost always results in permanent hypothyroidism and the subsequent need to take lifelong thyroid hormone replacement. Surgery is generally reserved for those patients suffering from airway compressive symptoms (Ríos et al., 2005).

1.5.4 – Thyrotoxicosis Management

The treatment of thyrotoxicosis can be split into symptomatic treatment and the establishment of normal thyroid hormone levels. In order to treat the symptomatic tachyarrhythmia, beta blockers are used to reduce the heart rate. There are three different modalities of treatment that are currently employed for the treatment of thyrotoxicosis; thionamide therapy, surgery and radioiodine treatment. The treatment should be tailored to the specific needs of each patient with the benefits and risks of each therapy fully explained.

1.5.4.1 - Thionamide Therapy

Thionamides are a class of antithyroid drugs that work through the inhibition of thyroid hormone synthesis. The main two medications used in the UK are carbimazole and propylthiouracil (@NICEcomms, 2023). Thionamides work through being actively transported into the thyroid gland where they inhibit the organification of iodine to the

tyrosine residues in thyroglobulin (Cheetham, 2021). The medications act as a preferred substrate for iodination by thyroid peroxidase (**Figure 1.7**). Thionamides are used in GD patients who want to potentially avoid or defer their ablative therapies in the form of radioiodine or thyroid surgery. In some fortunate cases, remission from GD can be achieved.

Patients treated with thionamides, typically take between three to eight weeks to become euthyroid through the blockage of new hormone synthesis. If there is already any formed T4 and T3 stored in the colloid, this must be secreted and metabolised before any significant clinical improvement is seen. Thionamides can also act to suppress lymphocytic infiltration into the thyroid and as a result, modulate GD (Burch & Cooper, 2015).

1.5.4.2 - Surgery

Surgery involves either a subtotal thyroidectomy or a total thyroidectomy. Since the turn of this century, surgical practice has shifted towards that of total thyroidectomy (Mittendorf & McHenry, 2001; England & Atkin, 2007; Selwyn et al., 2023). This is because the accurate prediction of how much tissue needs to be left, in order to achieve a euthyroid state is not possible as too many variables exist. Patients need to be clearly counselled regarding the risks of the surgery; recurrent laryngeal nerve damage, a postoperative haematoma, post-operative hypocalcaemia and the ongoing need to take lifelong thyroxine (Smithson et al., 2019). The surgery should be performed by a high-volume thyroid surgeon due to the proven reduced complication rate associated with high volume practice (Adam et al., 2017). This has been further backed up by work from the 'Getting It Right First Time Programme' orchestrated by NHS England (Gray et al., 2021).

1.5.4.3 - Radioactive Iodine Treatment

RAI treatment involves a single oral dose of medication with no requirement for an inpatient stay. At present, it is recommended as first line treatment for most cases of GD (Onyebuchi et al., 2020). The radioactive iodine damages DNA, resulting in the death of thyroid cells and a general reduction in thyroid size and function (Hertz & Roberts, 1946).

1.6 – Thyroid Cancer (TC)

Thyroid cancer (TC) encompasses a spectrum of pathological variants that are heterogeneous in clinical behaviour (Fagin & Wells, 2016). Effective, accurate, and timely diagnosis is crucial to the decision-making surrounding the treatment options. TC is classified into four main histological types; papillary thyroid carcinoma (PTC), follicular thyroid carcinoma (FTC), medullary thyroid carcinoma (MTC) and anaplastic thyroid carcinoma (ATC). The fifth edition of the Classification of Endocrine and Neuroendocrine Tumors was published by the World Health Organization in 2022, further updating the classification making changes to the nomenclature, grading and prognostics as a result of the increasingly recognised pathological features and molecular profile (**Figure 1.11**). Thyroid tumours with a predominant follicular growth pattern exhibit a *RAS*-like molecular profile, whilst thyroid tumors with a *BRAF*-like molecular profile demonstrate papillary features (Yoo et al., 2016). Detection and characterisation of this molecular profiling is helpful in terms of the identification of therapeutic targets.

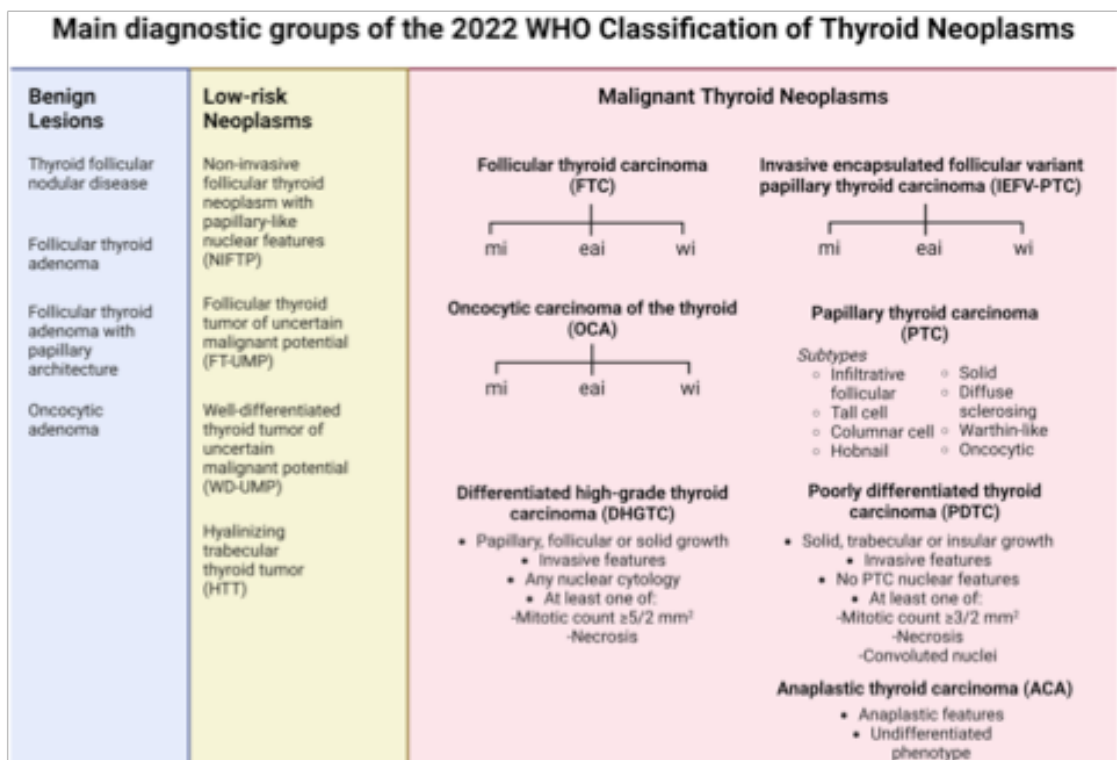


Figure 1.11 – An overview of the main diagnostic groups of the 2022 WHO classification of thyroid neoplasms (Juhlin et al., 2022)

In the fifth edition of the WHO guidelines, the term 'Hürthle' cell carcinoma is discouraged, being deemed a historical misnomer with preference being given to oncocytic carcinoma of the thyroid.

1.6.1 – Differentiated Thyroid Cancer

TC are predominantly epithelial in origin and can be subdivided into differentiated, poorly differentiated and the undifferentiated, anaplastic thyroid cancers (Hu et al., 2021). The differentiated thyroid malignancies can be either PTC or FTC which in most cases tend to behave indolently and possess a 'good prognosis' (Kilfoy et al., 2009). They are classified as 'differentiated' as they arise from thyroid follicular cells and retain the ability to uptake iodine. The 'differentiated' malignancies result from the dysregulation of the protein kinase pathways (Prete et al., 2020). PTC typically demonstrates lymphomatous spread to cervical lymph nodes, whilst FTC metastasises through a haematogenous route. Patient survival rates at ten years following diagnosis with differentiated thyroid cancer are between 92 and 98% (Mitchell et al., 2016). This contrasts with poorly differentiated ATCs which possess only a 5% five-year survival rate (Faten et al., 2023).

1.6.2 – Papillary Thyroid Cancer

PTC is the most common thyroid cancer, accounting for up to 90% of total cases (Rossi et al., 2021). However, within PTC there are recognised variants, some of which have a tendency to behave aggressively (Silver et al., 2011). Women unfortunately have an established three to four-fold increased risk of developing TC than men and this is consistent throughout the world especially with regards to PTC (Kilfoy et al., 2009).

1.6.2.1 - Papillary Thyroid Microcarcinoma

Papillary thyroid microcarcinoma (PTMC) is a PTC in which the tumour is a maximum of 1cm diameter (Noguchi et al., 2008). The vast majority cause no issues and are clinically silent. They are typically found incidentally following surgery for benign thyroid disease or within autopsies. The commonality of PTMC, alongside the excellent prognosis, has led to many feeling it too harsh to term this disease an actual 'cancer' (Kaliszewski et al., 2019). However, within this subtype there are aggressive PTMC cases that are termed occult PTMC, which can present with lymph node metastasis (Wada et al., 2003).

The clinical management of these ‘incidentalomas’ is a challenge, due to the obvious difficulty in predicting their aggressiveness. Whether surgery is actually indicated is one thing but also the extent of the surgery required to effectively treat the disease can be difficult to anticipate (Kaliszewski et al., 2019). There has been a general trend towards a de-escalation in the management of PTMC with time. The American Thyroid Association (ATA) has recommended surveillance as an option for PTMC with low-risk features (Haymart et al., 2017). In the UK, the practice has moved towards that of thyroid lobectomy for patients with PTMC with no other existent risk factors but active surveillance is also advocated for within the NICE guidelines (NICE, 2023).

The decision-making surrounding surgery versus surveillance needs to be patient centred (Yoshida et al., 2020). Undergoing an operation is a significant undertaking for the patient but at the same time provides reassurance that the PTMC has been removed, whilst surveillance presents an element of uncertainty. There is also the argument that surveillance versus operative management results in more trips to the hospital, culminating in a greater financial cost to the healthcare provider alongside further stress and disruption to the patient’s life. The main concern for PTMC patients is that they are undergoing surgery with a risk of morbidity that is not justified by PTMC’s low risk of mortality and recurrence. This highlights the need for further research which may help with the identification of PTMC that display more aggressive features that need addressing surgically; the identification of exosomal miRNA biomarkers could contribute to the surveillance and management strategy surrounding PTMC.

1.6.2.2 - Noninvasive Follicular Thyroid Neoplasm with Papillary-Like Nuclear

Features

Noninvasive Follicular Thyroid Neoplasms with Papillary-Like Nuclear Features (NIFTP), previously known as Encapsulated Non-invasive Follicular Variant Papillary Thyroid Carcinoma, are a ‘borderline’ thyroid tumour that are associated with an excellent clinical outcome. NIFTP have features that resemble that of PTC but are not considered to be malignant. NIFTP are considered to be of particularly low clinical risk for the adverse outcomes such as tumour recurrence or metastasis because they are contained within a capsule (**Figure 1.12**). The diagnosis of NIFTP can only be made after histological examination of the entirety of the tumour and is based upon strictly defined inclusion

and exclusion criteria (Zajkowska et al., 2020). According to the original diagnostic criteria, histological examination of NIFTP should demonstrate an encapsulated nodule, with cells exhibiting a follicular growth pattern and nuclei typical of PTC (Seethala et al., 2017). NIFTP should not display any features of vascular or capsular invasion, tumour necrosis or high mitotic activity.

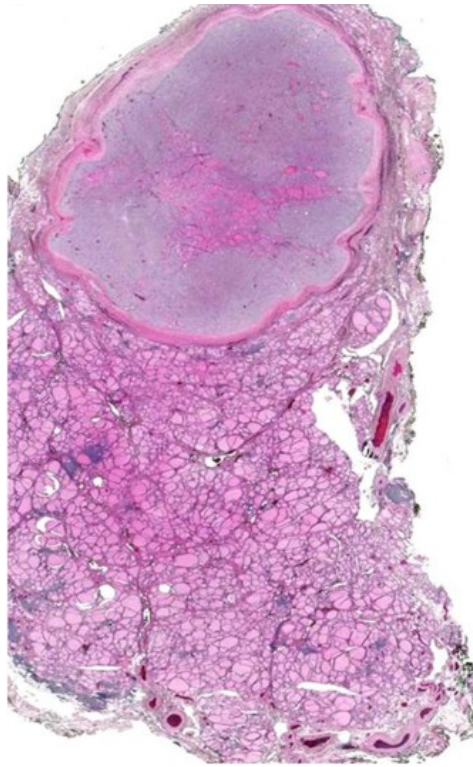


Figure 1.12 – H&E staining of a NIFTP identifiable within its well-formed sclerotic capsule. (Seethala et al., 2017)

1.7 - Undifferentiated Thyroid Cancers or Anaplastic Thyroid Cancer

Undifferentiated or ATCs are rare, highly aggressive thyroid tumours that account for between 2 and 3% of total thyroid malignancies (Faten et al., 2023). They are known as undifferentiated as their cells do not resemble those of typical thyroid cells (**Figure 1.12**). Patients presenting with ATC commonly present with a rapidly enlarging thyroid mass with the disease having metastasised at the time of presentation. Diagnosis with thyroid core biopsy is often preferred as it helps in the differentiation of ATC from that of thyroid lymphoma (Vander Poorten et al., 2022). Unlike differentiated thyroid cancers, which seldom possess mutations in the p53 tumour suppressor gene, between 50 to 80% of undifferentiated, ATC possess mutations in p53 (Manzella et al., 2017).

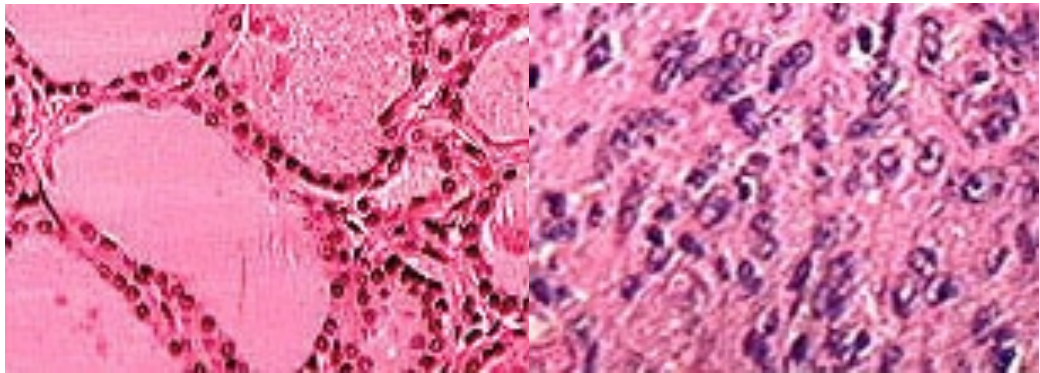


Figure 1.13 – Comparison between the normal architecture of normal thyroid tissue (**left-hand side**) compared to that of the chaotic disorganised histological architecture of ATC (**right-hand side**) (Agarwal & Bychkov, 2024)

1.7.1 - Medullary Thyroid Cancer

Medullary thyroid carcinoma (MTC) is a rare neuroendocrine tumour that arises from the parafollicular cells or C cells within the thyroid gland. They are of neural crest origin and typically present in the upper two thirds of the thyroid gland. The C cells themselves produce calcitonin, which acts to oppose the action of parathyroid hormone (PTH). Calcitonin and carcinoembryonic antigen (CEA) can be utilised as serum tumour markers (DeLellis et al., 1978; Machens et al., 2007). MTC are rare, making up between 3 to 5% of all thyroid malignancies but around 5 to 10% of all paediatric thyroid cancers (Starenki & Park, 2016). One quarter of the cases of MTC are inherited in an autosomal dominant pattern as either part of the multiple endocrine neoplasia type 2 (MEN-2) or familial MTC, however they can arise sporadically due to mutations in the RET proto-oncogene (Hofstra et al., 1994). Patients with suspected MTC should have serum calcitonin and biochemical screening for pheochromocytoma performed pre-operatively (Mitchell et al., 2016). Genetic screening for the RET mutation is mandatory due to its strong association with the disease and this needs to be undertaken in a dedicated cancer centre, supported by a dedicated Thyroid MDT (Niederle et al., 2014). All patients with MTC should receive a total thyroidectomy and central compartment node clearance (level VI). In the case of RET oncogene positivity, the patient's family should be screened for this, counselled appropriately and offered age-appropriate prophylactic thyroidectomy.

1.8 – Increasing Incidence of Thyroid Cancer

TC is currently the most common endocrine malignancy and the fifth most common malignancy in women in the USA (@NCICancerStats, 2022). Since the 1970s, TC has increased in incidence worldwide and was until recently the most rapidly increasing cancer diagnosis in the USA (Kaliszewski et al., 2023). Between the early 1990s and 2015 there was a 175% increase in the incidence of TC. The increasing incidence associated with the disease has led to a projected 7% increase in the mortality rate by 2035 (@NCICancerStats, 2022). However, this increase in incidence has not been equal across all subtypes of TC. It has been PTC that has increased at a significantly faster rate than other TC (Rossi et al., 2021). Despite this undoubted increase in TC incidence, this has not been mirrored by an increase in the diseases' overall associated mortality rate as might be expected (**Figure 1.14**).

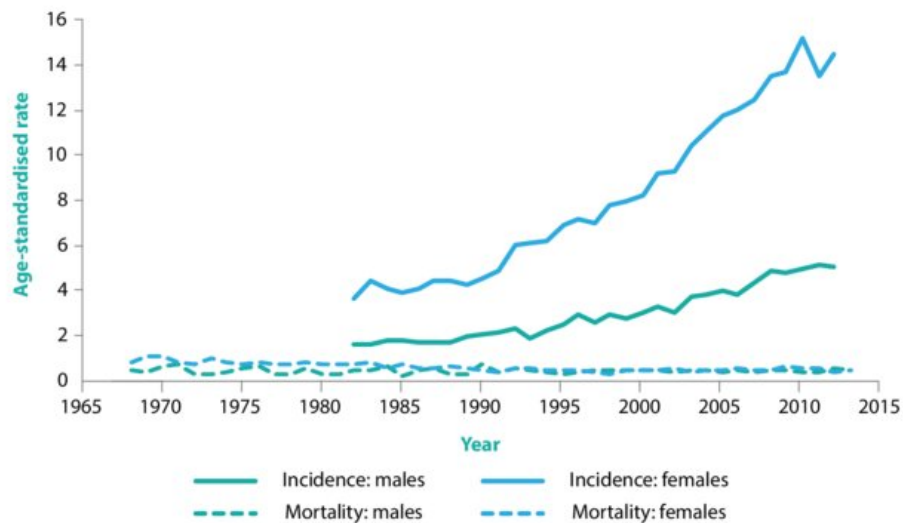


Figure 1.14 - Age-standardised thyroid cancer incidence and mortality rates per 100,000 males and females in Australia, 1968 to 2013. (Carter & Barratt, 2017)

1.8.1 – The ‘Overdetection’ of TC

As highlighted, the increase in incidence of TC has been primarily driven by PTC (Lim et al., 2017). Some researchers have speculated that the incidence patterns for TC are as a result of over-diagnosis due to increasing radiological imaging being carried out whilst others suggest a multifactorial causality (Kaliszewski et al., 2023). Without doubt, improvements within imaging and diagnostics along with overzealous imaging have played their part in the increased detection rate of TC (Brito et al., 2013). Alongside this,

the increasing rate of worldwide obesity and radiation exposure are also seen as risk factors (Seib & Sosa, 2019). Consideration also has to be given to day-to-day cumulative radiation exposure within our environment alongside that of medical diagnostic radiological imaging. A study examining the rates of TC in Belarus at the fallout sites from the Chernobyl nuclear disaster demonstrated increased rates of malignancy (Mahoney et al., 2004). Rates were significantly higher amongst children due to preexisting iodine deficiency resulting in increased susceptibility to the radiation as a result of the uptake of iodine uptake from the radioactively contaminated environment (Pacini et al., 1997). Thirty years following the nuclear disaster, nearly 11,000 TC cases have been reported among those who were children or adolescents at the time of the accident in Ukraine, Belarus and the most contaminated regions of Russia (WHO, 2016).

A number of cross-sectional studies of patients with PTC have added to the evidence that obesity is associated with increasingly aggressive types of PTC (Kim, 2013; Choi, 2015). As to how obesity has such an effect upon the development of PTC is not entirely clear, but laboratory-based studies have identified that insulin resistance and the likes of insulin-like growth factor 1, oestrogen, leptin and TSH could all be playing a role (Kim et al., 2013).

Improved imaging quality of the thyroid gland has undoubtedly led to the increased diagnosis of subclinical thyroid disease, which in turn has led to the 'over-detection' of PTC and consequently its over treatment (Wiltshire, 2016). These PTCs may have otherwise gone undetected, never requiring surgical input but instead the patients are left with the unwanted, potentially unnecessary knowledge that they are harbouring an indolent cancer. This can be demonstrated through the incidence of palpable nodules in men and women being at approximately 5% from clinical examination, whilst the use of ultrasound scanning has increased the detection rate of thyroid nodules to between 50 and 70% within the general population (Mitchell et al., 2016). The incidence rates throughout the world are not wholly equal however, and this is directly affected by the amount of GDP spent on healthcare and private healthcare investment in different parts of the world (Wang et al., 2023). The effect of access to imaging on diagnosis has been demonstrated by an interesting study carried out in the States, by Morris *et al.* in which they identified that PTC diagnosis was positively correlated with college education, white-collar employment and family income whilst negatively correlated with not

possessing health insurance, unemployment, non-white ethnicity and lack of high school education (Morris et al., 2013). An example of a country in which the effect of ultrasound imaging on TC diagnosis is evident is in South Korea. TC screening was promoted by health-care providers and the media there. As a result, the incidence of thyroid cancer increased fifteen-fold between 1993 and 2011 with the increase unsurprisingly being predominantly in PTC diagnosis (Ahn et al., 2014).

TC has been identified in between 5 and 10% of patients who have passed away from other causes, inferring the presence of subclinical, indolent disease that goes undetected within the general population (Harach et al., 1985; Martinez-Tello et al., 1993). Despite the increased detection rate, the mortality rate from thyroid cancer has remained stable. As a result, the evidence presented raises the question as to whether the treatment related morbidity associated with surgery delivers a justifiable survival benefit (Kitahara & Sosa, 2016). In addition to improved radiological imaging, histopathological interrogation of thyroid specimens and molecular pathology testing has also improved. This in turn has subsequently brought about more definitive diagnoses of thyroid cancer (Poller & Johnson, 2017). Part of the increased focus upon the diagnosis of PTMC has resulted from the improved histological examination (Roti et al., 2006).

1.8.2 - Radiation Induced TC

An issue associated with the increased rate of radiological imaging within the last few decades has been the resulting radiation induced cancers throughout the body (Ron, 2003). The thyroid is one of the most radiosensitive organs in the body in part due to its superficial anatomical location within the neck. Increased exposure to imaging, especially CT scanning in adults has led to an increasing risk of developing PTMC (Zhang et al., 2015) as these imaging modalities carry a much greater dose of radiation compared to that of traditional radiographic methods (Mettler et al., 2008).

With this link between TC and radiation being established, it has been postulated that radiation associated PTMC may constitute a completely different subtype of TC (Bresciani et al., 2019). It has been identified that these radiation related PTC possess a unique somatic mutation compared to that of other TC and can present with a higher

frequency of RET chromosomal rearrangements (Ciampi & Nikiforov, 2007; Hamatani et al., 2008).

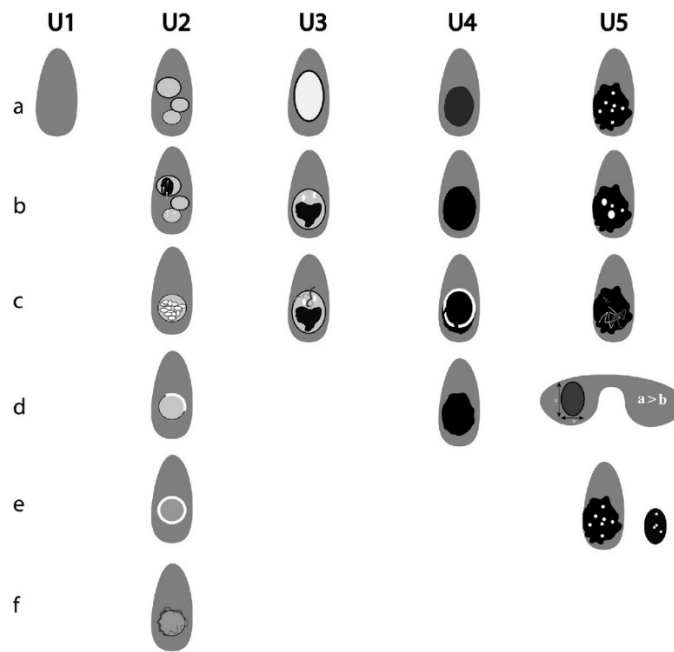
1.9 – The Investigation of TC

Thyroid nodules, as described by the ATA, are “discrete lesions within the thyroid gland, radiologically distinct from surrounding thyroid parenchyma” (Cooper et al., 2009). The incidence of thyroid nodules in the general population stands at 40% (La Vecchia et al., 2015). It is clear, that the vast majority of these thyroid nodules are harmless but the real difficulty lies within identifying which of these ‘nodules’ are malignant or possess malignant potential.

Ultrasound scanning (USS) is an extremely sensitive method in which to detect and characterise thyroid nodules and has the advantage of being both non-invasive and cost-effective (Wong & Ahuja, 2005). The main investigation of choice of potentially malignant thyroid nodules is through fine needle aspiration cytology (FNAC) under ultrasound guidance. The combination of both the cytology and ultrasound imaging are used to make a diagnosis of thyroid malignancy and determine ongoing management.

1.9.1 - British Thyroid Association (BTA) - Ultrasound Grading of Thyroid Nodules

USS is a vital diagnostic tool in the investigation of thyroid nodules and helps increase the diagnostic yield of cytology for FNAC. Ultrasonographers in the UK are instructed to use the U grade table in order to classify the nodules through their ultrasound appearances (**Figure 1.15**).



U1. <u>Normal</u> .
U2. <u>Benign</u> : (a) halo, iso-echoic / mildly hyper-echoic (b) cystic change +/- ring down sign (colloid) (c) micro-cystic / spongiform (d & e) peripheral egg shell calcification (f) peripheral vascularity.
U3. <u>Indeterminate/Equivocal</u> : (a) homogenous, hyper-echoic (markedly), solid, halo (follicular lesion). (b) ? hypo-echoic, equivocal echogenic foci, cystic change (c) mixed/central vascularity.
U4. <u>Suspicious</u> : (a) solid, hypo-echoic (cf thyroid) (b) solid, very hypo-echoic (cf strap muscle) (c) disrupted peripheral calcification, hypo-echoic (d) lobulated outline
U5. <u>Malignant</u> (a) solid, hypo-echoic, lobulated / irregular outline, micro-calcification. (? Papillary carcinoma) (b) solid, hypo-echoic, lobulated/irregular outline, globular calcification (? Medullary carcinoma) (c) intra-nodular vascularity (d) shape (taller >wide) (AP>TR) (e) characteristic associated lymphadenopathy

Figure 1.15 - Thyroid nodules and their associated ultrasound features (U1 to U5) (Weller et al., 2020)

FNAC is considered for all cases in which the nodules have suspicious ultrasound features (U3 to U5). If a nodule appears to be smaller than 10mm in diameter on USS, then FNAC is not recommended unless there are clinically suspicious lymph nodes seen on the USS also (Mitchell et al., 2016).

1.9.2 - BTA – Royal College of Pathologists Thy System - Fine Needle Aspiration

Cytology (FNAC) Guidelines

Following ultrasound evaluation of a thyroid nodule, FNAC is the gold-standard investigation in the evaluation of thyroid nodules (Cramer, 2000). In the UK, the RCPATH thyroid reporting system was developed through building upon the existing British Thyroid Association (BTA) guidelines back in 2009 (Mitchell et al., 2016) (**Table 1.1**). This is used in conjunction with the ultrasound “U” classification (**Appendix 1**) of thyroid nodules which has been developed by the BTA as part of their 2014 guidelines.

Table 1.1 - RCPATH FNAC Thyroid Classifications - thyroid nodule scoring (Cross et al., 2024)

Thyroid FNAC Diagnostics Categories		
<u>Score</u>	<u>Cytological Features</u>	<u>Recommendation</u>
Thy 1/ Thy 1c	Non-diagnostic	Reconduct ultrasound assessment and/or repeat FNAC Action – FNAC should be repeated
Thy 2/ Thy 2c	Non-neoplastic – if this correlates with clinical and radiological findings	No follow up if no suspicious USS feature and no clinical suspicion of thyroid cancer
Thy3a	Sample exhibits cytological/nuclear or architectural atypia or features raising possibility of neoplasia. 'a' for 'atypia'	Repeat ultrasound and FNAC If a second Thy3a cytology obtained, then discuss at MDT and consider a diagnostic hemithyroidectomy
Thy3f	Follicular carcinoma 'f' for 'follicular'	Diagnostic hemithyroidectomy is recommended Consider total thyroidectomy in lesions >4cm
Thy4	Suspicion for thyroid malignancy but do not allow for the confident diagnosis	Discuss at MDT Diagnostic hemithyroidectomy is recommended
Thy5	Diagnostic of thyroid cancer Sometimes it is possible to be confident of malignancy but not of tumour type	Discuss at MDT Surgical plan as appropriate

Thyroid FNA for detection of TC demonstrates a sensitivity for malignancy of between 65% and 98% and a specificity of between 76% and 100%. There is an associated false-negative rate of 0 to 5%, a false positive rate of 0-5.7% and an overall accuracy of between 69-97% (Belfiore, 2001; (Haberal et al., 2009). Alongside this, like any diagnostic procedure it is very much dependent upon the individual operator.

Despite USS and FNA working together to improve the diagnostic accuracy of TC, there are unfortunate shortcomings and inaccuracies associated with the tests as highlighted. A diagnostic test that is able to act as an indicator of the pathology of the TC alongside its underlying future behaviour would be welcome.

1.9.3 - American College of Radiology (ACR) - Thyroid Imaging Reporting and Data System (TI-RADS)

These aforementioned USS grading and FNAC are UK based and do not fully translate to an international thyroid audience. In the USA, the American College of Radiology (ACR) utilise the Thyroid Imaging Reporting and Data System (TI-RADS) (Figure 1.16). This was established in order to develop a risk-stratification system in order to help inform medical professionals which nodules warrant FNA and which nodules ultrasound follow-up is adequate, alongside when to leave nodules alone as such. The aim being to provide evidence-based recommendations for the management of thyroid nodules on the basis of a set of well-defined sonographic features or terms that can be applied to thyroid lesion (Grant et al., 2015).

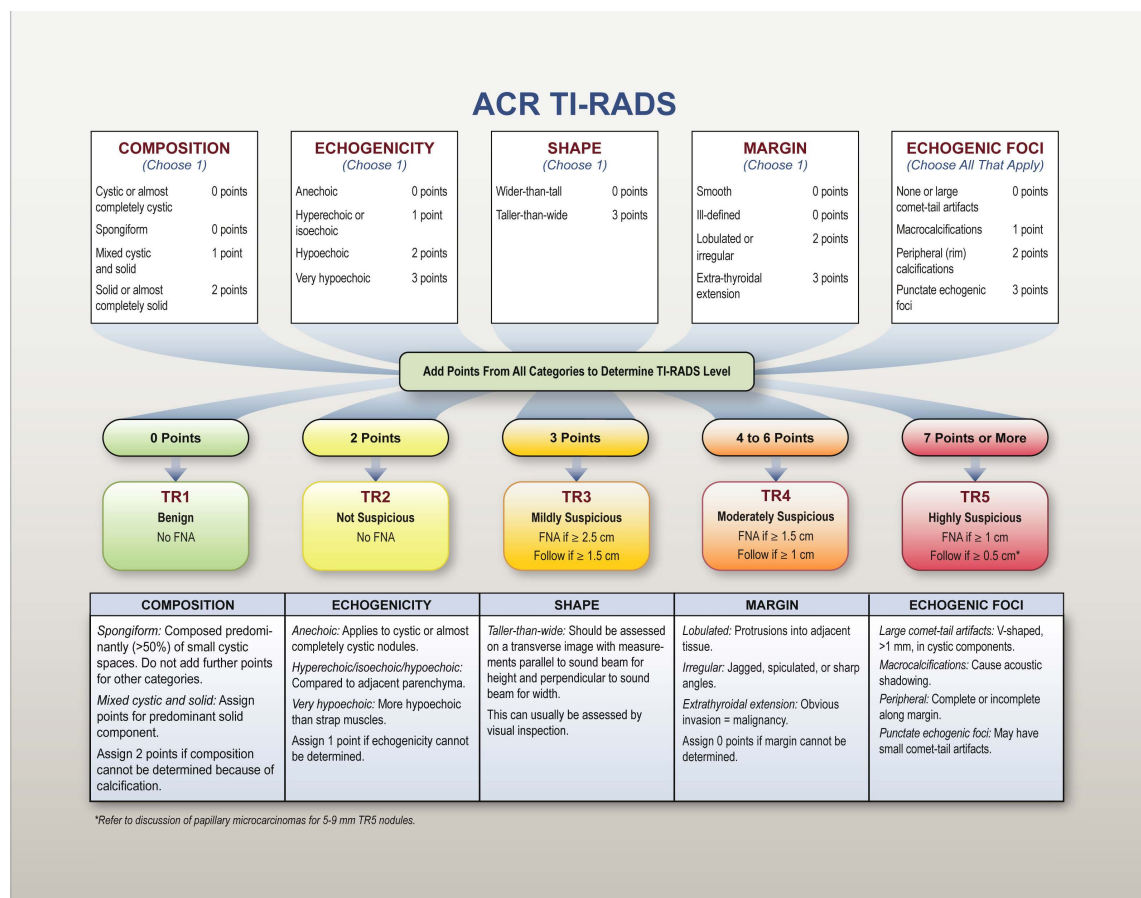


Figure 1.16 - Five categories (TR1-TR5) on the basis of the ACR Thyroid Imaging,

Reporting and Data System (TI-RADS), TR levels, and criteria for fine-needle aspiration or follow-up ultrasound

1.9.4 – The Bethesda System for Reporting Thyroid Cytopathology

The first edition of the Bethesda System for Reporting Thyroid Cytopathology (TBSRTC) was published in 2010. The system has enabled cytopathologists to use a standardised, category-based system for FNAC reporting. The third edition which was published in 2023, assigns a single name to each of the six diagnostic categories: (i) nondiagnostic; (ii) benign; (iii) atypia of undetermined significance; (iv) follicular neoplasm; (v) suspicious for malignancy; and (vi) malignant. The nomenclature has also been updated in order to align with the current WHO classification of thyroid cancer.

1.9.5 – American Joint Committee on Cancer (Staging) – Thyroid Cancer Staging – 8th Edition

TC should be staged as per the AJCC thyroid cancer staging system (Tuttle et al., 2017) (**Appendix 1**). Tumour (T) describes the size of the cancer, node (N) describes whether the cancer has spread to any surrounding lymph nodes and metastases (M) describes whether or not the cancer has spread to any other parts of the body (Mitchell et al., 2016). The staging system is divided into four separate groups from AJCC stage 1 to AJCC stage 4. Younger patients with differentiated TC possess a better long-term outlook than older people (Rong-liang et al., 2016). As a result, the staging system for patients under the age of 55 with differentiated thyroid cancer is different to those aged over 55 years. There are two stages for those aged under 55 whilst there are four stages for people over the age of 55.

Post-operatively the use of an 'R' classification can be used to provide an indication as to the amount of residual disease. The AJCC staging is also available for ATC and MTC (Perrier et al., 2019).

1.10 – Management of TC

All treatment decisions should be made pre-operatively within a dedicated Thyroid MDT setting. The primary curative treatment modality for the management of TC is surgical and this should be performed by a nominated surgeon in a cancer centre who has

received specific training within the scope of thyroid oncology (Adam et al., 2017) (Meltzer et al., 2019). Alongside this, adjuvant radioiodine ablative therapy can also be used. Chemotherapy is reserved for palliative cases of MTC and some cases of ATC. Patients should be given access to a TC clinical nurse specialist who will be able to provide information with regards to the ongoing treatment plans and acts as a vital point of contact for the patient (Vidall et al., 2011).

1. Surgical Management

Within the context of thyroid cancer, the surgery can be classified as diagnostic for patients with a Thy3f or Thy4 cytology report for whom a diagnostic hemithyroidectomy would be recommended (**Table 1.1**). Total thyroidectomy is recommended for patients with tumours greater than 4cm in diameter. Subtotal thyroidectomy should not be used in the management of thyroid cancer. Patients with metastases in the lateral compartment should undergo a therapeutic central and lateral compartment neck dissection.

Following surgical management, patients then need to be risk stratified for any further risk of disease recurrence. Low risk patients have the following characteristics; non local or distant metastases, resection of all macroscopic tumours, no evident tumour invasion of locoregional tissues or structures and that the tumour itself does not display any aggressive histological features or angioinvasion. This is in contrast to high-risk patients, who demonstrate the following characteristics; extrathyroidal invasion, incomplete macroscopic tumour resection and distant metastases.

2. Radioactive Iodine

RAI is recommended in patients who have a TC of more than 1cm in diameter following total thyroidectomy or subtotal thyroidectomy (Mitchell et al., 2016). The three primary goals of RAI therapy in well differentiated thyroid cancer are for remnant ablation, adjuvant therapy or the treatment of known disease. The fact that the thyrocytes keenly absorbs iodine (**Figure 1.6**) provides a means in which to deliver targeted treatment directly to the thyroid gland. RAI is a nuclear medicine treatment, used to treat hyperthyroidism since the early 1940s. This has the effect of not only killing the cells but also reduces the amount of thyroxine made by the thyroid gland and the size of the

gland. RAI remnant ablation (RRA) is used when a total thyroidectomy has been carried out, or in the treatment of residual, recurrent or metastatic disease.

As the TC cells can become undifferentiated this can cause them to lose their NIS expression, leading to them being unable to uptake RAI and not responding to the treatment (Schmidt et al., 2017). A higher level of TSH within the blood will aid in the uptake and effectiveness of RAI (Lawal et al., 2017). This can be achieved through not taking the prescribed levothyroxine that a patient would normally be taking in these circumstances alongside abiding by a low iodine diet for one to two weeks prior to RAI treatment. Unfortunately, through intentionally inducing a state of hypothyroidism this will result in the patient developing the unpleasant symptoms associated with hypothyroidism (**Figure 1.8**). To avoid this complication the use of injected human recombinant TSH prior to treatment has superseded cessation of thyroxine replacement as the normal standard of care (Ma, 2010).

RAI treatment may be offered to patients with metastatic disease that are iodine avid in uptake. Metastatic disease is a poor prognostic marker with regards to long term survival (Cooper et al., 2009). Of these patients, two thirds of them will go on to develop RAI refractory thyroid carcinoma (RRTC) of which only 42% will achieve a cure (Durante et al., 2006) ((Schlumberger et al., 2014).

The short-term effects that RAI treatment can induce are; neck tenderness and swelling, nausea and vomiting, swelling and tenderness of the salivary glands, dry mouth and taste changes. There have been reported documented risks of infertility associated with RAI in both genders (Soltani et al., 2023). RAI is contraindicated in pregnant or breastfeeding women. This protects the baby from radiation exposure and potential damage to the thyroid gland as the foetal thyroid begins to concentrate iodine from 12-weeks gestation (Gorman, 1999).

1.11 – Thyroglobulin as a Tumour Marker

1.11.1 - Post Operative Thyroglobulin Monitoring

Thyroglobulin (Soares et al.) is a 66kDa glycoprotein produced exclusively by the thyroid follicular cells and can be used as a primary biochemical tumour marker for patients with differentiated TC (Li, 2022). The goal of Tg monitoring is to detect TC recurrence. The follow up for TC revolves around clinical examination, measurement of serum Tg, TSH and thyroglobulin antibody (Mitchell et al., 2016). The normal value for Tg is 3 to 40 nanograms per millilitre (ng/ml) in a healthy patient (Peiris et al., 2019). Generally speaking, if a TC recurs following surgery, more Tg will be made. The monitoring of Tg levels in the identification of recurrence works best if the patient has had a total thyroidectomy, whilst the prediction of recurrence can be more difficult following thyroid lobectomy. Alongside this the RAI ablation of the residual thyroid tissue allows for improved quality interpretation.

Tg should be checked in all those patients with differentiated TC, but no sooner than six weeks after surgery (Mitchell et al., 2016). However, a rising serum Tg during the postoperative period must be interpreted cautiously. This could be due to the enlargement of non-cancerous residual thyroid tissue left behind during the surgery and does not act to confirm whether there is any actual cancer recurrence; Tg is not a tumour specific marker. As well as this, if there is not an accurate pre-operative Tg obtained then it is difficult to ascertain whether the post-operative measure provides an accurate post-operative representation. Postoperative serum Tg can act as an important prognosticating factor and work to guide clinical decision making and management surrounding the delivery of RAI treatment. However, there is no optimal value with regards to Tg which will provide a guarantee surrounding the overall efficacy of the RAI (Haugen et al., 2016).

1.11.2 – Preoperative Measurement of Thyroglobulin

Dispute exists as to the role of preoperative serum Tg as a predictor of malignancy within identified thyroid nodules. The opinion of the ATA is that they do not advocate the measurement of preoperative thyroglobulin (Haugen et al., 2016). This is in contrast to the work done by the European Prospective Investigation into Cancer and Nutrition (EPIC) study which demonstrated a strong association between preoperative

measurements of thyroglobulin and thyroid cancer risk. Rinaldi *et al.* looked at 357 patients with TC and matched them with control subjects. TC was associated positively with Tg and negatively associated with TSH level. An elevated Tg level was most strongly associated with FTC than PTC (Rinaldi *et al.*, 2014). In the study, there was a statistically significant difference in Tg levels between the TC patients and the control patients up to eight years prior to their diagnosis of TC.

1.12 - Extracellular Vesicles

Extracellular Vesicles found within various physiological fluids throughout the body, including blood, urine, saliva, lymph and seminal fluid (Möller & Lobb, 2020). EVs are classified as per the International Society for Extracellular Vesicles (ISEV) MISEV guidelines (Welsh, 2024). Exosomes, fall within the category of EVs and are membranous vesicles that are released by cells throughout the body (Bobrie et al., 2011). Exosomes or small EVs are endosomal in origin and typically range in size between 30 nm to 150 nm, in contrast to microvesicles (MVs) (100-1000 nm) which are released by membrane blebbing and apoptotic bodies (1000-5000 nm) which are released when cells die by apoptosis (Menck et al., 2020) (**Figure 1.17**). Exosomes are involved in intercellular communication and are highly stable within a variety of bodily fluids which positions them as ideal biomarkers for clinical analysis (Ludwig & Giebel, 2012).

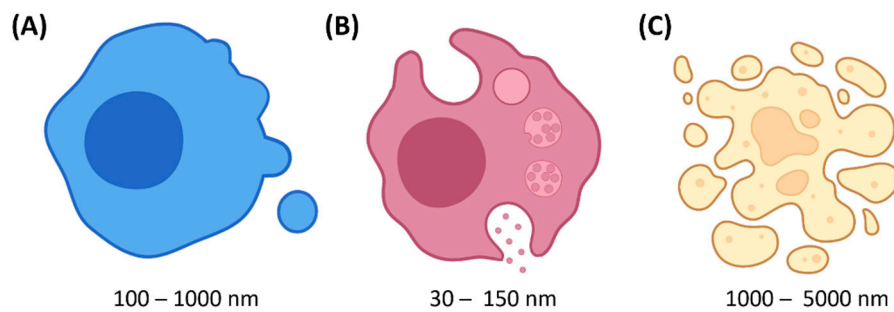


Figure 1.17 – Different types of EV

(A) Microvesicles – produced through direct budding at the plasma membrane

(B) Exosomes or sEV – released by exocytosis of multivesicular bodies formed through inward budding of the late endosome

(C) Apoptotic bodies – fragments of dying cells

(Delcorte, 2022)

Exosomes contain information in terms of proteins, non-coding RNAs, miRNAs, long-non-coding RNAs and circular RNAs that are unique to the cell of origin (Théry et al., 2018) (**Figure 1.18**). The significance of exosomes within intercellular communication and the role that they play within health and disease is becoming increasingly realised. This is at odds with when they were first identified and labelled as ‘platelet dust’ following their discovery in the supernatant of sheep red blood cells (Wolf, 1967). Intercellular communication occurs when exosomes deliver their cargo of proteins, DNA and RNA to recipient cells through endocytosis, receptor-ligand interactions or fusion with the plasma membrane (Kalluri & LeBleu, 2020). Through this intercellular material

transfer and subsequent involvement in the regulation of gene expression, exosomes play a significant role within cell proliferation, differentiation and immune responses (Gangadaran et al., 2023).

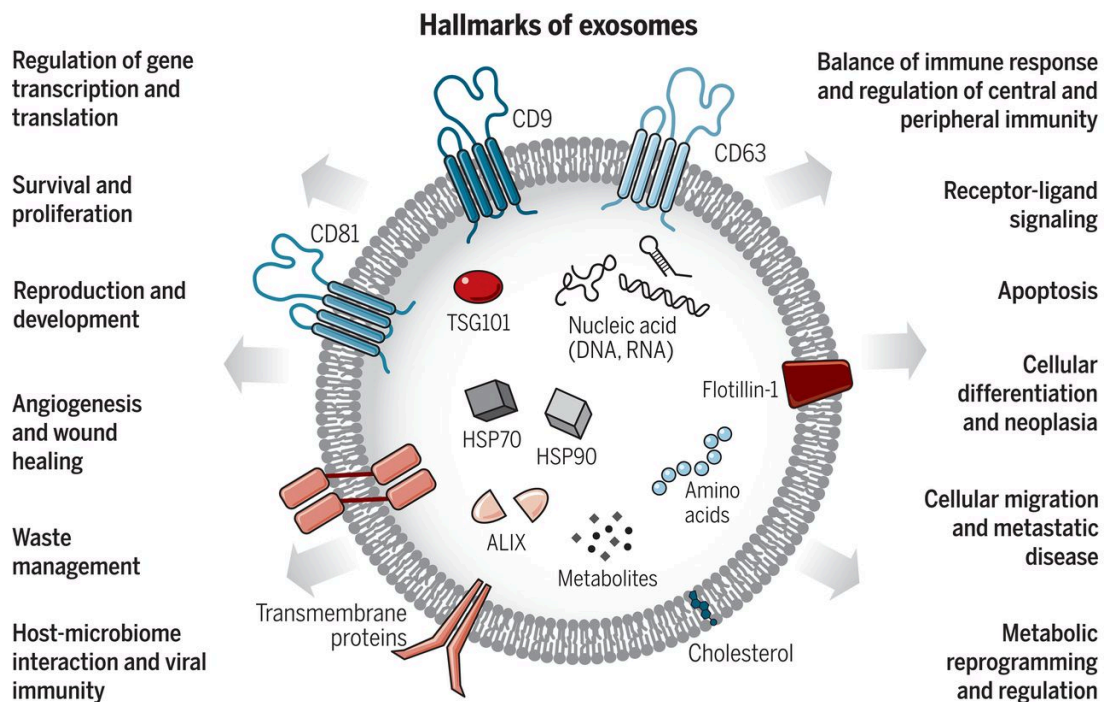


Figure 1.18 - The surface and intracellular content of exosomes and how they exert an influence upon their surrounding cellular environment (Kalluri & LeBleu, 2020)

1.12.1 – The Biogenesis of sEV/Exosomes

Exosomes form from early endosomes and are between 30-150 nm in size with a membrane rich in lipids and a density ranging between 1.15 and 1.19 g/ml (Théry et al., 2009). After the endocytosing of exogenous substances to form endosomes, the inward budding of the endosomal membrane entraps cytoplasmic proteins, nucleic acids and lipids to form multivesicular bodies (MVB) through a series of intracellular interactions. MVB fuse with the cell membrane, releasing the intraluminal vesicles as exosomes (**Figure 1.19**) (Mathivanan et al., 2010). On their secretion from cells, exosomes can be captured by neighbouring cells or alternatively they can enter the circulation through which they have the opportunity to be taken up by different tissues.

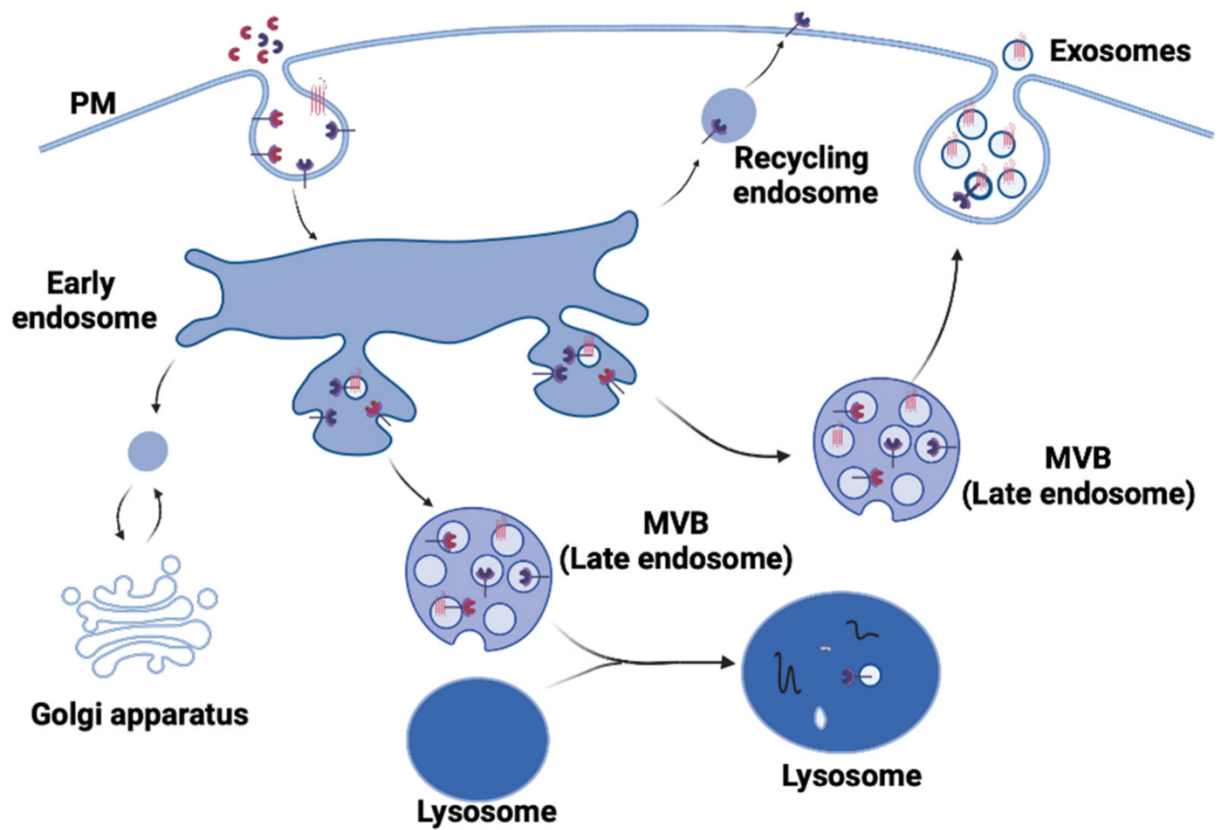


Figure 1.19 - The biogenesis of exosomes from their formation as multivesicular bodies to their release as exosomes (Krylova & Feng, 2023)

1.12.2 - Exosome Isolation

There have been difficulties and controversies surrounding the isolation of pure populations of exosomes. The gold standard method traditionally has been through differential centrifugation and ultracentrifugation. However, in recent years, new methods of isolation, including immunomagnetic separation, size-based isolation and microfluidics all of which possess inherent advantages and disadvantages. To try and standardise the exosome field, the ISEV have published their guidelines, “Minimum Information for Studies of Extracellular Vesicles” (MISEV) proposing standardised methods in which to isolate extracellular vesicle populations (**Figure 1.20**) (Théry et al., 2018).

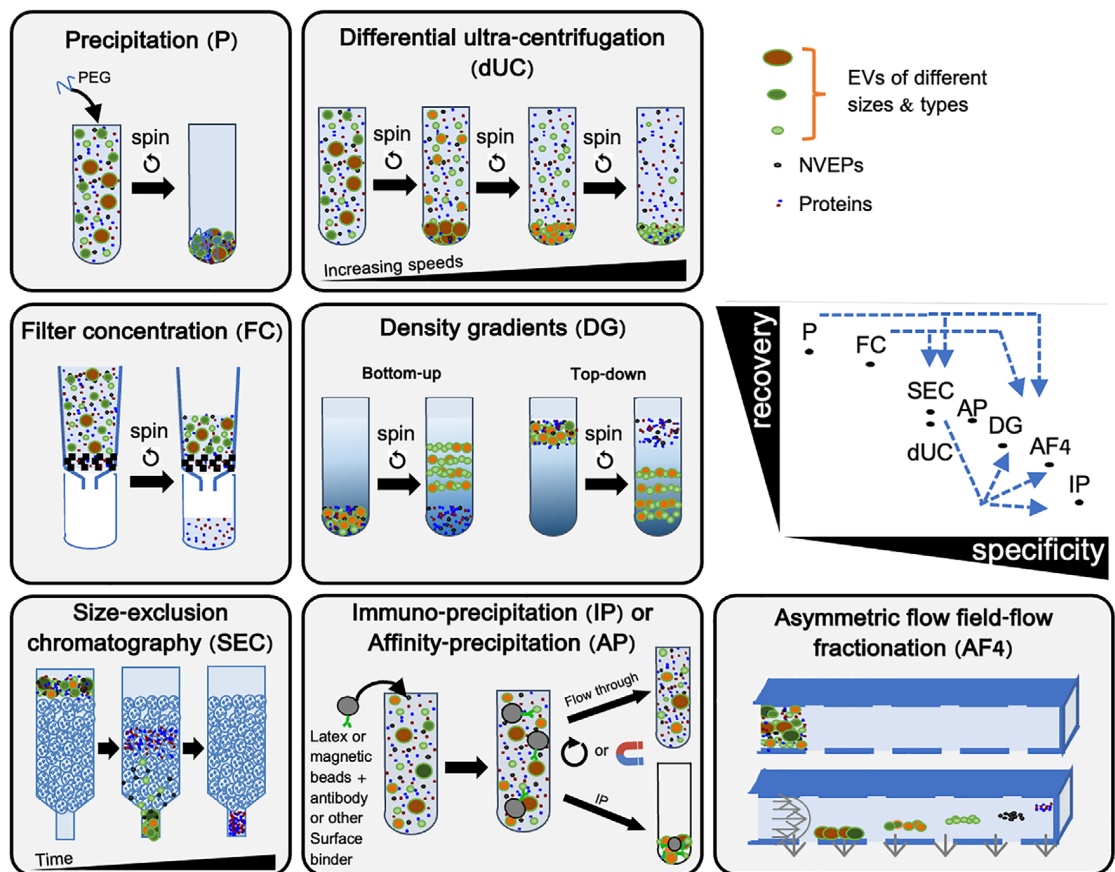


Figure 1.20 - MISEV 2024 - Different methods of EV separation and concentration. Also displayed is a demonstration of their methods and their recovery versus specificity. A combination in methods can be used to increase specificity as demonstrated through the blue arrows (Welsh, 2024)

Differential ultracentrifugation is most commonly used to isolate EVs. The principle revolves around the increasing centrifugal forces to EV containing fluid in order to eliminate donor cells or tissues. Alongside this density gradient or cushions, size exclusion chromatography, fluid flow-based separation and charge and molecular recognition-based separation techniques are all utilised. As emphasised by the MISEV guidelines the choice of separation and concentration methods must be informed by study specific factors and no ‘one-size-fits-all approach’ is applicable to all studies. Alongside this the MISEV consensus group is not in direct agreement as to how best to isolate exosomes. At the end of 2015, according to a worldwide ISEV survey, differential ultracentrifugation was the most commonly used primary EV separation technique (Gardiner et al., 2016). Following separation and isolation of sEVs is then helpful to be

able further quantify and analyse sEV populations. This has been done with both NTA and through flow cytometry.

1.13 - NTA – Quantification and Analysis of sEVs

The Nanosight LM10 enables the quick, accurate, analysis of the size distribution and concentration of nanoparticles between the size range of 20 to 1000 nanometres (nm) and is far more sensitive than flow cytometry (Dragovic et al., 2011). The Nanosight LM10 is capable of detecting particles in a range of 10^6 to 10^9 particles per ml. Most conventional flow cytometry is able to detect nanoparticles in the size of 300 nm to 500 nm, and at a best-case minimal detection limit of about 150 nm through the use of optimised triggering (Botha et al., 2021). However, nanoscale flow cytometry is undergoing further rapid development which is leading to significant improvements in the detection of nanoparticles (Lian, 2019).

The NTA technology works through a laser beam refracting at a low angle as it enters the sample. This then results in a thin beam of laser light illuminating the particles throughout the sample. Particles resident within the beam are visualized using a conventional optical microscope fitted with a video camera (**Figure 1.21**). This collects the light that has been scattered from the particles within the field of view. Three videos are taken, each of a sixty seconds duration, with a frame rate of thirty frames per second. The particle movement is then analysed through the NTA 2.4 software.

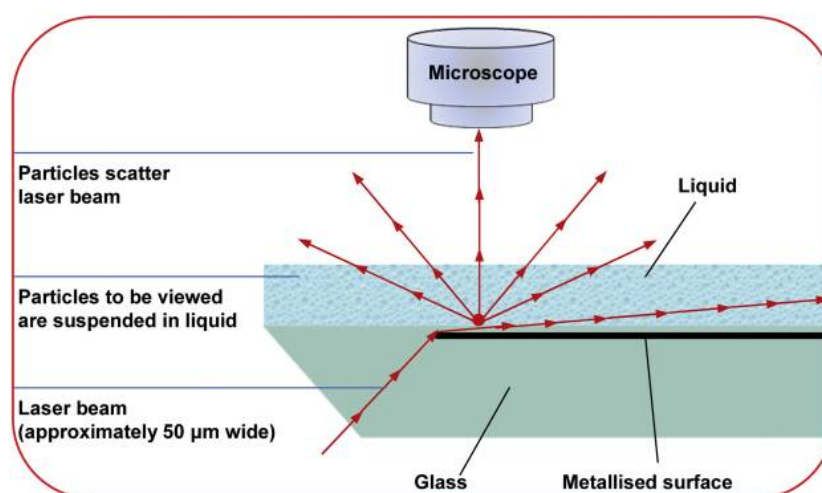


Figure 1.21 – Nanosight LM10 laser mode of action. (Dragovic et al., 2011)

NTA measures the Brownian motion of nanoparticles whose speed of motion, or alternatively diffusion coefficient, is related to the particle size through the Stokes-

Einstein equation (1924, The Stokes-Einstein law for diffusion in solution). The Stokes-Einstein equation is widely used to describe small spherical particles diffusion within liquid media.

The NTA laser light illuminates particles in suspension and a video camera captures the scattered light that is produced. The NTA software, through the tracking of the Brownian motion of the individual vesicles, measures the size and the concentration of the sEVs. The nanoparticles can be visualised on the monitor display (**Figure 1.22**). This visualisation of the nanoparticles on the screen allows for the validation of the data provided by the NTA software.

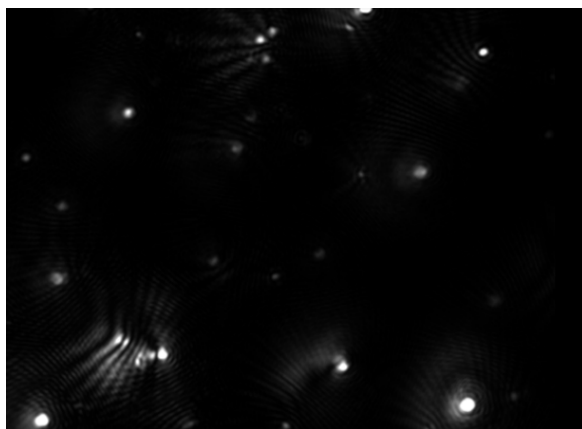


Figure 1.22 – NTA 2.4 software enabling the visualisation of sEVs. The bright dots of varying sizes are individual nanoparticles between 20 and 1000 nm in diameter

1.13.1 - NTA Advantages

NTA has a number of advantages, in that it allows for a large number of vesicles to be analysed with1in a rapid timeframe, typically analysing 1000 particles within one minute. Alongside, this any potential shrinkage is reduced as the nanoparticles being held within a liquid suspension, which in the case of this study was DMEM. The required sample volume and preparation is minimal compared to that of more sophisticated methods such as electron or atomic force microscopy. However, flow cytometry technology is rapidly catching up and evolving, enabling it to be able to detect smaller and smaller particles. A disadvantage of Nanosight LM10, is that it is unable to determine the actual endogenous origin of the vesicles (Théry et al., 2018)

A number of other methods have been used to both measure and characterise EVs. As mentioned, flow cytometry is destined to have a greater role to play in EV studies and this has been identified and developed by van der Pol and Welsh in their report, 'Minimum information to report about a flow cytometry experiment on extracellular vesicles' as part of the Extracellular Vesicle Flow Cytometry Working Group (van der Pol et al., 2022).

1.14 - The Use of NTA in the detection of Exosomes in Thyroid Disease

A number of studies have utilised NTA in terms of characterising sEVs within thyroid disease. This work has been predominantly performed on plasma or serum samples within the context of TC and AITD rather than originating from 'tissue on-chip' experiments.

1.14.1 – Thyroid Cancer (TC)

Zabegina *et al.* looked to isolate EVs and thyroid specific surface molecules followed by further miRNA analysis (Zabegina et al., 2020). The EVs were isolated from the plasma of patients who had either follicular adenoma (FA) ($n=30$) or FTC ($n=30$) through differential ultracentrifugation. A Nanosight NS300 analyzer (Malvern Panalytical Ltd) was used with data being processed using NTA 3.2 software. The concentration of nanoparticles ranged from 1.5 to 3.6×10^{10} and the size distribution from 40 nm to 120 nm with the majority being within the size range of 60 to 80 nm. The exosomal markers CD9 and CD63 were also detected on the surface of isolated vesicles by a CytoFLEX (Beckman Coulter, Miami, Florida, USA) research flow cytometer.

Rappa *et al.* in their study, similarly looked at EVs that had been isolated from the plasma of patients with PTC ($n=6$) prior to surgery and compared them to those of gender and age-matched healthy controls ($n=10$) (Rappa et al., 2019). The number and size of the EVs were quantified using NTA and data analysis was performed with NTA 3.0 software. Significantly higher numbers of plasma EVs ($p = 0.025$) were found in PTC patients than in healthy controls, but the average size of the EVs was similar between the two groups. The authors concluded that EV concentrations within plasma could be used to distinguish PTC patients from healthy individuals.

1.14.2 - Autoimmune Thyroid Disease (AITD)

Along with exosomes being implicated in the development of thyroid cancer, exosomes have also been postulated to play a role within the inflammatory response and propagation of AITDs. Rodríguez-Muñoz *et al.*, looked at the role of ‘circulating MVs’ in AITD. In their study, thirty-three patients with GD ($n = 33$), twenty-nine with HT ($n = 29$), and forty-five healthy thyroid disease-free subjects ($n = 45$), were studied; blood plasma was obtained from all patients (Rodríguez-Muñoz *et al.*, 2015). In order to isolate the exosomes, differential centrifugation of the blood was performed at 1500 x g for an initial 20 minutes, then 1500 x g for a further 20 minutes to ensure removal of platelets. In order to then isolate the MVs centrifugation at 18,500 x g was performed for 30 minutes. The size distribution of the MVs in the resultant supernatant from this centrifugation were then examined by Nanosight LM10 and NTA 2.3 software. The population size varied from 50 nm to 600 nm (**Figure 1.23**). Rodríguez-Muñoz *et al.* in their study did not present any comparative data regarding differences in particle size between the thyroid disease and control groups studied.

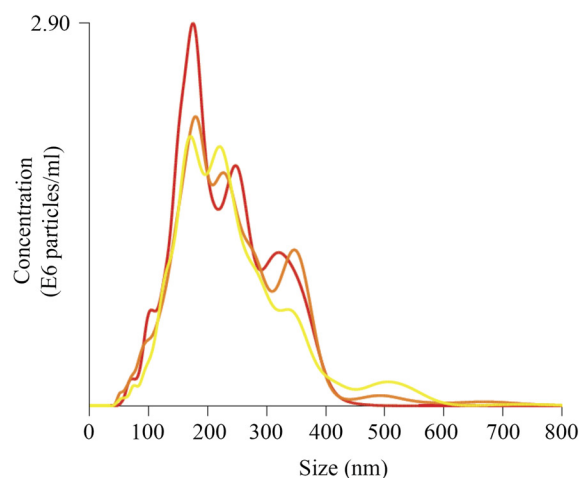


Figure 1.23 - NTA graph demonstrating particle size distribution (nm) and respective concentration (E6 particles/ml) for GD, HT and thyroid disease-free subjects (Rodríguez-Muñoz *et al.*, 2015)

Cui *et al.* (2019) examined the role that exosomes play within the inflammatory response of HT (Cui *et al.*, 2019). The exosomes were extracted from serum from patients with HT ($n = 30$) and healthy controls ($n = 30$). The exosomes were isolated by ultracentrifugation as per Théry *et al.* (2018). The size of the serum exosomes was analysed through the use of NTA NS300 (Nanosight). A uniform size distribution was

demonstrated with a major peak for HT exosomes demonstrated at 95 ± 5 nm (**Figure 1.24**). Transmission electron microscopy (Biosystems) analysis of HT exosomes revealed vesicles with diameters of between 30 to 100 nm, consistent with the size of sEVs.

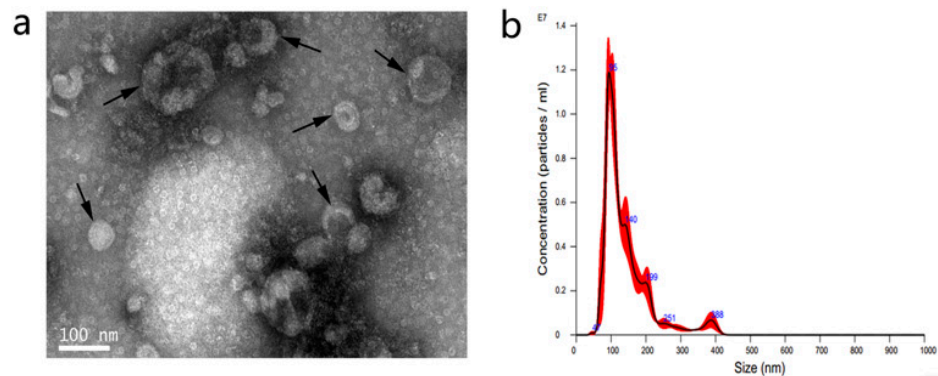


Figure 1.24 – **a.** TEM analysis of EV morphology and size. A representative image of serum exosomes from a patient with HT is shown. Scale bars = 100 nm. **b.** NTA – Particle-size distribution of serum exosomes from a patient with HT. (Cui et al. 2019)

The same team led by Cui *et al.* looked at the role of circulating exosomes in patients with GD (GD-EXO) ($n = 26$) and whether they could induce an inflammatory immune response. Comparison was between 26 patients with GD ($n=26$), 7 patients with Graves orbitopathy ($n=7$) and 26 healthy controls (HC-EXO) ($n=26$). Again, ultracentrifugation was used to isolate EV and NTA was performed using the ZetaView (Particle Metrix, Germany). The NTA analysis demonstrated that the diameter peak of the nanoparticles extracted from the serum of GD patients was 87.8nm in the GD-EXO (Cui et al., 2021) (**Figure 1.25**). The healthy control (HC-EXO) results were not presented as a comparison within their paper.

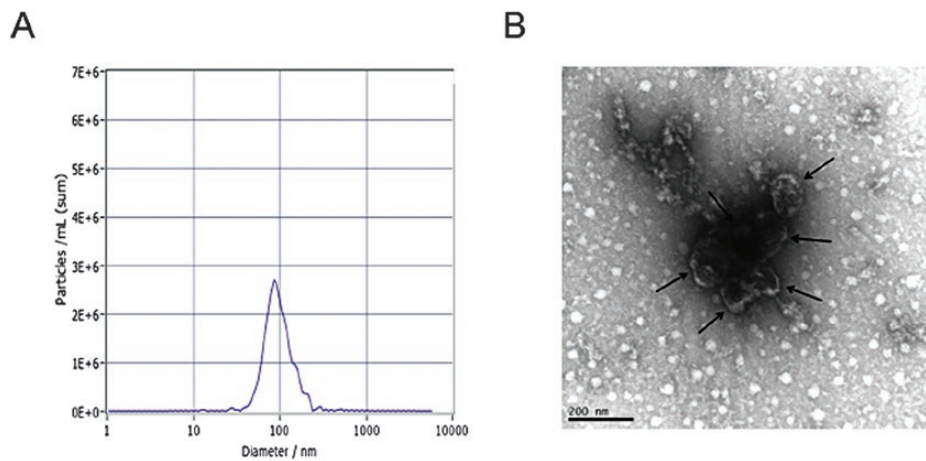


Figure 1.25 – a. NTA was used to measure the diameter of GD-EXO; the NTA results of HC-EXO, which served as controls for GD-EXO, are not shown in the figure. **b.** TEM was used to observe the size and morphology of GD-EXO. The scale bar = 200 nm. (Cui et al., 2021)

1.14.3 – Thyroid Cell Lines

Wise *et al.* conducted cell culture experiments in space, under microgravity conditions. Incubation of human thyroid follicular cell lines (FTC-133) took place for twelve days on the International Space Station under the effect of prolonged microgravity alongside a control group back on Earth. The team used size exclusion chromatography in order to isolate the exosomes followed by NTA to assess both exosome size and concentration. For the flight module samples, the particle size ranged from that of 94.3 to 114.9 nm with a mean value of 106.8 nm. Whilst for the ground module, the particle size ranged from 92.1 to 129.6 nm with a mean value of 107.3 nm. NTA in both experiments detected particles in keeping with the size of sEV (Wise et al., 2021).

Grzanka *et al.* looked at EVs isolated from different thyroid cancer cell lines. In this study, the quantification of the EVs was through flow cytometry and confocal microscopy (Grzanka et al., 2022). Flow cytometry demonstrated that the EV diameters varied from 2 μm to 6 μm which are too large for sEVs. Each of the cell lines released EVs of variable sizes. Alongside this the cytometric analysis showed that the number of EVs secreted, varied between the different cell lines, with the PTC cell line (TPC-1) secreting 18.4 per 100 cells and the thyroid SCC cell line (CGTH) secreting significantly more at 444 per 100 cells (**Figure 1.26**). The results for normal thyroid follicular cell lines (NTHY) were comparable to the FTC cell line.

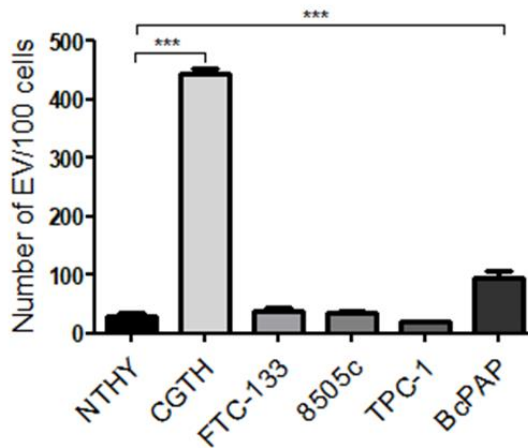


Figure 1.26 – The average number of EVs released by thyroid cell lines per 100 cells. The data is shown as mean \pm standard deviation (SEM). *** $p < 0.001$
 NTHY – normal thyroid follicular cell line; CGTH – thyroid SCC cell line; FTC-133 - lymph node metastasis of FTC cell line; 8505C – undifferentiated TC cell line; TPC-1 – PTC cell line; BcPAP – metastatic PTC cell line (Grzanka et al., 2022)

As demonstrated a multitude of studies have examined the release of EVs within the context of thyroid pathology for both their size and concentration with differing environmental conditions. To date the majority of these studies have revolved around cell lines and serum. Direct comparison between distinctly different thyroid pathologies alongside healthy controls has been lacking in publications. The current study aimed to address this through maintaining three different types of thyroid pathology on ‘tissue-on-chip’ technology and utilising NTA to examine differences in sEV size and quantity between the pathology types.

1.15 – Exosomal miRNAs Biomarkers

microRNAs (miRNAs) are endogenous, non-protein coding single stranded RNAs that contain on average 22 nucleotides (O'Brien et al., 2018). The expression of miRNAs is initiated within the cell nuclei through the transcription of miRNA genes. MiRNAs play an essential role within post-transcriptional processes, being involved in regulating gene expression and thus the proteins responsible for a number of cellular functions (Filipowicz et al., 2008). MiRNAs have been detected in exosomes isolated from bodily fluids which makes them easily accessible to sample. In this respect, they hold great promise in terms of their potential as non-invasive novel biomarkers which could help in accurate disease diagnosis and prognostication (Romano et al., 2021).

Within different cancer processes miRNAs have been demonstrated to be increased or reduced which may provide an indication as to the cancer disease staging or the level of progression. For instance, within non-small cell lung cancer (NSCLC), increased expression of exosomal miR-451a within the plasma of NSCLC was associated with tumour progression, recurrence and ultimately a poor disease prognosis (Kanaoka et al., 2018).

1.15.1 – The Role of Exosomes within Health

Exosomes have been recognised to play a critical role in various physiological and pathological processes including that of cancer, pregnancy disorders, cardiovascular disease and immune responses (Isola & Chen, 2017) (Figure 1.27).

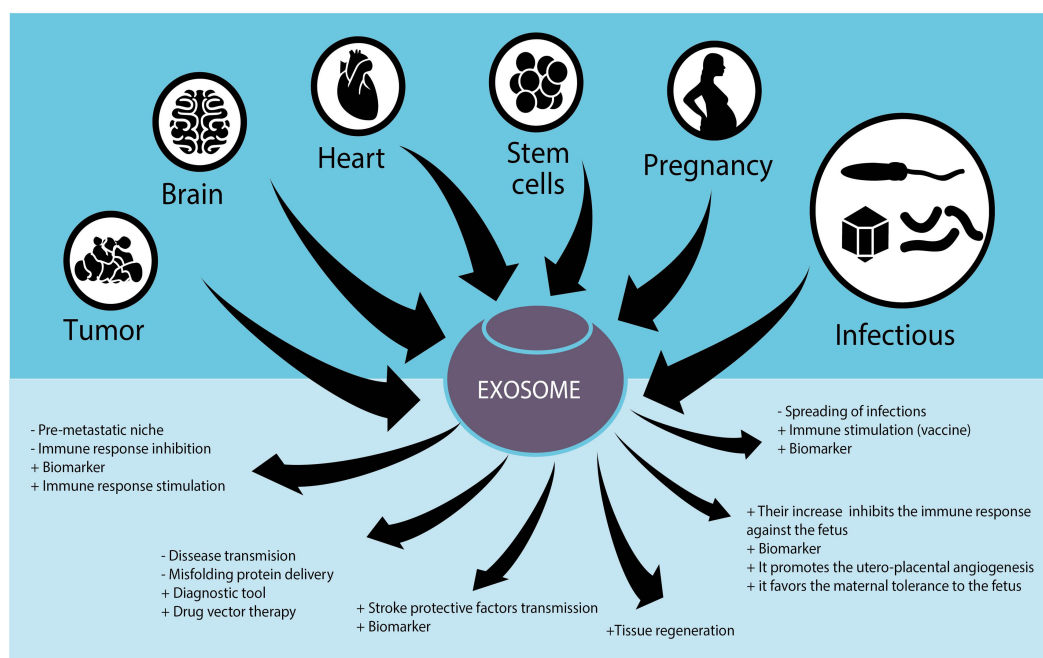


Figure 1.27 - The various roles exosomes play within normal health and disease processes (De Toro et al., 2015)

A functioning immune system is reliant upon exosomes. Exosomes are involved in communication with the immune system in both immunosuppressive and immune activating functions. Dendritic cells release exosomes which have a role in the activation of T cells, but also in the transfer of antigens between dendritic cells (Corrado et al., 2013). The communication between neurons is dependent on exosome release. The secretion of exosomes is triggered through the neurotransmitter glutamate. Studies examining the role of neural exosomes within the brain have demonstrated that overall,

they present a protective function to the neuron as they improve the stress tolerance of the neuron when they were under oxidative stress (Frühbeis et al., 2013; Fröhlich et al., 2014).

1.15.2 - Exosomes and Cancer

Exosomes from cancer cells have been implicated in cancer progression through the transfer of oncogenic proteins and nucleic acids (Dai et al., 2020). In turn, they are able to contribute and play a role in angiogenesis, tumorigenesis, cell proliferation, progression and metastasis. It has been demonstrated that tumour cells generally secrete more exosomes than healthy cells and that the development of cancer can induce changes in the molecular make-up of the exosomes (Zhang, 2020).

Exosomes, due to their stability and ability to communicate between distant cells, have been heralded as contributing to cancer metastasis through the creation of pro-tumour environments (Rana et al., 2013). Exosomes play a key role through interacting within the tumour microenvironment. The tumour microenvironment (TME) is made up of extracellular matrix, stromal cells and immune cells such as B and T lymphocytes, natural killer cells and tumour associated macrophages. Within this TME, exosomes play a key role in the signalling between cancer cells and any other surrounding cells (Dai et al., 2020).

1.15.2.1 - Cancer-Associated Fibroblasts-derived Exosomes

Cancer associated fibroblast (CAF)-derived exosomes (CDEs) are one of the main drivers of oncogenic transformation. The mechanism through which CDEs enhance the growth of cancer cells is through the inhibition of mitochondrial oxidative phosphorylation, consequently leading to an increase in glycolysis and glutamine dependent reductive carboxylation in cancer cells (Zhao et al., 2016). CDEs that are released by CAF can contribute to further progression of cancer and even drug resistance through the regulation of the cancer stem cells (CSCs) (Huang et al., 2019). Richards and colleagues in their study identified the effect the chemotherapy agent, gemcitabine, had upon exosome release and consequent cancer cell survival. Gemcitabine, which is used to treat pancreatic ductal adenocarcinoma increased the levels of the exosomes which led to increased proliferation and further survival of cancer cells thus demonstrating the role that exosomes can have in terms of cancer progression despite therapeutic

treatment (Richards et al., 2017). The gemcitabine-exposed CAFs were exposed to an inhibitor of exosome release, GW4869, which reduced the survival in co-cultured epithelial cells. This demonstrates the role that CDEs play in chemotherapeutic drug resistance.

1.15.2.2 - Exosomes within Angiogenesis and Metastasis

Within oral squamous cell carcinoma (OSCC), miRNA 210-3p is upregulated in exosomes isolated from the CAL-27 OSCC cell lines compared to that of the juxta-cancerous tissue which acted in which to induce tube formation in human umbilical vein endothelial cells (HUVECs) thus exhibiting pro-angiogenic properties (Wang et al., 2020). CDEs have also been shown to activate endothelial cells to support tumour angiogenesis. For example, the exosomes derived from hypoxic glioblastoma cells have been shown to be inducers of angiogenesis (Zhang, 2015), whilst hypoxic K562 leukaemia cells release miR-210 enriched exosomes that are able to promote the angiogenic activity of endothelial cells (Tadokoro et al., 2013).

It also appears that exosomes may play a critical role in the spread of tumour cells throughout the body. A study by Wei *et al.*, highlighted that exosomes from pancreatic cancer cells (Panc-1 PC cell line) expressing the Ephrin (Eph) receptor A2 act to induce cell migration through phenotypically altering recipient cells (Wei et al., 2020). In contrast, in the field of NSCLC, the expression of miRNA-let7e containing exosomes was able to impair further lung cancer metastasis (Xu et al., 2021). It is hypothesised that exosomes influence metastasis through their effect on epithelial-to-mesenchymal transition (EMT) (Jingwen et al., 2022). The EMT process involves disruption of cell-to-cell adhesion and the cell polarity, remodelling of the cytoskeleton and changes in the cell-matrix adhesion. This leads to the increased migratory and invasive properties of malignant cells (Mastronikolis et al., 2023).

1.16 - Exosomes and TC

As previously highlighted, there are many issues that need to be urgently addressed in the diagnosis, treatment and the prognostication of TC which have become even more pressing considering its rapidly increasing worldwide incidence (**Figure 1.14**). Liquid biopsy has the potential to provide a novel, progressive approach through the identification of circulating exosomes (**Figure 1.28**) (Romano et al., 2021).

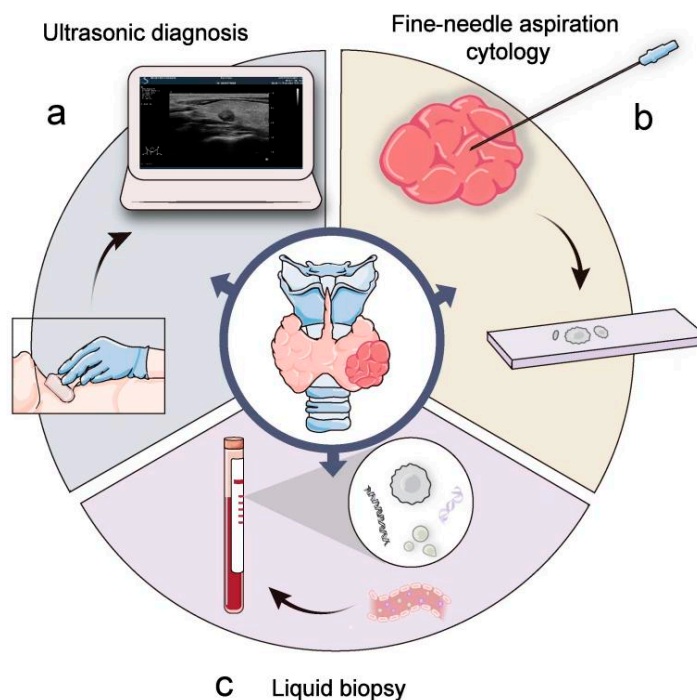


Figure 1.28 - Liquid biopsy acting alongside other thyroid cancer diagnostic techniques (Wang, 2023)

The first observation of thyroid EVs was in the thyroid gland of a bat during its awakening from hibernation. Nunez *et al.* with the use of electron microscopy in 1974 was able to observe small extracellular vesicles lying within the colloid, close to the apical plasma membrane of the cell (Nunez *et al.*, 1974). The accumulation of EVs was postulated to be part of the process enabling arousal from hibernation and the increased TPO production and extracellular iodination that would be necessary for thyroid hormone production.

As discussed, cancer cells secrete exosomes that are able to contribute to tumour progression, angiogenesis and metastasis and this is true within the thyroid also (see Section 1.10.5.2) (**Figure 1.29**) (Feng *et al.*, 2020). Exosomes produced by tumour cells create conditions which favour tumour progression, angiogenic switch induction, vascular permeability and the ability to escape the immune system (Wu, 2019). The number of exosomes is significantly higher in TC patients than compared to that of healthy subjects further suggesting that exosomes contribute to TC progression (Hardin, 2018).

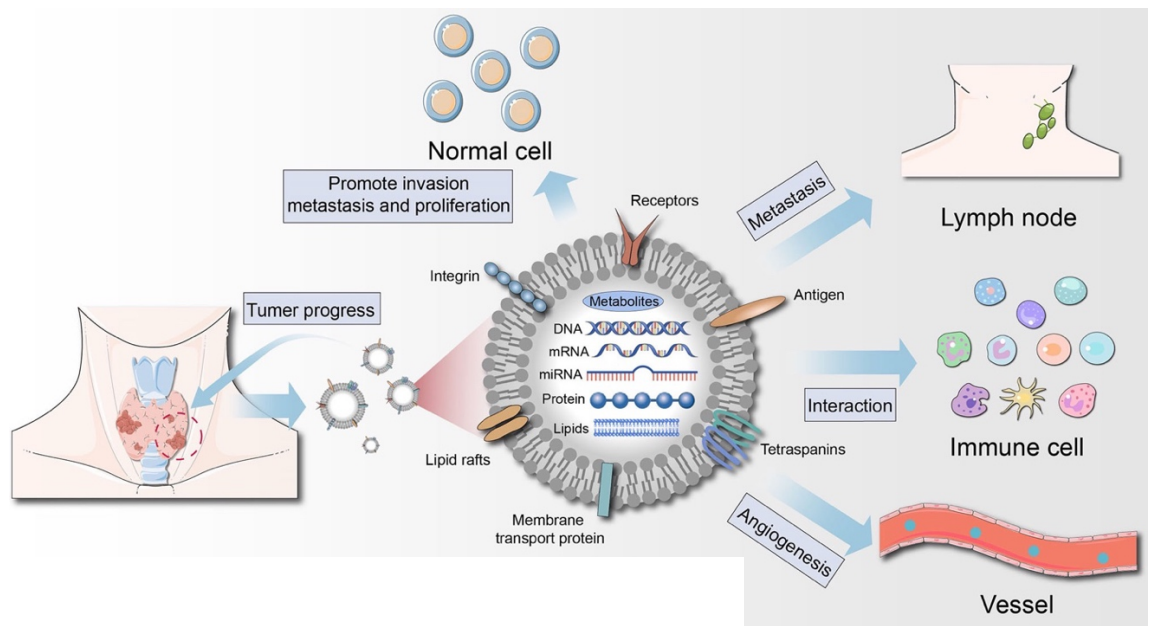


Figure 1.29 - The roles that thyroid cancer-derived exosomes play in cancer progression (Feng et al., 2020)

As tumour derived exosomes originate from the parent cell, they can provide a snapshot of the molecular makeup of the tumour cell, thus providing the potential to act as a non-invasive method of diagnosis and classification of TC. Currently diagnosis revolves around ultrasound scanning and fine needle aspiration cytology (**Section 1.9**). As described, the diagnosis and treatment of TC, especially PTC, is a contentious issue and within current practice it could be argued it results in unnecessary surgeries with associated morbidity (Jensen et al., 2020). The BTA Ultrasound Guidelines and RCP Thy Cytology guidelines can leave both patients and clinicians with both an element uncertainty and anxiety regarding the management of the thyroid especially on the receipt of a FNAC Thy3 result (Lakhani et al., 2011; Weller et al., 2020; Nair et al., 2021; Dimitriadis et al., 2023). The 2017 overall malignancy rate for Thy3 nodules presented in the 2017 National BAETS Audit report was 25.7%, from a sample of 6,373 cases (Chadwick et al., 2017). Nair and Dimitriadis at their respective centres report higher rates of malignancy compared to this national data which further highlights the potential inconsistency of inter-centre variability. The development of a more accurate pre-operative diagnosis in the form of liquid biopsy would add to both the diagnostic evidence and and certainty to both the clinician and patient (Rappa, 2019).

1.16.1 - Exosomes and PTC

PTC, the most prevalent TC, has a tendency in which to behave indolently but the presence of lymph node metastasis represents a poor prognostic sign (Zhan et al., 2022). Alongside there is a clinical need to identify the more aggressive PTC variants that have the propensity to metastasise which is limited through current diagnostic techniques. A number of studies have looked at miRNA contained within the exosome isolates of PTC. Lee and colleagues demonstrated that exosomes derived from a PTC cell line possessed increased levels of miR-146b and miR-222 compared to exosomes released from cell lines originating from benign thyroid. From their work they advocate that these exosomal miRNAs can act as biomarkers to aid in the detection of recurrent PTC (Lee et al., 2015).

Recently, Capriglione *et al.* compared exosomal miRNA expression in the plasma of patients with PTC and that of healthy controls and found downregulation of exosomal miR181a-5p, miR24-3p, miR382-5p, and miR146a-5p in the PTC group (Capriglione, 2022). Similarly, Wang *et al.* examined exosomes within the plasma of patients with PTC through an Exiqon PCR panels. They found that miR-34a-5p, miR-346 and miR-10a-5p were all elevated in the plasma of patients with PTC when compared to that of healthy individuals with nodular goitres (Wang et al., 2019). Their findings led to the proposition of a three-microRNA panel, which may help to distinguish PTC from standard nodular goitre. These findings do demonstrate that to establish a diagnostic tool a panel of miRNAs that are dysregulated may need to be identified rather than one sole microRNA which is either over or under expressed.

Within the context of disease progression surrounding PTC, it is important to consider lymph node metastasis (LNM) and to be able to identify those patient's that possess PTC that may then metastasise as this will have a direct effect upon patient management. Jiang *et al.* looked to identify the expression of plasma exosomal miRNAs in patients with PTC and LNM. In total, 49 patients ($n = 49$) with LNM were included and 15 patients ($n = 15$) that had no evidence of LNM. The exoRNeasy Serum/Plasma Maxi Kit was used to isolate the exosomes followed by reverse transcription quantitative PCR (RT-qPCR). Their findings demonstrated that miR-146b-5p and miR-222-3p enhanced both the

migration and invasive ability of the PTC cells and ultimately their ability to metastasise to lymph nodes (Jiang et al., 2020).

Looking at the underlying mechanistic action of the miRNAs within PTC and their effect upon carcinogenesis. Samsonov *et al.* explored the miRNA profile of exosomes within the plasma of patients ($n = 60$) with PTC and FTC. They found that the development of PTC is associated with specific changes within exosomal miRNA profiles (Samsonov et al. 2016). miRNA-31 was found to be overrepresented in the plasma exosomes of patients with PTC compared to that of patients with benign tumours. The identification of miRNA-21 helped in distinguishing benign tumours from that of FTC. This demonstrates that miRNA may have a role to play in differentiating individual histopathological subtypes of thyroid cancer. Feng *et al.* in their study, demonstrated that exosomal miRNA-21-5p released by hypoxic human PTC cell lines, BCPAP and KTC-1 enhanced angiogenesis in human umbilical vein endothelial cells (HUVEC) (Feng et al., 2020). The exosomal miRNA-21-5p was found to be elevated in the serum of PTC patients also, suggesting that this miRNA acts to stimulate angiogenesis and encourage PTC progression.

1.16.2 - Exosomes and GD

In AITD, antigen presenting cells (APCs) release exosomes with major histocompatibility complexes (MHC) on their surface which then migrate to secondary lymph nodes. This in turn can indirectly activate more antigen specific T cells resulting in the development of AITD (Shenoda & Ajit, 2016). Many small, scale studies suggest that exosomes from GD patients play a role in the promotion of the inflammatory response and the consequent pathogenesis and development of GD. Cui *et al.* looked at extracting serum exosomes from 26 healthy controls ($n = 26$), 26 GD patients ($n = 26$) and 7 with Graves' ophthalmopathy ($n = 7$). Western blotting (WB) was employed to determine exosomal total protein content, thyrotropin receptor, insulin-like growth factor 1 (IGF-1R), heat shock protein 60 (HSP60) and CD63 expression. It was found that IGF-1R and HSP60 expression was significantly higher in the GD exosomes and the Graves' ophthalmopathy exosomes compared with the healthy control serum. From this it has been postulated that GD exosomes may induce an inflammatory response through the TLR/NF- κ B signalling pathway (Cui et al., 2021).

An elevated level of EVs have been detected in the plasma of GD patients when compared to that of controls, using flow cytometry. The samples were obtained from 15 patients with GD ($n = 15$) in the acute phase of hyperthyroidism and then following a 17 to 26 month course of treatment. These were compared to that of 14 healthy controls ($n = 14$). The treatment of the GD patients with thiamazole significantly reduced ($p < 0.01$) the number of microvesicles (MVs) but not to the same level as seen in the healthy controls (Mobarrez et al., 2016). The authors wisely concluded that the MVs along with hormones could well be acting in which to propagate the disease and be contributing to immune disruption.

In GD, autoantibodies bind to the TSHR expressed on the surface of the thyroid follicular epithelial cells, stimulating the growth of the thyroid as well as the synthesis and release of T4 (**Figure 1.10**). Edo *et al.* (2019) found that anti-thyrotropin receptor antibodies were detectable in the exosomes secreted by normal benign thyroid follicular cell lines (NTHY-ori 3-1) and those from TC cell lines (8305C, 8505C, and FTC-133). As a result, Edo *et al.* isolated these TSHR expressing exosomes from cell lines and found that these TSHR expressing exosomes were able to sequester the autoantibodies and reduce the activation of thyroid function through the use of an *in vitro* binding assay. This hypothesis needs to be further trialled and replicated to fully elucidate the role of these TSHR expressing exosomes and identify if there is any therapeutic utility.

Although studies are investigating exosomal miRNAs in the pathogenesis of GD, the role in which these miRNAs play has yet to be fully elucidated. It has identified that miRNA levels in the plasma exosomes in patients with GD can be either upregulated or downregulated relative to healthy controls and that these are associated in turn with disease progression (Hiratsuka, 2016). Hiratsuka *et al.* looked at circulating exosomal miRNAs using the miScript miRNA PCR Array in serum obtained from seven intractable GD patients ($n = 7$), seven GD patients whom were in remission ($n = 7$), and seven healthy controls ($n = 7$). The team found that in the serum of GD patients in remission, the levels of miR-23b-5p and miR-92a-3p was significantly increased compared to the intractable GD patients. However, in the intractable GD patients the levels of miR-let-7g-3p and miR-339-5p were decreased when compared to GD patients in remission. The differences in exosomal microRNA are likely to be responsible, at least in part, for the pathogenesis and propagation of GD especially within the intractable cohort.

To date, there is a lack of studies highlighting the role of exosomal miRNAs in GD pathogenesis. Ongoing basic scientific clinical research is key for further clinical development and application of exosomes.

1.16.3 - Exosomes within HT

Exosomal surface protein markers including Hsp60 and Hsp70 are able to mediate immunomodulatory effects along with that of immune responses (Taha et al., 2019). Cui *et al.* (2019) compared the serum exosomes of healthy patients ($n = 30$) to those of HT patients ($n = 30$) and was able to demonstrate that the exosomes from patients with HT expressed higher levels of the inflammatory factor Hsp60 and that this was also strongly correlated with serum TPOAb and thyroglobulin antibodies. In addition, it has been shown that Hsp60 is structurally homologous with the structures of both TPO and Tg and as a result, Hsp60 may well be acting as an autoantibody within the immunological development of HT (Gammazza et al., 2014).

Identification of the structural homogeneity may deliver a potential therapeutic benefit to the disruption of the secretion of exosomes. This may in the future deliver a benefit in relation to the reduction of inflammation and the subsequent pathogenesis of AITD.

1.17 - The Development of Microfluidics and 'Tissue-On-Chip'

Technology

Microfluidics is the science and technology of systems that are able to process or manipulate small volumes of fluids, using channels with dimensions of tens to hundreds of micrometres (Niculescu et al., 2021). The development of microfluidics has been a multidisciplinary team effort in areas such as molecular analysis, biodefence, molecular biology and microelectronics (**Figure 1.30**) (Whitesides, 2006). In terms of analysis, the origins lay in the development of gas-phase chromatography, high pressure liquid chromatography and capillary electrophoresis. These methods have enabled the development of a plethora of devices with high sensitivities, despite only a small volume (<1 μL) of sample being required.

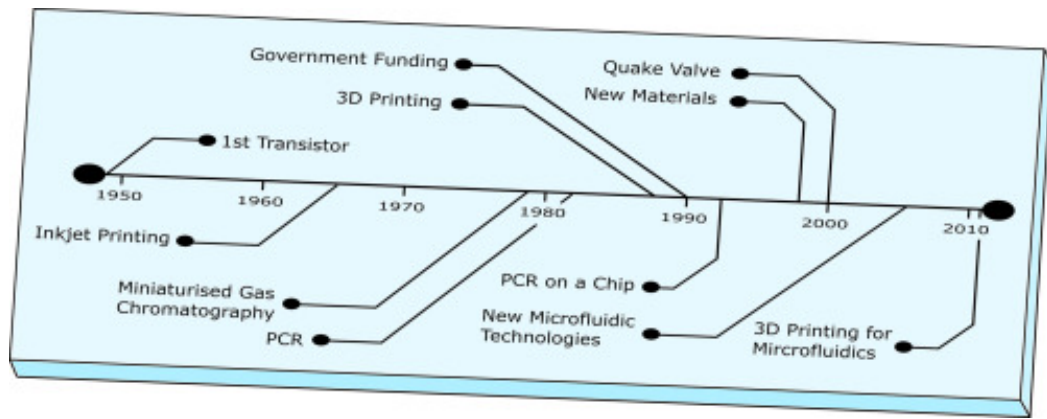


Figure 1.30 - Timeline demonstrating the development of microfluidic technology (Convery & Gadegaard, 2019)

The growth of the technology has continued through the further development of plastics suitable for the construction of microfluidic systems. The majority of the work has centred around polydimethylsiloxane (PDMS), an optically transparent, biologically inert, soft elastomer (McDonald et al., 2000). The advent of 3D printing has also catalysed the development of microfluidic devices (Su, 2023). 3D printing has made it possible to fabricate a microfluidic device from a computer-assisted design model, which has significantly reduced the time taken from design of the device to subsequent experimentation. The impact of 3D printing has been heralded as the ‘third industrial revolution’.

To date the most successful commercial application of microfluidic technology is the inkjet printhead. In 2020, the global inkjet market was valued at \$41.2 billion and it is estimated to hit \$67.7 billion by 2030 (Precedence Statistics, 2023). Microfluidics has many potential applications, but the current thesis focusses on using it for manufacturing tissue-on-chip devices which have the potential to aid with decision making in the clinical setting, leading to person centred treatment.

1.17.1 – Microfluidics Fluid Dynamics

Microfluidics exploits the small size of the microchannels to generate laminar flow. Within laminar flow, the fluid moves in parallel smooth layers (or laminae) as opposed to ‘turbulent flow’ in which the fluid is constantly being subject to mixing and irregular fluctuations in movement (**Figure 1.31**). Fluid flow within the body tends to be of laminar flow (Saqr et al., 2020).

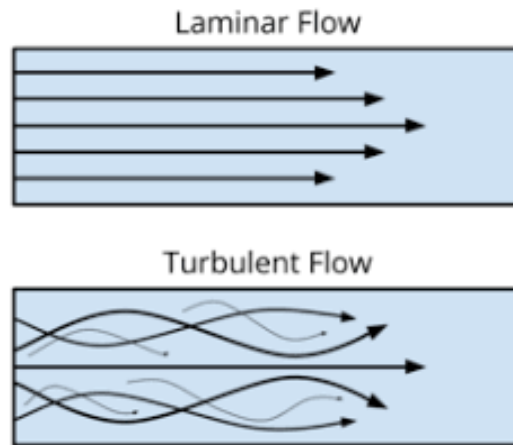


Figure 1.31 - A comparison of *laminar* and *turbulent* flow
 Taken from (@theconstructor2, 2021)

To generate laminar flow, a slow motion of a relatively viscous fluid is required to pass through a small flow channel. Within the profile of laminar flow, small concentric cylinders can be visualised towards the direction of flow. At the outermost aspect of the tube, the fluid velocity is zero and increases to a maximum level at the centre of the tube (Li, 1988).

1.17.1.1 – Reynolds Number

The Reynolds number, is based on several fluid characteristics and is a unitless indicator of whether fluid is either laminar or turbulent (**Figure 1.32**) (Falkovich, 2023). Values that are below 2000 are considered laminar flow, whilst values more than 2000 are considered turbulent. There is no cut off value as such that marks the transition from laminar to turbulent flow, it is a gradient.

$$\text{Reynolds Number (Re)} = \frac{\rho V D}{\mu}$$

ρ = density of fluid (kg/m³)

V = velocity of fluid (m/s)

D = pipe diameter (m)

μ = fluid viscosity (kg/ms)

Figure 1.32 - Reynolds Number Calculation: The Reynolds number is a mathematical quantity that links average flow, tube diameter, the fluid's mass density and its absolute viscosity (Reynolds, 1883; Uruba, 2019)

Within a microfluidic device, laminar flow with a low Reynolds number is desired as this allows for the easy manipulation of the fluid and smooth ordered flow and better mirrors the *in vivo* environment (Bureau et al., 2023).

1.17.2 - Different Types of Microfluidics

Passive microfluidic flow can be driven through the force of gravity, hydrostatic pressure, surface tension or osmotic pumps. These do not rely on external forces such as syringe drivers. These passive devices utilise surface tension, pressure driven gravity, osmosis, vacuum suctioning and the most frequently utilised, capillary forces (Xu et al., 2020). A relevant example are the lateral flow devices used for COVID-19 self-testing (Peto et al., 2021). As a result of capillary flow, the small liquid droplet travels along the surface of the application pad until it reaches an antibody and test control strips. Active microfluidics refers to the manipulation of the working fluid through active components such as pumps or valves. In this project, pressure driven flow is achieved through a syringe driver (**Figure 2.2c**) (Riley et al., 2019) (Foster et al., 2021).

1.18 - Microfluidics within Personalised Medicine

Microfluidics can play a role within personalised cancer treatment. Within the clinical setting, drug efficacy and tolerability can be highly variable within the target population and this is true across a spectrum of human disease processes. The aim of personalised medicine is to tailor treatments to each patient in order to achieve optimal clinical outcomes (Goetz & Schork, 2018). Through personalisation of the therapeutic approach delivered to each patient, which is currently usually quite standard for all patients, there is the potential to lower treatment toxicity and lead to an improvement in patient quality of life.

The response of a patient to a drug can be determined based upon the status of their personal biomarkers or the severity or extent of progression of their disease, which can be predicted based upon the presence of atypical cells (Califf, 2018). The development of microfluidic systems/tissue on-chip technology has the potential to aid in the delivery

of the most efficacious drugs to the patient, as well as optimising drug dosage which will lead to a reduction in side effects. The aim is that microfluidic models could offer a means through which to reduce the trial and error associated with treatment, which if not successful, can allow the cancer to progress, impairing further treatment and ultimately patient outcome.

This technology can act as a platform for disease and therapeutic treatment in that it has the potential to reduce reliance upon animal models which have limited transference to that of human clinical models (Ma et al., 2021) (Ingber, 2022). Microfluidic/tissue-on-chip technology enables microenvironmental factors, such as oxygen, growth factors, mechanical forces, along with spatial configurations to be tightly controlled when investigating tissue outside of the body, all of which have the ability to influence tumour progression (Ayuso et al., 2022). Microfluidic models can be coupled with detection and analysis platforms, miniaturising what were previously largescale laboratory tasks into a single chip device. If validated and mass-produced this would result in clinical benefit, and huge savings, in time and costs.

1.18.1 – Organ-on-Chip/Tissue-on-Chip Technology

Organ-on-Chip/Tissue-on-Chip systems are based on microfluidic technology and involve the continuous perfusion and removal of waste from a tissue sample, *ex vivo*, in a manner mimicking that of the natural circulatory system (Bower et al., 2017). The systems involve a combination of biomaterial technology, cell biology and engineering, creating a miniature platform (Singh et al., 2022). Organ-on-chip are micro-scale systems that replicate the human body for drug testing and disease monitoring with the ethical aim in which to replace animal models.

From a patient tissue sample, multiple pieces of the same initial tissue sample can be perfused on a number of parallel devices. This allows for the study of a number of variables through replicates of the 'same' type of tissue. Alongside this technology can enable further disease modelling, toxicity testing, comparisons of drug responses and further personalisation of drug selection (**Figure 1.33**).

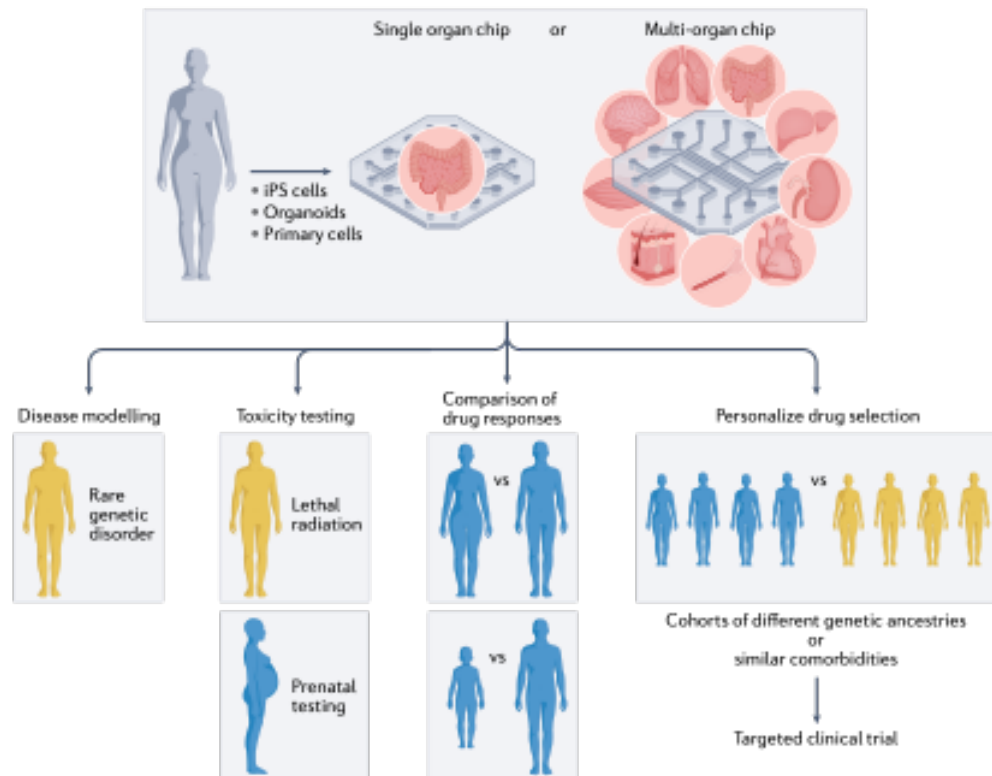


Figure 1.33 - The far-reaching applications of tissue-on-chip technology within disease research and management (Ingber, 2022)

Single organ-on-a chip systems are systems with only one organ or tissue modelled and allow the evaluation of the response of a specific organ to a compound. These can take on the form of either tissue biopsies or engineered tissues (**Table 1.2**). Multi-organ systems on the other hand examine the interaction of one organ with another, through the exchange of metabolites and signalling molecules (Leung et al., 2022).

Table 1.2 - Examples of the use of organ-on-chip technology in a number of different organ environments. Taken from (Singh et al., 2022)

Organ on a Chip	Applications/Model
Lung on a Chip (Engineered tissue)	Model a pulmonary oedema <i>in-vivo</i> environment for human airways, to study viral infection (Huh, 2015; Si, 2021)
Brain on a Chip (Vatine <i>et al.</i> - Engineered tissue) (Coquinco <i>et al.</i> - Biopsied tissue)	Blood Brain Barrier functioning (Vatine et al., 2019) Neural Network (Coquinco & Cynader, 2015)
Heart on a Chip (Engineered tissue)	Electrical stimulation, cardiac electrophysiology and different heart diseases (Ribas, 2016; Gaudriault, 2020; Kim, 2013)
Liver on a Chip (Engineered tissue)	Liver specific Protein Synthesis (Tostões et al., 2012)
Kidney on a Chip (Engineered tissue)	Drug induced nephrotoxicity (Wilmer et al., 2016), Glomerular filtration (Musah et al., 2017)
Skin on a Chip (Engineered and Biopsied tissue)	Dermal diffusion testing, toxicology studies, efficacy testing, wound healing, inflammation, repair, ageing and shear stress studies (Wufuer et al., 2016; Ponmozhi et al., 2021)
Gut on a Chip (Engineered tissue)	Drug pharmacokinetics, host-gut microbiota cross talk, and nutrition metabolism (Xiang et al., 2020)

1.18.2 - Head and Neck Cancer - Tissue-on-Chip Technology

Since 2010, the biomicrofluidics group at the University of Hull have been developing tissue-on-chip devices for the maintenance of *ex vivo* samples. The aim being in which to measure the response of human tissue to treatment and through that determine the optimal course of therapy for the patient. The tissue-on-chip devices in Hull are active microfluidic devices being maintained under a constant flow of medium with removal of waste by the action of a Harvard PhD 2000 pressure driven syringe pump. Through experimentation, the optimum flow rate for each device and for every tissue is a flow rate of between 2 and 6 $\mu\text{L}/\text{min}$.

Tissue-on-chip methodology has been used in order to try and address the question surrounding radio-resistance in head and neck squamous cell carcinoma (HNSCC). Carr, et al. (2014) and Cheah, et al (2017), both utilised bespoke microfluidics devices designed and manufactured in Hull in order to investigate this. Being able to evaluate a

tumour's response to irradiation *ex vivo* from a biopsy provides a potential avenue to guide individual treatment decision making. This study was able to demonstrate that the HNSCC samples from different patients demonstrated varying responses on being treated with a variety of irradiation doses which supports the theory surrounding patient's variability in response to irradiation.

Chemotherapy agents such as paclitaxel, cisplatin and 5-fluorouracil have also been perfused through microfluidic platforms. Hattersley *et al.* used a microfluidic tissue on chip device in which to perfuse squamous cell carcinoma biopsies which were exposed to cisplatin and 5-fluorouracil under continuous flow for seven days (Hattersley *et al.*, 2012). The results demonstrated a reduction in cell viability and proliferation on comparing the chemotherapy exposed group with that of the unexposed group.

The use of H&E by Hattersley *et al.* (2012) and Bower *et al.* (2017) confirmed the presence of morphologically intact tissue following maintenance on the microfluidic device used to maintain head and neck SCC tissue. This was then further verified by a consultant histopathologist who reported on the tissues whilst blinded to whether they had been maintained on the device and to the treatment applied.

1.18.3 – Thyroid - Tissue-on-Chip Technology

The perfusion device developed in Hull allows for the use of precision cut tissue slices (PCTS) which has been shown to maintain the 3D architecture and functionality of thyroid tissue over a 96-hour period (**Section 2.2**) (Riley *et al.*, 2019). The perfusion device was developed to act as a drug screening platform for RAI treatment, in order to help try and assess radioiodine refractivity which occurs in around 10% of patients suffering from thyroid cancer (**Figure 1.34**). The aim was to see whether these patients could be identified using *ex vivo* tissue-on-chip technology in a personalised manner.

The microfluidic technology developed in Hull is the only such technology in the literature which has maintained *ex vivo* thyroid tissue on a perfusion device. Foster *et al.* maintained *ex vivo* thyroid tissue from GD patients treated with and without dexamethasone or methimazole, with the aim of isolating and analysing EV miRNA released from the tissue (Foster *et al.*, 2021). They found variability in the levels of miRNA-146a and miRNA-155 between patients, however the administered treatments

had no effect on levels of miRNA-146a and miRNA-155. This preliminary study provided a platform to examine the miRNA profile of tissue-specific EVs released in to the microfluidic effluent of diseased thyroid tissue.

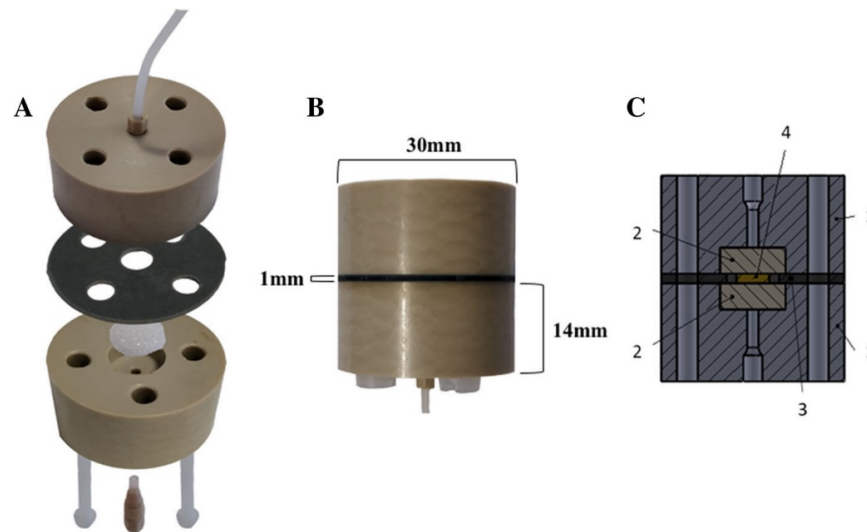


Figure 1.34 – PCTS Device developed at the University of Hull (Riley et al., 2019)

A major advantage of all the tissue-on-chip systems developed at the University of Hull, is that they allow both the continual measurement of secretions from the tissue maintained on the devices. Through the collection of the effluent flowing over the tissue, and tissue recovery following experimentation, both of these can then be investigated using laboratory analytical techniques. For example, haematoxylin and eosin (H&E) staining allows morphological analysis; immunohistochemistry has the ability to detect markers of interest previously shown to be affected by the intervention under examination, including apoptotic and proliferation markers; and finally, protein and RNA can be extracted from the tissue to measure changes at the molecular level (Riley et al., 2019; Foster et al., 2021; Haigh et al., 2023).

1.19 – Thesis Aims

It is clear, that exosomes play a role within TC and GD, however the exact mechanisms are yet to be elucidated. If a reliable, exosomal miRNA biomarker can be identified within the context of PTC this may ultimately provide clinicians with the confidence to place PTC ‘under surveillance’ rather than being managed surgically. It may also enable clinicians to predict which PTC may have a tendency to metastasise or which PTMCs behave aggressively. The long-term aim would be the development of a cost effective, accurate liquid biopsy. This ‘holy grail’ development would have the potential to circumvent current investigations and limit the surgical management of PTC and prevent ‘overtreatment’. The benefits would be far reaching, first and foremost to the patients but also clinicians. This is alongside the financial savings in a healthcare system with increasingly finite resources.

The aim of the study is to determine whether thyroid disease-specific sEVs could be isolated from different thyroid pathologies maintained on the perfusion device for a 6-day period and whether distinct sEV miRNA signatures exist between the three thyroid pathologies investigated; EMG, GD and PTC.

The plan is to take biopsies of EMG tissue ($n=10$), GD tissue ($n=10$), and PTC ($n=10$), divide each into a minimum of 6 pieces and incubate these under continuous perfusion on tissue-on-chip devices for 6 days. Following incubation, effluent will be collected, EV size and concentration will be analysed through nanoparticle tracking analysis (NTA) and sEVs will be isolated using differential ultracentrifugation steps. Following collection of the effluent, this will be analysed for exosomal content with guidance and input from the current MISEV guidelines (Théry et al., 2018).

The aims for the study are as follows:

- To study the basic histoarchitectural structure and assess the viability of thyroid tissue following maintenance on a ‘tissue-on-chip’ device for 144 hours with H&E staining
- To identify if the size of sEVs changes for different types of thyroid tissue, i.e. EMG, GD and PTC, maintained on a tissue-on-chip device over a six day period
- To identify if the three different types of thyroid tissue perfused on the ‘tissue-on-chip’ devices produce significantly different quantities of sEVs

- To identify classical exosomal markers (CD63 and CD81) through western blotting (WB) techniques in thyroid exosomal and tissue lysates
- To identify if different thyroid pathology types exhibit differential expression of CD markers on WB analysis
- To Identify differential miRNA expression through QIAGEN miRNA sequencing between the thyroid pathologies of EMG, GD and PTC
- To validate these results further using RT-qPCR for miRNA found to be significantly different through the miRNA sequencing using the GeneGlobe-integrated RNA-seq Analysis Portal

Chapter 2 – Materials and Methods

2.1. Obtaining Tissue for Tissue-on-Chip Devices

2.1.1 - Ethical Considerations

Ethical approval for the study was obtained from the National Research Ethics Service, North East Newcastle and North Tyneside (15/NE/0412) and from Hull University Teaching Hospitals NHS Trust Research and Development (R1925). In addition to the acquisition of a small piece of tissue from patients undergoing surgery for either GD, TC or a benign thyroid condition, an amendment was made to the ethics, during the research study, in order to obtain blood samples from the respective patients at the time of surgery. This was approved by the local research and ethics committee. It is essential to note that tissue was only obtained when there was sufficient sample for both pathology and the experimental research so as not to compromise patient care in anyway.

A copy of the respective consent form and the research participant information form, approved by the LREC and used to generate the written informed consent are included in Appendix 6.

2.1.2 - Patient Selection

Patients undergoing thyroid surgery at Castle Hill Hospital, Hull University Teaching Hospitals NHS Trust were approached and consented as appropriate on the day of surgery. The patients' notes were reviewed prior to the surgery following communication with the ENT theatre booking clerk. The Consultant's assessment of the patient with regards history and presentations, obtained during a presurgery clinic, were reviewed alongside the results from any blood tests (especially thyroid function tests, TFTs and thyroid receptor antibody, TRAb), thyroid USS and FNAC results to provide an indication of the thyroid pathology to be resected. A total of 29 patients were included in the study, 19 females and 10 males, with an age range of 19–83 years (**Table 2.1**).

Table 2.1 – Patient characteristics in study

Sample	Tissue Type	Tumour Stage	Age	Gender	Analysis techniques used
1 THTHY2	Hürthle Cell Carcinoma	pT2 NO	60	F	WB
2 THTHY3	GD	-	60	F	miRNA Seq, RT-qPCR
3 THTHY4	PTC	pT2 N1a	60	M	NTA, miRNA Seq, WB
4 THTHY5	PTC	pT3a N1b R1	83	M	NTA, miRNA Seq
5 THTHY6	Hürthle Cell Carcinoma	pT2 NO	74	M	NTA
6 THTHY7	GD	-	49	F	NTA, miRNA Seq
7 THTHY8	EMG	-	59	F	NTA, miRNA Seq, RT-qPCR
8 THTHY9	PTC	pT2 RO	50	F	NTA, miRNA Seq, RT-qPCR
9 THTHY10	EMG	-	51	F	NTA, miRNA Seq
10 THTHY11	Metastatic FTC	-	54	F	miRNA Seq
11 THTHU12	PTC	pT3b N1a R1	61	M	NTA
12 THTHY13	EMG	-	75	F	NTA, miRNA Seq
13 THTHY14	GD	-	42	M	NTA, WB
14 THTHY16	PTC	pT3b N1a R1	53	M	miRNA Seq, RT-qPCR
15 THTHY17	PTC	pT3a N1b R1	32	F	miRNA Seq, RT-qPCR
16 THTHY18	GD	-	40	M	miRNA Seq, RT-qPCR
17 THTHY20	GD	-	35	F	miRNA Seq, RT-qPCR
18 THTHY21	EMG	-	55	F	miRNA Seq
19 THTHY22	GD	-	70	F	miRNA Seq

20 THTHY23	EMG	-	42	F	RT-qPCR
21 THTHY24	EMG	-	68	F	miRNA Seq, RT-qPCR
22 THTHY25	EMG	-	48	M	RT-qPCR
23 THTHY27	EMG	-	50	F	RT-qPCR
24 THTHY29	GD	-	51	F	RT-qPCR
25 THTHY32	PTC	pT3 N1a R2	20	F	RT-qPCR
26 THTHY33	GD	-	57	M	RT-qPCR
27 THTHY34	PTC	pT3 N1b	27	M	RT-qPCR
28 THTHY35	PTC	pT3b N1b R2	19	F	RT-qPCR
29 THTHY36	GD		51	F	RT-qPCR

Tissue type: GD – Graves’ disease; PTC – Papillary thyroid cancer; EMG – euthyroid multinodular goitre; FTC – Follicular thyroid cancer

Gender: M – Male; F – Female

Analysis techniques used: NTA – Nanoparticle tracking analysis; WB – western blotting; miRNAseq – microRNA sequencing; RT-qPCR – reverse transcription-quantitative polymerase chain reaction

Written, informed, consent was obtained from all eligible patients for the study. The original copy of the research consent form was placed in the patients’ notes and a photocopy was kept in a secure folder following the assigning of a unique identifier number, by which the laboratory specimen would be known as from that point onwards (pseudo anonymisation). A log and storage location of all the samples obtained were recorded in the Head and Neck Tissue Log located on a secure location on the University of Hull - One drive.

Final histopathology following surgical resection confirmed the pathology of the tissue samples obtained.

2.1.3 - Tissue Sampling

The tissue sample was removed at the time of surgery from the thyroid gland. The thyroid sample was then placed within Dulbecco’s modified Eagles’ medium (DMEM; GE

Health-care, Yeovil, Somerset, UK) containing 10% (v/v) foetal bovine serum (FBS; Thermofisher, Loughborough, UK), penicillin/streptomycin (0.1 U/ml and 0.1 mg/ml respectively, GE healthcare), 0.4 mM glutamine (GE Health-care) and 2.5 µg/ml Amphotericin B (Life Technologies, Paisley, UK) and immediately transferred over to the laboratory. The biopsy sample was immediately prepared for loading on to the microfluidic devices, with the aim to have the biopsies loaded on to the microfluidic devices within 1 hour of resection (**Section 2.2.1**).

2.1.4 - Blood Sampling

Blood was obtained with a view to screen for the presence of specific miRNA identified in the exosomes released from the tissue. The blood was obtained on the insertion of a cannula into a patient prior to anaesthetic induction, thus minimising any need for a further venepuncture attempt and any subsequent discomfort for the consenting patient. The blood was collected in a gold topped vacutainer containing a silica clot activator (Beckton Dickinson, Vacutainer Bottles, Plymouth, UK). The blood was collected from the operating theatre prior to anaesthetic induction and removal of thyroid tissue.

Upon receipt of the blood sample in the Daisy Laboratory, the collection tube was centrifuged at 3000 x *g* for 5 minutes at 4°C (Beckman Coulter Ltd, High Wycombe, UK), to separate the serum. The serum was then aliquoted in 210µl volumes into 1.5ml microcentrifuge tubes (Sarstedt, Leicester, UK) and stored in the -80°C freezer for preservation.

2.2 - Fabrication of the microfluidic culture device – Precision Cut Tissue Slices (PCTS) device

Two polyether ether ketone plastic plates (PEEK; Direct Plastics, Sheffield, UK), both 30 mm × 14 mm in size (**Figure 2.1**), were milled centrally to produce threaded axial holes to which inlet and outlet ethylene tetrafluoroethylene tubing (ETFE; 0.8mm internal diameter; Kinesis, IDEX Health & Science, Cambridge, UK) was attached via coned adapters (LabSmith, Mengel Engineering, Denmark). In addition, four 1/4 inch (6.35 mm) holes were made in both PEEK plates to allow the insertion of metal screws (RS components, Leeds, UK), in order to secure the unit following sample addition. A central cylindrical recess (10 mm × 4 mm) was drilled in each PEEK plate to house a porous

sintered Pyrex disc (The Lab Warehouse, Grays, UK). Finally, a silicone gasket (30 mm diameter, 1 mm thickness sheet silicone) with a 6 mm central hole to create a tissue well, was placed between the two PEEK plates.

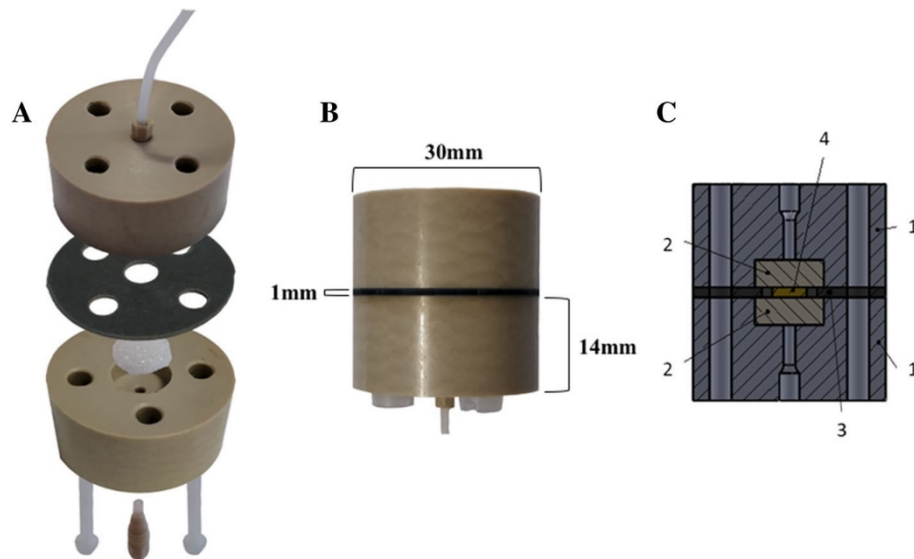


Figure 2.1 - PCTS Culture Device (Riley et al., 2019)

- A. Photograph that demonstrates the assembly of the device showing the two PEEK plastic plates, which sandwich together housing a silicone gasket to create a tissue well between two sintered Pyrex discs. ETFE tubing was connected via coned adapters.
- B. Photograph of an assembled PCTS culture device with the external dimensions
- C. A schematic diagram of the PCTS culture device. The respective component parts are labelled numerically. 1 – PEEK plastic plates, 2 – glass sintered Pyrex disk, 3 – central silicone gasket, 4 – tumour tissue sample

2.2.1 – Tissue Processing and Preparation

Following transport of the tissue from the operating theatre to the laboratory class II tissue culture cabinet, the tissue was transferred into a Petri dish whilst still being bathed within DMEM. Where possible the tissue was divided into three separate pieces using scalpels; one was transferred to 4% paraformaldehyde (PFA; Sigma/Merck, Dorset, UK) for tissue fixation for 24h before processing (**Section 2.4**). One of the samples was placed in a 2ml CryoPure tube (Sarstedt, Nümbrecht, Germany) and cryofrozen through the use of liquid nitrogen. The cryofrozen sample was then subsequently stored in the -80°C freezer whilst the final one was processed for loading on to the tissue-on-chip devices. This piece of tissue was immobilised onto the vibratome tissue holder using superglue and sliced at a thickness of 350 µm in ice-cold phosphate buffered saline (PBS) using a vibratome (Leica VT1200S, Milton Keynes, UK) with a blade speed of 0.1 mm/s

and amplitude of 2.5mm. A skin biopsy punch (Stiefel, Middlesex, UK) was used to generate PCTS of 5 mm in diameter from the resulting 350 μ m slice. Each PCTS was weighed individually prior to insertion into their respective tissue-on-chip device.

Prior to each experiment the PCTS device and tubing were washed out with 70% ethanol in order to clean and sterilise the device and also to check flow through the device. Once constructed, with screws *in situ*, the device was checked to see that it was fully patent and that DMEM was able to flow freely through each device.

2.3 – PCTS Device Set Up

‘Complete medium’ consisting of DMEM containing 10% (v/v) exosome depleted foetal bovine serum (FBS; Thermofisher), penicillin/streptomycin, glutamine and Amphotericin B (as described in **Section 2.1.3**), was loaded into a 20 ml syringe (Becton Dickinson, Wokingham, UK) and connected to the 2-part adapter and ETFE tubing via a 0.22 μ m filter (Millipore, Watford, UK) (**Figure 2.2. (A)**).

Each of the 5mm punch biopsy specimens were labelled numerically within each dish following weighing. The PCTS was loaded onto a 70 μ m nylon porous membrane (FALCON, Corning Brand, Durham, USA) positioned on top of the sintered disc in the inlet PEEK plate, and the outlet PEEK plate, containing a second sintered disk was then secured in place using metal screws (RS components, Leeds, UK) (**Figure 2.2. (B)**). The syringe containing complete medium was connected to a Harvard PhD 2000 syringe pump (Harvard, Cambridge, UK), which provided a pressure driven perfusion rate of 2 μ l/min (**Figure 2.2 (C.)**).

The culture device was maintained at 37°C inside an incubator (Covatutto 24 Eco, Novital, Lonate Pozzolo, Italy) for 6 days in total (144 hours). Media coming off each chip was collected in 15 ml polypropylene tubes (Sarstedt, Nümbrecht, Germany) on a daily basis from day 1 to day 6 of each respective experiment (**Figure 2.2 (C.)**). DMEM remaining in the input syringe at day 6 was kept as a control for the baseline of bovine EVs. Collected medium was stored at -80°C until required for further processing.

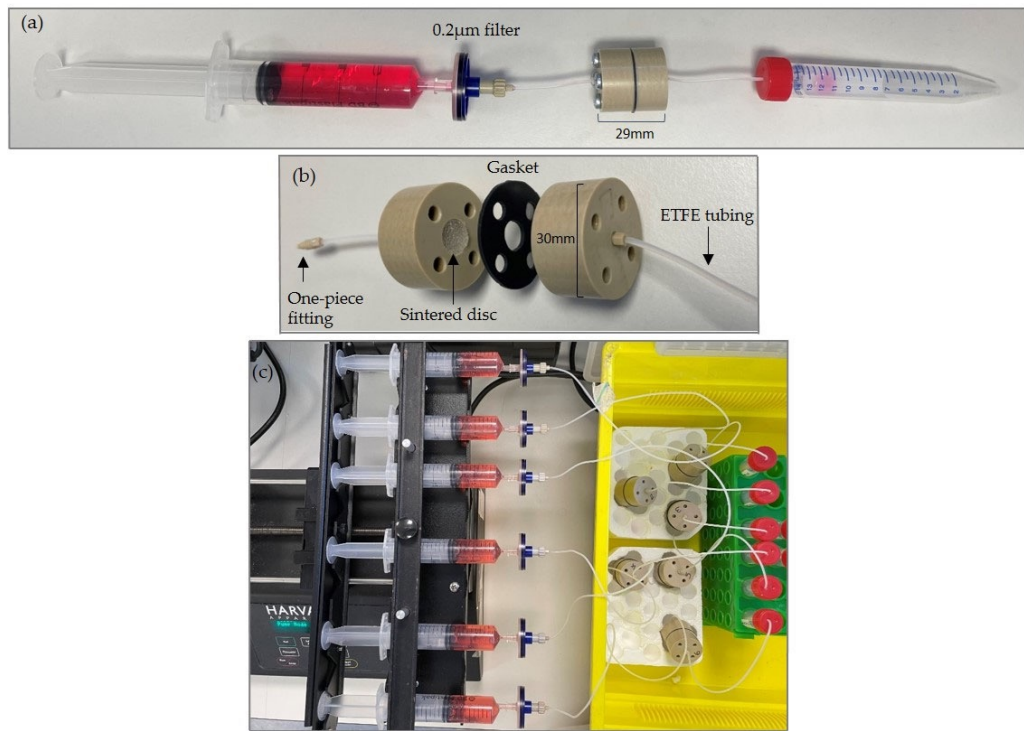


Figure 2.2 - Set-up of the PCTS perfusion device constructed from PEEK plastic
A. Complete syringe > PCTS device > collection tube set-up
B. Deconstructed PCTS device
C. Perfused devices connected to the syringe pump and 37°C incubator

2.3.1 - PCTS Device and Flow Calculations

The numerical values of Reynolds number and velocity (**Figure 2.3**) are provided for 3 points 0.25 mm away from the tumour slice boundary (Kennedy et al, 2019). The Reynolds numbers obtained are values characteristic of laminar flow at the K_1 and K_2 permeability conditions. Computer simulation of the fluid flow within the tissue-on-a-chip platform was performed. Firstly, permeability of the sintered disc does not affect flow velocity field, with minimal changes observed in velocity values. Further, due to the axisymmetric configuration, the chip provides a uniform and controlled flow and the fact that the flow in the chip is directed along the axis of the sample prevents tissue deformation.

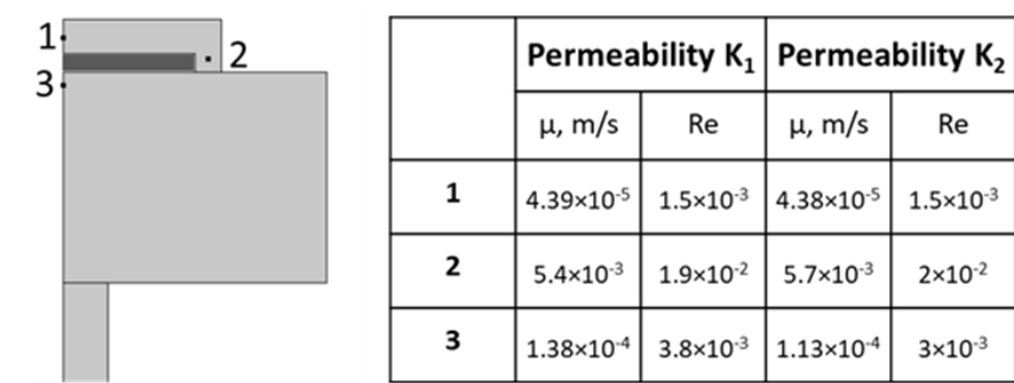


Figure 2.3 – The points studied for the calculation of the Reynolds number and the velocity of fluid are indicated numerically as three separate sites (1, 2 and 3). K_1 permeability ($1 \times 10^{-11} \text{ m}^2$) and K_2 permeability ($1 \times 10^{-9} \text{ m}^2$) are for the velocity fields surrounding the central tissue well.

2.4 - Histo-Architectural Analysis

Following the 6 day experiment, the PCTS devices were disassembled and the post-culture tissue samples were fixed in 4% (w/v) PFA for a period of 24 hours. Both pre-experiment (**Section 2.2.1**) and post culture PFA fixed tissues were transferred to embedding cassettes and dehydrated through an ethanol gradient (70%, 90%, 95%, 100%) for 30 minutes each followed by a further 50 minutes in 100% ethanol and 2 changes of xylene for 30 and 45 minutes. Finally, the samples were impregnated with molten paraffin wax (Epredia Histoplast Paraffin PE, Fisher Scientific, Loughborough, UK), by incubating in two different wax baths for 1 hour each at 55°C. The samples were then placed in an embedding mould, covered in molten wax and allowed to set with the cassette base in place, for 1h on a cold plate. The PFA fixed, paraffin embedded (FFPE) tissues were sectioned using a Leica RM2135 microtome at 5 μm thickness (Leica, Milton Keynes, UK) and mounted on StarFrost Slides (Waldemar Knittel, Braunschweig, Germany), previously treated with VECTABOND® (Vector Laboratories, California, USA) reagent to increase tissue adherence (VectorLabs, 2024).

In order to visualise cell architecture within the thyroid tissue, FFPE sections were stained with haematoxylin and eosin (H&E). Haematoxylin is employed to demonstrate nuclear structures whilst Eosin is used to show cytoplasmic and positively charged structures such as mitochondria (Fischer et al., 2008). H&E staining was performed as per established protocol (Bower et al., 2017). Briefly, the slides were dewaxed in warm

Histoclear for a total of 5 minutes and subsequently rehydrated through graded ethanols (100%, 90% and 70%) for 5 minutes each. The slides were placed in running tap water for a total of 1 minute, before submerging in Harris Haematoxylin for 5 minutes. The slides were then rinsed in running tap water for 10 seconds before staining with 1% filtered Eosin in water for 5 minutes. The slides were initially rinsed with 100% ethanol through the use of a squirty bottle before transferring through three changes of 100% ethanol, ten dips in each. The sections were then cleared through two changes of Histoclear (Fisher Scientific, Loughborough, Leicestershire, UK) for 2 minutes each. The slides were then mounted with 22 X 50 mm cover slips (Scientific Laboratory Supplies, Nottingham, UK) using Pertex mounting medium (Cell Path, Newtown, UK).

Tissue morphology, both pre and post experiment was examined by Dr Lazlo Karsai, Consultant Head and Neck Pathologist, Hull University Teaching Hospitals NHS Trust.

2.5 – Determination of size and concentration of particles using Nanoparticle Tracking Analysis (NTA)

Malvern Panalytical (Malvern, UK) have developed the technique of Nanoparticle Tracking Analysis (NTA) sized between approximately 20 nanometers (nm) to 1000 nm in diameter (**Section 2.5.1**). Using this method, a series of instruments have been developed to count and determine the size of nanoparticles held in liquid suspension.

2.5.1 - LM10 – Nanosight NTA System

For the purpose of the current study, an LM10 Nanosight NTA System (Malvern Panalytical, Malvern, UK) based at the Daisy Laboratory, Castle Hill Hospital, was used.

The LM10 Nanosight instrument (Malvern Panalytical, Malvern, UK) (**Figure 2.4**), is based upon a conventional optical microscope fitted with a scientific camera. The technology uses a laser light source (65 mW), with a wavelength of 405 nm (blue), to illuminate the particles in the sample and the scattered light is captured by the camera attached to the microscope and displayed on the connected personal computer which is running the NTA software (NTA v.3.4).

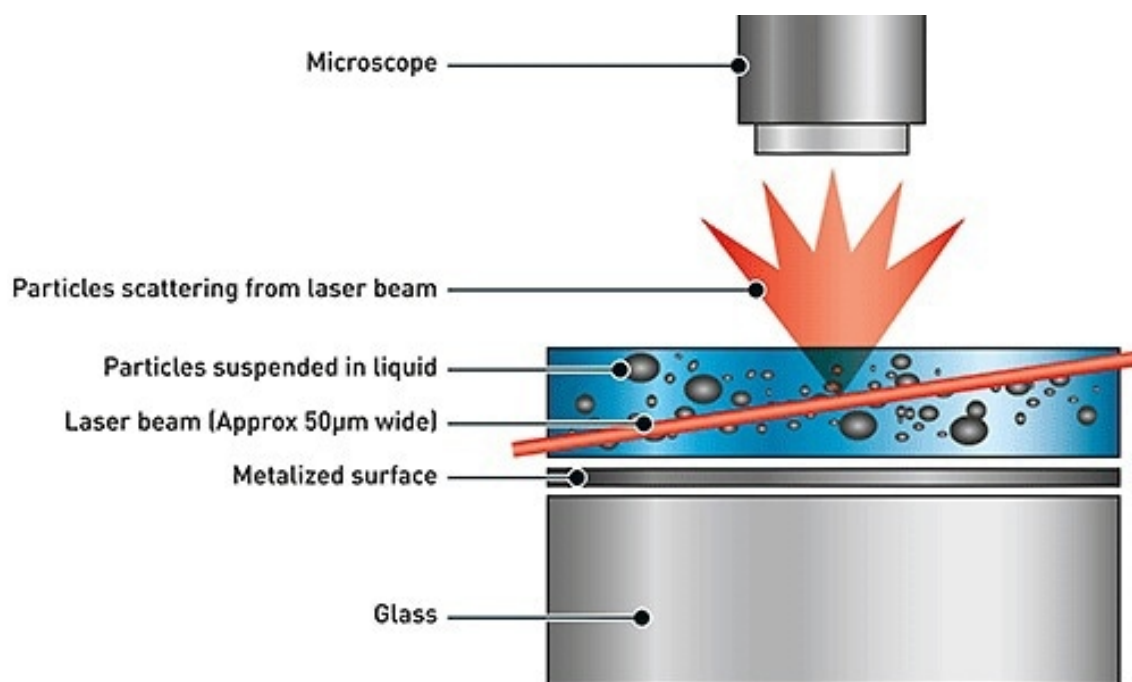


Figure 2.4 - Demonstrating the LM10 Nanosight and the interaction of the nanoparticles held in liquid suspension with the laser beams (Panalytical, 2015)

The NTA uses the principles of Brownian motion to determine the size of the particles present, simultaneously enabling the determination of particle concentration. Results are displayed as a frequency size distribution graph and are exported in various, user-selected formats including spreadsheets and video files. The LM10 is proven with most nanoparticle classes down to 20nm (dependent upon particle density) dispersed in a wide range of solvents (Griffiths et al., 2020).

2.5.2 - Nanosight LM10 Preparation

The Nanosight laser module was removed from the storage bag and the window was cleaned with white soft lint free tissue (Kimtech Science, Reigate, UK) and 10% ethanol. Butane duster (RS components, Corby, UK) was then sprayed into the ports in order to remove any moisture and residual fluid. The lid was screwed on finger tight with the screws provided. This was done in a diagonal formation in order to obtain an even pressure distribution. The laser cable was plugged into the support and the tissue-on-chip effluent, in a 1 ml plastic syringe (Becton Dickinson, Wokingham, UK), was connected to the lower port of the Nanosight device and used to fill the sample chamber until the sample emerged from the upper port. The housing was placed on the

microscope stage and the lint free tissue was placed appropriately underneath the module to capture any drips and to minimise spillage.

2.5.3 - Computer Screen and NTA 3.4 Software

In the NTA 3.4 software, the standard measurement tab was selected and under the standard operating procedure, the number of captures was set to 3 and the time of capture to 60 seconds. The name of the script was saved appropriately with its' respective name. The laser was switched on and the camera started. The stage was aligned appropriately with the laser, making sure the laser line was visible in the centre of the field of view, with the 'thumbprint' slightly to the right of this, using the microscope eye pieces. At this point the image was reverted back to the computer screen, by sliding the arm out on the microscope. The laser line was now apparent on the computer screen, at which point it was moved to the left of the screen just out of view. The nanoparticles were brought in to focus and the run was started. The runs track particles with light scattering properties during the 3 x 60 second runs, with advancement of the sample after each 60 second run. Once the three runs were complete, the particle detection/image processing was adjusted to detect the true particles (red cross in centre of each) and the analysis completed and exported, from which a pdf of the results was saved. The pdf provides histograms of each run to show the size distribution as well as dot plots to show the size and intensity. The mean size (nm) is also provided as well as concentration in both particles/ml and particles/frame. The Nanosight was flushed through with 10% ethanol between each sample and with 70% ethanol at the end, in order for it to be cleaned and left for storage. The housing was placed back in the bag, being careful to cover the crystal module with the tissue provided.

In addition to the tissue-on-chip effluent, the DMEM from the input syringe at day 6 was also analysed on the Nanosight, in order to obtain a baseline particle count from the exosome-depleted FBS. Dilution of the tissue-on-chip effluent was performed initially with the filtered PBS and then subsequently following optimisation with the DMEM medium (**Section 3.7.2**). The diluent was checked on the Nanosight in order to ensure a particles/frame reading of between 30-80 for the dilution.

2.6 - NTA - Materials and Methods

An aliquot of effluent (exosome depleted DMEM), which had run through the tissue-on-chip perfusion device containing thyroid tissue, was collected on a daily basis from each individual device from day 1 to day 6. In addition, an aliquot of the input DMEM from the 20ml syringe at day 6 was taken for analysis. All effluent samples from thirteen patients (**Appendix 4; Table 4.2**), from each device, at each daily timepoint were run through the Nanosight LM10 to measure the particle mean size (nm), particles/ml and particles/frame. The NTA software provided both a mean and a standard deviation for each of the samples following the three separate runs for each of the measured parameters.

The particles/ml and particle/frame readings for each individual device, at each timepoint had the corresponding reading from the day 6 syringe input subtracted from them. This was done with the intention of removing any background particle measurements that may have entered the effluent, as a result of the exosome depleted DMEM being held within the syringe for 6 days. These values were calculated as follows:

$$\text{Particles/ml for each device} = (\text{Particles/ml in device effluent}) \text{ minus } (\text{Particles/ml in day six syringe input})$$

For each sample loaded onto the PEEK perfusion devices during preparation, the mass of each sample loaded onto the device was noted down in milligrams (mg). This allowed for the normalisation of the concentration of particles/mg of starting material (particles/ml/mg) thus providing a direct comparison between samples, similar to that performed by Foster et al, (2021).

Statistical Analysis

Basic analysis was performed on Microsoft Excel. Further analysis and statistical tests including two-way Analysis of Variance [ANOVA] with Bonferroni post-hoc correction, were carried out using GraphPad PRISM 9 to determine differences overtime in particle mean size and particles/ml/mg.

2.7 - Isolation of total EV content from tissue-on-chip effluent using differential ultracentrifugation

EVs were isolated from the effluent coming from the tissue-on-chip device using sequential centrifugation steps (Théry et al., 2006).

2.7.1 - Bench top centrifugation steps

Initially, the combined tissue-on-chip effluent from day 2 to day 6 was combined from all devices, filtered through a 0.2µm filter and centrifuged at 400 x *g* for 10 minutes at 4°C in a 50 ml tube (Sarstedt, Nümbrecht, Germany) in order to remove floating cells (Eppendorf 5810R, Stevenage, UK). This created the supernatant – S1. Day 1 was excluded due to concerns that the day 1 effluent contained cellular debris from the tissue preparation process.

The S1 supernatant was then transferred over into a new 50 ml tube and centrifuged at 2000 x *g* for 10 minutes at 4°C to generate supernatant S2. This supernatant was aliquoted into 1.5 ml microcentrifuge tubes and centrifuged at 10,000 x *g* at 4°C for 30 minutes to generate supernatant S3.

2.7.2 - Ultracentrifugation

S3 supernatants, generated above, were transferred into 4.7 ml OptiSeal centrifuge tubes (Beckman Coulter, High Wycombe, UK). Each tube was capped and an OptiSeal Tube spacer (Beckman Coulter, Brea, USA) was added to each tube to support the neck. All tubes were weighed on a 4-digit analytical balance to within 0.01 g of the opposing tube, in order to balance the ultracentrifuge. Tubes were placed in a pre-cooled TLA-110 fixed angle rotor before centrifuging at 100,000 x *g* at 4°C for 1 hour (Beckman Optima MAX-XP).

Following the first ultracentrifugation the supernatant was discarded and the tubes inverted in the OptiSeal tube rack for 10 minutes to remove all the supernatant. The pellet was washed by filling each tube with PBS that had been filtered through 20 nm filters (ThermoFisher Scientific, Loughborough, UK) before being ultracentrifuged again at 100,000 x *g* at 4°C for 1 hour. The resulting supernatant was discarded and the tube

remained inverted in the Optiseal tube rack to dry the pellet before storage at -80°C, prior to downstream applications including RNA and protein extraction.

2.8 - Western Blotting (WB) Analysis of Exosomal Content

What follows is an established protocol to identify the expression of the tetraspanin markers on the EVs isolated from the tissue-on-chip effluent using the ThermoFisher Bolt System (ThermoFisher Scientific, Loughborough, UK) (Kowal et al., 2017).

2.8.1 - Protein Extraction

Protein was extracted from ultracentrifuged pellets (**Section 2.7.2**) using 100 µl of Radioimmunoprecipitation assay buffer containing PhosSTOP – phosphatase inhibitor cocktail (PhosSTOP™) and protease inhibitor cocktail complete ULTRA (Sigma/Merck, Gillingham, UK). Pellets from replicate tubes (from day 2 onwards) were lysed in the 100 µL of RIPA buffer to concentrate the protein. The lysates were incubated for 15 minutes on ice before vortexing and sonication for 3 minutes to fully disrupt the EVs and release protein content. Centrifugation at 4°C for 15 minutes at 16,000 x *g* pelleted exosomal debris and the supernatant was analysed for protein content using the Pierce™ BCA protein assay kit (ThermoFisher Scientific). Tissue lysates were prepared via the same method, following the mincing of the tissue with scalpels, but using 300 µL of RIPA buffer and a tube pestle in which to encourage cell lysis.

A non-reducing sodium dodecyl sulphate (SDS), polyacrylamide gel electrophoresis method was used, utilising the Bolt™ System (ThermoFisher) to detect the classic exosomal markers CD9, CD63 and CD81 (**Table 3.2**).

2.8.1.1 - Pierce BCA protein quantification assay

Protein concentration within cell and tissue lysates was quantified using the Pierce BCA protein assay kit (ThermoFisher Scientific, Waltham, USA) according to the manufacturer's instructions. Standards were prepared using a 2000 µg ml⁻¹ Bovine Serum Albumin (BSA) stock ampule provided in the kit; briefly, stock was diluted in ddH₂O to yield 9 standards (0, 25, 125, 250, 500, 750, 1000, 1500 and 2000 µg/ml). Standard or unknown sample (25 µl) were added in duplicate to a 96 well microplate before 200 µl of mixed working reagent (50-parts reagent A: 1-part reagent B) was added. The plate was agitated on a plate shaker (30 seconds) before incubation at 37 °C

for 30 minutes. After cooling the plate to room temperature absorbance was measured at 570 nm on a plate reader Thermo Scientific Multiskan FC. The average absorbance of the blank standard (0 µg/ml BSA) was subtracted from the average measurement of all other standards and unknown samples. A standard curve was plotted of protein concentration (µg/ml) vs. absorbance (570 nm) (Example given in **Figure 2.5**) allowing the protein concentration of each unknown to be determined (within the linear range of the assay only).

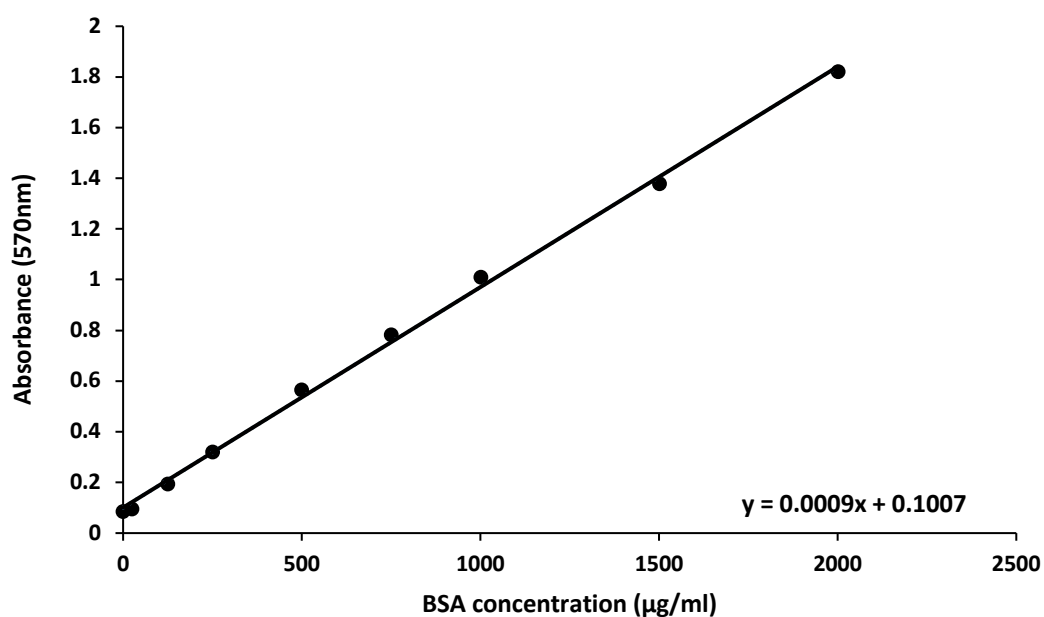


Figure 2.5 - Representative linear standard curve produced using Pierce BCA assay kit. Graph shows absorbance values (570 nm) of standards with known concentration of BSA from 0 – 2000 µg/ml

2.8.2 - Electrophoresis

The amount of lysate required for 5 µg of protein was calculated and transferred to a microfuge tube, where possible and an equal volume of 2 x bolt sample buffer was added. For those samples with low protein concentrations, the maximum volume of 30 µl was used and 10 µl of 4 x sample buffer was added. The lysate/sample buffer mix was heated at 70°C for 10 minutes.

2.8.3 - Preparation of Western Blot Reagents

The bolt system gel running tank was used. The gel holding cassette was clamped into the chambers with the anode connectors aligned to the centre. Both chambers were

filled to the level of the cathode with 1 x 2-(N-morpholino)ethanesulfonic acid (MES) running buffer (**Appendix 2**). The comb and the tape were removed from the precast 4-12% Bis/Tris gels (Thermofisher) (NW04120BOX) and the gel was placed and clamped into the chamber with the wells facing forwards. MES buffer (1x) was used to fill the chambers up to the fill line. Each well was washed out several times with the 1 x MES buffer.

The prepared samples (**Section 2.8.1**) and the respective markers (See Blue 6 µl and Magic Mark 3 µl; Thermofisher) were loaded into appropriate wells, before the lid was placed onto the tank and the electrode cords plugged into the power supply. The gel was run for approximately 40 minutes at 150 V until the dye front was approaching the end of the gel. The gel was removed from the cassette using the opening tool to unsnap the plastic surround and the gel was transferred onto polyvinylidene fluoride (PVDF) membrane.

2.8.4 - Western Transfer using the semi-dry Trans-Blot® Turbo™ transfer system

Following electrophoresis, the Trans-Blot® Turbo™ transfer system (Biorad, Watford, UK) was used to transfer proteins from the gel onto the PVDF membrane to immobilise them prior to antibody labelling according to the manufacturer's instructions. Each Trans-Blot® pack consisted of a base layer and a top layer. Both base and top layers contain a stack of filter papers soaked in buffer, with the base layer having the addition of a layer of PVDF membrane. The base layer was lifted out using a pair of flat tipped forceps and placed into the Trans-Blot® drawer. Following the removal of excess gel, the main portion of the gel was transferred carefully onto the PVDF membrane. Care was taken at this point not to move the gel around once it has been placed. The top portion of the Trans-Blot® transfer pack was placed on top of the gel to form a sandwich and any bubbles were removed via the use of a plastic roller. The lid of the Trans-Blot® drawer was clamped firmly into position and placed into the Trans-Blot® Turbo™ machine. Transfer was achieved using the standard settings of 25 V for 30 minutes.

2.8.5 - Membrane Preparation and Blocking

Once protein transfer had taken place, the membrane was removed from the sandwich and placed in a plastic staining tray and non-specific binding sites were blocked for 1

hour with 5% (w/v) milk powder in 0.1% PBS-Tween-20 (**Appendix 2**) at 4°C with end-to-end rocking.

Following blocking, the milk powder was removed and replaced with the appropriate primary antibody, diluted at an appropriate concentration in 5% (w/v) milk powder in PBS-Tween-20. A minimum of 3ml of antibody was used to cover the membrane and incubated overnight at 4°C with gentle rocking from end to end.

The membrane was then washed using 0.1% PBS-Tween-20. Initially two quick rinses with the PBS-T were used to remove any excess antibody, followed by 3 washes of 10 minutes duration with constant end to end rocking.

To detect the mouse primary antibody a 1:5000 dilution of mouse IgG κ binding protein conjugated to horse radish peroxidase (HRP) (Santa Cruz, insight Biotechnology, Wembley, UK) in 5% (w/v) milk powder was incubated with the membrane for 1 hour at room temperature with gentle rocking. Note; in order for this binding protein to work the initial primary antibody needed to be a murine IgG κ isotype. Following a further 3 washes as previously described, the membrane was removed from the PBS-T and drained by placing the edge onto absorbent paper and placed onto a clean piece of transparent projector film.

Super Signal West Stable (SSWS) peroxide solution (Thermofisher; prepared by adding 1 ml of Regent A to 1 ml of Reagent B), was applied, 1 ml per membrane for 5 minutes, in the dark, to react with the HRP and produce light. In order to create an even spread of the peroxide solution a second piece of clean, transparent projector film was laid over the membrane during incubation, taking care to remove any air bubbles.

Following incubation, the membrane was removed from the transparent projector film and drained onto absorbent paper. The membrane was quickly transferred between two fresh, clean projector films and secured in a developing cassette. It was essential to orientate the membrane correctly to aid with the interpretation of the western blot. A piece of x-ray film with the top left corner cut off to aid orientation, was removed from its packaging (in the dark room) and placed swiftly on top of the membrane in one motion, so as not to blur the location of the bands.

A five-minute exposure of the blot with the film occurred, before the cassette was opened and the film removed carefully, ready for developing.

2.8.6 - Film Development

Film development took place within a dark room with only the use of a red safe light to prevent fogging of the film. The film was lifted directly upwards from the membrane and placed immediately into a tray containing developer solution (Ilfosol 3, Ilford, Mobberley, UK) and agitated until bands appeared. The film was transferred into a 10% acetic acid bath, before fixation in Ilfosol 3 rapid fixer (Ilford). Once fixed (when the film became transparent), the film was removed from the fixer, washed under running tap water and hung up and allowed to dry completely.

2.9 - Extraction of RNA from exosomes using the QIAGEN miRNeasy microkit

For the extraction of the RNA, the QIAGEN miRNeasy microkit (QIAGEN, Hilden, Germany) was used following the manufacturer's instructions, briefly described below.

2.9.1 - RNA Extraction Procedure

Qiazol lysis reagent (Qiagen, Maryland, USA 700 μ L) was added to one of the exosome pellets, isolated by ultracentrifugation (**Section 2.7.2**). The tube was vortexed vigorously for 2 x 30 seconds before the lysate was transferred to the second tube and the process repeated. This was repeated for all of the replicate exosome pellets to concentrate the RNA being extracted.

The lysate was then transferred to an RNase free microfuge tube (Qiagen) and incubated at room temperature for 5 minutes to promote the dissociation of the nucleoprotein complexes. To extract RNA from the lysate, 140 μ L of chloroform (Merck/Sigma-Aldrich) was added to the tube and capped before vigorous shaking for 15 seconds. The tube was incubated at room temperature for 2-3 minutes, prior to centrifugation at 12,000 x *g* for 15 minutes at 4°C. The process of centrifugation enabled the generation of three phases, an upper, clear aqueous phase which contained the RNA, a white interphase containing DNA and a lower red organic phase which contained proteins and lipids. The upper aqueous phase was transferred to a clean RNase free tube, before the addition of 1.5 volumes of 100% ethanol (~525 μ l), with thorough mixing to precipitate the RNA.

Immediately, 700 μ L of the sample, including any precipitate that may have formed, was transferred on to a RNeasy MinElute spin column, provided in the miRNeasy micro kit (Qiagen), which had been placed in a 2 ml collection tube. The lid on the column was closed gently to prevent any spill before centrifugation at $>8000 \times g$ for 15 seconds at room temperature. The flow through was discarded before the application and centrifugation steps were repeated with the remaining sample. Again, any flow through was discarded and the collection tube reused each time.

Buffer RWT (700 μ L), provided in the extraction kit was then added to the RNeasy MinElute spin column and the lid closed gently before centrifugation at $>8000 \times g$ for 15 seconds to wash the column and help purify the sample. The flow through was discarded again and the column was further washed with 500 μ L of Buffer RPE (provided) with centrifugation at $>8000 \times g$ for 15 seconds. Ethanol (80%) was prepared from 100% ethanol by dilution with RNase-free water (Qiagen) and 500 μ L was pipetted onto the RNeasy MinElute spin column. Again, the lid was closed gently and centrifuged for 2 minutes at $>8000 \times g$ to wash the spin column membrane.

The RNeasy MinElute spin column was removed carefully from the collection tube so that the column did not come into contact with any of the flow through, to prevent carryover, and placed in a clean 2 ml collection tube. The column was then centrifuged at full speed for 5 minutes, with the lid open, in order to dry the membrane. In order to ensure that damage did not occur to the lids of the spin column, it was important that the spin columns were placed into the centrifuge with at least one empty position between the columns. It was also vital that the lids orientation was opposite to that of the rotatory direction of the ultracentrifuge. Leaving the lid open ensured that no ethanol was carried over during RNA elution. The collection tube and flow through were discarded.

To elute the RNA, the RNeasy MinElute spin column was placed into a new 1.5 ml RNase free collection tube and 14 μ L of RNase-free water was added directly to the centre of the spin column membrane. The lid was closed gently and the tube centrifuged for 1 minute at full speed in a microfuge. The elution with 14 μ L of RNase-free water resulted in a 12 μ L total RNA eluate.

2.10 - RNA quantification using the Biochrom SimpliNano Spectrophotometer

SimpliNano (Holliston, USA) possesses a sample port which enables users to quickly and accurately measure samples. The sample port comprises two fibre optics which are fixed 0.5 mm apart. The sample was loaded into the space between the two-fibre optics. The initial step was to add 2 μ L of RNase-free water to the sensor in order to act as a reference sample. The OA/100%T button was pressed to calibrate the device. This blank reference was used for all the subsequent samples and was performed twice. The 2 μ L of RNase-free water was removed and the sample port cleaned with lint free tissue before application of the RNA sample.

To quantify the RNA, 1 μ L of eluate from the spin column (**Section 2.9.1**) was placed onto the centre of the port in order to be in contact with both port probes. Care was taken not to introduce bubbles into the sample. The results button was pressed on the display and the concentration (μ g/ml) and both A260/A280 and A260/A230 readings were recorded.

The A260/280 nm absorbance ratio provides an indication of the purity of the RNA and whether there was any DNA contamination. Pure RNA preparations have expected ratios of ≥ 2.0 . The 260/230 ratio should also be > 2.0 (Thermofisher Scientific, 2024). A ratio that is lower than this is generally indicative of contamination with protein or guanidinium thiocyanate which is a reagent that is often used in RNA purification, which absorbs over the 230–260 nm range.

2.11 - miRNA sequencing - QIAGEN, Hilden, Germany

In total 15 RNA samples were prepared and sent to QIAGEN in Germany for microRNA sequencing. An equal balance of pathologies was selected with five samples being EMG, five of GD and five of PTC. The selected samples had been stored at -80°C following RNA extraction and were sent via express courier to Germany on dry ice as per instructions from QIAGEN.

2.11.1 - QIAGEN Quality Control (QC) – miRNA: Quantative Polymerase Chain

Reaction Quality Control (qPCR-QC)

The QC of the samples was performed with 2 μ L RNA, leaving 5 μ L RNA for library preparation. In order to determine the sample quality, a qPCR assay was performed. The aim of the qPCR was to determine the expression levels of specific miRNA in the samples. Following quality control at QIAGEN, 14 samples were selected for processing with one of the GD samples excluded.

2.11.2 - Library preparation and sequencing

The library preparation was done using the QIAseq miRNA Library Kit (QIAGEN). A total of 1 ng or 5 μ L total RNA was converted into miRNA NGS libraries. After adapter ligation, unique molecular indicators, UMIs, were introduced in the reverse transcription step. The cDNA was amplified using PCR (24, 22 cycles) and during the PCR, UMIs were added. After PCR the samples were purified. Library preparation was quality controlled using capillary electrophoresis (Tape D1000). Based on quality of the inserts and the concentration measurements the libraries were pooled in equimolar ratios. The library pool(s) were quantified using qPCR. The library pool(s) were then sequenced on a NextSeq (Illumina Inc.) sequencing instrument, according to the manufacturer's instructions. Raw data was de-multiplexed and FASTQ files for each sample were generated using the bcl2fastq2 software (Illumina inc.).

Eight of the fourteen samples sent had 5 μ L of RNA remaining for the further RT-qPCR and these samples were returned to the Daisy laboratories, at Hull.

2.12 - RT-qPCR using Individual miRCURY LNA PCR Assays

Results from the miRNA sequencing were validated using RT-qPCR using individual SYBR green miRCURY LNA PCR assays (Qiagen). The miRCURY LNA RT kit allows for the polyadenylation of the miRNA and the reverse transcription in one single step.

2.12.1 - cDNA synthesis using QIAGEN kit (339340) with UniSp6 spike

The miRCURY LNA reverse transcriptase (RT) Kit enables the fast and convenient miRNA polyadenylation and reverse transcription in a single reaction step. The following method demonstrates first-strand cDNA synthesis using UniSp6 Spike-in as an internal

cDNA synthesis control and the miRCURY LNA RT Kit. cDNA was synthesised from sEV RNA extracted from 20 different tissue-on-chip effluent samples.

Preparation of the UniSp6 cDNA synthesis RNA spike-in mix

The vial containing the UniSp6 was spun down before opening and then resuspended in 80 µl nuclease-free water. These were then mixed by vortexing and centrifuged briefly. The vial was left for at least twenty minutes, on ice, to ensure all the cDNA had entered solution.

2.12.2 - Polyadenylation and cDNA synthesis

Each RNA was thawed on ice and a volume equivalent to 50 ng was added to an RNAase free microfuge tube and made up to 6.5 µl with RNAse free water. The following steps were prepared on ice. MiRCURY RT 5x reaction buffer (2 µl) was added to the RNA along with 0.5 µl of the UniSp6 spike in and 1 µl of 10x miRCURY RT enzyme mix. These volumes were increased in an equal ratio between one another if a larger volume of RT reaction master mix was required.

For each experiment a no-template control was included to control for contamination. The prepared cDNA was used at a 1:30 dilution and the PCR was prepared in 96-well plates (Applied biosystems/Fisher Scientific MicroAmp Fast Optical 96-well reaction plate).

2.12.3 - PCR Thermal Cycler

The samples were incubated for sixty minutes at 42°C in a thermal cycler and then five minutes at 95°C, in order to heat inactivate the reverse transcriptase. The samples were then cooled by placing on ice.

Following incubation on the thermal cycler, the samples were either used immediately in the real-time PCR reaction or were stored, undiluted, at 2-8°C for up to four days, or up to 5 weeks at a temperature between -15°C and -30°C.

2.12.4 - Quantitative, Real Time PCR (RT-qPCR) using Individual miRCURY Locked

Nucleic Acid (LNA) PCR assays

The miRCURY SYBR green PCR kit and miRCURY LNA miRNA PCR assays were used to amplify miRNA of interest. The miRCURY LNA miRNA PCR assays are individual miRNA PCR primer sets that provide sensitive and specific miRNA quantification from small total RNA samples. The short, high-affinity, LNA-based primers bind directly to a miRNA sequence. The system enabled a simple and accurate two-step quantitative PCR process based on SYBR Green detection. The miRNA is converted by reverse transcription into a cDNA using a miRNA-specific primer and is then amplified by PCR using the miRNA-specific short LNA primer. LNA has been critical in enabling the successful quantitation of miRNA through RT-qPCR (Lunn et al., 2008).

The 2 x miRCURY SYBR Green Master Mix contains the QuantiNova DNA polymerase, which is inactive at room temperature. In order for the QuantiNova DNA polymerase to be activated, the PCR protocol must start with an initial incubation for two minutes at 95°C (Biaassoni & Raso, 2020).

Preparation of the miRNA LNA PCR Assays

The miRNA LNA PCR tube, containing each specific miRNA primer (PCR primer mix), was centrifuged prior to opening, 220 µL of nuclease free water was added to the tube and incubated at room temperature for 20 minutes. The tube was then vortexed and briefly centrifuged.

Preparation of 'Neat' cDNA

The cDNA was diluted 1:30 by adding 58 µL of RNAase-free water to 2 µL of cDNA, this was labelled 'Neat'. Further dilutions of the 'Neat' cDNA were trialled, from 1:10 to 1:50.

The PCR reaction mix was prepared as shown in **Table 2.2**, multiplying the volumes up appropriately for greater numbers of tubes, always ensuring at least two more tubes worth of mixture was prepared than was needed, to ensure the mixture did not run out when aliquoted. ROX, a fluorescent passive reference dye, was added to the PCR reaction mix. ROX's level of fluorescence does not change during the PCR process.

Normalization of qPCR data using ROX reduces the influence of well-to-well variability (Biosystems, 2015).

Table 2.2 - Preparation of PCR Reaction Mix

Component	Volumes for 1 x run (μL)	Volumes for 10 x runs (μL)
2xmiRCURY SYBR Green Master Mix	5	50
ROX reference dye	0.5	5
PCR primer mix	1	10
RNase-free water	0.5	5
Total	7	70

Following the preparation of the reaction mixes they were mixed thoroughly and $7\mu\text{L}$ was dispensed into each appropriate well of a 96-well PCR plate (Applied Biosystems/Fischer Scientific MicroAmp Fast Optical 96-well reaction plate). This was followed by $3\mu\text{L}$ of prepared cDNA following the plate layout. The plate was transported to the university and centrifuged briefly at room temperature in a plate spinner.

Using the ABI Real-Time PCR StepOne Plus machine (Applied Biosystems, Warrington, UK). The step one software was used to select the standard 2 hour program using the Quantification standard curve, with SYBR Green Reagents (with Melt Curve). The cycles used for amplification are shown in **Table 2.3**.

Table 2.3 - PCR cycling temperatures and times

Step	Time	Temperature	Ramp Rate
PCR initial heat activation	2 minutes	95°C	Maximal/fast mode
Denaturation	10 seconds	95°C	Maximal/fast mode
Combined annealing/extension	60 seconds	56°C	Maximal/fast mode
Number of cycles	40		
Melting curve analysis		$60-95^{\circ}\text{C}$	

Initial data analysis was performed using the software supplied with the real-time PCR instrument to obtain raw C_T values.

2.13 - Analysis of PCR Data using the Qiagen PCR Analysis Tool

The expression of miRNA species in each of the thyroid samples was analysed using the GeneGlobe Data Analysis tool from Qiagen

(<https://geneglobe.qiagen.com/gb/analyze>).

In order to start analysing the data, select:

- PCR
- miRNA
- miRCURY LNA miRNA PCR Panels & Assays

Following that, then select the miRCURY LNA miRNA PCR Data Analysis

Handbook:

[https://dataanalysis2.qiagen.com/static/templates/miRCURY LNA miRNA PCR Data Analysis Handbook 190930.pdf](https://dataanalysis2.qiagen.com/static/templates/miRCURY_LNA_miRNA_PCR_Data_Analysis_Handbook_190930.pdf)

- Upload/Select
- Upload Dataset
- Product type = assays
- Species = Human (YAHs)
- Plate format = 96-well
- Upload file
- Example file format, must be Excel (xls):

miRNA #	miRNA ID	Assay Catalog #	Normal Control Group	Normal Control Group	Normal Control Group
1	hsa-miR-142-5p	YP00204722	27.925755	26.07041	26.223831
2	hsa-miR-9-5p	YP00204513	None	32.65381	38.8189
3	hsa-miR-150-5p	YP00204660	24.334599	23.718548	23.287169
4	hsa-miR-27b-3p	YP00205915	23.839155	23.074007	22.944405
5	hsa-miR-101-3p	YP00204786	25.21303	23.359682	23.902048
6	hsa-let-7d-5p	YP00204124	25.198746	24.225424	24.139067
7	hsa-miR-103a-3p	YP00204063	25.148733	25.035772	23.97102
8	hsa-miR-16-5p	YP00205702	22.630583	21.420828	21.520142
9	hsa-miR-26a-5p	YP00206023	21.060686	20.049652	20.067286
10	SNORD68	YP00308017	23.67738	23.259106	22.92256

- Example 2, where there are 3 repeats/ wells per sample:

miRNA #	miRNA ID	Assay Catalog #	Benign 1 Control group	Benign 1 Control group	Benign 1 Control group	Benign 2 Control group
1	UniSp6	YP00203954	18.99499512	18.98188591	18.93069839	None
2	hsa-miR-16-5p	YP00205702	31.05362511	30.20783806	30.40629768	29.78098679
3	hsa-miR-320c	YP00205706	30.52452469	30.39354706	30.55754662	27.74220467
4	hsa-miR-375-3p	YP00204362	None	None	36.55085373	34.80684662
5	ssc-miR-7-5p	YP002102959	None	38.67356873	36.86163712	35.84365463

- If the file will not upload, even in the above format. Download the file below, delete example data, and copy and paste your data directly into the file provided by QIAGEN and then re-attempt the upload:

- https://view.officeapps.live.com/op/view.aspx?src=https%3A%2F%2Fdataanalysis.qiagen.com%2Fstatic%2Ftemplates%2FmiRCury_miRNA_qPCR_Assay_Template.xlsx&wdOrigin=BROWSELINK
- Click Submit
- One can then check the uploaded data to see if the data has been uploaded correctly
- Go onto sample manager
- The designated group names may need to be altered:
 - For example, even though 'benign' set is designated as Control Group on the excel file, it will designate this set as Group 1.
 - Change designation for Control Group here.

Job Details		Group Definition							
Benign 1	Control Group	Benign 1.1	Control Group	Benign 1.2	Control Group	Control Group			
Benign 2	Control Group	Benign 2.1	Control Group	Benign 2.2	Control Group	Control Group			
Benign 3	Control Group	Benign 3.1	Control Group	Benign 3.2	Control Group	Control Group			
Benign 4	Control Group	Benign 4.1	Control Group	Benign 4.2	Control Group	Control Group			
Benign 5	Control Group	Benign 5.1	Control Group	Benign 5.2	Control Group	Control Group			
Graves 1	Group 1	Graves 1.1	Group 1	Graves 1.2	Group 1	Group 1			
Graves 2	Group 1	Graves 2.1	Group 1	Graves 2.2	Group 1	Group 1			
Graves 3	Group 1	Graves 3.1	Group 1	Graves 3.2	Group 1	Group 1			
Graves 4	Group 1	Graves 4.1	Group 1	Graves 4.2	Group 1	Group 1			
Graves 5	Group 1	Graves 5.1	Group 1	Graves 5.2	Group 1	Group 1			
Graves 6	Group 1	Graves 6.1	Group 1	Graves 6.2	Group 1	Group 1			
Cancer 1	Group 2	Cancer 1.1	Group 2	Cancer 1.2	Group 2	Group 2			
Cancer 2	Group 2	Cancer 2.1	Group 2	Cancer 2.2	Group 2	Group 2			
Cancer 3	Group 2	Cancer 3.1	Group 2	Cancer 3.2	Group 2	Group 2			
Cancer 4	Group 2	Cancer 4.1	Group 2	Cancer 4.2	Group 2	Group 2			
Cancer 5	Group 2	Cancer 5.1	Group 2	Cancer 5.2	Group 2	Group 2			
Cancer 6	Group 2	Cancer 6.1	Group 2	Cancer 6.2	Group 2	Group 2			
Other 1	Group 3	Other 1.1	Group 3	Other 1.2	Group 3	Group 3			

For example:

- Select the reference miRNA
- Highlight and press 'Add>>'
- These will now appear on the right in the Selected miRNA box.

Select 'Yes' for, 'Are your samples serum, plasma, another body fluid, or other cell-free source?'

Internal Amplification Controls;

- UniSp6 should already be selected if this miRNA has been used.

Lower Limit Detection;

- Use Single C_T Cut-Off
- Set to 40; if sample C_T is high

T-Test & p-Value Calculation;

- T-test: select 'Un-Paired'
- P-value: select '2-Tail'

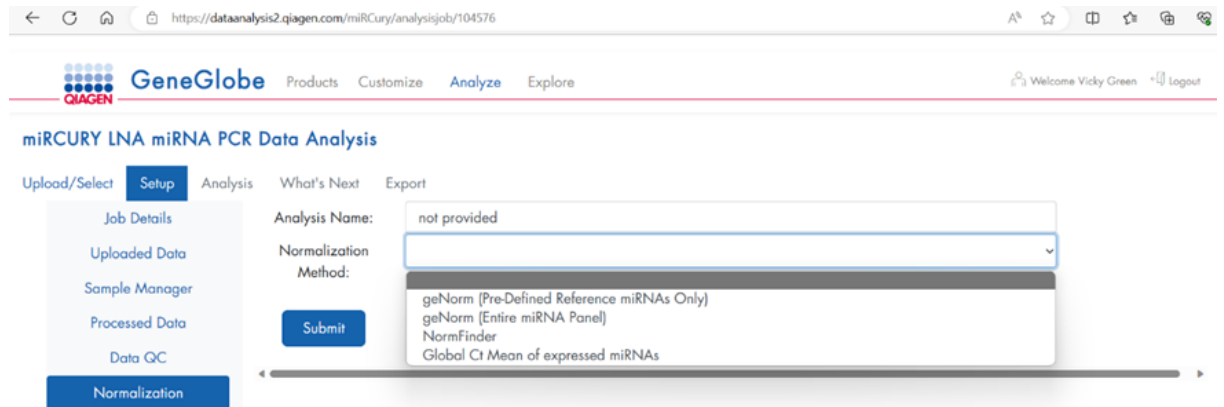
Compare each Test Group to Control Group ONLY: do **NOT** select this

Click Submit

Click analyse the Processed Data and the Data QC

Normalisation;

- Name the analysis
- Select Normalisation Method



- Initially run with geNorm (Pre-Defined miRNA's Only)
- Select NormFinder for more than two stable/ housekeeping genes
- Once a Normalisation Method is selected, details on each method are provided. For example;

Normalization Method:

geNorm (Pre-Defined Reference miRNAs Only)

This method calculates a normalization factor based on multiple reference miRNA for more accurate and reliable normalization of miRNA expression data. It is based on the principle that the expression ratio of any two reference miRNAs (using standard deviation of log-transformed reference miRNA ratios) should be identical in all samples. Stability measures will be returned which are the average pairwise variation between a reference miRNA and all other reference miRNAs using stepwise exclusion of the worst scoring miRNAs. The predefined miRNAs or up to ten miRNAs from the entire panel with the best gNorm-calculated stability measures are listed if their value is less than 1.5. For more details, see:

Reference: Vandesompele J, De Preter K, Pattyn F, Poppe B, Van Roy N, De Paeppe A, Speleman F. Accurate normalization of real-time quantitative RT-PCR data by geometric averaging of multiple internal control miRNAs. *Genome Biol.* 2002 Jun 18;3(7):RESEARCH0034. PubMed ID: 12184808.

miRNA ID	hsa-miR-16-5p	hsa-miR-320c	Arithmetic Mean	Average Arithmetic Mean
Stability Factor	N/A	N/A		
Reference miRNA	<input checked="" type="checkbox"/>	<input checked="" type="checkbox"/>		
Control Group	Benign 1	31.05	30.52	30.79
Control Group	Benign 5.2	31.17	29.97	30.57

- Then click Submit
- Go to Analysis
- Results will be shown as Fold Regulation, Fold Change, Average ΔCt , $2^{-\Delta Ct}$, as well as Plots & Charts

The results can be exported from the Export tab as an Excel or PDF
'What's Next' can be selected for additional analysis.

Materials and Methods - Acknowledgements

A huge thank you is owed to Dr Victoria Green, Senior Postdoctoral Researcher, for teaching me the necessary laboratory skills in which to carry out these experiments. The thank you extends to Miss Hannah Beattie, PhD candidate, to whom I taught the set-up of the PEEK devices and she as a result helped with the set-up of the experiments in the latter part of the study. Miss Beattie also helped in the centrifugation and ultracentrifugation of samples and the extraction of RNA, ready for the microRNA sequencing. I hope that the skills Miss Beattie learnt will help with the further continuum of this research. The work presented in this thesis was carried out by myself, the candidate, independently in the laboratory except where explicitly acknowledged above. Acknowledgement regarding individual's respective contributions has been reflected in the resulting publication in the International Journal of Molecular Sciences (IJMS).

Chapter 3 - Histoarchitectural analysis of thyroid tissue, NTA analysis of thyroid tissue on chip effluent, western blot analysis of thyroid exosomal and tissue lysate

In order to delineate an exosomal miRNA profile of thyroid disease using tissue-on-chip technology, the first aim was to prove that thyroid tissue is viable on chip for a six-day period. In order to prove this, three individual scientific laboratory techniques were performed. Firstly, histoarchitectural analysis of thyroid tissue that had been 'on-chip' was performed both pre and post perfusion on chip for six days. Following this, NTA was carried out on effluent samples collected at daily time points throughout the experiment from different thyroid pathologies in an attempt to quantify and characterise the effluent sEV content. This was followed up with western blot (WB) analysis of thyroid exosomal and tissue lysate to identify classical exosomal tetraspanin markers. An effort was also directed towards understanding how different types of thyroid pathology behave on chip.

3.1 - Histoarchitectural analysis of thyroid tissue

The morphological integrity of tissues is defined as the preservation of general architecture including epithelial structures and spatial relationships to the stroma (Vaira et al., 2010). One obvious histological feature of cell death is that of nuclear degeneration (Galluzzi et al., 2018). The initial sign is that of pyknosis, which results from the condensation of chromatin into small, densely Haematoxylin-stained masses (Burgoyne, 1999). Later this nuclear material becomes further fragmented (karyorrhexis) and breaks down with a loss of the nucleus (karyolysis) (Majno & Joris, 1995). The denaturation of the cytoplasmic proteins results in formation of an amorphous cytoplasmic mass which stains intensely with eosin.

The H&E staining allows for the visualisation of the structure, distribution of cells and any morphological changes within a tissue sample (**Section 2.4**) (**Appendix 3**).

3.2 - Materials and Methods

The thyroid biopsies were obtained and processed as described in Section 2.1, being immediately prepared on collection from theatre ready to be maintained on the 'tissue-on-chip' device. The fresh tissue (without incubation on the device) and tissue following

six days of perfusion was fixed in 4% (v/v) paraformaldehyde for a period of 24 h and following that placed in 70% ethanol ready for processing (**Section 2.2.1**). Samples were dehydrated and embedded with molten paraffin wax before being sectioned at 5 μm thickness. These sections were then mounted and stained with H&E (**Section 2.4**).

3.3 - Results

H&E staining was performed on the following samples EMG ($n=5$), Graves ($n=6$) and PTC ($n=5$). Following staining, the slides were examined and photographed at both x10 and x40 magnification to provide both an overall appreciation of cellular architecture as well as a detailed image. A second opinion was sought from Dr Karsai, Consultant Head and Neck Pathologist at Hull University Teaching Hospitals NHS Trust; with regards to the viability of thyroid tissue-on-chip at 144 hours. Representative examples are shown for each type below, all data are shown in **Appendix 3**.

3.4 - Thyroid Tissues Images (Pre-Culture and Post-Culture) at x10 and x40 Magnification

3.4.1 - Euthyroid Multinodular Goitre (EMG)

Each thyroid lobule is made up of an aggregation of follicles, which are the structural and functional units of the thyroid gland. The follicles are lined by follicular cells and are filled with a homogenous gelatinous material called colloid (**Figure 3.1** and **Figure 3.2**). The thyroid gland stores its secretory substances within the follicle lumina. Each of the follicles are able to store several weeks supply of thyroid hormone within the colloid. The connective tissue septa, that are derived from the capsule, invade the parenchyma and act to provide a conduit for blood vessels, lymphatic vessels and nerve fibres. **Figure 3.2** demonstrates EMG tissue that has been maintained on chip. The variability in the architecture of the individual pieces of tissue maintained on the devices can be appreciated at day six.

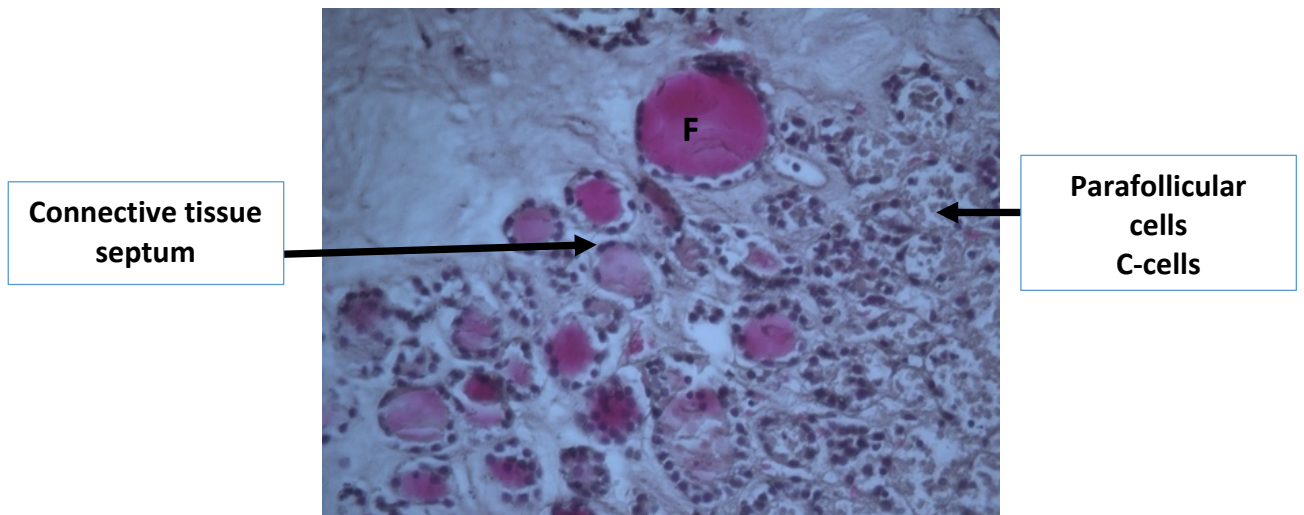
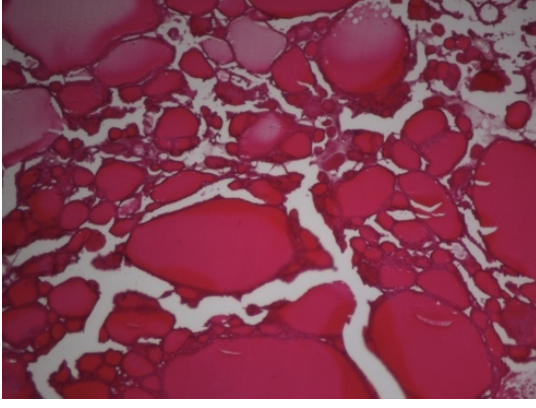
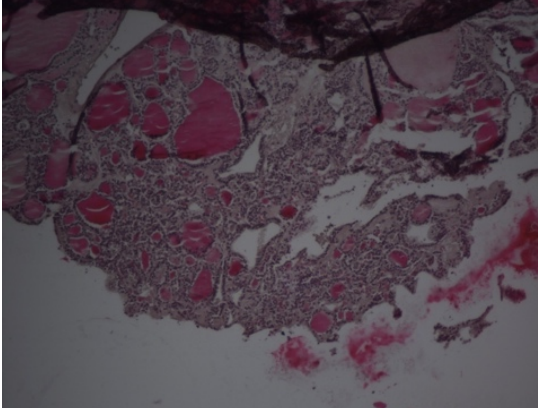
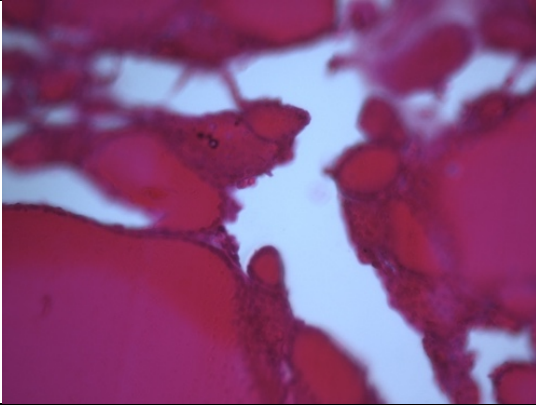
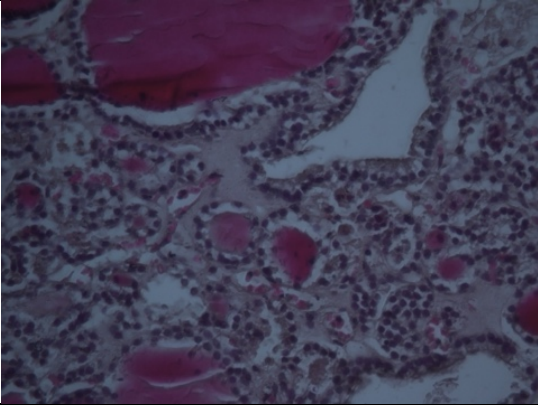
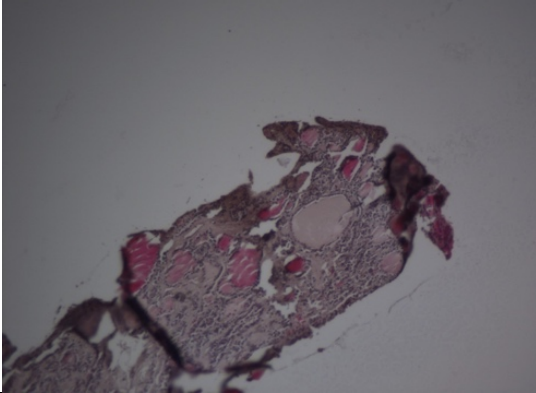
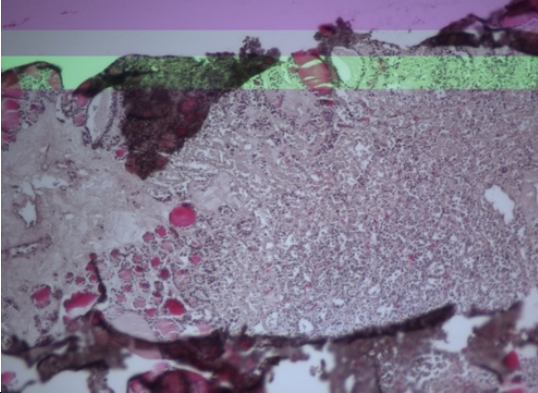
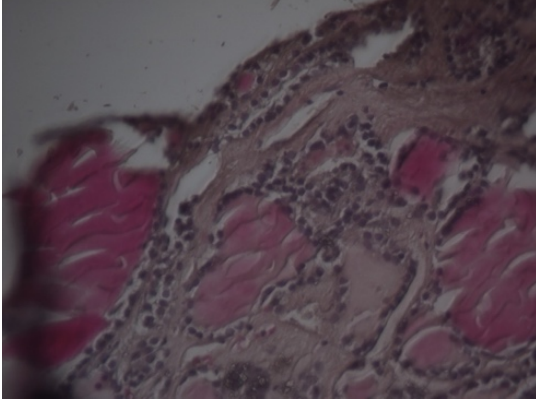
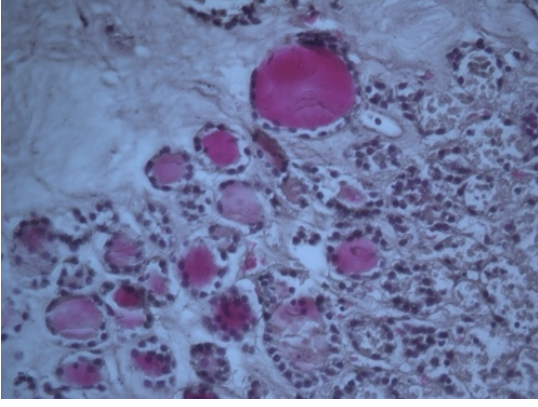


Figure 3.1 – EMG thyroid tissue architecture at x40 magnification following maintenance on the ‘tissue-on-chip’ device for a period of six days. (F) demonstrates a colloid filled follicle. As can be appreciated on the periphery of the follicles are connective tissue septa, which provide an avenue for blood vessels and lymphatics. C-cells can be appreciated which are typically found within the basal lamina of the thyroid follicles.

EMG – Fresh Tissue – Pre-culture (x10 + x40)	EMG – Post-culture – Device 1 (x10 + x40)
	
	
EMG – Post-culture – Device 2	EMG – Post-culture – Device 3
	
	

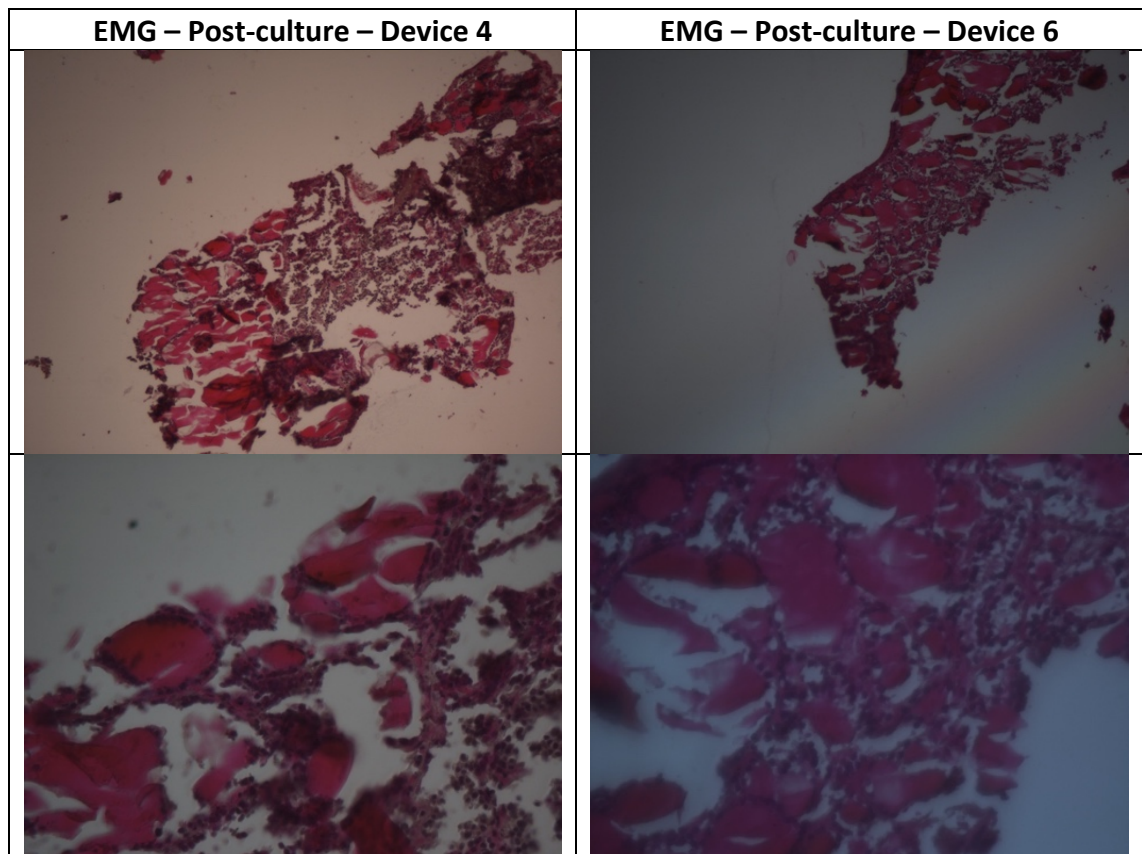


Figure 3.2 – EMG thyroid tissue of 5 μm thickness pre and post maintenance on a ‘tissue-on-chip’ device (x10 and x40 magnification). Images from 5 devices are displayed, all from the same patient.

3.4.2 – Graves Disease (GD)

GD H&E staining is characterised by hyperplastic thyroid follicles with papillary infoldings (**Figure 3.3; Figure 3.4**). The nuclei are often round, basally located and rarely overlap. The stroma in GD may exhibit infiltration by inflammatory cells, including lymphocytes, plasma cells, and macrophages and an increased vascularity (Aly & Satturwar, 2023). It is worth noting that the blood vessels within the thyroid gland may be more prominent, dilated, and congested due to the increased metabolic demand and thyroid hormone production. **Figure 3.3.** demonstrates GD tissue that has been maintained on chip.

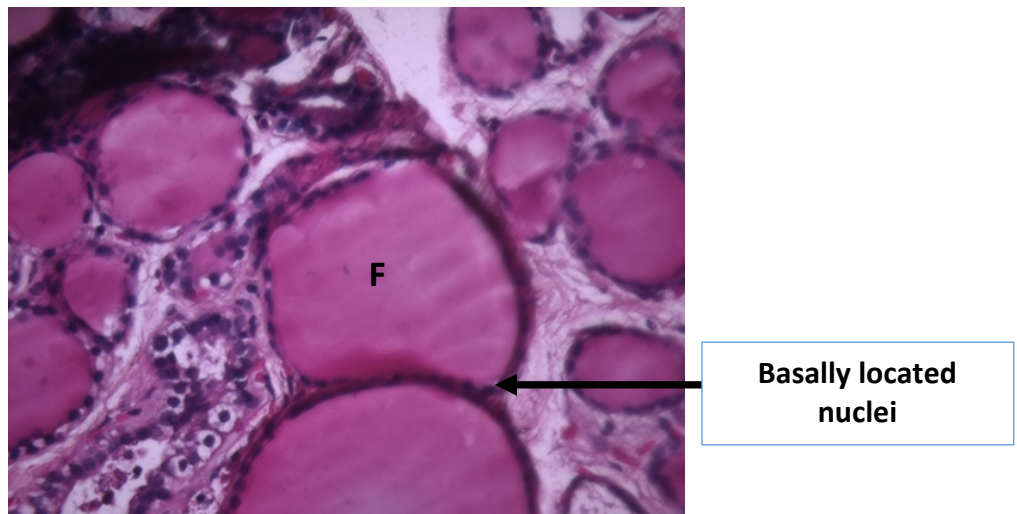
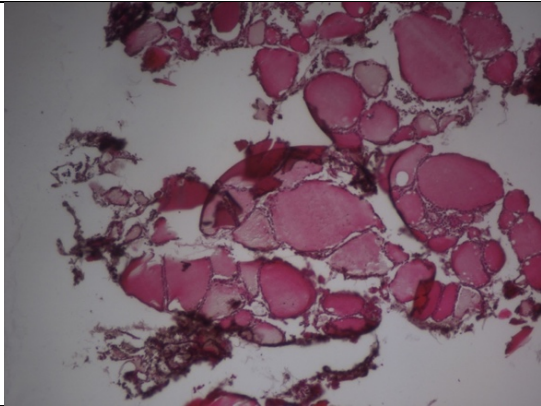
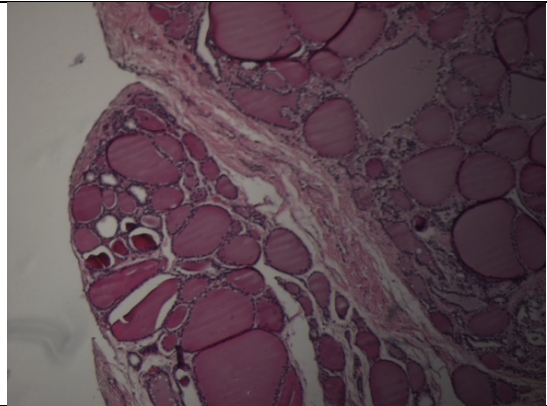
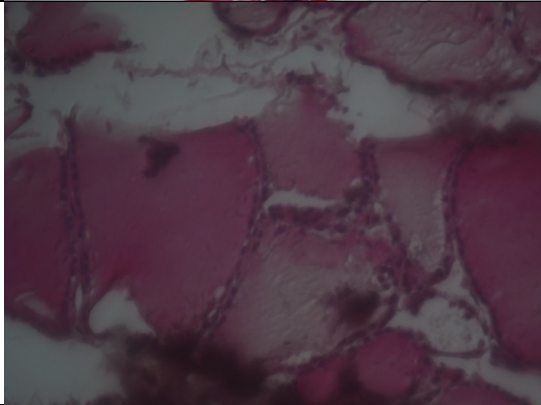
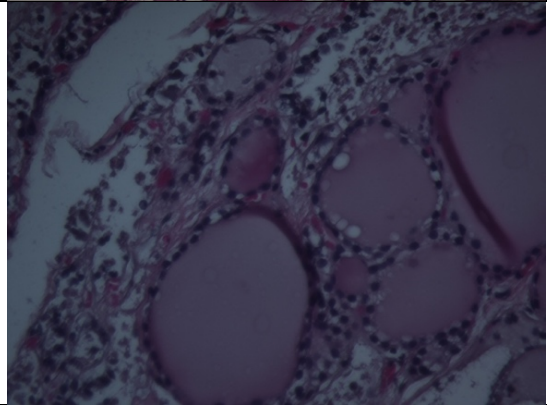
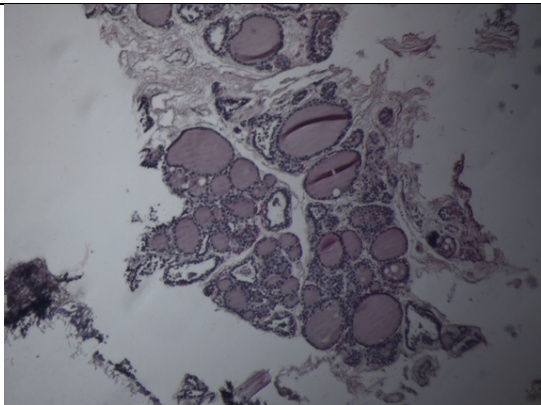
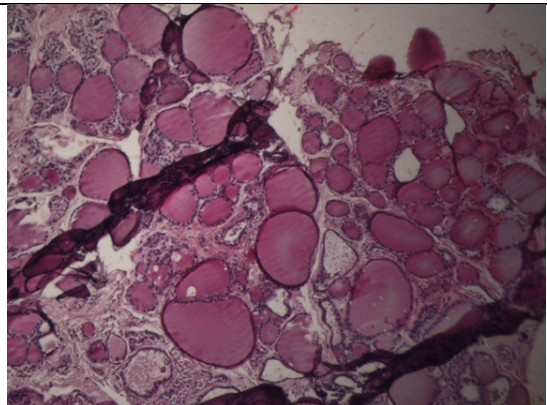
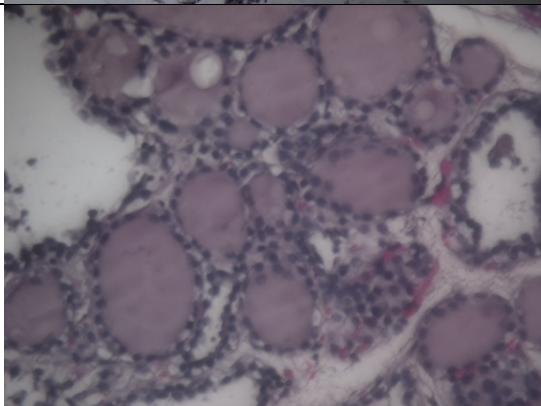
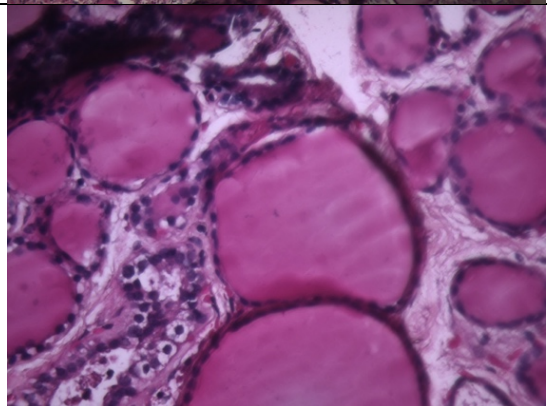


Figure 3.3 – GD tissue architecture at x40 magnification following maintenance on a tissue-on-chip device for a total of six days. (F) demonstrates a colloid filled follicle. Relative to the EMG H&E figure (**Figure 3.1**), the follicles are hyperplastic with a greater number appreciated on a x40 magnification.

GD – Fresh Tissue – Pre-culture (x10 + x40)	GD – Post-culture – Device 1 (x10 + x40)
	
	
GD – Post-culture -Device 3	GD – Post-culture – Device 4
	
	

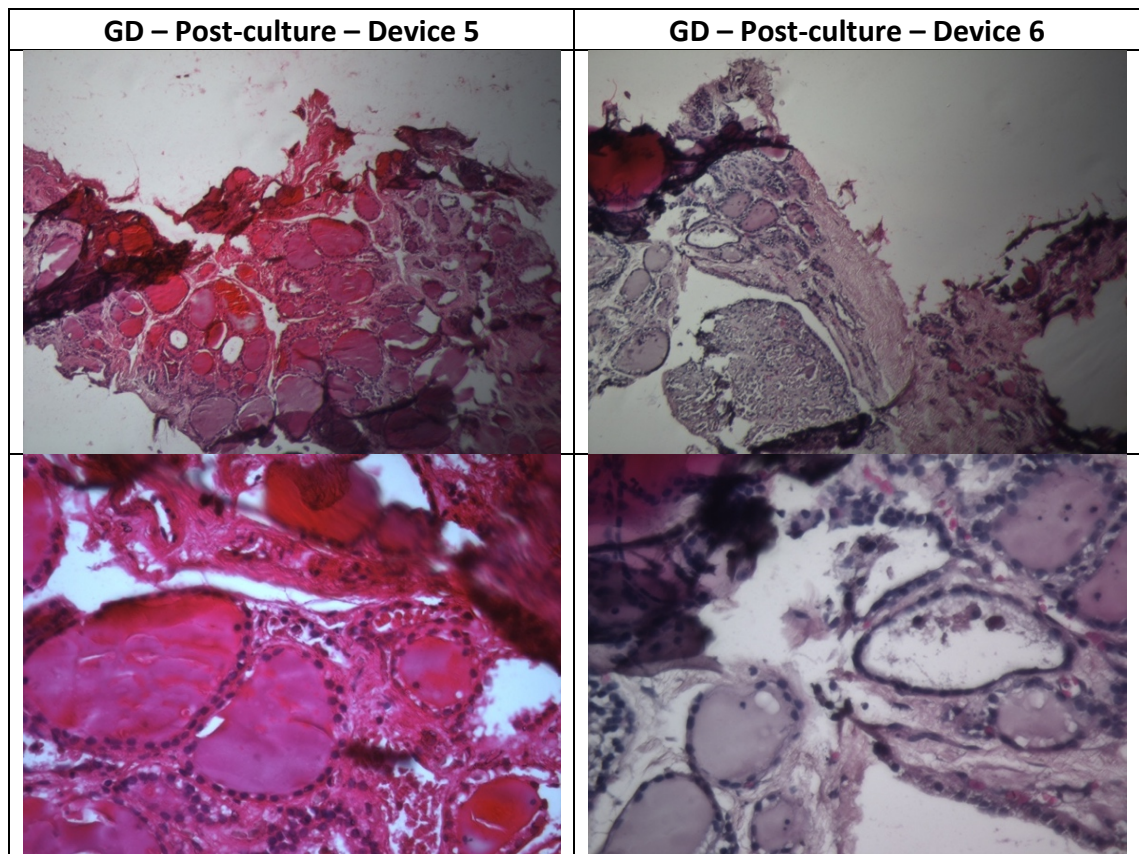


Figure 3.4 – GD tissue 5 μm thickness pre and post maintenance on a ‘tissue-on-chip’ device (x10 and x40 magnification). Images from 5 devices are displayed, all from the same patient

3.4.3 – Papillary Thyroid Cancer (PTC)

PTC demonstrates characteristic histoarchitectural features such as nuclear enlargement, elongation and overlapping of the nuclei (**Figure 3.5**). Alongside this there can be prominent papillae alongside fibrovascular cores (Xu, 2023). The histological subtypes of PTC are continually under review as per the World Health Organisation (WHO) Classification (Jung et al., 2022). Their nuclear membranes demonstrate irregular nuclear contours, nuclear grooves and nuclear pseudoinclusion.

Some of the samples demonstrated evidence of neoplastic papillae and tumoral fibrous stroma, features which mark its’ difference to that of benign EMG thyroid tissue (**Figure 3.5**). Psammoma bodies are also representative of PTC, they are formed through focal areas of infarction of the tips of the papillae which attract calcium that are then deposited within the dying cells (**Figure 3.6**; Device 4) (Johannessen & Sobrinho-Simões, 1980). A point to be aware of is that many thyroid lesions can present with a papillaroid architecture that can mimic PTC and this presents obvious diagnostic challenges.

Pathologies that can mimic PTC include Hashimoto's Thyroiditis and tissues demonstrating post-FNA changes (Kunjumon, 2016). As can be seen there is intra-tumour variation in cellularity and follicle size. However, these differences are retained in the tumour tissue throughout culture (**Figure 3.6**).

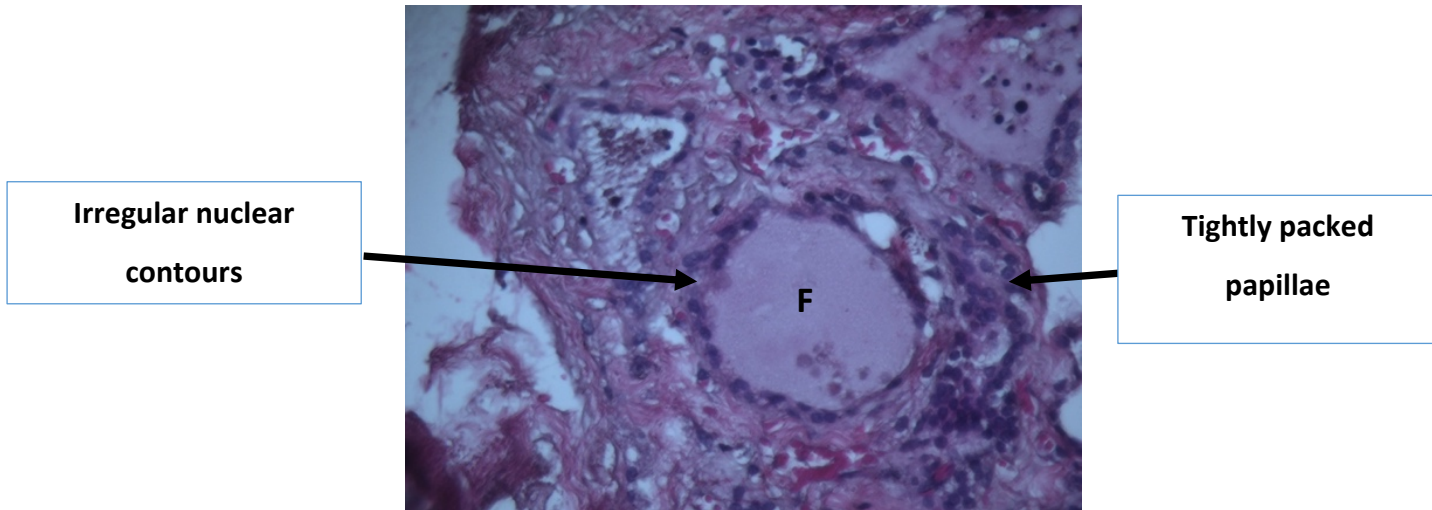
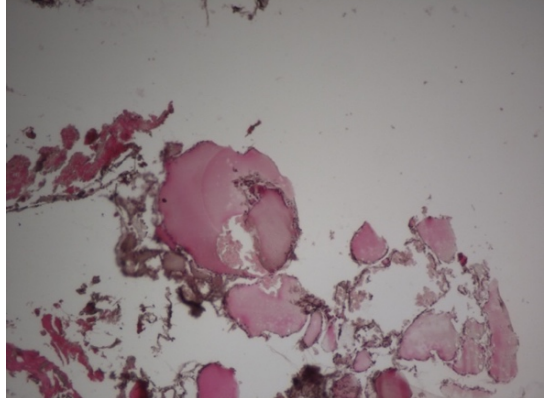
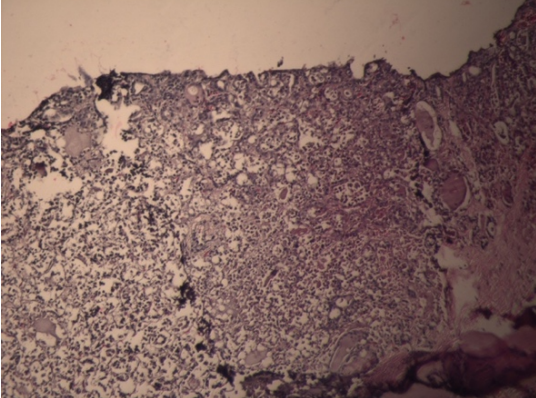
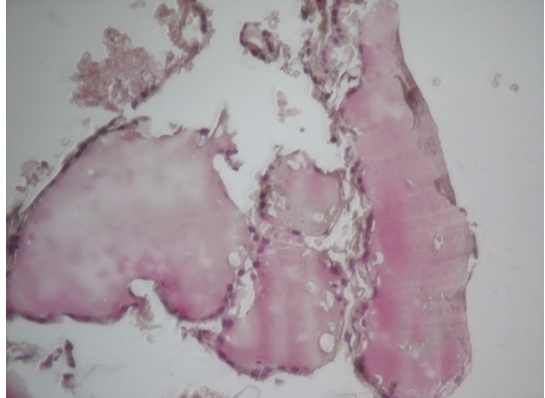
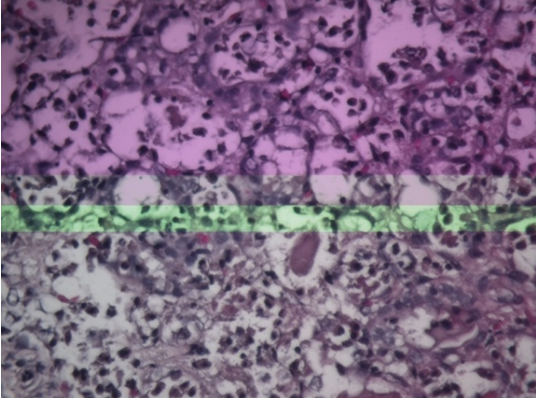
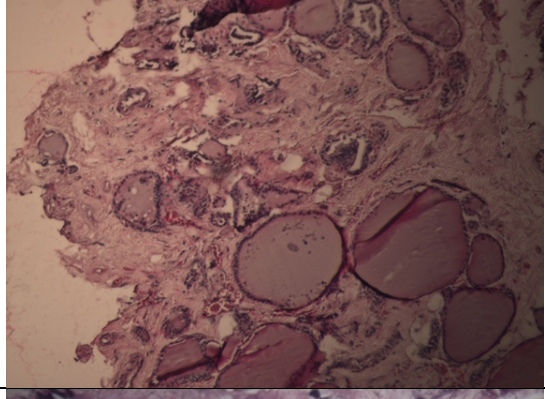
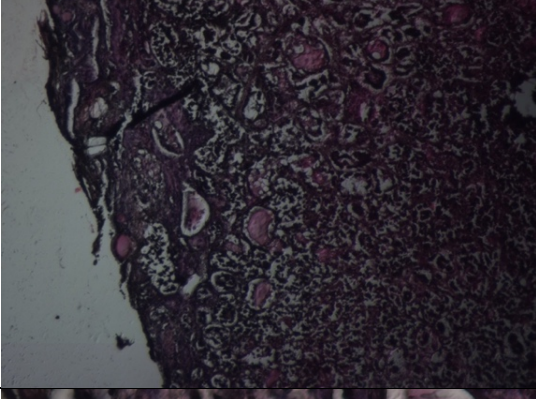
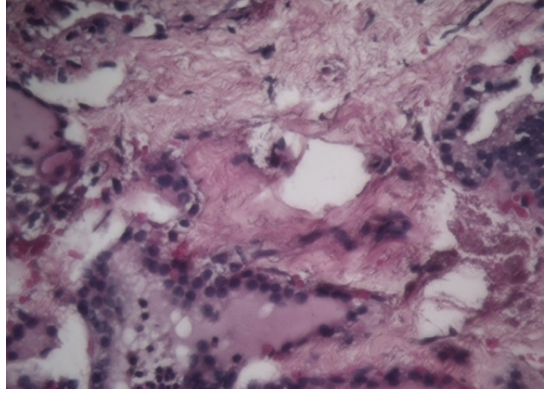
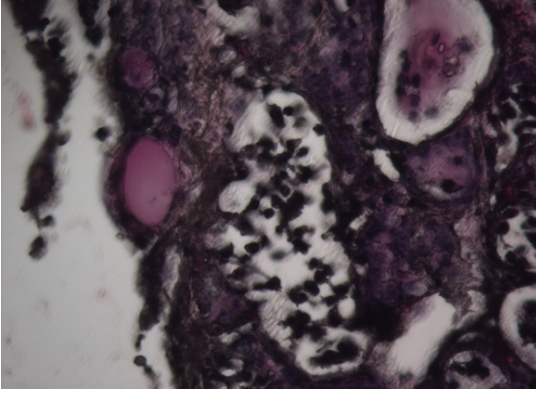


Figure 3.5 – PTC tissue architecture at x40 magnification following maintenance on a tissue-on-chip device for a total of six days. (F) demonstrates a colloid filled follicle

PTC – Fresh Tissue (x10 + x40)	PTC – Post-culture – Device 1 (x10 + x40)
	
	
PTC – Post Culture - Device 2	PTC – Post Culture - Device 3
	
	

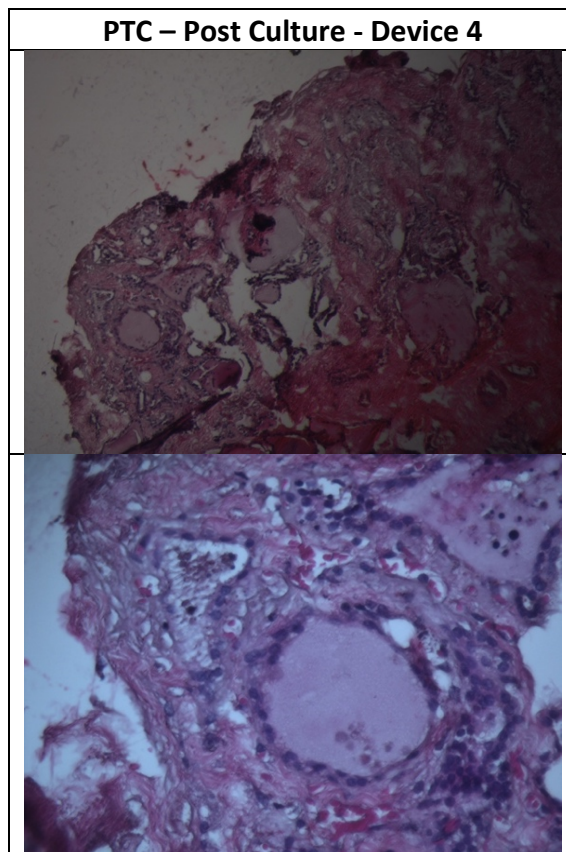


Figure 3.6 - PTC tissue 5 μm thickness pre and post maintenance on a tissue-on-chip device (x10 and x40). Images from 4 devices are displayed, all from the same patient sample demonstrating the intra-tumour variability.

3.5 - The use of Nanosight Tracking Analysis (NTA) to determine the size and concentration of small Extracellular Vesicles (sEVs) produced by thyroid tissue maintained on a tissue-on-chip device

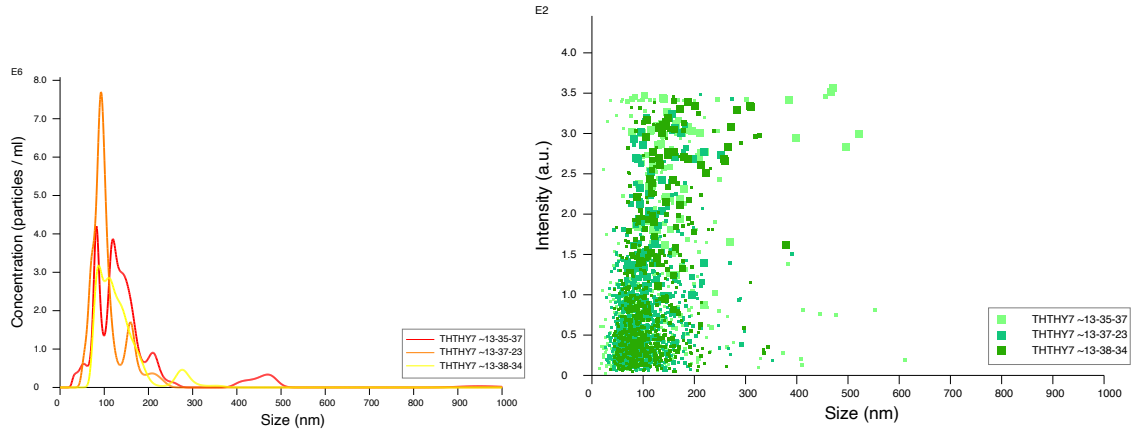
3.5.1 - The Role of NTA as per the Minimal Information for Studies of Extracellular Vesicles (MISEV) Position Paper 2023

In the 2018 MISEV guidelines, recommendations were made that the particle number and size can be measured through the use of light scattering technologies such as NTA (Théry et al., 2018). However, the guidelines do advise an element of caution in terms of quantification of EV as the technique itself is not EV specific. For example, within the context of dynamic light scattering, the technology can register co-isolated particles such as lipoproteins and protein aggregates which will provide a higher than intended reading for EVs. In the most recent MISEV 2023 Position Paper, NTA is recommended alongside atomic force microscopy, diffraction-limited fluorescence microscopy, dynamic light scattering and electron microscopy, super-resolution microscopy and single-particle interferometric reflectance imaging sensing (Welsh, 2024).

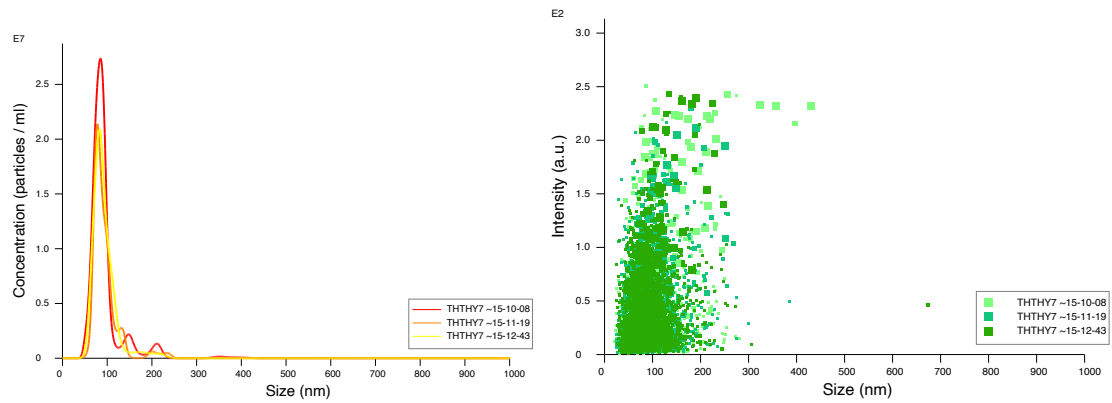
3.6 - Particle Mean Size and Particles/ml

An overall mean value for the particle size and particles/ml was obtained for each individual experiment on each respective day. Following the effluent being run through the Nanosight LM10, the NTA software provided a graphical representation. **Figure 3.7** demonstrates representative data from each individual day for one device over the 6 days of incubation. A data sheet with values for the particle mean size (nm) and particles/ml was also obtained for each sample (**Figure 3.8**). For this particular sample, it shows that the size of the majority of the particles is below 200 nm throughout the experiment but the density of the dots looks to deplete after day 4.

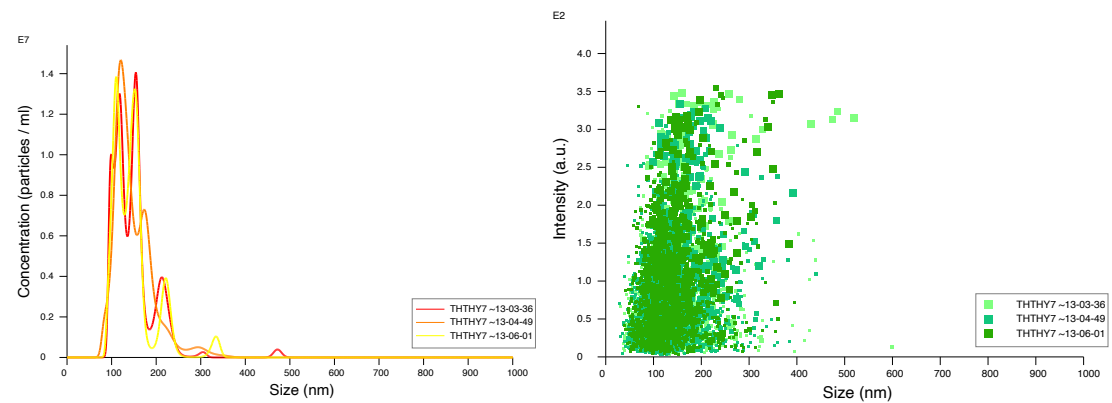
A. GD - Device 3, Day 1



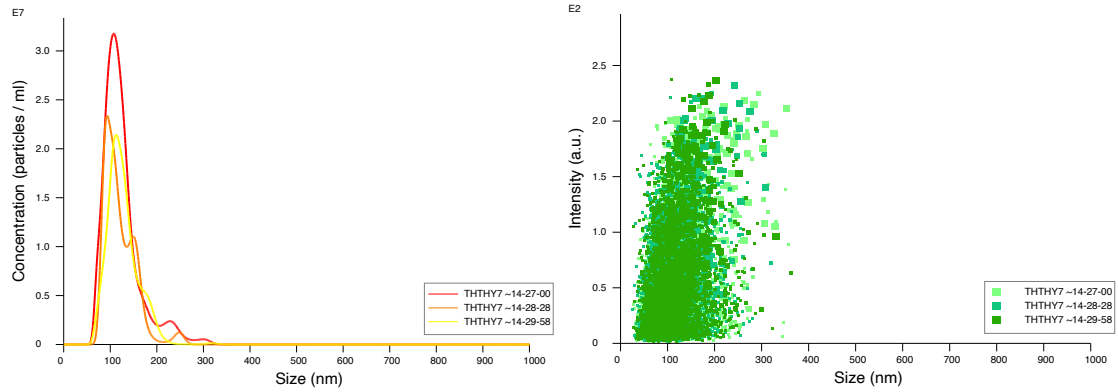
B. GD - Device 3, Day 2



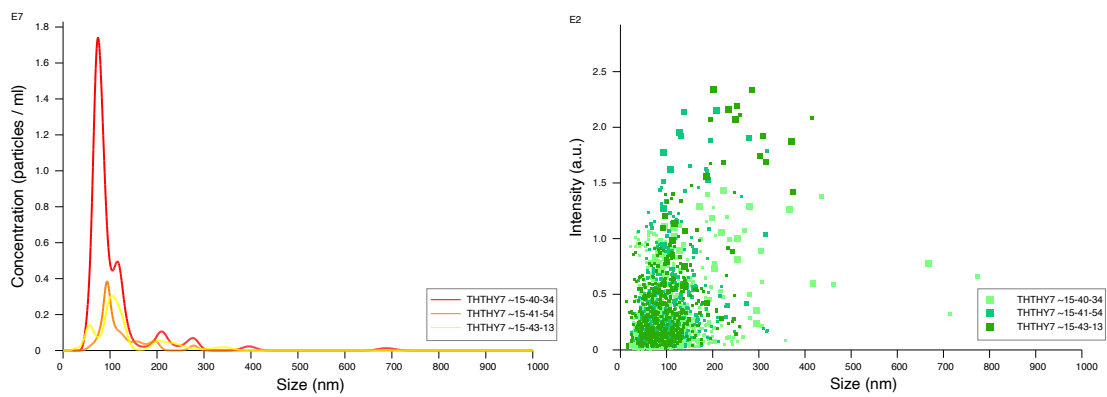
C. GD - Device 3, Day 3



D. GD - Device 3, Day 4



E. GD - Device 3, Day 5



F. GD - Device 3, Day 6

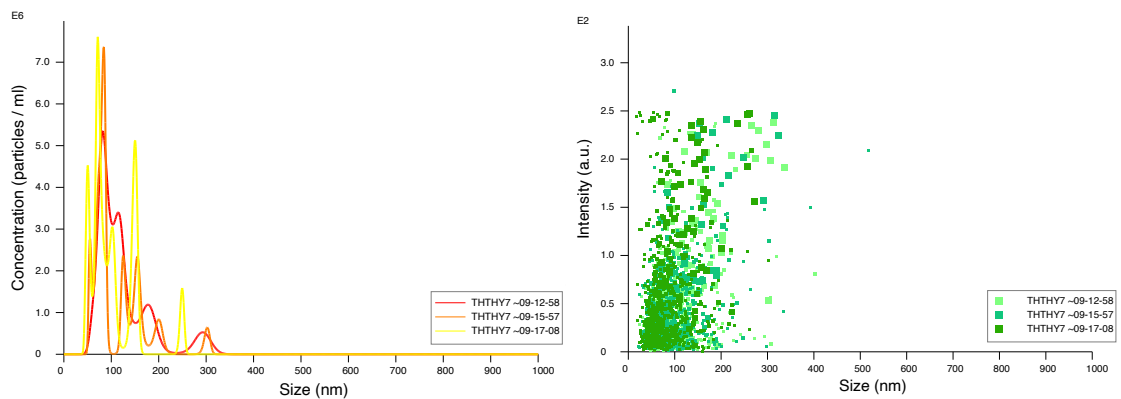


Figure 3.7. NTA data output of size (nm) vs. concentration (particles/ml) for each sample, and intensity dotplot (a.u.). Data from GD Device 3, Sample I (**Appendix 4, Table 4.1**) or the six days of the experiment are shown as a representation. The x axis provides the size (nm) and y axis the concentration (particles/ml) and intensity (a.u.)

Stats: Mean +/- Standard Error	
Mean:	79.1 +/- 2.6 nm
Mode:	66.0 +/- 3.9 nm
SD:	26.8 +/- 1.4 nm
D10:	56.6 +/- 1.5 nm
D50:	70.3 +/- 2.0 nm
D90:	108.8 +/- 10.1 nm
Concentration:	6.01e+08 +/- 2.85e+08 particles/ml
	32.9 +/- 15.6 particles/frame
	48.6 +/- 29.3 centres/frame

Figure 3.8. Numerical data provided by the NTA software for the GD Sample I, (**Appendix 4, Table 4.1**) Device 2, Day 3 effluent. A mean size is provided, alongside a mode, standard deviation of the mean and values for D10, D50 and D90 size. The D90 figure is the diameter value which encompasses 90% of all the particles measured; and similar for the D50 and D10.

3.7 – NTA Results

3.7.1 - Optimisation Studies

It was found that running the undiluted tissue effluents gave high concentrations of particles (>E+09 particles/ml), outside of the highest reading threshold of the instrument. The number of particles/ml should optimally lie within the range of between E+07 and E+09 total particles/ml, this is because of a combination of laser brightness and camera sensitivity and the need to differentiate particles from camera noise (Filipe et al., 2010). Trials using a 1:2, 1:4 and 1:8 dilution of the effluent with 20nm filtered PBS were carried out to determine the most appropriate dilution factor for the effluent. The results of the dilution series (**Figure 3.9**) demonstrates that a minimum dilution of 1:8 is required to bring the concentration of the particles within the appropriate range of detection for the NTA. Even after a 1:8 dilution however there remained considerable variation in the number of particles detected per ml over time (**Figure 3.9B**).

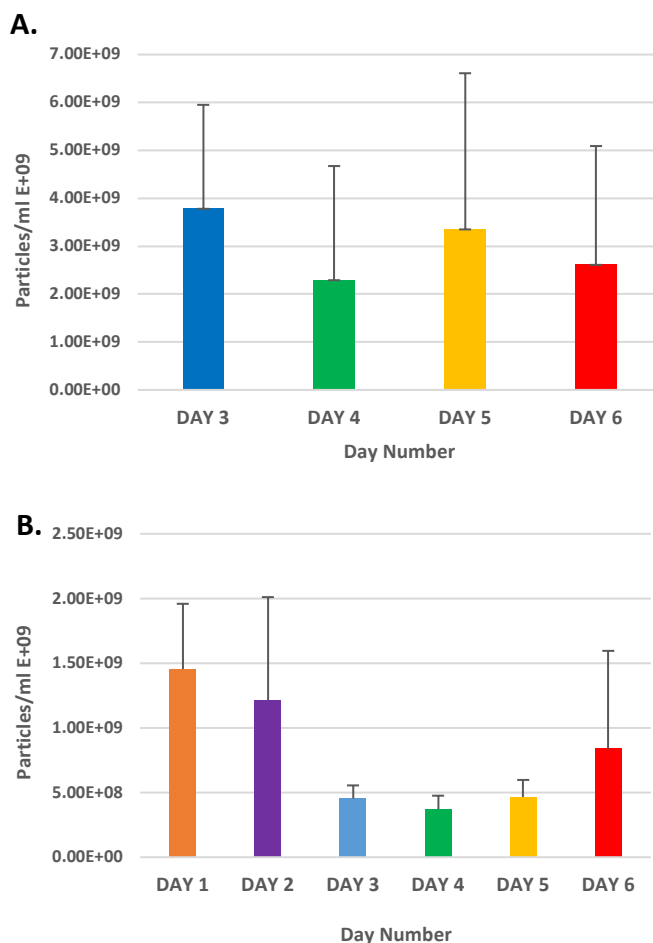


Figure 3.9. A – Sample A (**Appendix 4, Table 4.1**) for Day 3 to Day 6 mean particles/ml E+09 at a 1:2 dilution in filtered (20nm) PBS. **B** – Sample B (**Appendix 4, Table 4.1**) for Day 1 to Day 6 mean particles/ml E+09 at 1:8 dilution with DMEM

3.7.2 - Use of DMEM as a Dilution Agent rather than Filtered PBS

Initially the dilution of effluent was performed with 20 nm filtered PBS. However, due to the expense of the filters, it was proposed to use DMEM without any supplements as an alternative. This was first analysed to determine if it contained sufficiently low numbers of particles to act as a diluent (**Figure 3.10**).

Three separate runs were performed on the Nanosight, using both the 20 nm filtered PBS and un-supplemented DMEM and the concentration of particles was noted (**Figure 3.10** and **Table 3.1**).

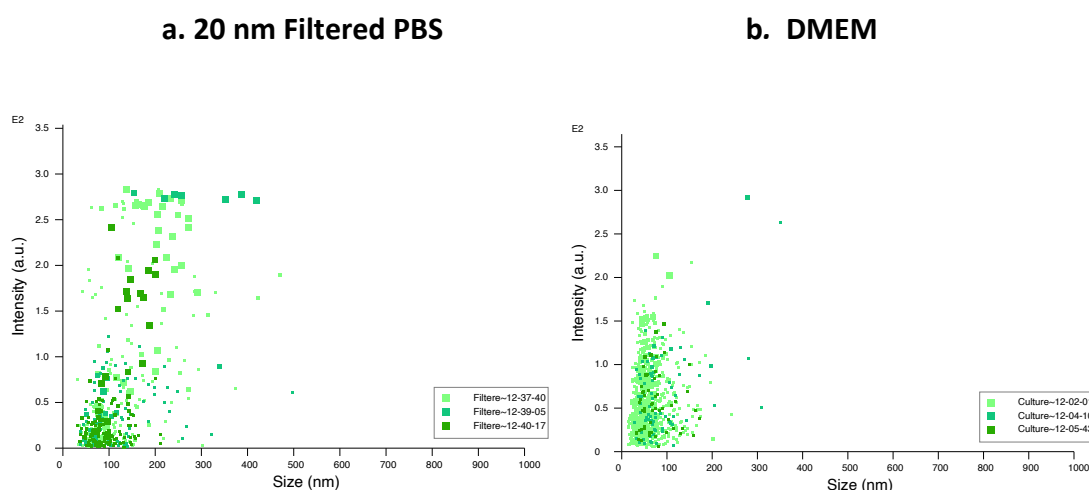


Figure 3.10. NTA output of size (nm) vs. intensity (a.u.) for both **filtered PBS (a)** and **DMEM (b)**

Table 3.1 - Results from three comparative runs of the Filtered (20 nm) PBS and the DMEM particles/frame plus a calculated average particles/frame across the three runs

Filtered PBS	Particles/frame	Standard Deviation
Run 1	36.6	+36.6
Run 2	4.9	+1.6
Run 3	1	+0.6
Average Particles/frame	14.17	
Unsupplemented DMEM	Particles/frame	
Run 1	94.9	+93.2
Run 2	5	+3.9
Run 3	3.4	+3.1
Average Particles/frame	34.43	

Statistical comparison of the data from **Table 3.1** with an unpaired T test gave a non-significant value ($p= 0.582$) between the average number of particles/frame in the Filtered PBS and DMEM. This led to the decision that the effluent should be diluted for analysis with DMEM rather than the 20 nm filtered PBS.

It was noted however, that the non-supplemented DMEM, used for dilution, developed a progressively greater number of background particles, relative to the length of time that the bottle had been opened. This is despite the filtered PBS and DMEM being prepared within the Class II tissue culture hood under sterile conditions (**Figure 3.17**). The reason for the increased presence of particles overtime is unknown. However, it may be due to contamination with nanoparticles in the filtered air, precipitation of factors after opening and changing the protected atmosphere or plastic nanoparticles.

Therefore, the DMEM used to dilute the effluent was always 'quality checked' prior to its use with the NTA. Following three runs through the Nanosight, if the readings came back as equal to or below 30 particles/frame, this culture medium would be used for the dilution of the effluent samples.

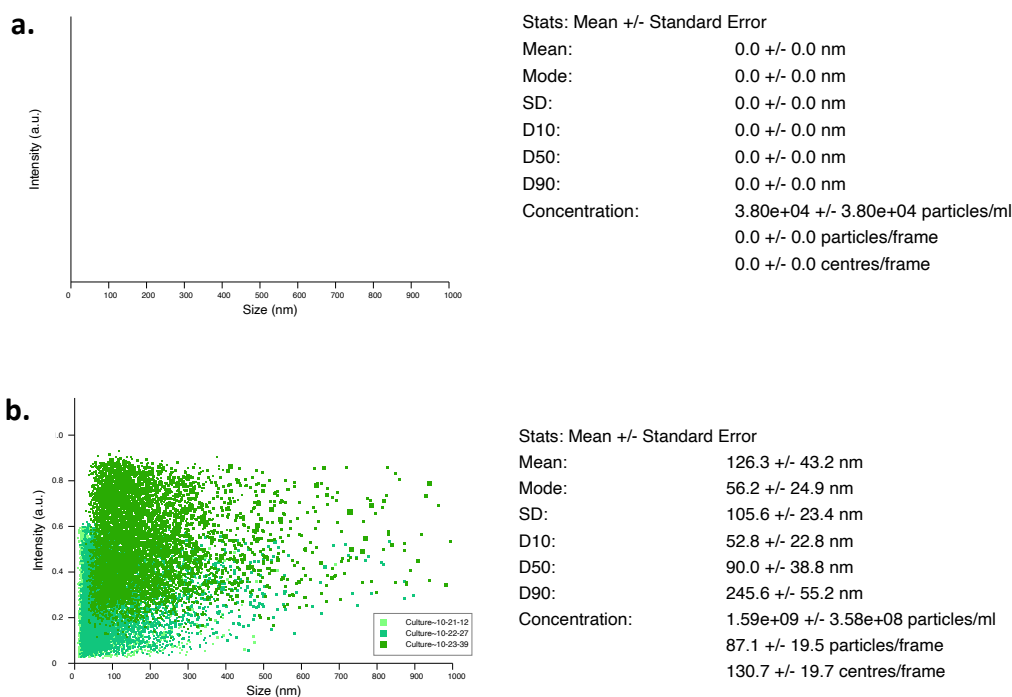


Figure 3.11. NTA output of size (nm) vs. intensity (a.u.) for a **freshly opened bottle of DMEM (Galluzzi et al.)** compared to that of one that has been **open for a 2-week period (b.)** and left in the laboratory fridge with the lid closed

3.7.3 – Degradation of Polypropylene into Plastic Nanoparticles

With the evidence of the increase in particles in the DMEM overtime, this raised concerns surrounding the degradation of the plastic syringes that houses the input medium. There is widespread acknowledgement of the presence of plastic microparticles from the degradation of plastics within the marine environment (Viel et al., 2023). It is known that polypropylene, polyethylene and polystyrene are all sources of microplastics. The syringe and the plastic tubes used to store the daily effluent were made of polypropylene which is as a polyolefin and a high-molecular weight hydrocarbon. Polypropylene tubes 15 ml, (Sarstedt) were used to collect the effluent in addition to the DMEM syringe input which was housed in a 20 ml BD polypropylene

plastic syringe (Becton Dickinson) for a period of six days. Polypropylene has been shown to produce microplastics at a rate three times that of polystyrene (Nakatani, 2021). Degradation within the natural environment is thought to occur due to photodegradation from sunshine irradiation alongside autoxidation. The polypropylene within the current study was kept out of direct sunlight within the laboratory, but there may have been a level of plastic degradation within the experimental set-up overtime.

In order to determine whether the nanoplastics were contributing to the readings obtained in this study, glass syringes were tested alongside the plastic syringes (**Figure 3.12**).

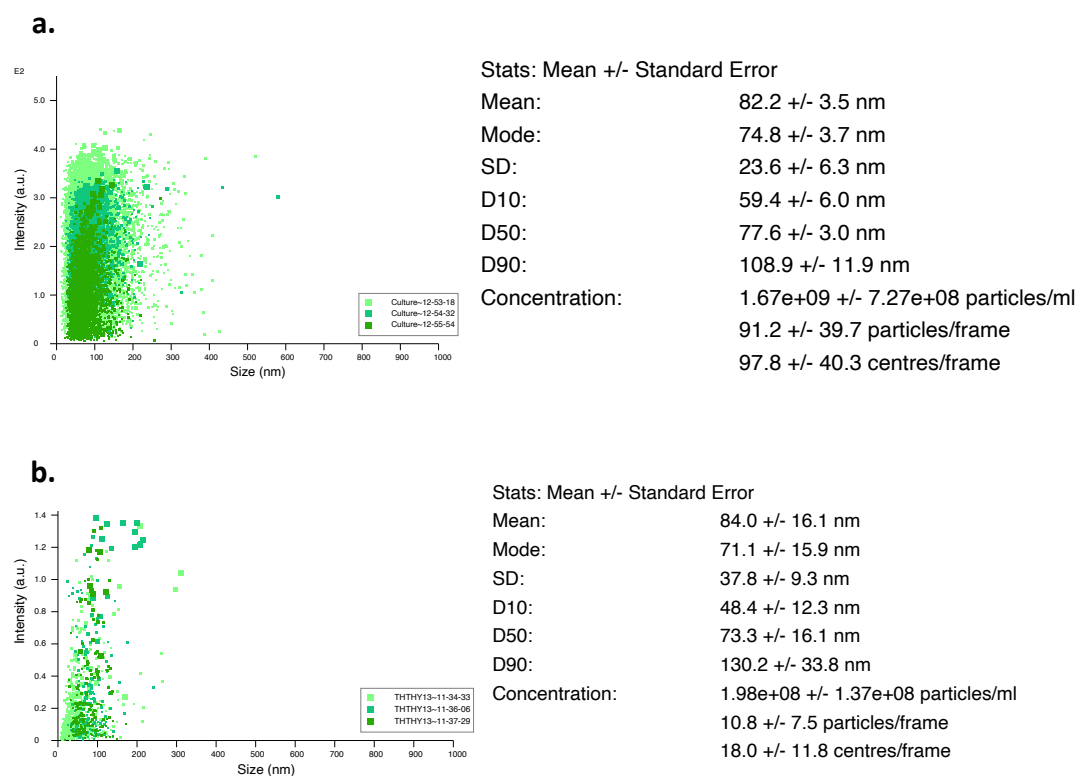
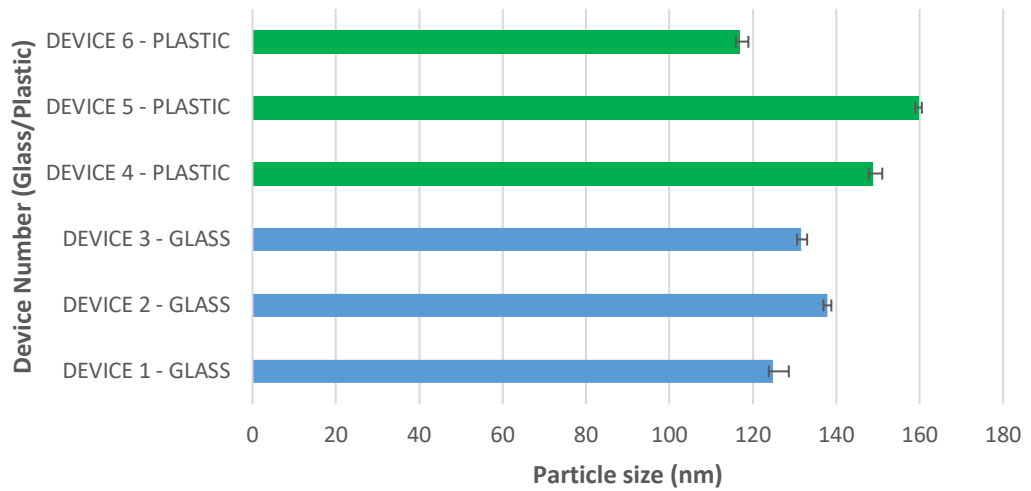


Figure 3.12. NTA output of size (nm) vs. intensity (a.u.) for DMEM that has been left in the **plastic syringe (a.)** and a **glass syringe (b.)** for 1 week

Trial of the glass syringes alongside the standard plastic syringes took place over a 4-day period. Particle size (nm) and Particles/ml were both examined to attempt to identify if there was any significant difference in the readings obtained in the plastic syringes compared to those of the glass syringes. The range in raw data for the devices for particle size (nm) for the plastic syringes was 116.9 nm through to 168.6 nm whilst in the glass syringes the range was 114.4 nm through to 144.5 nm. There was greater

variability with the particles/ml readings from the plastic syringe across the four days with the range in the glass being from 5.64E+08 to 2.94E+09 and the plastic readings being from 4.40E+07 to 3.26E+09 particles/ml. No significant difference in particle size or concentration was observed between the medium housed in plastic or glass syringes; particle size (nm) ($p = 0.20$) and particles/ml ($p = 0.26$), unpaired t test (**Figure 3.13** and **3.14**).

a.



b.

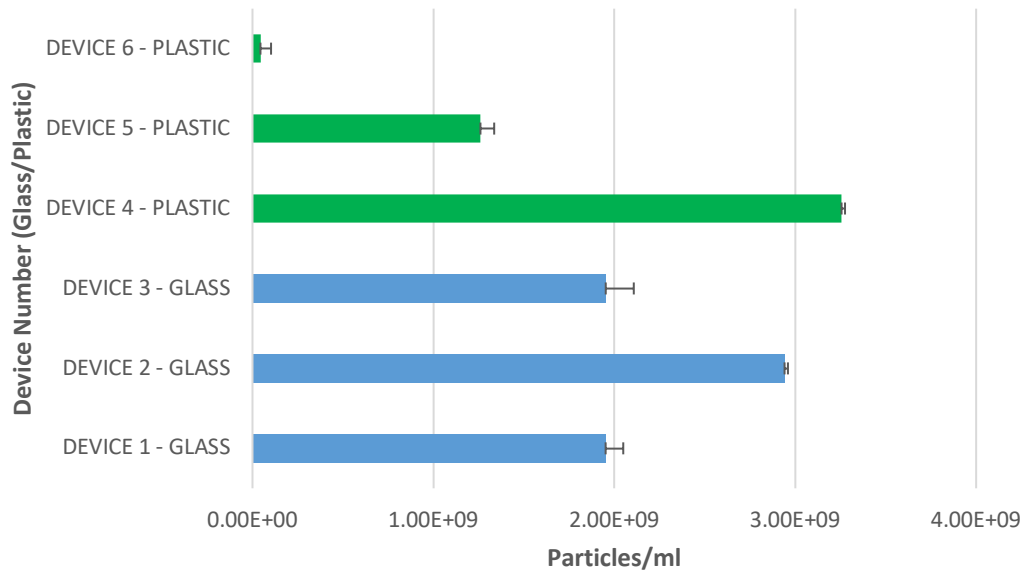


Figure 3.13. Comparison of particle size (nm) and particles/ml in **sample m** (Appendix 4, Table 4.1) day 4 effluent that has been run through a ‘tissue-on-chip’ device using either plastic or glass syringes for each individual device
a. Sample m. particle mean size (nm; x axis) in effluent run through the tissue-on-chip device using either plastic or glass syringes (y axis)
b. Sample m. particles/ml (x axis) in effluent run through the tissue-on-chip device via either plastic syringes or glass syringes (y axis)

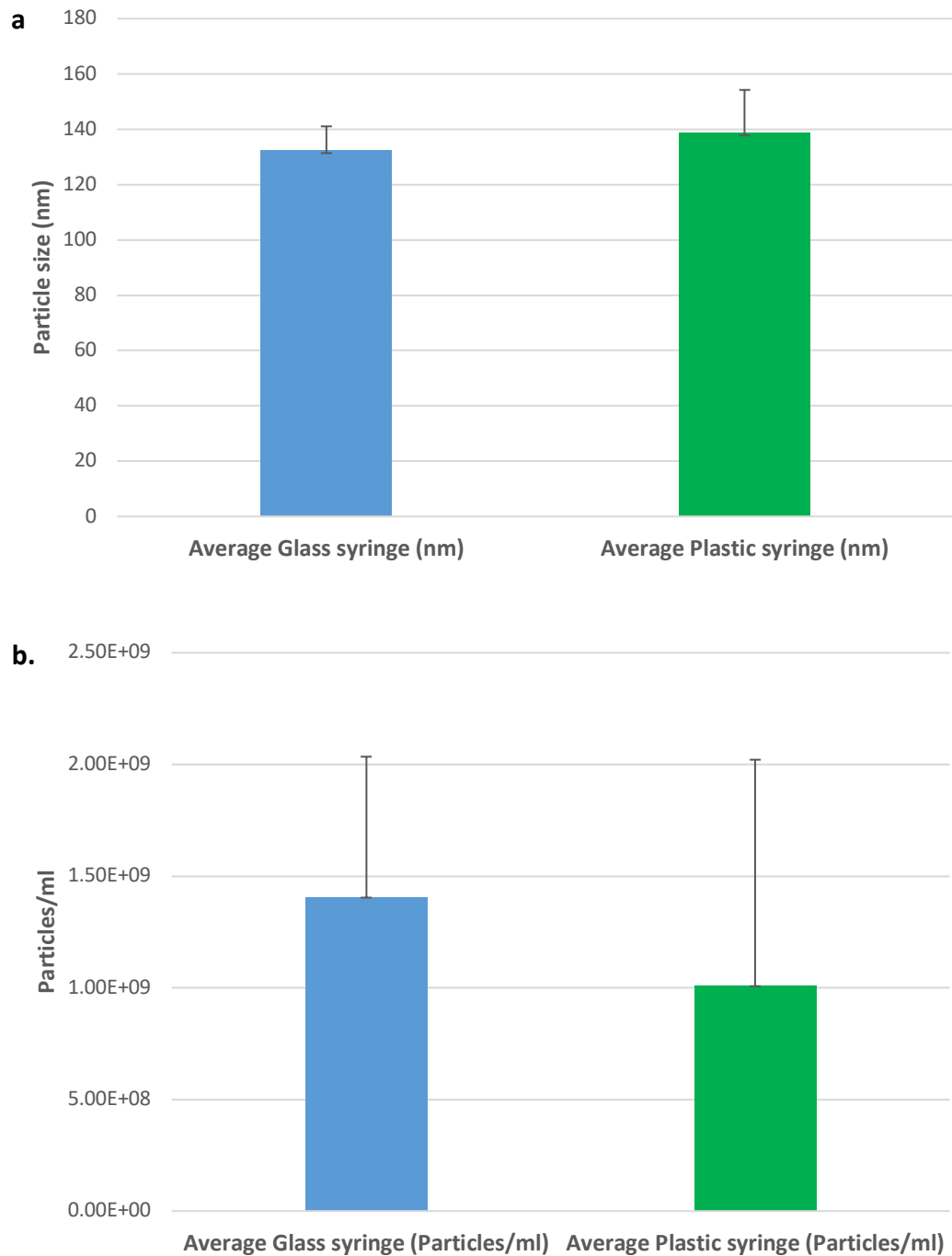


Figure 3.14. Average particle size (nm) (a.) average particles/ml (b.) in the glass or plastic syringes across the four days

With these findings demonstrating no statistically significant difference between the plastic or glass syringes, along with the fact that there were multiple issues with the glass syringes sticking leading to the syringe pumps stalling, the decision was made to continue with plastic syringes due to their reliability. The effects of any plastic nanoparticle production could be accounted for by measuring the input media alone at each time point and subtracting from the value for the effluent.

3.8 – NTA determination of Particle Size (nm) and Concentration in Particles/ml/mg in the tissue-on-chip effluent of EMG, GD and TC Tissue maintained on a PEEK *ex vivo* device

3.8.1 – Particle size

The aim was to identify if there was a statistically significant difference in sEV particle mean size between the EMG, GD and PTC pathologies. For each sample studied, a mean size with standard deviation was obtained for each day of collection. There was a noted variability in size between the devices from the same patient, highlighted in the figure showing all devices for sample I (**Appendix 4; Table 4.1**) on Day 3 (**Figure 3.15**).

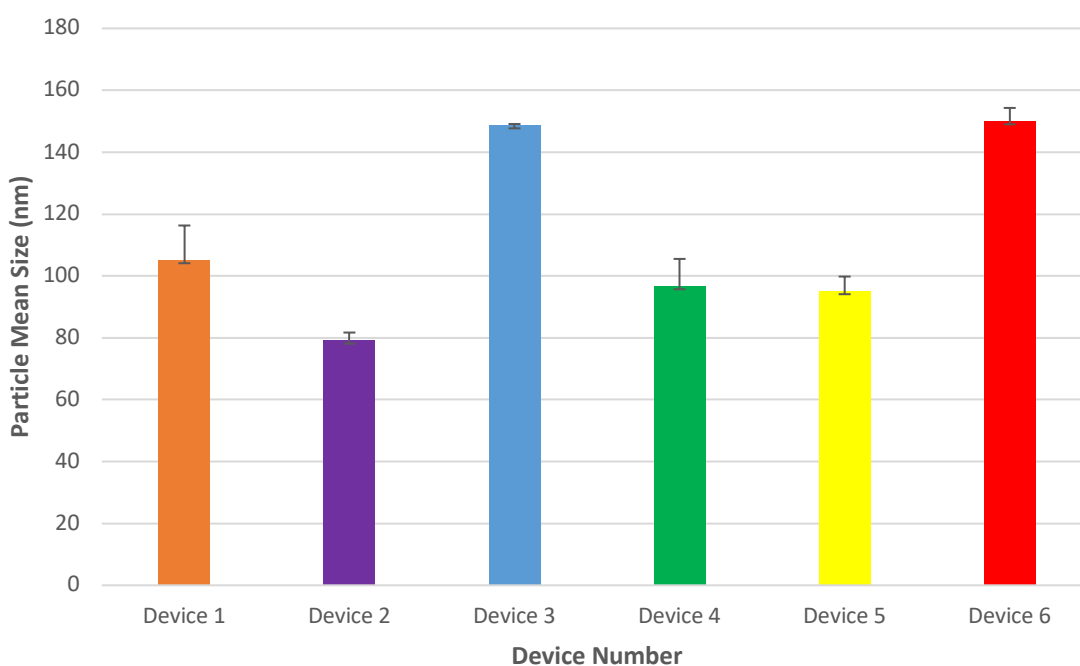


Figure 3.15. Sample I, GD Day 3 – particle mean size (nm) vs. device number (1 to 6). Error bars = standard deviation (STDEV). NTA three runs performed per device sample

In total, thirteen samples were analysed, but only eleven were run at a dilution of 1:8 thus allowing for their direct comparison (**Appendix 4; Table 4.1**). The first two samples, **a.** and **b.** were used for optimisation studies as previously outlined (**Section 3.7.1**). Seven of the analysed samples were TC ($n = 7$), with 4 of these being PTC, 1 of which was FTC, and 2 being Hürthle Cell neoplasms. With regards to the other thyroid pathologies studied, 2 were GD ($n = 2$) and 3 were EMG ($n = 3$) (**Appendix 4**).

The samples which were excluded from the overall analysis were **A.** – Hürthle Cell Carcinoma and **H.** – GD. The rationale behind this was that their effluent samples could not be directly compared to the others in the study as the effluent had not been diluted at the uniform 1 in 8 dilution factor.

The data from **sample G.** and **sample M.** despite being performed with glass syringes and glass collection tubes, were included in the overall analysis and comparison. The individualised graphs for particle size (nm) for each sample are located in **Appendix 4** for review. There was variability but no trends were observed.

Over the 6-day maintenance period on the tissue-on-chip device, the effluent coming from the chip was collected daily from all 11 patient samples and analysed using NTA for particle size (nm) (**Figure 3.16**). The average size of particles released from the EMG ($n = 3$), GD ($n = 2$) and TC tissue ($n = 6$) samples, over the 6-day period was 116.9 ± 16.8 nm, 140.1 ± 41.4 nm and 131.3 ± 16.8 nm respectively. In all the cases, the size range was between 80 nm and 187 nm, falling within the expected range for exosomes/sEVs demonstrating no significant change over time (Two Way ANOVA).

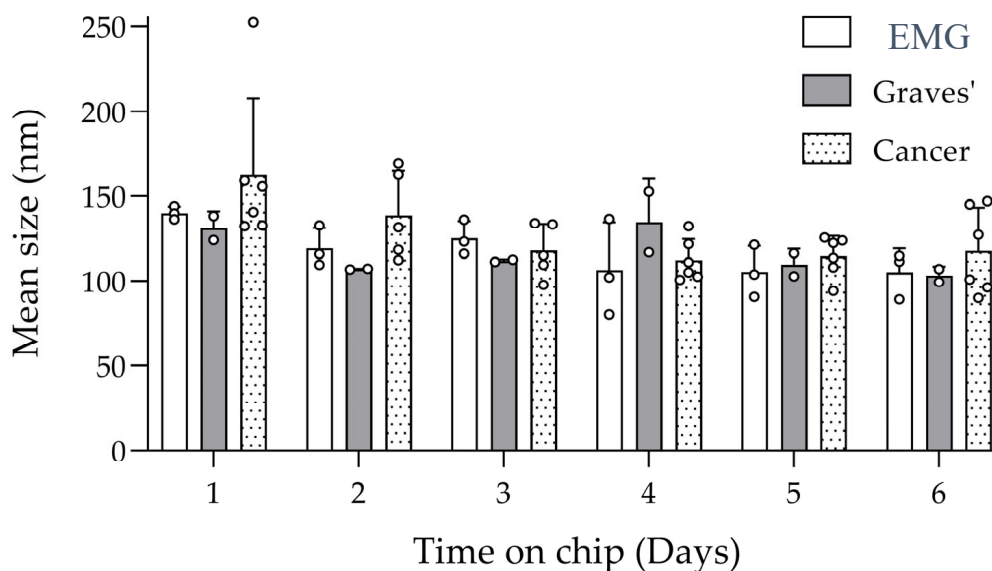


Figure 3.16 - NTA of EVs showing particle mean size (nm) in the effluent (1:8 dilution with serum-free DMEM) collected from EMG ($n = 3$), GD ($n = 2$) and TC ($n = 6$), tissue maintained for 6 days on a tissue-on-chip device. No significant difference in particle size was observed over time (p value – 0.1960) or between tissue types (p value – 0.9752) (two-way Analysis of Variance [ANOVA] with Bonferroni post-hoc correction).

The mean number of particles/ml/mg produced by the thyroid tissue over a 6-day period demonstrated that the concentration of particles between samples was variable, having normalised the different weights of starting material; values ranged between 1.1×10^6 and 2.84×10^8 particles/mL/mg (**Figure 3.17**).

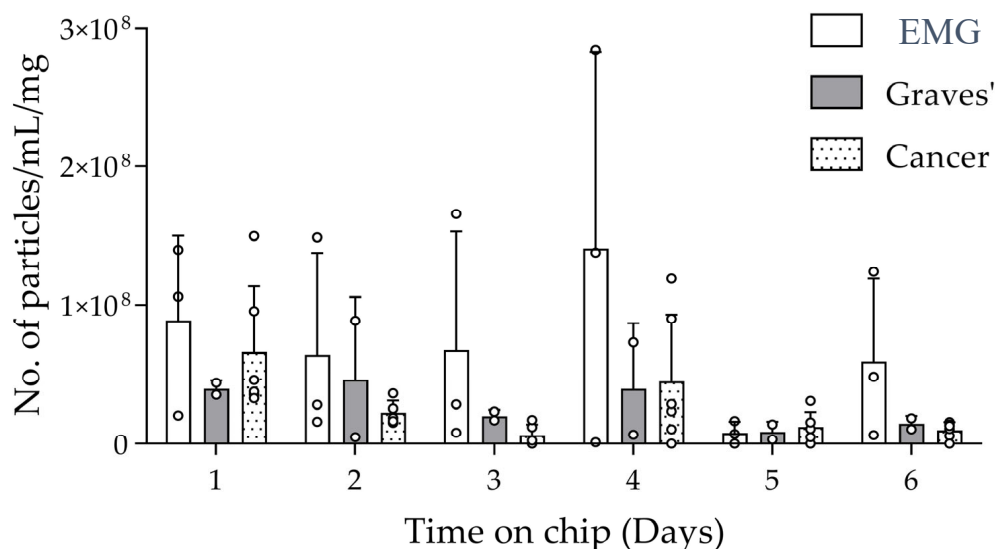


Figure 3.17 - NTA of EVs showing particle concentration (particles/ml/mg) in the effluent (1:8 dilution with serum-free medium), collected from EMG ($n = 3$), GD ($n = 2$) and TC ($n = 6$) tissue maintained for 6 days on a tissue-on-chip device. No significant difference in particle size or concentration was observed over time (p value – 0.0534) or between tissue types (two-way Analysis of Variance [ANOVA] with Bonferroni post-hoc correction)

The means of the EMG sample were greater than the other pathologies on 5 out of 6 days of measurement. Despite the observed variation this was not statistically significant, either between different pathologies or as a result of the time the tissue had spent on the 'tissue-on-chip' device. As an overall summary, both days 1 and day 4 demonstrate the greatest number of particles/ml/mg produced. The tissue on chip seemed to be the most productive in terms of particles produced on day 4 which may suggest that the tissue may have adapted to its' tissue-on-chip environment

3.9 - Western Blotting Analysis of Thyroid sEVs and Tissue Lysates

MISEV guidelines specify that alongside the quantification of EVs, one should identify protein markers that are specific for exosomal content (Théry et al., 2018). Currently, no clear gold standard method exists for the isolation and identification of exosomes. Exosomes have up until now been predominantly isolated through differential

ultracentrifugation, but additionally now there are number of products on the market such as ExoQuick (Palo Alto, California, USA) and Total Exosome Isolation Reagent (ThermoFisher Scientific, Waltham, USA), which allow for rapid exosome isolation. Rather than relying on one method for exosome identification, a combination of methods are advised (Théry et al., 2018). These include transmission electron microscopy along with various instruments for analysis of nanosized objects (e.g., ZetaViewTM, qNanoTM, and NanoSightTM systems), and WB for verification using markers such as CD9, CD63, and CD81 tetraspanins, known to be expressed on sEVs (JA et al., 2024; Welsh et al., 2024).

3.9.1 - The Detection of Exosomal Tetraspanins

EVs are highly enriched in tetraspanins (Andreu et al., 2014). Tetraspanins are integral membrane proteins expressed on the cell surface and are able to interact with a large number of transmembrane and cytosolic signalling proteins (Hemler, 2005). The tetraspanins CD9, CD63, CD81, CD82 and CD151 have all been identified on a number of endocytic membranes and are recognised as exosomal markers (Andreu et al., 2014). CD9 was the first identified exosomal marker by Théry *et al.* in dendritic cells (Théry et al., 1999). The tetraspanins CD9, CD63 and CD81 are the established markers of sEV (Kowal et al., 2016) (**Table 3.2**).

Table 3.2 - The role of CD9, CD63 and CD81 and their respective molecular weights (kDa)

Tetraspanin	Details	Molecular Weight
CD9	A type IV transmembrane glycoprotein. It is thought that CD9 plays a role in cell-cell adhesion and signal transduction.	24kDa
CD63	A lysosomal membrane glycoprotein that translocates to the plasma membrane following platelet activation.	CD63 core protein: 26 kDa Glycosylated CD63: 30-60 kDa
CD81	A type III transmembrane protein. It is believed to be involved in both cell growth and signal transduction.	22-26 kDa

WB is the most commonly used method used to detect EV proteins (Welsh, 2024, Minimal information for studies of extracellular vesicles (MISEV 2023: From basic to

advanced approaches). The MISEV guidelines specify that the EV samples should be loaded side by side from the source in a specified amount.

3.9.2 - WB in Thyroid Exosome Detection

Two studies to date have looked at identifying levels of exosomal molecular chaperones in thyroid cancers with the aid of WB. Luo *et al.* looked to compare the proteome profiles of serum purified-exosomes (SPEs) from PTC patients with lymph node metastasis (LNM) ($n=3$), compared to that of PTC patients without LNM ($n=3$) and healthy donors ($n=3$) (Luo et al., 2018). The study was able to identify 697 differentially expressed proteins in the SPEs of PTC patients with LNM. Serum samples from the patients were ultracentrifuged to isolate the exosomes and the exosomal markers CD63 and Annexin 1 were validated through WB analysis. Alongside this, specific proteins associated with cancer cell metastasis talin-1 (TLN1), integrin beta chain-2 (ITGB2), proto-oncogene SRC (SRC) and calpain small subunit 1 (CAPNS1) were significantly more expressed in the serum exosomes of a patient with TC LNM, compared to those without LNM on WB (**Figure 3.18**).

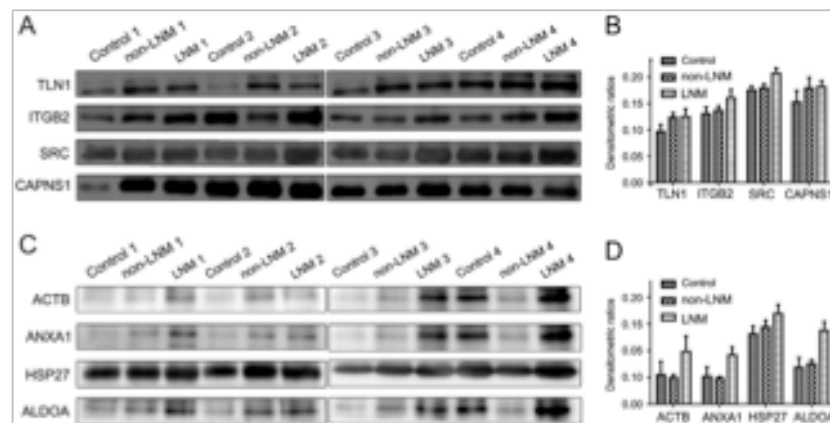


Figure 3.18 – A and C. WB validation of differentially expressed proteins in serum-derived exosomes from thyroid cancer patients. ‘Control 1-4’ are healthy volunteers, ‘non-LNM 1-4’ – PTC patients without LNM and ‘LNM 1-4’ – PTC with LNM B and D. histogram demonstrating optical density of each immunoreactive band

The results obtained demonstrated a similar pattern to that of the mass spectrometry results, but due to small sample size, statistically significant differential expression of the proteins was not demonstrated.

Chaperone proteins have been attributed to the development and progression of cancer. Findings have suggested that the number of chaperone proteins can be attributed to tumour cells having an accelerated metabolism, growth, and division rate. These chaperone proteins can be pathogenic and cause diseases being known as chaperonopathies (Paladino et al., 2021). Carusso Bavisotto *et al.* looked at the levels of chaperone proteins within circulating plasma exosomes (Caruso Bavisotto et al., 2019). The chaperone proteins Hsp27, Hsp60, Hsp70 and Hsp90 along with Alix and CD81 were quantified in the plasma exosomes of patients with PTC and benign goitre, before and after thyroid surgeries using WB (**Figure 3.19**). The chaperone proteins of Hsp27, Hsp60 and Hsp90 were present in the exosomes of both benign and PTC. In the PTC cohort, the levels of the heat shock proteins were higher prior to surgery than in the benign goitre patients (**Figure 3.19A.**). In the benign group, the chaperones were more localised to that of physiological sites, whilst in the PTC they were more abundant within the cytoplasm. Carusso *et al.* from their findings concluded that the chaperone proteins may themselves be secreted by EV and be contributing to carcinogenesis alongside holding promise as biomarkers.

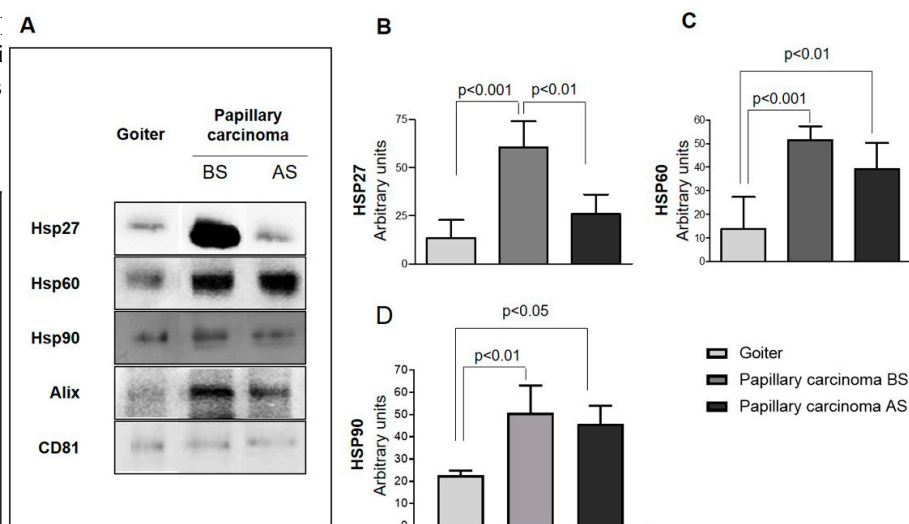


Figure 3.19 – Comparative WB data looking at exosomal molecular chaperones for PTC before and after surgery along with goitre

A. WB showing the presence and levels of Hsp27, Hsp60 and Hsp90 before (**BS**) and after (**AS**) surgery and in benign goitre

B. Hsp27 – higher prior to PTC removal ($p < 0.01$) and relative to benign goitre ($p < 0.001$)

C. Hsp60 - higher prior ($p < 0.01$) to and after PTC ($p < 0.001$) removal relative to benign goitre

D. Hsp90 - higher prior ($p < 0.01$) to and after PTC ($p < 0.05$) removal relative to benign goitre

WB for tetraspanins on thyroid EV, isolated from thyroid tissue maintained on chip, has not been performed to date, apart from the previous work in the group by Foster *et al* (Foster et al., 2021). This work therefore builds upon this previous body of work, but also looks to evaluate the presence of exosomal markers within TC, Graves and EMG thyroid disease.

3.10 - WB Analysis of 'Tissue-on-Chip' Thyroid Exosomal Samples

The effluents from the tissue-on-chip devices were combined from all chips setup from two patient samples; one with Hürthle cell carcinoma and one with GD. More samples would have had WB analysis performed, but due to a lack of consistency in the results, the decision was made to move onto isolating the RNA. The day 1 effluent was omitted for all samples so that any cellular debris brought about by the device setup was excluded. This resulted in a volume of approximately 14 ml of effluent per chip. The sEVs were isolated from the effluent by ultracentrifugation (**Section 2.6**).

WB analysis (**Section 2.7**) using the protocol established by Kowal *et al.* 2017 (Kowal et al., 2017), using the ThermoFisher Bolt System (ThermoFischer Scientific, Waltham, USA), was then used to determine the expression of the tetraspanins CD9, CD63 and CD81. Following protein extraction using RIPA buffer (**Section 2.7.1**) the Bioinchronic Acid (BCA) assay was used to determine protein concentration.

BCA Protein Assay was performed on both the HCC exosomal lysate sample and the GD exosomal lysate sample prior to the WB in order to determine protein concentration.

3.10.1 - Exosome Lysate WB - TC - Hürthle Cell Carcinoma (HCC)

WB has been performed exosome lysates with the aim of identifying the classical exosomal markers CD63, CD81, and CD9 through the use of primary antibodies (**Section 2.7**) (see **Table 3.2**). Exosomal and cell lysates obtained from cell lines that are known to express these exosomal markers were run alongside the exosomal lysates from the tissue-on-chip device as positive controls; U87 cell lysate from glioblastoma, UMSCC exosomal lysate (floor of mouth SCC cell line), FaDu cell line exosome lysate from pharyngeal SCC. The Magic Mark™ XP Western protein standard was used to enable

protein molecular weight estimation directly on the WB. SeeBlue Pre-Stained Standard was used to help monitor protein electrophoresis and the efficiency of western transfer.

The first WB was ran with 30 μ l of the HCC exosome lysate. This was performed with the antibodies to CD9, CD63 and CD81 (1 in 500 concentration). The first blot failed and as a result this WB had to be redone. Fortunately, the second attempt led to detection of CD63 in the HCC exosome lysate in lane 5 (**Figure 3.20A**). Alongside this, CD81 and CD63 were detected in the cell line positive controls U87 cell lysate (**lane 2**), and UMSCC 12 (**lane 3**) exosome lysate.

As only quite a weak smear for CD63 and no CD81 was observed in the HCC exosome lysate it was decided to increase the volume of lysate added to the gel from 30 μ l to 60 μ l in order to increase the likelihood of detecting the exosomal markers (**Figure 3.26B**). CD63 and CD81 were detected in both UMSCC 12 exosome lysate (**lane 4**) and FadU exosome lysate (**lane 6**). CD81 was also detected in the UMSCC 12 exosomes isolated using an Invitrogen kit (**lane 7**). Neither CD63 or CD81 were detected in the HCC Exosome Lysate (**lane 9**), despite an increase in the volume of the HCC exosomal lysate added. Consequently, the decision was made to increase the concentration of the primary antibodies to 1 in 250. The same original blot was used and reprobed with the higher antibody concentrations of CD63 and CD81. Following this, strong expression of CD63 was found in the U87 cell lysate and both the Fadu and UMSCC 12 exosome lysates (Lanes 4, 6, 7) (**Figure 3.20C**). There was also detection of the glycosylated form of CD63 in the TC HCC exosome lysate in lane 9 after being left in the cassette for two hours. It has been recognised that different smear patterns can occur depending on the origin of the exosomes (Lötvald et al., 2014). CD81 was also present in all the cell line exosome lysates and the U87 cell line lysate, but was not present in the TC HCC exosomal sample.

Following this, an effort was made to see whether CD81 could be detected within TC HCC exosomal lysate without the presence of CD63. The WB was stripped with WB stripping buffer (**Appendix 3**) with the intention to strip the WB of the prior primary antibodies. A 1 in 500 dilution of CD81 primary antibody was used to detect CD81. Unfortunately, there was an issue with the stripping buffer as the anti-CD63 antibody

was not stripped off the WB and consequently CD63 was still detected on the WB (**Figure 3.20D**).

Despite several attempts at staining, even after stripping and starting again, no CD81 was detectable in the HCC exosomal lysates. Evidence of the CD81 antibody working however is evident from its' detection within other cell lines on the WBs. In this instance, CD9 was not detected but its' appearance would have overlapped with that of CD81, which would have made such detection difficult.

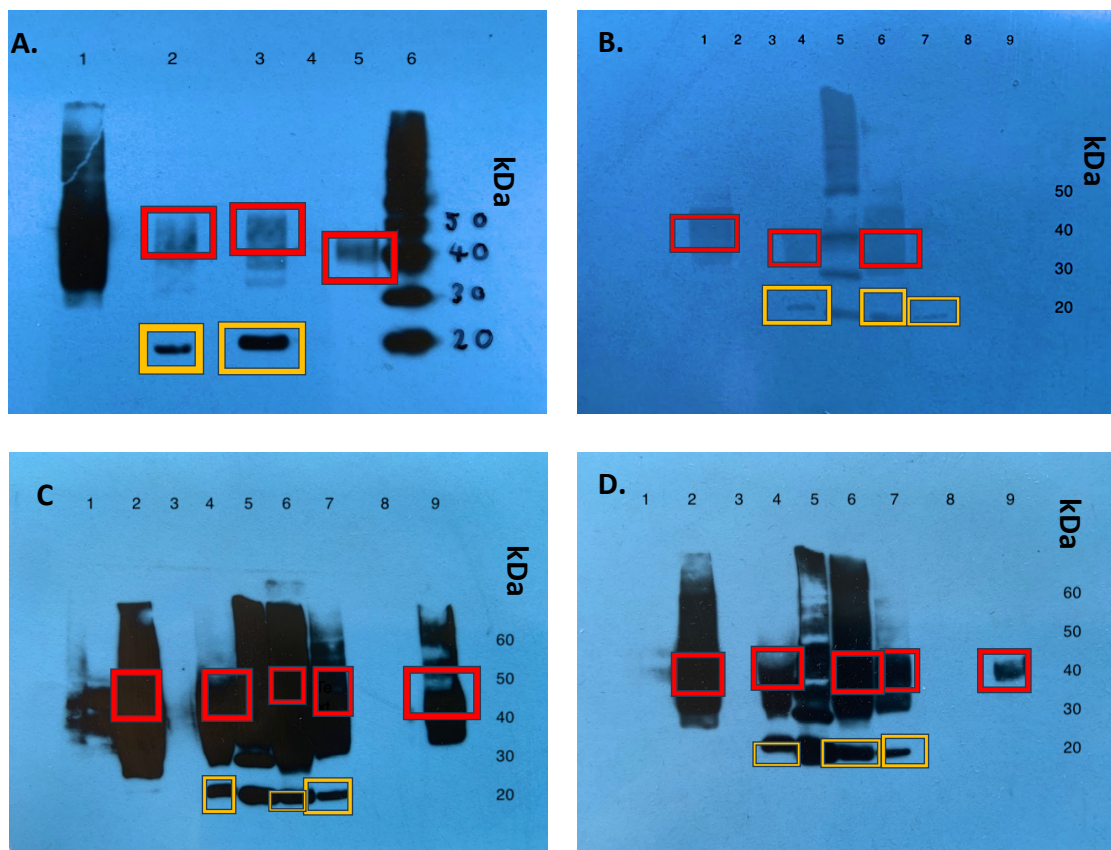


Figure 3.20 – WB of TC Hürthle Cell Carcinoma (HCC) and cell line positive control exosomes

A. Exosome Lysate WB - TC - HCC attempted detection CD63, CD81 and CD9 (1 in 500 dilution)

1 = SeeBlue, 2 = U87 cell lysate (5 µg), 3 = UMSCC 12 exosome lysate (5 µg), 4 = FaDu exosome lysate (5 µg), 5 = HCC Exosome Lysate (30 µl), 6 = Magic Mark

WB demonstrating detection of glycosylated **CD63 (red box)** (30-60 kDa) exosomal marker in the HCC exosome lysate (**lane 5**) and **CD81 (orange box)** (26 kDa) in U87 cell lysate (**lane 2**) and UMSCC exosome lysate (**lane 3**).

B. Exosome Lysate WB - TC HCC (60 µl) – attempted detection of CD63 and CD81 (1 in 500 dilution)

1 = SeeBlue, 2 = U87 cell lysate (5 µg), 4 = UMSCC 12 exosome lysate (5 µg), 5 = Magic Mark, 6 = FadU exosome lysate (5 µg), 7 = UMSCC 12 exosome lysate (5 µg), 9 = HCC Exosome Lysate (60 µl)

C. Exosome Lysate WB - TC HCC (60 µl) – attempted detection of CD63 and CD81 (1 in 250 dilution)

1 = SeeBlue, 2 = U87 cell lysate (5 µg), 4 = UMSCC 12 exosome lysate (5 µg), 5 = Magic Mark, 6 = FaDu exosome lysate (5 µg), 7 = UMSCC 12 exosome lysate (5 µg), 9 = HCC Exosome Lysate (60µl)

D. Exosome Lysate WB - TC HCC (60 µl) – attempted detection of CD81 (1 in 500)

1 = SeeBlue, 2 = U87 cell lysate (5 µg), 4 = UMSCC 12 exosome lysate (5 µg), 5 = Magic Mark, 6 = FaDu exosome lysate (5 µg), 7 = UMSCC 12 exosome lysate (5 µg), 9 = HCC Exosome Lysate (60 µl)

3.10.2 - Exosome and Tissue Lysate WB - GD

Both exosomes collected from the effluent coming off GD maintained on the ‘tissue on-chip’ device following ultracentrifugation (**Section 2.3**) and a tissue biopsy of GD were lysed using RIPA buffer as outlined in the Materials and Methods (**Section 2.7**). The amount of protein in the lysate was determined using the Pierce™ BCA Protein Assay Kit (**Section 2.7.1**) and amounts were added to the gel as detailed in the figures. The gel was run and the WB carried out (**Section 2.7**), using CD63 and CD81 antibodies at a 1:500 dilution. However, in order to prevent the CD63 blotting obscuring the CD81, the CD81 was added first and then the film developed (**Figure 3.21A**), before the CD63 was subsequently added and the film developed again (**Figure 3.21B**). CD81 (orange box) was detected in the UMSCC exosome lysate (**lane 2**) as well as the GD tissue lysate using both 8.2µg (**lane 6**) and 16.4µg (**lane 8**) of lysate, but was not detected in the exosomes isolated from the GD tissue effluent (**lane 4**). Using the same WB, the CD63 antibody was then added to the WB membrane overnight at a 1 in 500 dilution. The added CD63 (red box) was detected in the GD exosome lysate (**lane 4**), and both of the tissue lysates (**lane 6 and 8**) as well as the UMSCC exosome lysate (**lane 2**).

B.

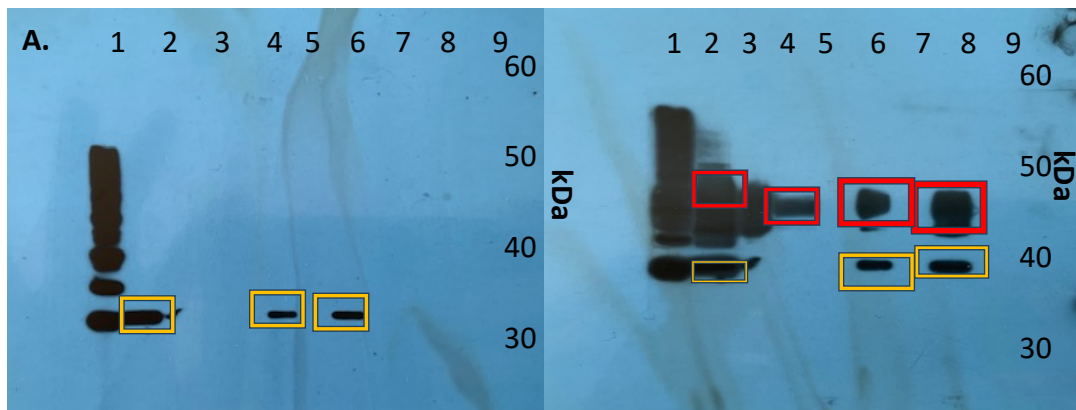


Figure 3.21 – WB of GD exosomal and tissue lysate and cell line positive control exosomes for attempted detection of exosomal markers **CD63 (red box)** and **CD81 (orange box)**

A. GD Exosome Lysate (8.2 µg) and Tissue Lysate (8.2 µg and 16.4 µg) – attempted detection of CD81 (1 in 500)

1 = Magic Mark, 2 = UMSCC12 exosome lysate (8.2 µg), 4 = GD Exosome Lysate (8.2 µg), 6 = GD Tissue Lysate (8.2 µg), 8 = GD Tissue Lysate (16.4 µg), 9 = SeeBlue

B. GD Exosome Lysate (8.2 µg) and Tissue Lysate (8.2 µg and 16.4 µg) – attempted detection of CD63 (1 in 500). The same blot as in A) was used and CD63 applied on top of the CD81.

3.11 - Discussion

3.11.1 - Histo-Architectural Analysis

The morphology of both freshly resected and post-on-chip culture (144 hours) *ex vivo* thyroid tissue sections was assessed by H&E staining by Dr Karsai, Consultant Head and Neck Pathologist at Hull University Teaching Hospitals NHS Trust; overall samples showed preservation of gross follicular morphology, with retention of tissue cohesion. This was true across the pathologies studied, of EMG, GD and PTC. Intra-tumour variation in cellularity and follicle size was clear, however these differences are retained in tumour tissue throughout culture (**Figure 3.2**). Previous work by Riley *et al.*, (2019) had validated the PCTS device but only for 96 hours, the current work further demonstrates the capabilities of this ‘tissue-on-chip’ device in terms of maintenance of thyroid tissue as the cellular architecture appears both intact and viable at 144 hours. This is the case with regards to three different types of thyroid tissue; EMG, Graves’ and PTC (Haigh *et al.*, 2023).

Riley *et al.*, utilised a Lactate DeHydrogenase (LDH) assay to assess cell membrane integrity throughout the 96-hour period (Kennedy *et al.*, 2019; Riley *et al.*, 2019). As

anticipated, levels of LDH were high at the beginning of the culture period and then decreased for the remainder of the experiment which they suggested showed that the thyroid tissue following introduction onto the 'tissue-on-chip' environment was able to recover from the initial insult and cellular damage that takes place during the set up. During the current study, levels of LDH were not measured as prior work performed by Foster *et al.* (2021) in which intentional lysis of thyroid tissue was carried out at 117 hours demonstrated a significant increase in LDH levels which was suggestive that the tissue was still viable at this time point, and was in line with other work by the group in head and neck squamous cell carcinoma (HNSCC) (Carr *et al.*, 2014; Cheah *et al.*, 2017; Kennedy *et al.*, 2019).

A further point of interest would be to determine whether certain types of thyroid tissue are able to adapt more effectively to the 'tissue-on-chip' environment. For instance, does the 'tissue-on-chip' environment suit the EMG non-diseased tissue rather than the malignant disease. This was examined by Riley *et al.* who measured thyroid hormone production (T4), and identified that the EMG tissue produced a significantly higher amount of T4 than the malignant thyroid tissue on chip. This fits with the fact malignancy results in functional differentiation and diminished expression of proteins central to thyroid hormone production and consequently reduced T4 production (Riley *et al.*, 2019).

3.11.2 – NTA Discussion

The Nanosight LM10 has enabled the detection of nanoparticles in the secretome released from different thyroid pathologies maintained on a 'tissue-on-chip' device. The mean size range of the particles produced by the three separate thyroid pathologies was between 80 nm and 187 nm which is in the size range expected of sEVs (Théry *et al.*, 2018). The unique PEEK 'tissue-on-chip' device used in the current study coupled with the use of exosome depleted medium and the methodology, enables one to be confident that sEVs are being isolated from maintained thyroid 'tissue-on-chip'.

3.11.2.1 – Particle mean size

The mean size of the nanoparticles detected at day one was increased when compared to the particle size of day two through to day six, however, this difference was not

statistically significant (p value – 0.1960). The increased particle size detected at day one was thought to be brought about through the preparation of the sample. The fine slicing of the tissue on the vibratome, along with further tissue manipulation during the weighing of the tissue and subsequent loading of it on the perfusion device will have resulted in cellular disruption. The cellular debris produced as a result of this disruption will culminate in a greater number of particles/ml but also have contributed to the release of particles with a greater mean size than that expected of sEVs. This day one finding may have been contributed to by non-vesicular extracellular particles (Jeppesen et al., 2023). These findings back up those made by Foster *et al.* 2021 in which particle size was again detected to be at its highest at day 1 but then subsequently decreased during the six days which was reported to be statistically significant (Foster et al., 2021). Foster *et al.* in their prior works were able to demonstrate that particle size released from the non-GD tissue was greater than that of the GD tissue but this was only deemed to be of statistical significance at one time point (0-4 hour time point). These results were of statistical significance but this is on the back of significant disruption to the tissue in this time frame following device loading. In the current study such a difference in particle size was not found between the different tissue pathology types this in part could be as a result of the small sample size for each respective pathology. In the Foster *et al.* study there was a greater sample size studied with regards to GD ($n = 7$) than when compared to this study ($n = 2$). Alongside this the Foster *et al.* study experienced a statistically significant decrease in particle size ($p < 0.0001$) over time which was not similarly observed in this study.

3.11.2.2 - Particles/ml/mg

Some of the samples that were run on the PEEK ‘tissue-on-chip’ device produced a generally lower number of particles/ml/mg compared to other samples. This was the case for instance in two samples of the same pathology in terms of PTC, **A.** and **C.** (**Table 4.2; Appendix 4**). The reason behind this is that the transfer of the tissue from the operating theatre and its subsequent slicing, handling and mounting may have led to irreversible damage to the tissue which may have had a direct effect upon the tissue’s functionality and capacity in which to produce sEVs. There could however be a number of reasons beyond the control of the laboratory, for instance within the operating

theatre; the thyroid tissue may have been devoid of blood supply prior to removal from the patient due to the nature of the operation or the tissue may not have been immediately placed in DMEM following removal from the patient and host blood supply. These factors would have unfortunately had detrimental effects upon the functionality of the thyroid tissue. The samples highlighted in terms of reduced sEV production were a PTC and hürthle cell carcinoma, which may not have been as resilient to environmental changes as the 'healthy' benign EMG tissue and as a result not recovered well from such an 'insult'. This may have consequently affected their ability in which to adapt to the 'tissue-on-chip' environment.

Particles were detectable in the tissue secretome across the six-day incubation period, however there was substantial variability between the days and between patient samples. Day 1 tended to demonstrate the greatest number of particles/ml/mg across the six-day period which again is most likely linked to the cellular disruption from preparation of the samples (**Appendix 4**). Interestingly, however, at day 4 there tended to be an unexplainable secondary peak in particles/ml/mg. Perhaps, this could in part be due to the tissue adapting to its' on-chip environment and establishing itself following the tissues transfer from an *in vivo* environment to the 'tissue-on-chip' device. It is known that culturing tissue samples with continuous perfusion, as in our study, improves circulation around the tissue biopsies and increases viability of the samples compared to static models and this timepoint may be when this is noticed (Schumacher et al., 2007). This is particularly notable in the EMG tissue, if the day 4 reading of particles/ml/mg is compared to that of the other days. Although only 3 samples of EMG were studied, it does raise the question whether the EMG tissue adapts to the perfusion environment 'better' than diseased thyroid tissue (Imparato et al., 2022). This could in part be further examined in the future through further in-depth study of tissue architecture on day 6 and whether the standard of the histoarchitectural integrity at day 6 correlates with the level of particle production. Alongside this, the level of T4 production by the benign tissue at day 6 could be measured to look at level of 'functionality' of the tissue at this timepoint whilst being maintained on the chip (Riley et al., 2019).

On comparison of our findings with those of other groups, the work has predominantly been performed on plasma or serum samples rather than that of the secretome of

thyroid tissue maintained on a 'tissue-on-chip' hence making direct comparisons limited. Rappa *et al.* identified significantly higher numbers of plasma EVs found in a cohort of 6 PTC patients ($n=6$) ($p = 0.025$) when compared to healthy controls ($n=10$) (Rappa *et al.*, 2019). This is in keeping with general experimental findings of increased exosome production by malignant cells compared to healthy, benign, cells (Zhang, 2020). The comparison in our study is limited by the fact there were no 'healthy' thyroid controls *per se*, as all the patients from whom we received samples had an element of thyroid disease, hence why they were undergoing a thyroid operation. In terms of potentially broaching this question in the future through the examination of plasma or serum samples, ethical approval was obtained which enabled the collection of serum from patients prior to anaesthetic induction *i.e.* with the disease *in situ*. These samples will allow for the future direct comparison of EVs in the serum of patients with different types of TC, GD and further AITDs such as HT. It would be worth considering having serum samples from individuals free of thyroid disease to act as 'healthy controls'.

One could argue from the current results presented that what has been isolated are simply cellular fragmentation from cell disruption and degradation and are not actually sEVs. The MISEV 2024 guidelines do advise an element of caution with the use of NTA to measure the diameter distributions due to the counting of co-isolates such as lipoproteins and large protein complexes along with EVs that are larger than a few hundred nm in size (Welsh, 2024). Hence, attempts were made in which to follow MISEV guidelines order to validate such findings and ensure robust methodology surrounding the isolation and identification of sEVs (Théry *et al.*, 2018). Therefore, a further molecular technique as per the MISEV guidelines was utilised in the form of western blotting (WB) in an attempt to examine and identify sEV markers within the exosomal and tissue lysates of thyroid tissue.

3.11.3 - WB Analysis

The results demonstrate that the exosomal marker CD63 was detectable in the TC HCC and GD exosome lysate. CD81 was detectable in the GD tissue lysate, but not within the exosomal lysate. These results demonstrate that classical exosomal markers can be detected through WB within both the thyroid tissue and exosomal lysate as per the MISEV guidelines. However, these results are not consistent throughout all samples,

despite every effort to ensure that the methodology was consistent throughout the experiments (Kowal et al., 2017). This mirrors the previous findings of Foster *et al.*, in which there was difficulty consistently detecting CD63 and CD81 in Graves' tissue and non-Graves tissue. Foster *et al.* were also unable to detect CD9 as was the case in the current study (Foster et al., 2021). Despite a lack of consistency in detection the results do add further evidence to the presented NTA data, that exosomes are being detected within the 'tissue on-chip' effluent. The WBs that were performed however, were only performed on two different thyroid pathology types and so do not demonstrate results for a broad range of thyroid pathology. A limitation of the study was that a WB was unfortunately not performed on a PTC sample. Future works should focus on identification of these exosomal markers within a broader range of thyroid pathology in an attempt to identify if differential expression of these exosomal markers exists between pathology. In an effort, to quantify and compare expression of exosomal markers in the future, densitometry techniques or Image Lab Software (BioRad, Hercules, USA) could be used to identify differential expression on WB. However, one of the main limitations was the amount of protein extracted from the samples and getting this the same between samples would be a challenge as some will inevitably have more exosomes to extract from than others. Alongside the detection of proteins, the detection of phospholipids present within the lipid bilayers has also been recognised as a means in which to detect the presence of extracellular vesicles (Skotland et al., 2017).

Despite the difficulties in the identification of CD9 in the exosomal lysate, Vlasov *et al.* was able to identify CD9 from a cell line (FRTL-5) originating from the thyroid gland of the Fisher rat grown in plastic culture flasks. Again, differential ultracentrifugation was performed and WB as per alternative protocols for the detection of CD9. Greater CD9 level on detection was shown to be correlated with higher Tg content in the ultracentrifuged pellet (Vlasov et al., 2016). Maggisano's team were able to identify CD63 through WB in two PTC cell lines and non-tumorigenic thyroid cells cultured in DMEM and with exosomes extracted through ExoQuickTC (Systems Bioscience, Pala, USA) (Maggisano, 2022).

The findings despite providing supporting evidence that exosomes are being isolated as per the MISEV guidelines but do not provide any diagnostic utility (Welsh, 2024). As recently emphasised by the MISEV 2024 guidelines, no single molecular class

measurement is able to quantify all EVs and there are no universal molecular markers of EVs. One also has to be aware of the shortcomings that WB possesses on interpreting these results within the context of identifying exosomal markers. WB is very sensitive when it comes to the detection of tiny concentrations of protein and possesses specificity re: the sorting of proteins into different sizes and charges. WB does require a skilled, trained laboratory technician with experience in the technique alongside experience in WB interpretation. The results do need to be interpreted cautiously as an erroneous result can easily result from an antibody reacting with a non-intended protein.

A point that needs to be considered is the process of exosome isolation through differential ultracentrifugation, which is a time intensive task which makes quick, efficient WB analysis difficult. Hopefully, this may be further circumvented through the use of exosome extraction kits and an automated WB process through the Jess Automated western blot machine. This may allow for the rapid assessment and identification of exosomal markers in future studies enabling a large through put of samples which will in turn produce more results. Microfluidics has also demonstrated progress as potential means of exosome isolation through immune-affinity techniques such as the ExoChip which facilitates exosome interaction with anti-CD63 antibodies and incorporates WB analysis (Mousavi et al., 2022).

13.12 – Conclusion

The use of dynamic microfluidic tissue perfusion to maintain functional, thyroxine producing benign and thyroid tumour tissue, for up to 4 days, has been demonstrated previously by Riley *et al.* (Riley et al., 2019). This work was further backed up by Foster et al. using a different microfluidic device whom demonstrated histoarchitectural maintenance at the 6-day mark in both Graves' and 'non-Graves' tissue. The findings by Haigh *et al.* surrounding the histoarchitectural analysis adds to the evidence surrounding the viability of thyroid 'tissue-on-chip' at 144 hours on a range of thyroid pathologies: EMG, Graves and PTC which is over the 96 hours previously demonstrated (Haigh et al., 2023).

In terms of future work, it would be of interest as to determine whether novel thyroid treatment modalities, such as the clinically-used TKIs, if used to treat the tissue-on-chip

have the capability in which to affect the thyroid architecture following treatment or the proliferative index through using IHC techniques such as Ki67 staining. In this respect such technology may be able to demonstrate the responsiveness of certain tumour types to drug regimens and open the door to personalised treatment regimens for TC.

The combination of NTA and WB provide confidence regarding the isolation of exosomes from thyroid tissue-on-chip effluent through differential ultracentrifugation. However, these findings are academic and as yet possess no implications for the diagnosis of thyroid disease. The process of ultracentrifugation of the effluent and consequent detection in exosomal lysates of exosomal markers provides confidence with regards to the isolation of thyroid exosomes through the described methodology (**Section 2.7** and **2.8**). Through the isolation of exosomes and extraction of miRNA and consequent miRNA sequencing the identification of an exosomal miRNA profile specific to a particular thyroid pathology, may help in the elucidation of a diagnostic profile for thyroid disease.

Chapter 4 - The use of miRNA sequencing and RT-qPCR in order to identify differences in miRNA expression in sEV released from EMG, Graves' and PTC tissue

4.1 - miRNA Sequencing Introduction

miRNA as previously described (**Section 1.12.3**), are a class of small RNA molecules (around 22 nucleotides) that have a vital regulatory role in multiple physiological and pathological processes. It has been recognised that miRNAs are vital regulators of cellular processes in the form of survival, proliferation and differentiation (Caterina et al., 2016). Following sequencing, miRNAs have been identified as biomarkers in terms of cancer classification, response to therapy and cancer prognosis (Chakraborty et al., 2023).

miRNA sequencing enables complete miRNA profiling and the identification of potentially unknown miRNA variants within disease states. The technique uses next-generation sequencing techniques (Potla et al., 2020). The miRNA sequencing method facilitates the sequencing of pools of small RNAs in a single sequencing run making it very time efficient. Once all the miRNAs in each sample have been quantified, their consequent expression levels can be compared between samples. In the current study, comparative miRNA levels between PTC, Graves' and EMG tissue have been investigated. After the normalisation of the number of mapped reads between the samples, statistical testing can then be used to determine differential gene expression. The miRNA sequencing workflow involves three main steps: The isolation of RNA; cDNA library construction and microRNA sequencing.

4.1.1 - Preparation of samples for miRNA sequencing

Twenty-four thyroid samples: Graves' ($n=6$), EMG ($n=6$) and TC ($n=11$), were processed for 'tissue on chip' incubation (Table 2.1).

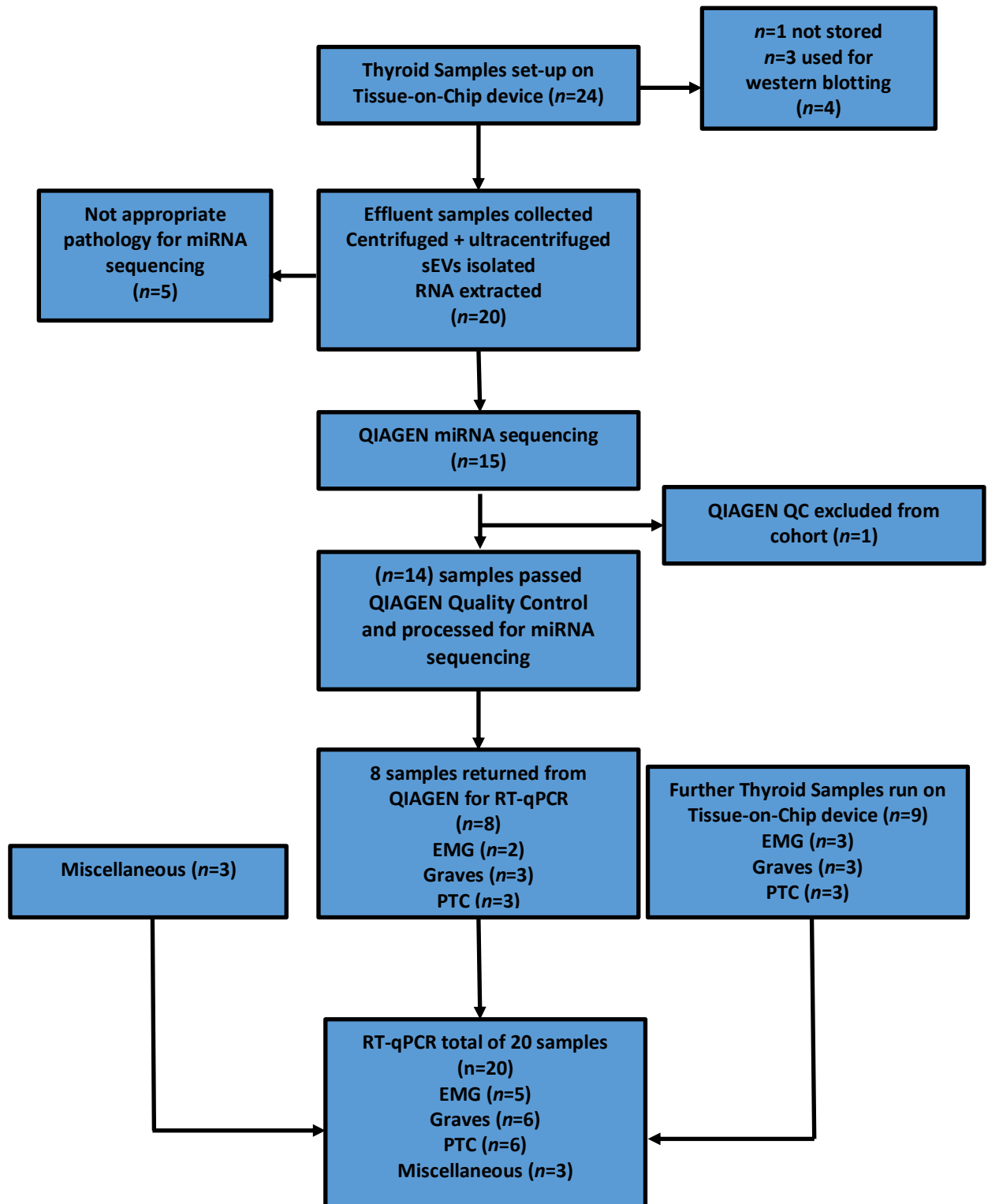


Figure 4.1 - Flow Chart demonstrating the processing of samples through miRNA sequencing and RT-qPCR

Effluent was collected from all devices over a 6-day period and processed for centrifugation and ultracentrifugation in order to isolate the exosomes (**Section 2.6**) for RNA extraction (**Section 2.8**).

Fifteen samples (**Table 4.1**), split equally between EMG ($n=5$), GD ($n=5$) and PTC ($n=5$), were selected for miRNA sequencing. The RNA was then extracted from the sEV pellets using the QIAGEN microRNA easy kit (**Section 2.8**). Following RNA extraction this was then sent on dry ice to QIAGEN - Hilden, Germany, for RNA quality testing and miRNA sequencing.

Table 4.1 - Breakdown of the EMG, GD and PTC samples with age and gender selected for QIAGEN RNA sequencing

EMG		GD		PTC	
Age	Gender	Age	Gender	Age	Gender
59	Female	53	Female	60	Male
51	Female	49	Female	83	Male
75	Female	40	Male	50	Female
55	Female	35	Female	53	Male
68	Female	70	Female	32	Female

4.1.2 - QIAGEN Qubit Quality Control RNA High Sensitivity Assay

QIAGEN performed the initial quality control of the RNA using the Qubit RNA high sensitivity (HS) assay, seven samples had RNA concentrations below the lower limit of detection (highlighted with *, **Table 4.2**).

Table 4.2. Qubit determined RNA concentration for the samples sent to QIAGEN

Sample	Sample ID	RNA Concentration (ng/ μ l)
1	THTHY3	17.5
2	THTHY4*	<1.35*
3	THTHY5*	<1.35*
4	THTHY7*	<1.35*
5	THTHY8	11.4
6	THTHY9	4.6
7	THTHY10*	<1.35*
8	THTHY13*	<1.35*
9	THTHY16	11
10	THTHY17	6.9
11	THTHY18	4.6
12	THTHY20	5.8
13	THTHY21*	<1.35*
14	THTHY22*	<1.35*
15	THTHY24	1.8

* samples were below the lower limit of detection of the Qubit RNA high sensitivity assay

The 7 samples which were below the limit of detection (Vaira et al.) of the assay were sent on for qPCR QC biofluids to evaluate the overall RNA sample quality. Despite there being a low RNA reading for these samples, personal laboratory experience from QIAGEN indicated that low RNA concentration was not necessarily a determinant of the total miRNA content and these were therefore processed for sequencing.

Following the qPCR QC of the exosome effluent, 14 out of the 15 samples were deemed by QIAGEN to be of a satisfactory quality for RNA sequencing, as miRNA had been detectable using RT-qPCR using the miRCURY LNA miRNA QC PCR Panel. This assay consists of 12 dedicated, predefined assays for identification of miRNA that are found within most tissues (miR-103, miR-191), controls for the quality of RNA isolation (UniSp2, UniSp4 and UniSp5) and assays looking at the quality of cDNA synthesis (UniSp6). Further testing showed that Sample 4, THTHY7, should be excluded from further analysis, which reduced the GD cohort to 4 samples.

4.2 - QIAGEN miRNA Sequencing

4.2.1 - Quality Control (QC) Checks

QIAGEN sequenced the isolated RNA over a month-long period, obtaining 31 million reads per sample. The minimum depth of sequencing required to detect the miRNAs that are expressed in one sample is 1,000,000 reads per library, mapped to the miRBase annotations. QIAGEN recommends allocating 5-10 million reads per sample (QIAGEN, 2024). The miRNA sequencing for the Hull samples was deemed to be of an 'excellent sequencing quality'. This was evidenced by QIAGEN in the high median Phred score obtained across all sample. The Phred score is logarithmically related to base calling error probabilities (Ewing & Green, 1998).

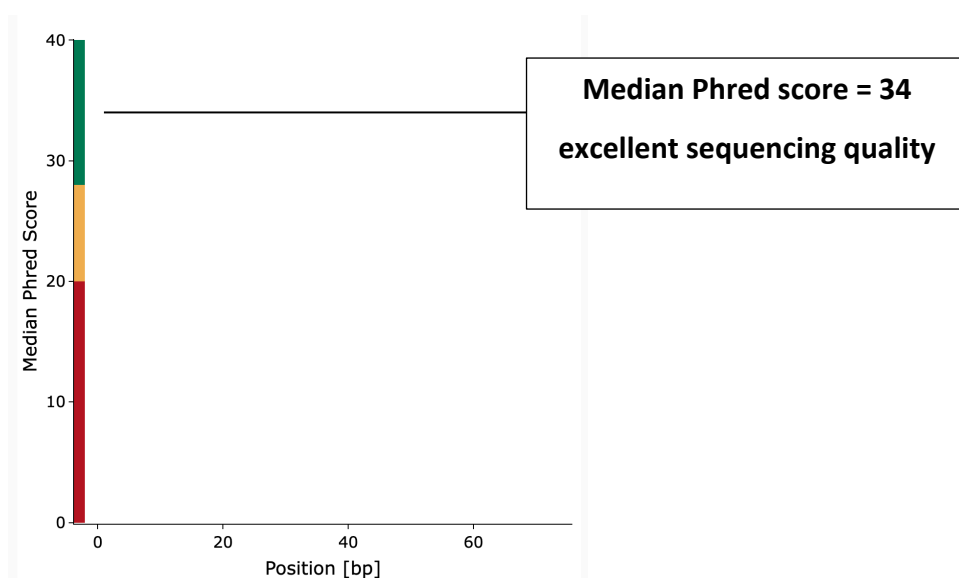


Figure 4.2 - Median Phred quality score for samples processed

The coloured bar on the y axis classifies the Phred values into three quality categories: poor (red, 0 to <20), medium (yellow, 20 to <28) and good (green, 28 and higher). The line at the level of 34 signifies the Median Phred Score for the Hull samples.

4.2.2 - QIAGEN miRNA Sequencing Methodology

A library was prepared from the RNA using the QIAseq miRNA Library Kit (QIAGEN). The QIAseq miRNA Library Kit is optimised to map miRNA down to ultralow input levels. A total of 1 ng or 5 µl total RNA was converted into miRNA Next Generation Sequencing libraries. After adapter ligation, unique molecular indices (UMIs) were introduced in the reverse transcription step. These UMIs are short, random nucleotide sequences that

can be attached to RNA prior to any amplification or sequencing. These UMIs enable the tracking of original molecules through the entire experimental process. The UMIs act as an internal control for managing library amplification bias (Potla et al., 2020). The cDNA was amplified using a PCR mix also containing the UMIs. After PCR the samples were purified prior to the library preparation, which was quality controlled using capillary electrophoresis (Tape D1000) and qPCR. Based upon the quality of the inserts and the concentration measurements the libraries were pooled in equimolar ratios. The final library pool was then sequenced on a NextGenSeq (Illumina Inc.) instrument.

All primary analysis was carried out using the CLC Genomics Server 22.0.2. The workflow “QIAseq miRNA Quantification” of CLC Genomics Server with standard parameters was used to map the reads to the miRBase version 22.

4.3 - Determination of Differential Gene Expression (DGE) between EMG, GD and PTC cohorts

DGE analysis was undertaken between the three different thyroid pathologies. The aim being to determine and identify differentially expressed miRNAs which may have the potential to discriminate thyroid pathologies; these were then confirmed and validated by RT-qPCR.

Mean Average (MA) Plots

Mean Average (MA) plots were generated in order to visualise differences in expression between the three pathologies. To generate the MA plot, the data was first transformed into M (\log_2 ratio) versus A (\log_2 mean average) scales, before plotting of these values against each other. The MA plot provides a visualisation of the differences between measurements taken in two samples, the higher the mean expression (\log_2 ratio) and the further away the miRNA is from 0 on X axis (\log_2 mean average), the more significant it is likely to be (McDermaid et al., 2019). Significant changes are defined as having a False Discovery Rate (FDR) of <0.01. The FDR is the rate at which features that are identified as significant are actually negative, in this case less than 1 in a 100 by chance.

4.3.1 - DGE miRNA analysis in sEV isolated from PTC tissue vs EMG tissue

On comparison of sEV miRNA expression between the PTC ($n=5$) and the EMG ($n=5$) samples there was no significant differential miRNA expression between the two, at either an FDR < 0.01 or <0.05 (**Figure 4.3**).

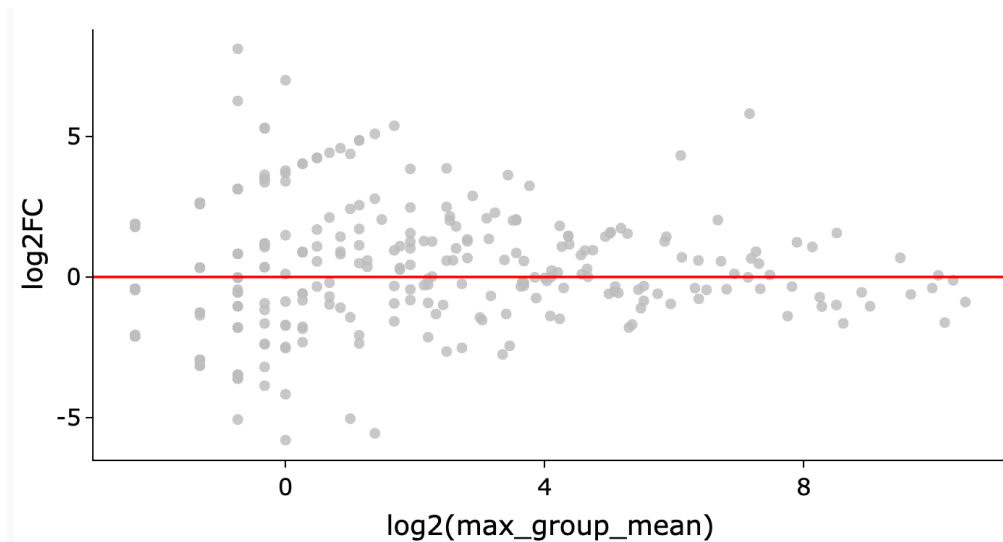


Figure 4.3 - MA Plot demonstrating DGE miRNA expression in sEV isolated from PTC and EMG Thyroid Pathologies. The red line is representative of the baseline of the EMG samples

4.3.2 - DGE miRNA analysis in sEV isolated from GD tissue vs EMG tissue

Comparison of miRNA expression from GD tissue sEVs ($n = 4$) with that of benign EMG tissue sEVs ($n = 5$) demonstrated that hsa-miR-375-3p, hsa-miR-7-5p, hsa-miR-382-5p and hsa-miR-127-3p were all significantly upregulated in GD derived sEV compared to EMG derived sEV (**Table 4.3** and **Figure 4.4**).

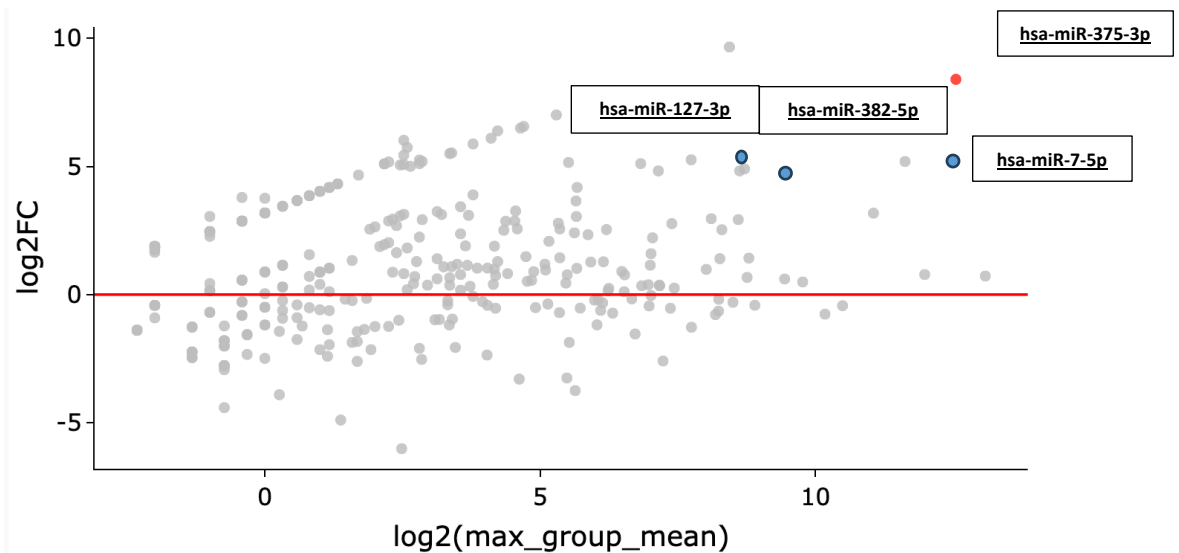


Figure 4.4 - MA Plot demonstrating DGE miRNA expression in sEV isolated from GD tissue and EMG. The red line is representative of the baseline of the EMG samples

Table 4.3 - sEV DGE miRNA expression in GD-derived sEV compared with EMG tissue-derived sEV showing Log2 fold change and FDR *p* value

miRNA	Log2 fold change	FDR <i>p</i> value
hsa-miR-375-3p	8.40	0.0004 (FDR <0.01)
hsa-miR-7-5p	5.19	0.0175 (FDR <0.05)
hsa-miR-382-5p	4.82	0.0321 (FDR <0.05)
hsa-miR-127-3p	5.26	0.0321 (FDR <0.05)

Comparison of miRNA levels in GD patient exosomes with EMG derived sEV miRNA demonstrated hsa-miR-375-3p to be highly differentially expressed having a log₂ fold change of 8.40 and this expression was accompanied by a highly significant FDR of 0.00044 (*p*<0.01). In addition, a further three miRNAs had an FDR *p* value of <0.05 in the form of hsa-miR-7-5p, hsa-miR-382-5p and hsa-miR-127-3p that demonstrated higher levels miRNA levels in GD sEV compared to EMG sEV.

4.3.3 - DGE miRNA analysis in sEV isolated from GD tissue compared to PTC-derived sEV

The comparison of sEV miRNA expression in GD tissue-derived sEV (*n*=4) and PTC tissue-derived sEV (*n*=5), also demonstrated that miR-7-5p and miR-375-3p were significantly higher in the sEV from GD tissue relative to the sEV isolated from PTC (**Table 4.4** and **Figure 4.5**).

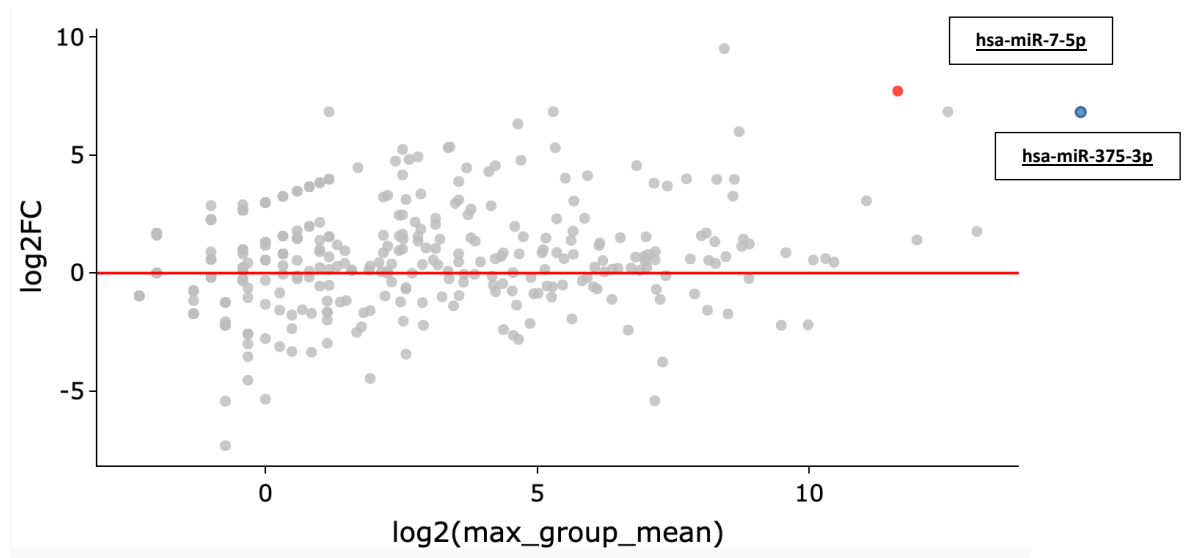


Figure 4.5 - MA Plot demonstrating DGE miRNA expression in sEV isolated from GD tissue and PTC. The red line is representative of the baseline of the PTC samples

Table 4.4 - sEV DGE miRNA expression in GD tissue-derived sEV compared with PTC derived sEV showing Log2 fold change and FDR *p* value

miRNA	Log2 fold change	FDR <i>p</i> value
hsa-miR-7-5p	7.72	0.0031 (FDR <0.01)
hsa-miR-375-3p	6.84	0.013 (FDR <0.05)

QIAGEN Software References

The following software packages were used for the generation of the QIAGEN miRNA sequencing report:

R (2024), DeSeq2 (MI, 2014), ggplot2 (, 2009), rmdformats (Barnier, J. Rmdformats. (2020). at <<https://github.com/juba/rmdformats>>), and plotly (@plotlygraphs, 2024).

4.4 – Reverse Transcription Quantitative Real-Time PCR (RT-qPCR) Analysis to validate QIAGEN miRNA sequencing results

4.4.1 - RT-qPCR Introduction

The employment of complementary techniques in order to answer a question fully always strengthens the reliability and accuracy of the results. It is recommended that following miRNA sequencing, validation takes place with Reverse Transcription Quantitative Real-Time PCR (RT-qPCR) analysis. RT-qPCR analysis is a relatively fast and simple laboratory procedure to perform (approximately 8 hours), instrumentation and expertise are widely available, so this has become the gold standard method for gene expression analysis (Wagner, 2013).

Typically, only a small number of biological replicates can be included in a single RNA-Seq experiment, usually limited due to the cost, but in contrast to this, multiple different RNA samples can be rapidly analysed in parallel using RT-qPCR. Increasing the number of biological replicates improves the power of statistical analyses with larger numbers reflecting the wider population.

4.4.2 - RT-qPCR Methodology

The results from the miRNA sequencing were validated through RT-qPCR (**Section 2.1**). cDNA was synthesised through the use of the miRCURY LNA reverse transcriptase (RT) kit with a UniSp6 Spike-in acting as the c-DNA synthesis control (**Section 2.11.1**). RT-qPCR was then carried out using the miRCURY SYBR green PCR kit and miRCURY LNA miRNA PCR assays (both Qiagen) (**Section 2.11.3**). PCR plates (96-well) were then prepared and loaded onto the ABI Real-Time PCR StepOne Plus machine (Biosystems). Raw C_T values were provided by the real-time PCR instrument.

The Role of UniSP6 in RT-qPCR

UniSP6 RNA spike-in acts as a control for the efficiency of the RNA isolation, cDNA synthesis and PCR amplification in the miRCURY LNA miRNA PCR kit. UniSp6 is an exogenous control and is added prior to the reverse transcription reactions, as a positive control and acts as a quality control that helps identify any experimental or technical anomalies. The UniSP6 level should be equal across all samples and acts as an inter-plate calibrator. However, the normalisation should always be performed using stably

expressed endogenous reference genes; an appropriate panel of which were provided by QIAGEN in the form of hsa-let-7c-5p, hsa-miR-191-5p, hsa-let-7e-5p, hsa-miR-16-5p, and hsa-miR-320c, which were the most “stable” miRNAs that possessed the lowest coefficient of variation between all samples used during the sequencing reactions.

4.4.3 - Samples used for RT-qPCR Analysis

The two miRNAs (hsa-miR-7-5p, hsa-miR-375-3p) which were found to be significantly different between the sEVs isolated from different thyroid pathologies through RNAseq ($FDR < 0.01$), were investigated further using RT-qPCR on a larger set of samples (EMG, $n=5$; GD, $n=6$; and PTC, $n=6$). The panel of five miRNA controls (hsa-let-7c-5p, hsa-miR-191-5p, hsa-let-7e-5p, hsa-miR-16-5p and hsa-miR-320c) were used to provide a stability index panel of miRNAs.

A total of eight samples which had sufficient RNA levels remaining, following the miRNA sequencing were returned and were available for RT-qPCR testing (**Figure 4.1** and **Table 4.5**). In addition, a further twelve samples were run on the ‘tissue on-chip’ devices which were a mixture of PTC ($n=3$), GD ($n=3$) and EMG ($n=3$). The sEVs were collected and RNA extracted as previously described (**Section 2.3, 2.6** and **2.8**).

Table 4.5 - Samples available for RT-qPCR, EMG, GD and PTC

EMG		GD		PTC	
n=5		n=6		n=6	
59	Female*	53	Female*	50	Female*
42	Female	40	Male*	53	Male*
68	Female*	35	Female*	32	Female*
48	Male	51	Female	20	Female
50	Female	57	Male	27	Male
		51	Female	19	Female

*Samples returned from QIAGEN for RT-qPCR ($n=8$)

4.5 - RT-qPCR Results

RNA concentration was determined for all samples using the Biochrom SimpliNano Spectrophotometer (Holliston, USA; **Table 4.6**), including those returned from QIAGEN, to identify if any degradation had occurred (**Section 2.9**). Of the 8 samples returned from Qiagen, it was shown that RNA degradation had occurred in six out of the eight samples. However, there was still sufficient material to prepare the cDNA; the

maximum amount of RNA that could be added, for all samples, was 50 ng. Using the RNA concentrations determined from the spectrophotometer, the volume required for 50 ng was calculated (**Table 4.6**).

Table 4.6. RNA concentration of the respective sEV RNA samples measured on the Biochrom SimpliNano Spectrophotometer and the volume of RNA required to provide 50 ng from cDNA synthesis

Sample	Diagnosis	Initial RNA Concentration (µg/ml) (Pre-Sequencing)	RNA Concentration (µg/ml)	Volume required for 50 ng of RNA (µl)
THTHY8	EMG	39.4	27	1.85
THTHY23	EMG		50.6	0.99
THTHY24	EMG	37.1	18.3	2.73
THTHY25	EMG		10	5.00
THTHY27	EMG		17.6	2.84
THTHY3	GD	91.1	85.5	0.58
THTHY18	GD	27.1	29.6	1.69
THTHY20	GD	23.9	13.2	3.79
THTHY29	GD		15.6	3.21
THTHY33	GD		73.9	0.68
THTHY36	GD		127.9	0.39
THTHY9	PTC	14.9	52.2	0.96
THTHY16	PTC	25.3	21.4	2.34
THTHY17	PTC	23	14.9	3.36
THTHY32	PTC		17.6	2.84
THTHY34	PTC		87.8	0.57
THTHY35	PTC		40.4	1.24
THTHY11	FTC		8	6.25

4.5 - Optimisation of RT-qPCR conditions

As per the methodology for RT-qPCR (**Section 2.11, 2.12**), the ‘Neat’ cDNA samples prepared were already diluted at a 1:30 dilution with RNAase-free water during their preparation. In order to determine the efficacy of the primers for detecting the specific miRNA, dilutions of the “Neat” sample were produced to verify that threshold cycle, C_T value, increased with increasing dilution. The C_T value, is the number of cycles of PCR required in order for the fluorescent signal to cross the threshold and be detected, i.e. a high C_T value demonstrates a small amount of the target miRNA. cDNA was therefore prepared at a 1:5, 1:10, 1:20 and 1:50 dilution of the “neat” cDNA. RT-qPCR was then performed using cDNA from both THTHY3, a GD sample and THTHY23, a EMG sample as

these had higher concentrations of RNA which should ensure there would be sufficient RNA for the following optimisation steps (**Table 4.6**). The samples were then probed with two of the control miRNA; hsa-miR-191-5p and hsa-miR-320c. As expected, increasing dilution of the THTHY3 and THTHY23 increased the respective mean C_T value (**Figure 4.6**), demonstrating that the primers were correctly detecting the miRNA in the sample and that the C_T value was increasing in accordance with an increasing level of dilution. The C_T value for hsa-miR-191-5p in the THTHY3 sample increased beyond 40 so the machine did not provide a C_T value, with dilutions of 1:20 and 1:50 resulting in the empty space for these samples on the graph **Figure 4.6**.

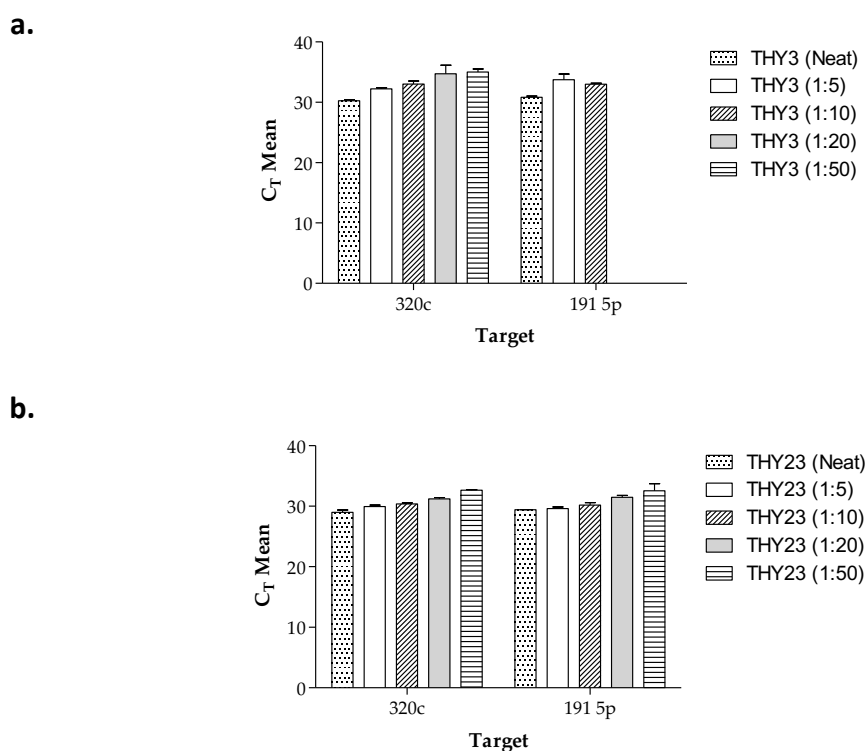
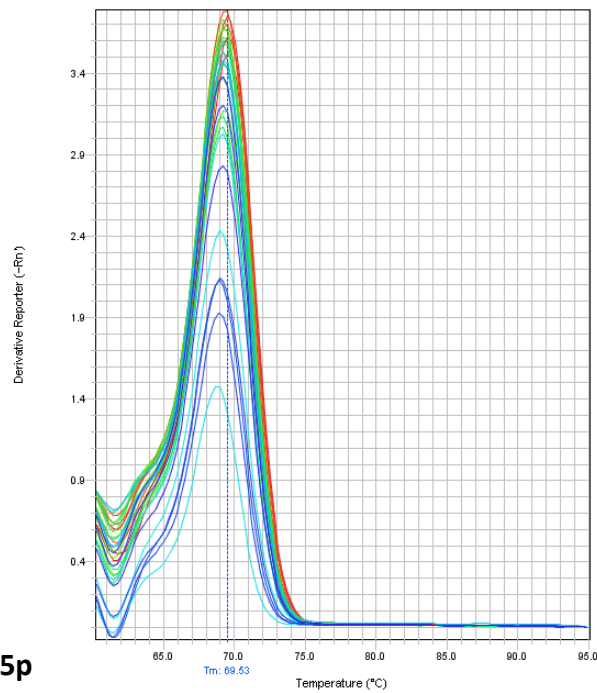


Figure 4.6 - Increasing mean C_T with increasing dilution of cDNA using hsa-miR-191-5p and hsa-miR-320c stable miRNA primers on THTHY3 (Galluzzi et al.) and THTHY23 (**b.**) RNA.

The melt curve analysis for THTHY3 and THTHY23 demonstrated high affinity binding for both sets of primers, hsa-miR-191-5p and hsa-miR-320, which further confirmed specific binding of the primers with little or no off-target interactions (**Figure 4.7**).

a. hsa-miR-320c



b. hsa-miR-191-5p

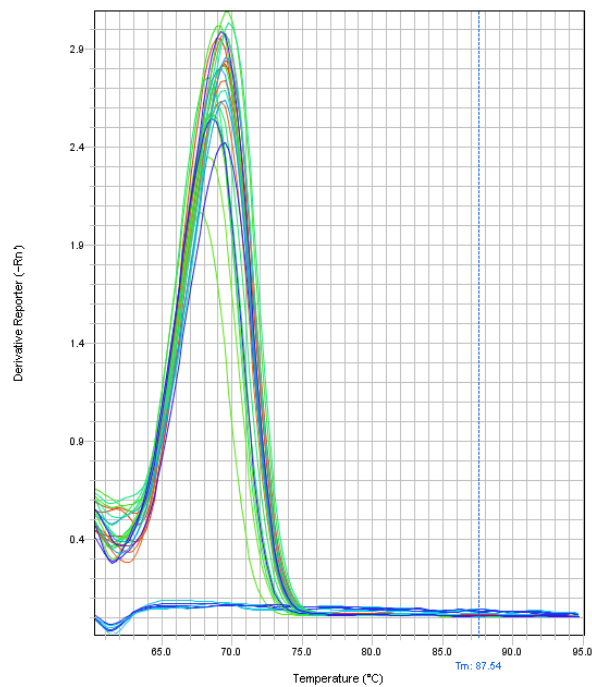


Figure 4.7 – (a.) Melt curve analysis demonstrating high affinity binding for hsa-miR-320c primer for both samples THTHY3 and THTHY23 at a number of varying concentrations. Different colours represent the different samples at each dilution in triplicate.

(b.) Melt curve analysis demonstrating high affinity binding for hsa-miR-191-5p primer for both samples THTHY3 and THTHY23 at a number of varying concentrations. Again, the different coloured traces represent different samples at each dilution in triplicate.

Following this preliminary work, the primers for the full range of stable miRNAs were tested on THTHY3, 23 and 36. The rationale behind focusing upon these samples was that they had the greatest RNA concentrations, which would ensure that there would be sufficient RNA to carry out these optimisation runs and still have enough for subsequent analyses. Refer to Appendix 4 for melt curves for THTHY3 (GD) and THTHY23 (EMG) which were tested for the presence of hsa-let-7c-5p, hsa-miR-16-5p which were part of the stable panel of primers alongside hsa-miR-375-3p and hsa-miR-7-5p which were two of the differentially expressed miRNA from the sequencing data (**Figure 4.8**). Both stable miRNAs were detectable in the cDNA samples of the two samples and demonstrated increases in their mean C_T value on dilution to 1:50, again demonstrating that the primers were working appropriately. Both hsa-miR-375-3p and hsa-miR-7-5p were detectable in the neat cDNA samples, however they were not detectable when the RNA was diluted (1:50).

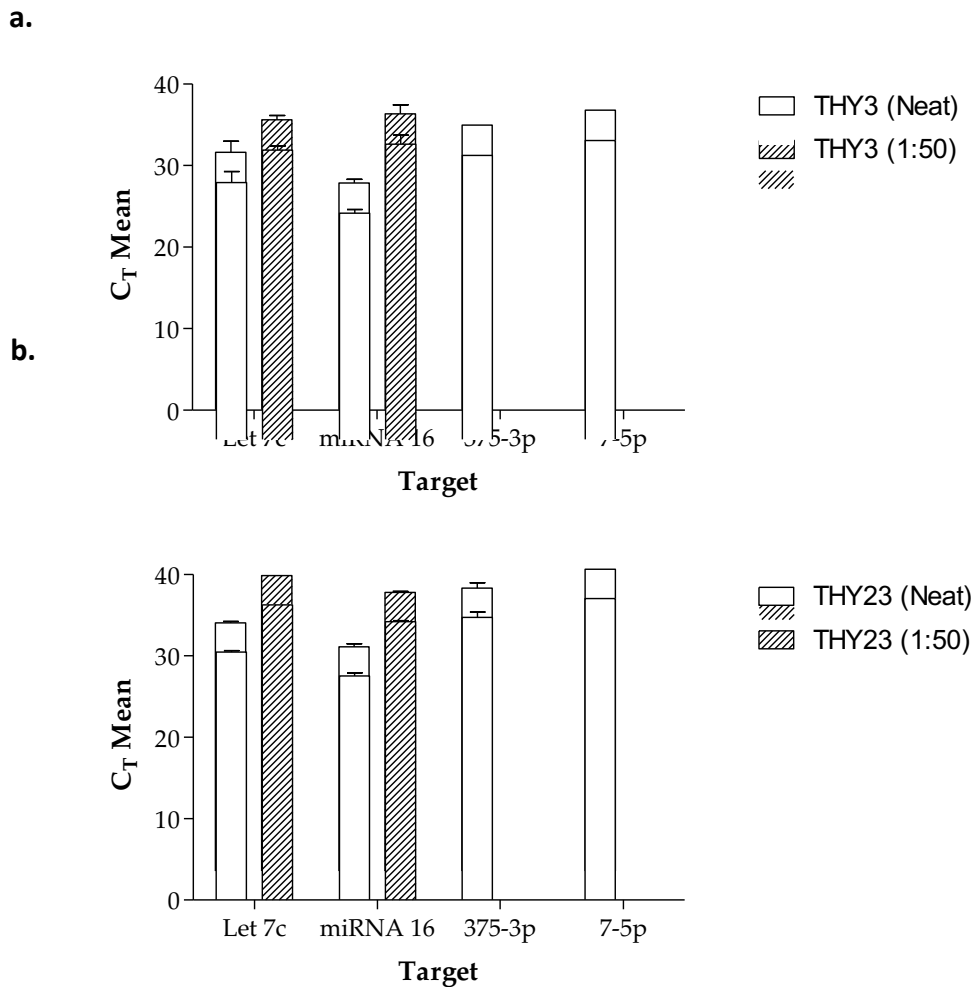


Figure 4.8 – (a.) Increasing mean C_T using hsa-let-7c-5p and hsa-miR-16-5p with increasing dilution of THTHY3 RNA. miR-375-3p and hsa-miR-7-5p were only detectable within the Neat THTHY3 sample
(b.) Increasing mean C_T using hsa-let-7c-5p and hsa-miR-16-5p with increasing dilution of THTHY23 RNA. miR-375-3p and hsa-miR-7-5p were only detectable in the Neat THTHY23 sample

Plotting the results for the RT-qPCR for the “Neat” samples for the stable miRNA (hsa-let-7c-5p and hsa-miR-16-5p) demonstrated that there was minimal variation between the samples (THTHY3, THTHY23 and THTHY36; **Figure 4.9**). This provided reassurance with regards to the stability index panel of miRNAs. On the whole, hsa-miR-16-5p demonstrated greater stability across the samples than hsa-let-7c-5p.

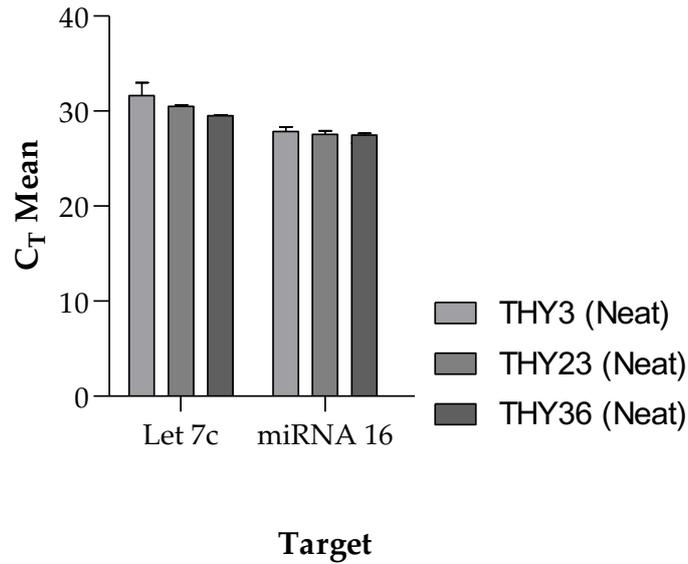
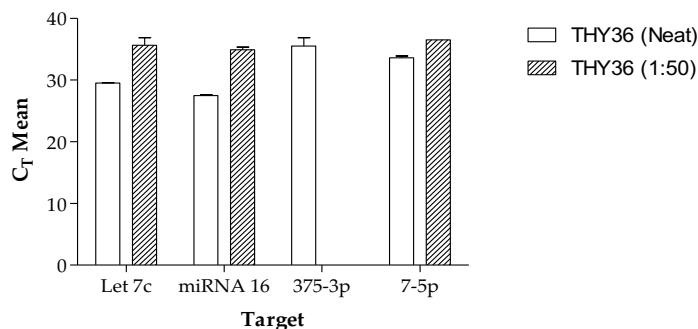


Figure 4.9 - Demonstrating mean C_T on detecting stable miRNA hsa-let-7c-5p and hsa-miR-16-5p, in the neat samples of THHY3 (GD), THHY23 (EMG) and THHY36 (GD)

4.5.1 - Determination of the Concentration of RNA to be used in RT-qPCR

In order to determine whether 50 ng of RNA was sufficient to be able to detect miRNAs, a trial with both 50 ng and 200 ng of RNA was performed. THHY36 was utilised as it possessed sufficient quantities of RNA to be used within these optimisation steps. An RT-qPCR was run with THHY36 at both 200 ng “Neat” and at an associated 1:50 dilution and also at 50 ng “Neat” with an associated 1:50 dilution against the two stable miRNA primers hsa-let-7c-5p and hsa-miR-16-5p as well as the two primers of interest hsa-miR-375-3p and hsa-miR-7-5p (**Figure 4.10**). Despite the reduced concentration of THHY36 at 50 ng, all of the miRNAs tested on the panel were detected in the “Neat” samples (**Figure 4.10 (a.)**). As expected, a higher C_T value in the 200 ng samples was obtained than when compared to that of the 50 ng samples (**Figure 4.10 (b.)**)

a. 50 ng - THTHY36



b. 200 ng - THTHY36

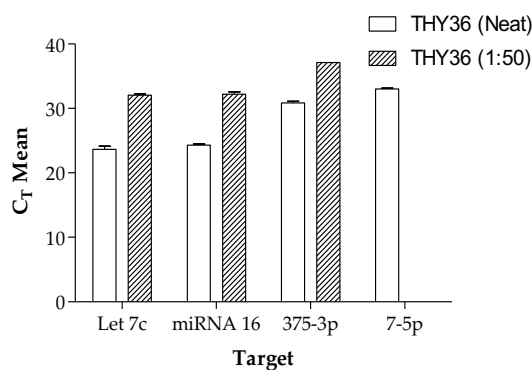


Figure 4.10 - C_T values obtained for hsa-let-7c-5p, hsa-miR-16-5p, hsa-miR-375-3p and hsa-miR-7-5p for THTHY36 at **(a.)** 50 ng Neat and 1:50 dilution and **(b.)** 200 ng Neat and 1:50 dilution

These runs demonstrated that using 50 ng of RNA to synthesise the cDNA was sufficient to detect both the stable miRNA and the miRNA of interest and would be used going forward. Starting with this level of RNA meant that all of the collected samples could be tested by RT-qPCR, even those with relatively low RNA yields.

4.5.2 - Assessing the consistency of the “stable” miRNA

Seventeen of the samples synthesised from 50 ng of RNA from a spectrum of the thyroid pathologies, were used to assess the stability index of miRNAs suggested by Qiagen for normalisation in the RT-qPCR reactions (**Figure 4.11**). There was minimal variability in the SP6 C_T values across all 17 samples which provides reassurance surrounding our methodology. The stable miRNAs investigated, included hsa-miR-191-5p and hsa-let-7e-5p which demonstrated slight variation in their CT values, however a similar pattern was seen for each primer indicating that this may be a result of pipetting errors.

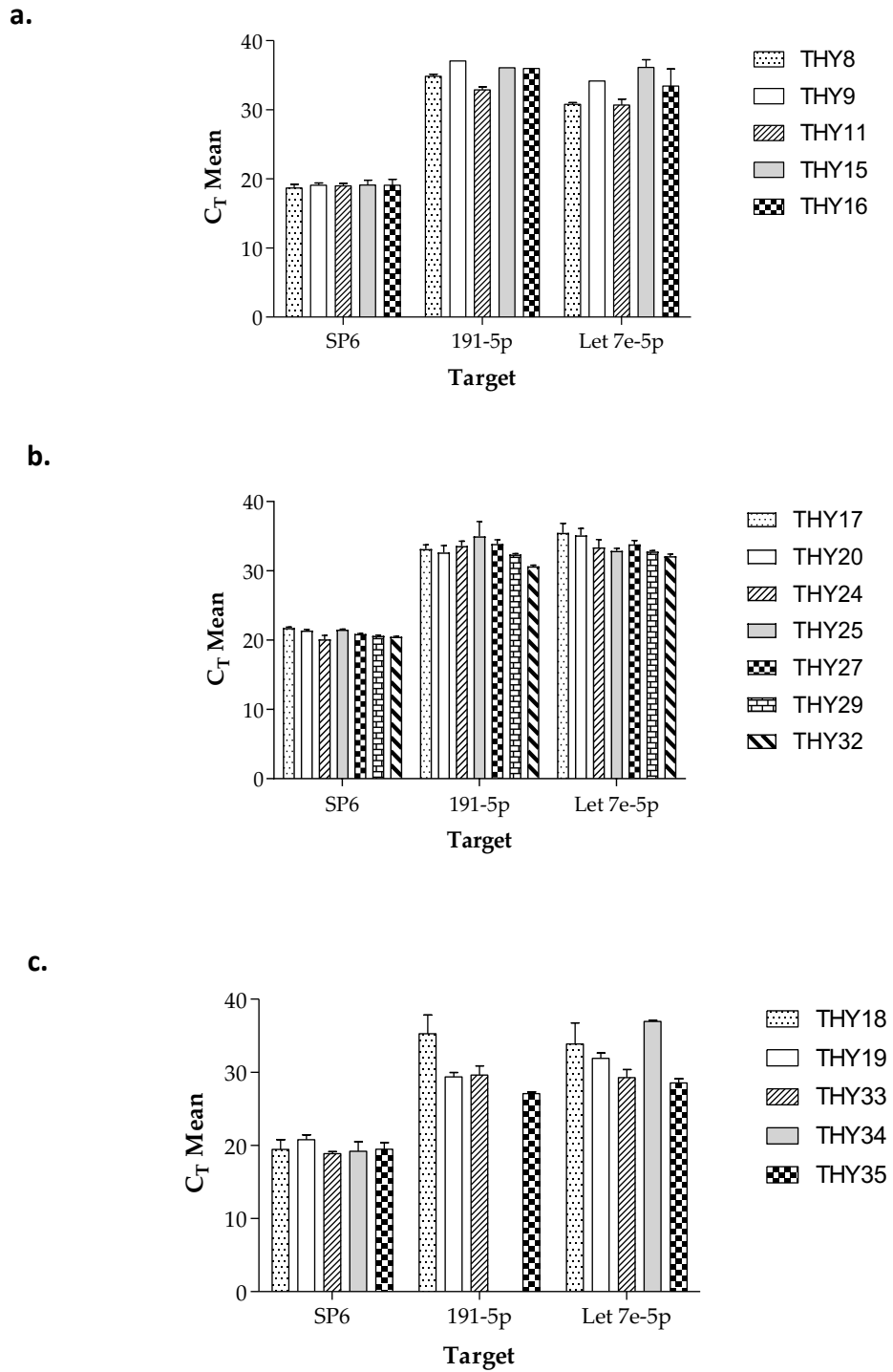


Figure 4.11. Bar chart demonstrating C_T values for 50 ng samples for detection of SP6, hsa-miR-191-5p and hsa-let-7e-5p “stable” miRNA:

(a.) THTHY8, THTHY9, THTHY11, THTHY15, THTHY16

(b.) THTHY17, THTHY20, THTHY24, THTHY25, THTHY27, THTHY29, THTHY32

(c.) THTHY18, THTHY19, THTHY33, THTHY34, THTHY35

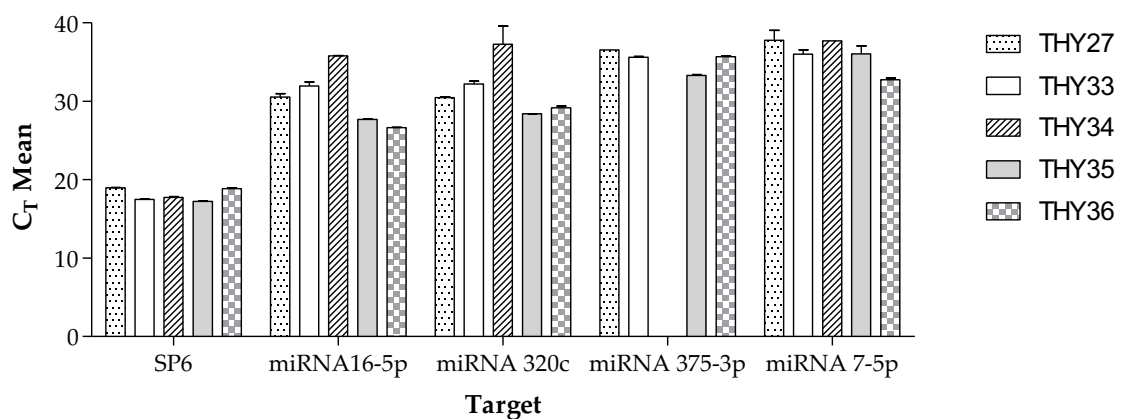
Blank spaces result from the C_T value being >40

4.5.3 - Assessing differentially expressed hsa-miR-375-3p and hsa-miR-7-5p across the seventeen thyroid samples

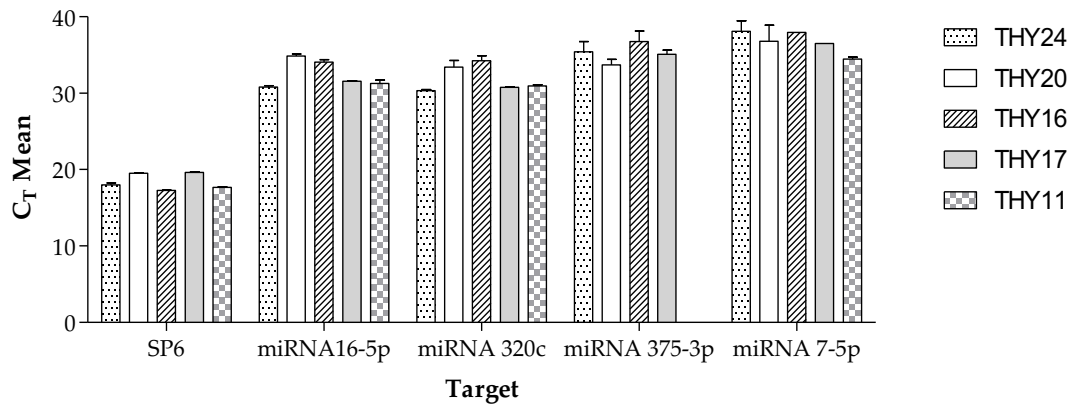
As a result of the previous optimisation and testing of the panel of potential stable miRNAs, it was decided that miR-16-5p and miR-320c were the most stable primers and would act as a reference to normalise the differentially expressed hsa-miR-375-3p and hsa-miR-7-5p.

Despite hsa-miR-16-5p and hsa-miR-320c being identified as stably expressed miRNAs across the samples, there was evidence of variability between the samples (**Figure 4.12 a to d**). The pattern of variation for each of these “stable” primers was similar between each sample, suggestive of human pipetting error rather than differential expression. Unsurprisingly, hsa-miR-375-3p and hsa-miR-7-5p, the miRNA of interest, demonstrated variability across samples. hsa-miR-375-3p was not detectable in sEV RNA extracted from six samples, demonstrating no predilection for a particular thyroid pathology. No clear pattern in the samples that do not express the hsa-miR-375-3p was demonstrated in terms of their thyroid pathology. However, to note, is that this miRNA was detected in all of the GD samples which is in keeping with the results of the miRNA sequencing where this miRNA was more highly expressed in the GD sEV compared to that of the Benign samples with an FDR p value of <0.01 .

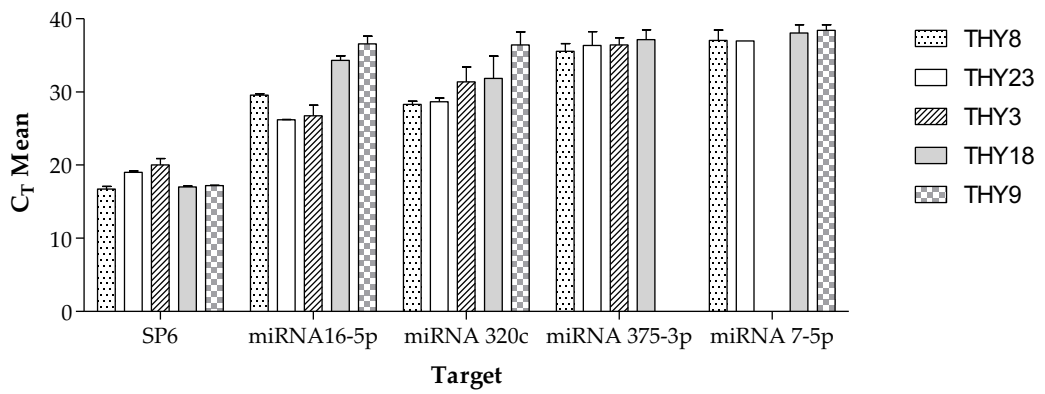
a.



b.



c.



d.

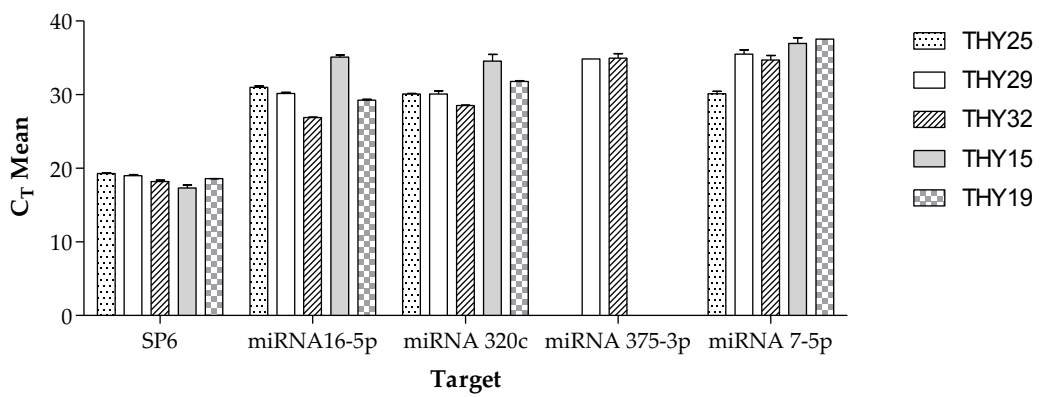


Figure 4.12 - Bar chart demonstrating C_T values for 50 ng samples for detection levels of SP6 (the spike in control) and hsa-miR-16-5p, hsa-miR-320c (“stable” miRNA), and hsa-miR-375-3p and hsa-miR-7-5p (genes of interest)

(a.) THTHY27, THTHY33, THTHY34, THTHY35 and THTHY36.

(b.) THTHY24, THTHY20, THTHY16, THTHY17 and THTHY11

(c.) THTHY8, THTHY23, THTHY3, THTHY18 and THTHY9

(d.) THTHY25, THTHY29, THTHY32, THTHY15 and THTHY19

4.6 - GeneGlobe-integrated RNA-seq Analysis Portal

In this study, four miRNAs were profiled on 60 samples; the two selected stable miRNAs in the form of hsa-miR-16-5p, and hsa-miR-320c and the differentially expressed miRNAs of interest hsa-miR-375-3p and hsa-miR-7-5p. Following obtaining the C_T values from the RT-qPCR these values were collated for each respective sample and then inputted into the QIAGEN RNA-seq Analysis Portal. For the miRNA of interest (miR-375-3p, miR-7-5p), the mean C_T value was ≥ 30 for all samples demonstrating that overall, there was low level of expression of these selected miRNA within the thyroid tissue sEVs.

The analysis portal on the Qiagen website was used (<https://geneglobe.qiagen.com/>).

The lower limit of detection was defined at the C_T cut-off of 40.

4.7 - miRNA Analysis Method

The data analysis web portal calculates fold change/regulation using the delta-delta C_T method, in which delta C_T is calculated between miRNA of interest and an average of reference miRNAs, followed by delta-delta C_T calculations (delta C_T (Test Group)-delta C_T (Control Group)). Fold Change is then calculated using $2^{(-\text{delta-delta } C_T)}$ formula.

The geNorm normalisation analysis was performed which involves the calculation of a normalisation factor based upon the two reference miRNAs, which in our case was the selected stable miRNAs, hsa-miR-16-5p and hsa-miR-320c (Vandesompele, 2002). Four different pathological groups were defined and all the samples assigned to one of these groups (**Table 4.7**).

Table 4.7 - Thyroid pathologies grouping for the GeneGlobe-integrated RNA-seq Analysis Portal

Group	Thyroid Pathology
Control Group	EMG
Group 1	GD
Group 2	PTC

4.7.1 - Differential expression of hsa-miR-375-3p and hsa-miR-7-5p in sEV isolated from GD tissue vs those from EMG

Following analysis using the Qiagen analysis tool, it was demonstrated that there are increased levels of hsa-miR-375-3p and hsa-miR-7-5p between in the GD tissue sEV compared to the EMG sEV demonstrated by the positive fold change increases observed (**Table 4.8**). Fold regulation change is a measure of quantity change between two populations for example a change from 20 to 40, would be a fold regulation change of 2.

Table 4.8 - Fold Regulation changes for GD vs EMG for the differentially expressed hsa-miR-375-3p and hsa-miR-7-5p

miRNA ID	Fold Regulation	Comments
hsa-miR-375-3p	6.18	B
hsa-miR-7-5p	2.64	B

The fold regulation changes of 6.18 for hsa-miR-375-3p in GD tissue-derived sEV relative to EMG tissue sEV support the findings from the QIAGEN RNASeq data in which hsa-miR-375-3p was found to be significantly differentially expressed with an FDR p value of <0.01 . However, the RT-qPCR findings are not as conclusive as the sequencing as in the 'Comments' section of the table, the B comment for both of miR-375-3p and miR-7-5p relates to the fact that the miRNA expression was low in both of the tested samples and that the associated p -value was greater than 0.05 and therefore not significant.

4.7.2 - Differential expression of hsa-miR-375-3p and hsa-miR-7-5p in sEV isolated from PTC vs those from EMG

The comparison of the PTC tissue-derived sEV miRNAs with the EMG tissue-derived sEV miRNA samples showed hsa-miR-375-3p to possess a fold regulation of 9.90 with an associated p -value of 0.0037 (**Table 4.9**). miR-7-5p possessed a fold regulation of 2.94 but this was not deemed to be statistically significant ($p = 0.405468$).

Table 4.9 - Fold Regulation changes for PTC vs EMG for the differentially expressed hsa-miR-375-3p and hsa-miR-7-5p

miRNA ID	Fold Regulation	p-Value
hsa-miR-375-3p	9.90	0.003730
hsa-miR-7-5p	2.64	B

The results from the Qiagen analysis portal demonstrate that hsa-miR-375-3p was detected at a level that is significantly greater ($p=0.037$) in the PTC tissue-derived sEVs compared to the EMG derived sEVs. This is in contrast to the results from the miRNA sequencing in which there were no identified differentially expressed miRNA detected between these two groups.

4.8 - Discussion

The findings from this study are evidence that ‘tissue on-chip devices’ can be utilised to isolate sEVs specifically from thyroid tissues which aids in differentially profiling thyroid pathology through their sEV miRNA profile. This study has identified two miRNAs (miR-375-3p and miR-7-5p) of potential significance within the development and pathogenesis of thyroid disease along with other miRNAs that may have a future role to play in diagnosis, treatment monitoring and disease prognostication. The findings from the RT-qPCR in part support the findings from the miRNA sequencing but have highlighted the need for a greater number of samples to be tested to help further substantiate and validate these findings.

4.8.1 - miR-375-3p

The miRNA which demonstrated the greatest differential expression from the sequencing results was miR-375-3p, which was significantly increased in GD sEVs compared to both EMG and PTC-derived sEVs. Despite there being no significant difference in miRNA-375-3p expression in PTC sEVs compared to EMG sEVs in the sequencing analysis, further comparison using RT-qPCR showed an elevation in the level of miR-375-3p in the PTC sEV compared to the EMG sEV. From these experimental findings, it can be hypothesised that miRNA-375-3p may play a role within the pathogenesis of both GD and PTC.

On review of the literature, most of the work on miRNA-375-3p has been studying it in relation to MTC. Censi *et al.* examined the plasma of patients with MTC ($n=68$)

compared to that of healthy individuals ($n=57$) and found miR-375-3p to be >100 times higher in the patients (Censi et al., 2021). The findings however highlight the role that miRNA-375-3p is playing within a wide scope of TC and the pressing need for this to be further elucidated.

A further study looking into MTC and circulating miRNAs as non-invasive biomarkers was carried out by Romeo *et al.* (Romeo et al., 2018). The plasma samples of healthy people ($n=36$) were compared to that of MTC patients ($n=36$), some of whom had been treated with the TKI, Vandetanib. Microarray analysis identified a panel of 51 miRNAs that were differentially expressed in MTC compared to the healthy controls. Further RT-qPCR analysis identified significantly higher miR-375 plasma levels in patients than the comparative healthy controls ($p<0.0001$), or in the subjects who were in remission of the disease ($p=0.0004$). Interestingly, increased miR-375 plasma levels in the MTC patients were shown to have an association with a reduced overall survival, thus further highlighting a potential role for the miRNA as a diagnostic marker, for monitoring of response to treatment or as a treatment target. In a separate study, Shi *et al.* looked to dissect the molecular mechanism of miR-375 within MTC and the pathway(s) that the miRNA may be targeting (Shi et al., 2017). The study examined the expression level of miR-375 in MTC with microarray data from Gene Expression Omnibus and they identified 1132 prospective targets for miR-375, concluding that higher expression of miR-375 was likely to have a role in MTC tumorigenesis.

Further investigation of miR-375 and its role as a diagnostic marker by Galuppini *et al.* demonstrated an upregulation of miR-375 in all MTCs ($n=130$) compared that of normal thyroid tissue ($n=30$) and that the level of expression was linked to that of the MTC size, thyroid capsule infiltration, lymph node metastasis and tumour staging (Galuppini et al., 2017). Lassalle *et al.* using thyroid cell lines identified that over-expression of miR-375 increased the sensitivity of the cells to the TKI Vandetanib (Lassalle et al., 2016).

4.8.1.1 - The role of miR-375-3p within the context of PTC

The DGE data in the current study demonstrated that miRNA-375-3p was not differentially expressed between PTC and EMG sEVs. However, RT-qPCR, with a slightly larger cohort of samples, demonstrated that miRNA-375-3p was detected at a higher level in the PTC sEV compared to the EMG sEV, with a fold regulation of 9.90 and p -value

of 0.0037, thus highlighting that it may well have a role to play within the pathogenesis of PTC. Conversely, Wang *et al.* (2016) postulate from their study that over-expression of miR-375 inhibits PTC cell proliferation and decreases the migration and the ability of human PTC cells to invade *in vivo* (Wang *et al.*, 2016). Their study concluded that miR-375 was down-regulated in human PTC tissues and cell lines which is in contrast to the RT-qPCR findings in the current study. It is clear that more research into the role of miR-375 is required in PTC, involving a larger cohort of patients.

4.8.1.2 - The role of miR-375-3p within the context of AITD

Within the context of AITD, Yamada *et al.* looked at the level of circulating miRNAs within AITD. Microarray analysis followed by RT-qPCR were utilised, analysing miRNA expression patterns in the serum of patients with GD ($n=17$) and HT ($n=27$) (Yamada *et al.*, 2014). It was shown that the serum levels of miR-375 from the Graves' patients were consistently elevated compared to the healthy controls ($n=20$). Again, this highlights the potential role that miR-375 might play within thyroid disease, but the study further implies that these miRNAs do not work in isolation of one another.

These findings do provide hope that this miRNA may open a gateway to personalised treatments within the field of thyroid oncology. More work is required to demonstrate any role in the pathogenesis of PTC and AITD, which overall possess a much higher incidence and disease burden than that of MTC.

4.8.2 - miR-7-5p

miR-7-5p was also found to be elevated in sEVs derived from GD tissue compared to both EMG (FDR p value <0.05) and PTC sEVs (FDR p value <0.01). Unfortunately, the RT-qPCR data did not further validate these results, and no significant difference was observed between the PTC and the benign samples.

Work by Hua *et al.* indicates a tumour suppressive role for miR-7-5p. Their work looked at the expression levels of miRNAs in PTC specimens ($n=14$), normal thyroid cancer tissue ($n=10$), and cell lines including normal thyroid follicular cells Nthy-ori 3-1, K1 PTC cells and human B-CPAP PTC cells (Hua, 2016). Results revealed that miR-7-5p expression was reduced in PTC tissue and PTC cell lines compared to that of adjacent normal thyroid

tissue and normal thyroid cells. *In vitro* experimentation, demonstrated that miR-7-5p acted to inhibit both cellular proliferation and suppress cellular migration and invasion through bringing about a G0/G1 arrest.

Interestingly, Saiselet *et al.* also found miR-375 to be up-regulated whilst miR-7-5p was downregulated in PTC tissue in comparison with normal tissue through small-RNA deep-sequencing. miR-7-5p has been shown to inhibit cell proliferation *in vitro* thus suggesting a tumour suppressive role (Saiselet *et al.*, 2015). Augenlicht's *et al.* study specifically focused upon the role miR-7-5p plays in inhibiting thyroid cancer cell proliferation and its targeting of the EGFR/MAPK and IRS2/PI3K signalling pathways (Augenlicht *et al.*, 2021). Their work was based on the transfection of two thyroid cell lines, TPC1 (PTC cell line) and HT-ori3 cells (normal follicular cell line), with miRNA-7-5p, TPC1 and HT-ori3 cells, which resulted in reduced proliferation. Their analysis of the global transcriptome, identified that miR-7-5p inhibits thyroid cell proliferation through modulation of the MAPK and PI3K signalling pathways. Thus, reduced expression of miR-7-5p would provide PTC with a proliferative advantage. This does have some resonance with findings in this study as miR-7-5p was found to be more differentially expressed in sEV from GD relative to PTC, suggesting that within PTC downregulation may be taking place.

4.8.3 – Conclusion

The findings from the miRNA sequencing demonstrate two highly differential expressed miRNAs within the context of thyroid disease in the form of miR-375-3p and miR-7-5p. Further analysis, through RT-qPCR and Gene-Globe RNAseq portal validated the differential expression of these miRNAs between the thyroid pathologies. It is clear from the literature, that miRNAs do not act in isolation and that a number of downstream targets are targeted within the context of disease pathogenesis and its propagation. Despite the limited sample size, two additional miRNAs; hsa-miR-382-5p, hsa-miR-127-3p (FDR p value <0.05) were identified in the GD vs EMG DGE analysis (**Section 4.2.3.2**) along with further miRNAs, not presented here, that were approaching statistical significance. Future work, should focus upon the two miRs, hsa-miR-382-5p and hsa-miR-127-3p, through RT-qPCR in order to further identify evidence of differential expression between thyroid pathologies. Tissue on chip technology has helped in identification of miRNAs of significance within the context of thyroid disease. Further

works need to delineate the downstream molecular pathways affected by the differential expression of these miRNAs, alongside validating the expression of miRNAs through RT-qPCR that were approaching statistical significance in the miRNA sequencing data.

Chapter 5 - Conclusion and Future Works

The management of thyroid disease poses significant clinical challenges within the arena of both thyroid oncology and AITD. The current 'over treatment' of PTC is a contentious issue and the diagnostic tools available lack the necessary sensitivity and specificity to resolve the issue (Belfiore & La Rosa, 2001). It can be argued that this is culminating in potentially unwarranted thyroid surgeries in a disease that may well be amenable to clinical surveillance (Jegerlehner et al., 2017). The identification of sEV miRNA biomarkers would help in establishing a diagnosis of both TC and AITD alongside the monitoring of response to treatment modalities and the discovery of therapeutic targets (Wang et al., 2023b). The aim of this study was to utilise 'tissue-on-chip' technology to help identify a differential sEV microRNA profile between the thyroid pathologies of EMG, GD and PTC (**Section 1.14**). NTA demonstrated that effluent from the perfused thyroid tissue on the 'tissue on chip' devices, possessed nanoparticles in keeping with the size range expected of sEVs (80 nm to 187 nm) (Théry et al., 2018) (**Section 3.4**). Further, WB techniques were able to identify the presence of classical exosomal markers (CD63 and CD81) in both thyroid exosomal preparations and tissue lysates (**Section 3.7**). Differential ultracentrifugation to isolate sEVs, RNA extraction, followed by miRNA sequencing led to the identification of two significantly differentially expressed miRNAs; miRNA-375-3p and miRNA-7-5p (FDR<0.01) (**Section 4.2**). In addition, miR-382-5p and miR-127-3p were also demonstrated to be differentially expressed between GD and Benign tissue using a slightly less-stringent cut off (FDR <0.05). The RNA sequencing results for the miRNAs, miRNA-375-3p and miRNA-7-5p were further examined and validated through RT-qPCR (**Section 4.2.4**). This 'tissue-on-chip' project has paved the way for further work to examine the mechanistic roles that these sEV miRNAs may exert within thyroid disease, as well as exploring their role as biomarkers.

Hopefully with the ever-expanding knowledge base, the monitoring of sEV miRNA biomarkers alongside other established biomarkers i.e. thyroglobulin, may have a role to play in post-treatment monitoring and provide increased clarity surrounding monitoring in the context of post TC surgery (Maggisano et al., 2022). The use of thyroglobulin as a biomarker of disease recurrence lacks sensitivity and needs to be approached and interpreted with an element of caution (Giovanella et al., 2023). The development of an effective diagnostic liquid biopsy within the field of thyroid oncology

would hopefully help negate the uncertainties associated with FNAC. The development of a liquid biopsy could ultimately deliver cost benefits to healthcare organisations worldwide when compared to repeat USS, FNAC, repeated thyroglobulin testing and in person clinical reviews (Zhou, 2020).

5.1 - Future Works

5.1.1 - Thyroid exosomal miRNAs effect upon gene regulation

One way the project can be developed is to investigate the effects that the four differentially expressed miRNAs have upon downstream target genes and the various molecular pathways, to further understand their role in thyroid disease. For instance, Augenlicht's group have looked at the role miRNA-7-5p plays through inhibiting thyroid cell proliferation in thyroid cell lines by targeting the EGFR/MAPK and IRS2/PI3K signalling pathways (Augenlicht et al., 2021). Ongoing work in the Hull group revolves around the two microRNAs identified (miRNA-7-5p and miRNA-375-3p).

It has been shown that miRNAs bind to specific sequences at the 3' untranslated region of their target mRNA in order to induce translational repression (Ipsaro & Joshua-Tor, 2015). The binding of miRNAs to the 5' untranslated region and coding region has the ability to silence effects on gene expression whilst interactions with the promoter region can induce transcription (Dharap et al., 2013). The full extent to which miRNA can affect gene regulation needs to be unravelled. In an attempt to start to address this there are international efforts to develop databases of miRNAs and the pathways that they affect, for instance the miRTar database which links miRNAs to metabolic pathways (Hsu et al., 2011) and the miR System, which provides pre-computed enrichments of target genes (Lu et al, 2012). As alluded to there are difficulties in identifying the downstream miRNA targets and a number of different techniques have been attempted such as CARP: Combined Analysis of RNA-seq and PRO-seq, which helps to dissect the gene regulatory networks that are triggered by miRNAs (Patel et al., 2020). Working with these databases, will help in the next steps of identifying the downstream effects of these miRNAs and the pathways that they have roles in regulating.

5.1.2 - Blood Serum

In order to broaden the scope of future studies, an amendment was made to the original ethics submission in order to collect blood samples from all patients from whom tissue biopsies were taken. This should allow correlation of the findings from the 'tissue-on-chip' effluent with that of the patient's serum through further sEV miRNA sequencing. Serum could be analysed in a number of ways: firstly, one could examine the serum of the different cohorts to see if the effluent-detected miRNAs display similarities with those of the miRNAs expressed within the serum. One could also look to see if there is any intra-patient correlation between the serum and the effluent detected miRNAs. This would have context if an individual patient had a particularly aggressive PTC and identifying if this was due to a difference in their sEV miRNA profile. In order to help examine differential miRNA expression within the serum it would be worthwhile recruiting thyroid disease-free healthy age matched controls. To date, more than twenty blood serum samples from patients whom are undergoing thyroid surgery have been obtained which have been centrifuged and stored in a -80°C freezer ready for retrospective analysis.

In terms of further developing the clinical utility of sEV miRNA biomarkers within the context of thyroid disease, it would be worthwhile correlating TC patients sEV miRNA biomarkers with follow up thyroglobulin levels. This would be particularly helpful within the field of TC as the follow up monitoring of the plasma may demonstrate changes in the sEV miRNA profile within the serum. Jiang *et al.* looked at PTC sEV miRNA expression in serum samples of patients with LNM ($n=49$) and without LNM ($n=15$) which demonstrated changes in sEV microRNA expression, it would be interesting to follow up a similar cohort in Hull who have undergone thyroid surgery and see if on longitudinal follow up if there are any significant changes (Jiang *et al.*, 2020). This approach could be used to assess patient response to RAI and whether this corresponds to a change in sEV miRNA profile (Li *et al.*, 2022). In time this may help in the selection of certain patient groups for RAI.

Whilst undertaking this study, the selection of patients was determined by the demographic of those requiring thyroid surgery. The age range of such patients was from 19 to 83 years. Obviously, the younger patients within the study are more likely to

be free of systemic disease than the older patients. As a result, the serum samples from these younger patients would possess the most utility in terms of analysis as their serum is less likely to contain sEV miRNAs from other systemic diseases (Alberro et al., 2021). For instance, one individual within the study was a 19 year old female, with a locally advanced PTC, pT3b pN1b, with no other comorbidities (see **Table 2.1**). Such a patient, would be a high yield sample for identifying PTC associated sEV miRNAs, but for a meaningful study a cohort of such patients, and healthy controls, would be needed.

5.1.3 - FNAC - TC Diagnostics

FNAC as previously discussed is one of the main stays of TC diagnosis. In order to assess FNAC's diagnostic sensitivity, if at the time of FNAC sampling a sample of tissue as well as being sent off for cytology for diagnosis was made available for maintenance on a 'tissue-on-chip' device or alternatively cultured as an organoid and its sEV miRNA profile from the tissue analysed, this would possibly add to the overall diagnostic utility (Laukienė et al., 2022). Alongside this, if a blood sample was taken at the time of diagnostic FNAC and analysed through RT-qPCR for specific miRNAs of interest, then the results from this could be corroborated with that of the analysis of effluent from the tissue of the FNAC. One could assess the FNAC analysis alongside the miRNAs from tissue-on-chip effluent, and blood if relevant samples were taken.

5.1.4 - Administration of Therapeutics

As alluded to by the works of Lasalle *et al.* and Romeo *et al.*, previously (**Section 4**) it would be of interest to identify if the administration of therapeutics, notably novel TKIs, to the thyroid 'tissue on chip' can modify the sEV miRNA profile (Lasalle et al., 2016) (Romeo et al., 2018). A logical place to start, based on the work in this thesis, would be to see if the miRNA expression of miRNA-375-3p and miRNA-7-5p, along with other miRNAs identified through the miRNA sequencing are affected by oncological treatments such as TKIs or other novel therapies. An interesting question to address would be whether such therapeutics can affect sEV miRNA profile of TC and induce a 'more benign' appearing miRNA profile and whether this could be used as a means to monitor treatment response and efficacy. Foster *et al.* in their prior works were able to incubate the 'tissue on chip' with dexamethasone or methimazole and looked at the drugs effect upon the sEV miRNA profile (Foster et al., 2021). The team were able to

determine that treatment with methimazole and dexamethasone increased the expression of both miRNA-146a and miRNA-155 in non-Graves' tissue. This work therefore demonstrates the ability of therapeutics to affect the miRNA profile of sEV microRNAs produced by tissue maintained on 'tissue-on-chip' devices which could be further extrapolated to different thyroid diseased pathology and treatment regimens.

5.2 - Limitations of Study

5.2.1 - Patient Selection and Sample Size

The main focal point of the study was the miRNA sequencing results for PTC ($n=5$), GD ($n=4$) and EMG ($n=5$). A limiting factor, is the time taken in which to identify suitable patients, set up the devices and collect samples. Fortunately, in Hull the patients do generously donate tissue to the study following consent which enables six devices to be set up per sample. The whole process for this sequencing was through QIAGEN and the expense obviously places limitations on the number of samples that can be sent for sEV miRNA sequencing. Even with this small cohort the results demonstrate two miRNAs of significance but this raises the question whether a greater sample selection would lead to the identification of a further differential panel of miRNAs. Hopefully, with the costs of sequencing reducing and improved sEV techniques developing this should enable increased sample analysis throughput.

5.2.2 - Tissue Availability and Sampling

The patient cohort demographic poses a limitation to the work. Having personally identified and consented the patients, I was aware that the patients were predominantly White British or White Caucasians from Eastern Europe. A number of studies performed on sEV miRNAs within serum to date have been performed on Chinese populations which have also identified miR-222-3p, miR-221-3p, and miR-146a-5p as potential biomarkers (Dai, 2017; Yu, 2012; Xuan, 2020). It would be worthwhile looking at whether ethnicity or local environmental factors have an effect upon miRNA profiles. One area of further interest may be in terms of the Hull-based Eastern European population whom present for thyroid surgery as to whether they were living in an area of significant 'fall out' from the Chernobyl nuclear disaster and if they received iodine supplementation at the time during childhood (Chen, 2021; Penha, 2018; Nikiforova, 2011). It would be of interest to see if the radiation had an effect upon their sEV miRNA

profile and if this could be extrapolated to where they were living at the time of the event. Rolling this 'tissue on chip' technology out to other centres throughout the world would help with sample acquisition and procuring more advanced cases of thyroid disease for study. At current, relations are being fostered with teams in India in order to help facilitate this.

Another restricting factor is the time required to set-up each sample, and the limited number of samples that were obtained some weeks. For example, if an operating list had three samples that were appropriate for the study realistically only one of them would be recruited. The reason being that the preparation and set up time of the 'tissue on chip' device is considerable. In the current study, 33 patients were recruited but with additional technical support it would have possible to double this number although this would have required substantial additional finances in terms of laboratory staffing but also the miRNA sequencing costs.

5.3 - 'Tissue-on-chip' technology and tissue viability

Each progressive study using thyroid 'tissue on chip' technology has demonstrated that the devices are able to maintain viable thyroid tissue over an increasing timeframe. Riley *et al.* (2019) using the PEEK 'tissue on chip' device demonstrated viable thyroid tissue following 72 hours 'on-chip' whilst the current work through the histoarchitectural H+E staining demonstrated intact thyroid follicles and architecture following 144 hours 'on-chip' (Haigh *et al.*, 2023). The question is how long can the tissue be maintained 'on chip'? Future LDH testing or the effluent will be required in order to ascertain viability. In terms of further work performed in order to assess viability of the thyroid tissue on chip further analysis of T4 production and LDH detection following intentional tissue apoptosis could be carried out (Kennedy *et al.*, 2019; Riley *et al.*, 2019). In order to further provide clarification surrounding thyroid tissue viability on chip then Poly (ADP-ribose) polymerase-1 (PARP levels) can be detected via flow cytometry in order to detect levels of apoptosis that are taking place (Los *et al.*, 2002). PARP is an enzyme involved in DNA repair which during apoptosis is cleaved by active caspase-3.

One benefit of extending the length of time in which the tissue is viable on the chip is that it enables the collection of a greater amount of effluent over the time course. This will ultimately provide a greater number of sEVs for collection, centrifugation and

analysis, furthermore the greater timeframe will potentially increase the effect of drugs upon the tissue resulting in a greater likelihood of being able to detect the effect upon the sEV miRNA profile over certain timeframes.

5.4 - Pathology

In terms of tissue, the study was limited to the patients that were undergoing thyroid resections at Hull University Teaching Hospitals NHS Trust. A drawback in term of sample selection is that one is not completely sure of the nature of thyroid tissue one is loading on the devices despite the USS and FNAC results. One will have to wait for approximately two weeks following the procedure to have the formal histopathological report. As a result, one loads the device on the presumption it is 'PTC' but that sample of tissue may well not be 'PTC'; it could be a disease-free sample of thyroid tissue or a completely different TC. In order, to officially determine this it would require the opinion of a histopathologist for each sample of tissue loaded on the 'tissue on chip' devices. This would most likely require the tissue samples following being on 'chip' being sent to the hospital based-laboratories for processing and sectioning to the standard required for slides at patient diagnostic level. This would come at considerable expense but would provide that clarity and peace of mind for future studies as to what 'exactly' is loaded on each chip.

A shortcoming of the study that could be argued is that the 'benign' EMG cohort is not actually a 'healthy' thyroid control cohort as they are still undergoing a thyroid operation which makes direct comparison limited. This is a difficult issue to address from the perspective of obtaining thyroid tissue as one can only obtain tissue ethically from consented patients undergoing thyroid surgery for an indicated reason following assessment by a clinician. From a gross, pathological perspective these are considered non-malignant but from time to time can be harbouring undiagnosed PTC or PTMC.

A means through which to obtain 'healthy' benign thyroid tissue would be through obtaining the thyroid tissue during a parathyroid operation or laryngectomy that is being undertaken not for the management of thyroid disease. With the view to obtaining healthy thyroid tissue, the parathyroid procedure would provide the best means through which to obtain non-diseased thyroid tissue. One has to be aware however though ethically that removing a small amount of thyroid tissue does pose a risk to the

patient in terms of a bleed into the neck during surgery and after surgery. The patient is at risk having undergone parathyroid surgery anyhow, but one cannot deny that the risk would be increased as a result of removing further thyroid tissue. In this respect, I feel obtaining ethical approval would be difficult due to the associated risk to the patient. Within the context of obtaining thyroid tissue from patients who have undergone laryngectomy I feel that this would have to be a very small subset of patients as the vast majority of patients who undergo a laryngectomy will be for T4 laryngeal squamous cell carcinoma in which the disease has invaded and involving the thyroid cartilage. I feel that these patients there will be a small burden of disease in the thyroid or micro-metastatic disease within the thyroid. If however, on the rare occasion, the patient was undergoing a laryngectomy for benign pathology then this sample of thyroid tissue would be ideal and plentiful.

5.5 - Flow cytometry and exosomal marker labelling

Flow cytometry has been shown to be able to detect sEVs and utilises tetraspanin exosomal markers to label sEVs (van der Pol et al., 2022). During the period of the study, the BD FACS Symphony A1 flow cytometer fitted with the small particle detector was used for a trial period. The flow cytometer was able to detect small particles in keeping with the size of sEVs. Again, exosomal markers anti-CD63 and anti-CD81 were used with appropriate fluorochromes. Detection was evident for samples but there was a lack of consistency in results and further optimisation steps were required before this could be used routinely. However, such technology demonstrates promise going forward surrounding sEV study (Kobayashi et al., 2024). Magnetic beads conjugated with antibodies against tetraspanins can be used for affinity isolation methods and Kobayashi *et al.* study demonstrated that flow cytometry techniques demonstrated reduced false positives for tetraspanin staining than when compared to that of differential ultracentrifugation in terms of identification of sEVs. Evidence is gathering that use of flow cytometers with tetraspanin antibodies can be more accurate in terms of isolation of sEV populations than differential ultracentrifugation. It does appear that there will be paradigm shift over to flow cytometry within the context of characterising sEV populations (Welsh et al., 2024). At current, the team in the laboratory are trialling effluent on the Paraytec CX300 Optical Particle Analysis Instrument (York, UK), a portable flow cytometer that can detect fluorescently labelled cells and sEV equally well.

5.6 - Microfluidics in the field of sEV Isolation and Detection

A key limiting factor within the field of sEV study is differential centrifugation. If the microfluidic devices had an inbuilt means through which to isolate sEVs this would circumvent the need for time consuming isolation techniques. This would allow direct isolation of the sEVs from 'tissue on chip' and would significantly increase throughput and subsequent analysis, assuming the issues of sensitivity can be addressed.

Recent studies have begun to look to use microfluidic devices in the detection of cancer associated exosomes using immune affinity methods. This method uses immunoaffinity interactions between antigens, exosome membrane proteins and monoclonal antibodies (Raju et al., 2022). Exosomal tetraspanin proteins such as CD9, CD81 and CD63 are bound by immunomagnetic beads that allow exosome isolation. A number of microfluidic devices have been developed in which to capture exosomes using similar technology. Wang *et al.* (2013) developed a device around a micropillar structure. This device was able to isolate exosome-like lipid vesicles and filter out proteins and cell debris. Fang *et al.* (2017) in their microfluidic device were able to analyse patient plasma samples for exosome content. In order to capture the exosomes, magnetic nanoparticles (Mag-CD63) were used against the CD63 antibodies. The study was able to identify that the amount of exosomal tumour marker EpCAM was much greater in breast cancer patient's plasma compared to healthy controls. Obviously, this would deliver huge time saving benefits compared with ultracentrifugation if such technology could be integrated into future works. The isolation of sEVs through the use of microfluidic devices has demonstrated significant progress and may well in the future be able to avoid the time-consuming process of ultracentrifugation to isolate sEVs.

5.7 - Conclusion

The project isolated sEVs in effluent from tissue maintained on 'tissue on chip' devices and identify four miRNAs: miRNA-375-3p, miRNA-7-5p, miRNA-382-5p and miRNA-127-3p which may well have a role to play in the pathogenesis of TC and AITD. In order to determine their utility as biomarkers in thyroid disease, further comparisons of the levels of the four miRNAs are required against the 'healthy' serum of controls. The 'holy grail' as mentioned would be the development of a non-invasive, cost effective 'liquid biopsy' within thyroid diagnostics. Of future interest, would be whether certain treatment modalities are able to modify the sEV miRNA profile of thyroid disease; this

would help to provide an indication regarding treatment response and disease recurrence. The advent of flow cytometry within EV research should contribute significantly to quicken sEV isolation and their subsequent analysis (Welsh et al., 2024).

In conclusion, the use of 'tissue-on-chip' technology enables the search for miRNA biomarkers in thyroid disease to be more specifically focused upon a thyroid pathology of interest. The work in this thesis has identified four exosomal miRNA candidates for further investigations being mindful that a large number of miRNAs are working together in thyroid disease states. To my mind, further work should be dedicated to the identification and validation of these findings within serum.

Reference list / Bibliography

(2024) *R: The R Project for Statistical Computing*.

@plotlygraphs (2024) *Data Apps for Production | Plotly*. Available online: / [Accessed.

@theconstructor2 (2021) *Laminar Flow and Turbulent Flow - The Constructor*. Available online: <https://theconstructor.org/fluid-mechanics/laminar-turbulent-flow/559432/> [Accessed 06/08/2023].

Adam, M., Thomas, S., Youngwirth, L., Hyslop, T., Reed, S., Scheri, R., Roman, S. & Sosa, J. (2017) Is There a Minimum Number of Thyroidectomies a Surgeon Should Perform to Optimize Patient Outcomes? *Annals of surgery*, 265(2).

Agarwal, S. & Bychkov, A. (2024) *Anaplastic thyroid carcinoma*. Available online: <http://www.pathologyoutlines.com/topic/thyroidUndiff.html> [Accessed 16/03/24].

Ahn, H., Kim, H. & Welch, H. (2014) Korea's thyroid-cancer "epidemic"--screening and overdiagnosis. *The New England journal of medicine*, 371(19).

Akamizu, T., Satoh, T., Isozaki, O., Suzuki, A., Wakino, S., Iburi, T., Tsuboi, K., Monden, T., Kouki, T., Otani, H., Teramukai, S., Uehara, R., Nakamura, Y., Nagai, M. & Mori, M. (2012) Diagnostic criteria, clinical features, and incidence of thyroid storm based on nationwide surveys. *Thyroid : official journal of the American Thyroid Association*, 22(7).

Alberro, A., Iparraguirre, L., Fernandes, A. & Otaegui, D. (2021) Extracellular Vesicles in Blood: Sources, Effects, and Applications. *International Journal of Molecular Sciences*, 22(15), 8163.

Allen, E. & Fingeret, A. (2023) *Anatomy, Head and Neck, Thyroid*.

Altayeb, A., Vanka, R., Bartholomew, P., Vennart, N., Vernazza, J., Stewart, K., Tsalidis, V., Narayanan, K., Weaver, J. U. & Razvi, S. (2022) The prevalence and significance of nonuniform thyroid radio - isotope uptake in patients with Graves' disease. *Clinical Endocrinology*, 97(1), 100.

Aly, Z. & Satturwar, S. (2023) *Graves disease*. Available online: <http://www.pathologyoutlines.com/topic/thyroidgraves.html> [Accessed 05/08/2023].

Antonelli, A., Ferrari, S., Ragusa, F., Elia, G., Paparo, S., Ruffilli, I., Patrizio, A., Giusti, C., Gonnella, D., Cristaudo, A., Foddìs, R., Shoenfeld, Y. & Fallahi, P. (2020) Graves' disease: Epidemiology, genetic and environmental risk factors and viruses. *Best practice & research. Clinical endocrinology & metabolism*, 34(1).

Armstrong, M., Asuka, E. & Fingeret, A. (2023) *Physiology, Thyroid Function*.

Augenlicht, A., Saiselet, M., Decaussin-Petrucci, M., Andry, G., Dumont, J. & Maenhaut, C. (2021) MiR-7-5p inhibits thyroid cell proliferation by targeting the EGFR/MAPK and IRS2/PI3K signaling pathways. *Oncotarget*, 12(16).

- Ayuso, J., Virumbrales-Muñoz, M., Lang, J. & Beebe, D. (2022) A role for microfluidic systems in precision medicine. *Nature communications*, 13(1).
- Bahn Chair, R., Burch, H., Cooper, D., Garber, J., Greenlee, M., Klein, I., Laurberg, P., McDougall, I., Montori, V., Rivkees, S., Ross, D., Sosa, J. & Stan, M. (2011) Hyperthyroidism and other causes of thyrotoxicosis: management guidelines of the American Thyroid Association and American Association of Clinical Endocrinologists. *Thyroid : official journal of the American Thyroid Association*, 21(6).
- Beck-Peccoz, P., Rodari, G., Giavoli, C. & Lania, A. (2017) Central hypothyroidism - a neglected thyroid disorder. *Nature Reviews. Endocrinology*, 13(10).
- Belfiore, A. & La Rosa, G. (2001) Fine-needle aspiration biopsy of the thyroid. *Endocrinology and metabolism clinics of North America*, 30(2).
- Bernal, J. (2005) Thyroid hormones and brain development. *Vitamins and hormones*, 71.
- Biassoni, R. & Raso, A. (2020) *Quantitative Real-Time PCR Methods and Protocols by Roberto Biassoni, Alessandro Raso (z-lib.org) (1).pdf*, 2023. Springer Science.
- Biosystems, A. (2015) *ROX passive reference dye for troubleshooting real-time PCR*. Available online: <https://assets.thermofisher.com/TFS-Assets/GSD/Application-Notes/co016741-rox-dye-for-qpcr-app-note.pdf> [Accessed].
- Bobrie, A., Colombo, M., Raposo, G. & Théry, C. (2011) Exosome secretion: molecular mechanisms and roles in immune responses. *Traffic (Copenhagen, Denmark)*, 12(12).
- Boelaert, K., Torlinska, B., Holder, R. & Franklyn, J. (2010) Older subjects with hyperthyroidism present with a paucity of symptoms and signs: a large cross-sectional study. *The Journal of clinical endocrinology and metabolism*, 95(6).
- Bogusławska, J., Godlewska, M., Gajda, E. & Piekietko-Witkowska, A. (2022) Cellular and molecular basis of thyroid autoimmunity. *European thyroid journal*, 11(1).
- Botha, J., Pugsley, H. & Handberg, A. (2021) Conventional, High-Resolution and Imaging Flow Cytometry: Benchmarking Performance in Characterisation of Extracellular Vesicles. *Biomedicines*, 9(2).
- Bower, R., Green, V., Kuvshinova, E., Kuvshinov, D., Karsai, L., Crank, S., Stafford, N. & Greenman, J. (2017) Maintenance of head and neck tumor on-chip: gateway to personalized treatment? *Future science OA*, 3(2).
- Brent, G. (2008) Clinical practice. Graves' disease. *The New England Journal of Medicine*, 358(24).
- Bresciani, L., Orlandi, E. & Piazza, C. (2019) Radiation-induced papillary thyroid cancer: is it a distinct clinical entity? *Current opinion in otolaryngology & head and neck surgery*, 27(2).

- Brito, J., Morris, J. & Montori, V. (2013) Thyroid cancer: zealous imaging has increased detection and treatment of low risk tumours. *BMJ (Clinical research ed.)*, 347.
- Burch, H. & Cooper, D. (2015) Management of Graves Disease: A Review. *JAMA*, 314(23).
- Bureau, L., Coupier, G. & Salez, T. (2023) Lift at low Reynolds number. *The European physical journal. E, Soft matter*, 46(11).
- Burgoyne, L. (1999) The mechanisms of pyknosis: hypercondensation and death. *Experimental cell research*, 248(1).
- Califf, R. (2018) Biomarker definitions and their applications. *Experimental biology and medicine (Maywood, N.J.)*, 243(3).
- Carr, S., Green, V., Stafford, N. & Greenman, J. (2014) Analysis of radiation-induced cell death in head and neck squamous cell carcinoma and rat liver maintained in microfluidic devices. *Otolaryngology - head and neck surgery: Official Journal of American Academy of Otolaryngology-Head and Neck Surgery*, 150(1).
- Carter, S. & Barratt, A. (2017) What is overdiagnosis and why should we take it seriously in cancer screening? *Public health research & practice*, 27(3).
- Caterina, C., Carlo, C. & Giuseppe, Z. (2016) MicroRNA in Control of Gene Expression: An Overview of Nuclear Functions. *International Journal of Molecular Sciences*, 17(10), 1712.
- Chadwick, D., Kinsman, R. & Walton, P. (2017) BAETS Audit National Report 2017.
- Chaker, L., Cooper, D., Walsh, J. & Peeters, R. (2024) Hyperthyroidism. *Lancet (London, England)*, 403(10428).
- Chaker, L., Razvi, S., Bensenor, I., Azizi, F., Pearce, E. & Peeters, R. (2022) Hypothyroidism. *Nature Reviews Disease Primers*, 8(1), 1-17.
- Chakraborty, A., Patton, D. J., Smith, B. F. & Agarwal, P. (2023) miRNAs: Potential as Biomarkers and Therapeutic Targets for Cancer. *Genes*, 14(7), 1375.
- Cheah, R., Srivastava, R., Stafford, N., Beavis, A., Green, V. & Greenman, J. (2017) Measuring the response of human head and neck squamous cell carcinoma to irradiation in a microfluidic model allowing customized therapy. *International journal of oncology*, 51(4).
- Cheetham, T. (2021) How to use thionamide anti-thyroid drug in the young– what’s new? *Thyroid Research*, 14, 18.
- Chiovato, L., Magri, F. & Carlé, A. (2019) Hypothyroidism in Context: Where We've Been and Where We're Going. *Advances in therapy*, 36(Suppl 2).

Chung, J.-K. (2012) *Sodium Iodide Symporter in Thyroid Carcinoma* | SpringerLink.SpringerLink.

Ciampi, R. & Nikiforov, Y. (2007) RET/PTC rearrangements and BRAF mutations in thyroid tumorigenesis. *Endocrinology*, 148(3).

Convery, N. & Gadegaard, N. (2019) 30 years of microfluidics. *Micro and Nano Engineering*.

Cooper, D., Doherty, G., Haugen, B., Kloos, R., Lee, S., Mandel, S., Mazzaferri, E., McIver, B., Pacini, F., Schlumberger, M., Sherman, S., Steward, D. & Tuttle, R. (2009) Revised American Thyroid Association management guidelines for patients with thyroid nodules and differentiated thyroid cancer. *Thyroid : official journal of the American Thyroid Association*, 19(11).

Coquinco, A. & Cynader, M. (2015) Use of a 3-Compartment Microfluidic Device to Study Activity Dependent Synaptic Competition | Springer Nature Experiments. *Springer Nature Experiments*(10.1007/978-1-4939-2510-0_8).

Corrado, C., Raimondo, S., Chiesi, A., Ciccia, F., De Leo, G. & Alessandro, R. (2013) Exosomes as intercellular signaling organelles involved in health and disease: basic science and clinical applications. *International journal of molecular sciences*, 14(3).

Cramer, H. (2000) Fine-needle aspiration cytology of the thyroid: an appraisal. *Cancer*, 90(6).

Cross, P., Chandra, A., Giles, T., Johnson, S. & Poller, D. (2024) The Royal College of Pathologists - Guidance on the reporting of thyroid cytology specimens, 2024(March).

Cui, X., Huang, M., Wang, S., Zhao, N., Huang, T., Wang, Z., Qiao, J., Wang, S., Shan, Z., Teng, W. & Li, Y. (2021) Circulating Exosomes From Patients With Graves' Disease Induce an Inflammatory Immune Response. *Endocrinology*, 162(3).

D'Aurizio, F., Kratzsch, J., Gruson, D., Petranović Ovčariček, P. & Giovanella, L. (2023) Free thyroxine measurement in clinical practice: how to optimize indications, analytical procedures, and interpretation criteria while waiting for global standardization. *Critical reviews in clinical laboratory sciences*, 60(2).

Dai, J., Su, Y., Zhong, S., Cong, L., Liu, B., Yang, J., Tao, Y., He, Z., Chen, C. & Jiang, Y. (2020) Exosomes: key players in cancer and potential therapeutic strategy. *Signal transduction and targeted therapy*, 5(1).

Danzi, S. & Klein, I. (2015) Amiodarone-induced thyroid dysfunction. *Journal of intensive care medicine*, 30(4).

Davies, T., Andersen, S., Latif, R., Nagayama, Y., Barbesino, G., Brito, M., Eckstein, A., Stagnaro-Green, A. & Kahaly, G. (2020) Graves' disease. *Nature reviews. Disease primers*, 6(1).

- Dayan, C. & Daniels, G. (1996) Chronic autoimmune thyroiditis. *The New England journal of medicine*, 335(2).
- De Toro, J., Herschlik, L, Waldner, C. & Mongini, C. (2015) Emerging roles of exosomes in normal and pathological conditions: new insights for diagnosis and therapeutic applications. *Frontiers in immunology*, 6.
- DeLellis, R., Rule, A., Spiler, I., Nathanson, L., Tashjian, A. & Wolfe, H. (1978) Calcitonin and carcinoembryonic antigen as tumor markers in medullary thyroid carcinoma. *American journal of clinical pathology*, 70(4).
- Dharap, A., Pokrzywa, C., Murali, S., Pandi, G. & Vemuganti, R. (2013) MicroRNA miR-324-3p Induces Promoter-Mediated Expression of RelA Gene. *PLoS ONE*, 8(11).
- Dimitriadis, P., Moinie, A., Michaels, J., Bance, R., Vijendren, A. & Mochloulis, G. (2023) Indeterminate thyroid nodules (Thy3): malignancy rate and characteristics in a study of 118 patients. *Annals of the Royal College of Surgeons of England*, 105(6).
- Doubleday, A. & Sippel, R. (2020) Hyperthyroidism. *Gland Surgery*, 9(1), 124.
- Dragovic, R., Gardiner, C., Brooks, A., Tannetta, D., Ferguson, D., Hole, P., Carr, B., Redman, C., Harris, A., Dobson, P., Harrison, P. & Sargent, I. (2011) Sizing and phenotyping of cellular vesicles using Nanoparticle Tracking Analysis. *Nanomedicine : nanotechnology, biology, and medicine*, 7(6).
- Durante, C., Haddy, N., Baudin, E., Leboulleux, S., Hartl, D., Travagli, J., Caillou, B., Ricard, M., Lumbroso, J., De Vathaire, F. & Schlumberger, M. (2006) Long-term outcome of 444 patients with distant metastases from papillary and follicular thyroid carcinoma: benefits and limits of radioiodine therapy. *The Journal of clinical endocrinology and metabolism*, 91(8).
- England, R. & Atkin, S. (2007) Total thyroidectomy is best operation for thyrotoxicosis. *BMJ : British Medical Journal*, 334(7596), 710.
- Ewing, B. & Green, P. (1998) Base-calling of automated sequencer traces using phred. II. Error probabilities. *Genome research*, 8(3).
- Fagin, J. A. & Wells, S. A. (2016) Biologic and Clinical Perspectives on Thyroid Cancer. *The New England journal of medicine*, 375(11), 1054.
- Fagman, H. & Nilsson, M. (2010) Morphogenesis of the thyroid gland. *Molecular and cellular endocrinology*, 323(1).
- Falkovich, G. (2023) Fluid Mechanics.
- Faten, L., Sarang, K., Phyu Thin, N. & Al O, G. (2023) Anaplastic Thyroid Cancer.

Feng, K., Ma, R., Zhang, L., Li, H., Tang, Y., Du, G., Niu, D. & Yin, D. (2020) The Role of Exosomes in Thyroid Cancer and Their Potential Clinical Application. *Frontiers in oncology*, 10.

Filipe, V., Hawe, A. & Jiskoot, W. (2010) Critical Evaluation of Nanoparticle Tracking Analysis (NTA) by NanoSight for the Measurement of Nanoparticles and Protein Aggregates. *Pharmaceutical Research*, 27(5), 796-810.

Filipowicz, W., Bhattacharyya, S. & Sonenberg, N. (2008) Mechanisms of post-transcriptional regulation by microRNAs: are the answers in sight? *Nature reviews. Genetics*, 9(2).

Fischer, A., Jacobson, K., Rose, J. & Zeller, R. (2008) Hematoxylin and eosin staining of tissue and cell sections. *CSH protocols*, 2008.

Foster, H., Wade, M., England, J., Greenman, J. & Green, V. (2021) Isolation and characterisation of graves' disease-specific extracellular vesicles from tissue maintained on a bespoke microfluidic device. *Organs-on-a-Chip*.

Fröhlich, D., Kuo, W., Frühbeis, C., Sun, J., Zehendner, C., Luhmann, H., Pinto, S., Toedling, J., Trotter, J. & Krämer-Albers, E. (2014) Multifaceted effects of oligodendroglial exosomes on neurons: impact on neuronal firing rate, signal transduction and gene regulation. *Philosophical transactions of the Royal Society of London. Series B, Biological sciences*, 369(1652).

Frühbeis, C., Fröhlich, D., Kuo, W., Amphornrat, J., Thilemann, S., Saab, A., Kirchhoff, F., Möbius, W., Goebels, S., Nave, K., Schneider, A., Simons, M., Klugmann, M., Trotter, J. & Krämer-Albers, E. (2013) Neurotransmitter-triggered transfer of exosomes mediates oligodendrocyte-neuron communication. *PLoS biology*, 11(7).

Galluzzi, L., Vitale, I., Aaronson, S., Abrams, J., Adam, D., Agostinis, P., Alnemri, E., Altucci, L., Amelio, I., Andrews, D., Annicchiarico-Petruzzelli, M., Antonov, A., Arama, E., Baehrecke, E., Barlev, N., Bazan, N., Bernassola, F., Bertrand, M., Bianchi, K., Blagosklonny, M., Blomgren, K., Borner, C., Boya, P., Brenner, C., Campanella, M., Candi, E., Carmona-Gutierrez, D., Cecconi, F., Chan, F., Chandel, N., Cheng, E., Chipuk, J., Cidlowski, J., Ciechanover, A., Cohen, G., Conrad, M., Cubillos-Ruiz, J., Czabotar, P., D'Angiolella, V., Dawson, T., Dawson, V., De Laurenzi, V., De Maria, R., Debatin, K., DeBerardinis, R., Deshmukh, M., Di Daniele, N., Di Virgilio, F., Dixit, V. M., Dixon, S. J., Duckett, C. S., Dynlacht, B. D., El-Deiry, W. S., Elrod, J. W., Fimia, G. M., Fulda, S., García-Sáez, A. J., Garg, A. D., Garrido, C., Gavathiotis, E., Golstein, P., Gottlieb, E., Green, D. R., Greene, L. A., Gronemeyer, H., Gross, A., Hajnoczky, G., Hardwick, J. M., Harris, I. S., Hengartner, M. O., Hetz, C., Ichijo, H., Jäättelä, M., Joseph, B., Jost, P. J., Juin, P. P., Kaiser, W. J., Karin, M., Kaufmann, T., Kepp, O., Kimchi, A., Kitsis, R. N., Klionsky, D. J., Knight, R. A., Kumar, S., Lee, S. W., Lemasters, J. J., Levine, B., Linkermann, A., Lipton, S. A., Lockshin, R. A., López-Otín, C., Lowe, S. W., Luedde, T., Lugli, E., MacFarlane, M., Madeo, F., Malewicz, M., Malorni, W., Manic, G., et al (2018) Molecular mechanisms of cell death: recommendations of the Nomenclature Committee on Cell Death 2018. *Cell Death & Differentiation*, 25(3), 486-541.

Galuppini, F., Bertazza, L., Barollo, S., Cavedon, E., Rugge, M., Guzzardo, V., Sacchi, D., Watutantrige-Fernando, S., Vianello, F., Mian, C. & Pennelli, G. (2017) MiR-375 and YAP1 expression profiling in medullary thyroid carcinoma and their correlation with clinical-pathological features and outcome. *Virchows Archiv : an international journal of pathology*, 471(5).

Gammazza, M. A., Rizzo, M., Citarrella, R., Rappa, F., Campanella, C., Bucchieri, F., Patti, A., Nikolic, D., Cabibi, D., Amico, G., Conaldi, P., San Biagio, P., Montalto, G., Farina, F., Zummo, G., Conway de Macario, E., Macario, A. & Cappello, F. (2014) Elevated blood Hsp60, its structural similarities and cross-reactivity with thyroid molecules, and its presence on the plasma membrane of oncocytes point to the chaperonin as an immunopathogenic factor in Hashimoto's thyroiditis. *Cell stress & chaperones*, 19(3).

Gangadaran, P., Madhyastha, R., Rajendran, R. L., Nakajima, Y., Watanabe, N., Velikkakath, A. K. G., Hong, C. M., Gopi, R. V., Muthukalianan, G. K., Gopalakrishnan, A. V., Jeyaraman, M. & Ahn, B.-C. (2023) The emerging role of exosomes in innate immunity, diagnosis and therapy. *Frontiers in Immunology*, 13, 1085057.

Gardiner, C., Di Vizio, D., Sahoo, S., Théry, C., Witwer, K., Wauben, M. & Hill, A. (2016) Techniques used for the isolation and characterization of extracellular vesicles: results of a worldwide survey. *Journal of extracellular vesicles*, 5.

Garrett, J., Tamir, H., Kifor, O., Simin, R., Rogers, K., Mithal, A., Gagel, R. & Brown, E. (1995) Calcitonin-secreting cells of the thyroid express an extracellular calcium receptor gene. *Endocrinology*, 136(11).

Gereben, B., Zavacki, A., Ribich, S., Kim, B., Huang, S., Simonides, W., Zeöld, A. & Bianco, A. (2008) Cellular and molecular basis of deiodinase-regulated thyroid hormone signaling. *Endocrine reviews*, 29(7).

Giovanella, L., Görges, R., Tuttle, R. M., Visser, W. E., Verburg, F. A., Borowczyk, M., Chiovato, L., Duntas, L., Feldt-Rasmussen, U., Knappe, L., Leenhardt, L., Magri, F., Rimmele, H. & Seregni, E. (2023) Thyroglobulin and thyroglobulin antibody: an updated clinical and laboratory expert consensus. *European Journal of Endocrinology*, 189(2).

Gish, D., Thomas, R., Melnick, S. & Nazir, S. (2016) Myxoedema coma: a forgotten presentation of extreme hypothyroidism. *BMJ Case Reports*.

Goetz, L. & Schork, N. (2018) Personalized medicine: motivation, challenges, and progress. *Fertility and sterility*, 109(6).

Gomberg-Maitland, M. & Frishman, W. (1998) Thyroid hormone and cardiovascular disease. *American heart journal*, 135(2 Pt 1).

Gorman, C. (1999) Radioiodine and pregnancy. *Thyroid : official journal of the American Thyroid Association*, 9(7).

Gray, W., Aspinall, S., Tolley, N., Day, J. & Lansdown, M. (2021) The volume and outcome relationship for thyroidectomy in England. *Langenbeck's Archives of Surgery*, 406(6), 1999.

Griffiths, D., Carnell-Morris, P., Wright, M. & (2020) Nanoparticle Tracking Analysis for Multiparameter Characterization and Counting of Nanoparticle Suspensions. *Methods in molecular biology (Clifton, N.J.)*, 2118.

Grzanka, M., Stachurska-Skrodzka, A., Adamiok-Ostrowska, A., Gajda, E. & Czarnocka, B. (2022) Extracellular Vesicles as Signal Carriers in Malignant Thyroid Tumors? *International journal of molecular sciences*, 23(6).

Haberal, A., Toru, S., Ozen, O., Arat, Z. & Bilezikçi, B. (2009) Diagnostic pitfalls in the evaluation of fine needle aspiration cytology of the thyroid: correlation with histopathology in 260 cases. *Cytopathology : official journal of the British Society for Clinical Cytology*, 20(2).

Haigh, T., Beattie, H., Wade, M., England, J., Kuvshinov, D., Karsai, L., Greenman, J. & Green, V. (2023) The Use of Tissue-on-Chip Technology to Focus the Search for Extracellular Vesicle miRNA Biomarkers in Thyroid Disease. *International journal of molecular sciences*, 25(1).

Hamatani, K., Eguchi H, Ito, R., Mukai, M., Takahashi, K., Taga, M., Imai, K., Cologne, J., Soda, M., Arihiro, K., Fujihara, M., Abe, K., Hayashi, T., Nakashima, M., Sekine, I., Yasui, W., Hayashi, Y. & Nakachi, K. (2008) RET/PTC rearrangements preferentially occurred in papillary thyroid cancer among atomic bomb survivors exposed to high radiation dose. *Cancer research*, 68(17).

Harach, H., Franssila, K. & Wasenius, V. (1985) Occult papillary carcinoma of the thyroid. A "normal" finding in Finland. A systematic autopsy study. *Cancer*, 56(3).

Hattersley, S., Sylvester, D., Dyer, C., Stafford, N., Haswell, S. & Greenman, J. (2012) A microfluidic system for testing the responses of head and neck squamous cell carcinoma tissue biopsies to treatment with chemotherapy drugs. *Annals of biomedical engineering*, 40(6).

Haugen, B., Alexander, E., Bible, K., Doherty, G., Mandel, S., Nikiforov, Y., Pacini, F., Randolph, G., Sawka, A., Schlumberger, M., Schuff, K., Sherman, S., Sosa, J., Steward, D., Tuttle, R. & Wartofsky, L. (2016) 2015 American Thyroid Association Management Guidelines for Adult Patients with Thyroid Nodules and Differentiated Thyroid Cancer: The American Thyroid Association Guidelines Task Force on Thyroid Nodules and Differentiated Thyroid Cancer. *Thyroid : official journal of the American Thyroid Association*, 26(1).

Haymart, M., Esfandiari, N., Stang, M. & Sosa, J. (2017) Controversies in the Management of Low-Risk Differentiated Thyroid Cancer. *Endocrine reviews*, 38(4).

Hemler, M. (2005) Tetraspanin functions and associated microdomains. *Nature reviews. Molecular cell biology*, 6(10).

Hertz, S. & Roberts, A. (1946) Radioactive iodine in the study of thyroid physiology; the use of radioactive iodine therapy in hyperthyroidism. *Journal of the American Medical Association*, 131.

Hofstra, R., Landsvater, R., Ceccherini, I., Stulp, R., Stelwagen, T., Luo, Y., Pasini, B., Höppener, J., van Amstel, H. & Romeo, G. (1994) A mutation in the RET proto-oncogene associated with multiple endocrine neoplasia type 2B and sporadic medullary thyroid carcinoma. *Nature*, 367(6461).

Hsu, J., Chiu, C., Hsu, S., Huang, W., Chien, C., Lee, T. & Huang, H. (2011) miRTar: an integrated system for identifying miRNA-target interactions in human. *BMC bioinformatics*, 12.

Hu, J., Yuan, I., Mirshahidi, S., Simental, A., Lee, SC & Yuan, X. (2021) Thyroid Carcinoma: Phenotypic Features, Underlying Biology and Potential Relevance for Targeting Therapy. *International journal of molecular sciences*, 22(4).

Huang, T., Guan, X. & Fu, L. (2019) Therapeutic targeting of the crosstalk between cancer-associated fibroblasts and cancer stem cells. *American journal of cancer research*, 9(9).

Imparato, G., Urciuolo, F. & Netti, P. A. (2022) Organ on Chip Technology to Model Cancer Growth and Metastasis. *Bioengineering*, 9(1), 28.

Ingber, D. (2022) Human organs-on-chips for disease modelling, drug development and personalized medicine. *Nature reviews. Genetics*, 23(8).

Ingoe, L., Phipps, N., Armstrong, G., Rajagopal, A., Kamali, F. & Razvi, S. (2017) Prevalence of treated hypothyroidism in the community: Analysis from general practices in North-East England with implications for the United Kingdom. *Clinical endocrinology*, 87(6).

Ipsaro, J. & Joshua-Tor, L. (2015) From guide to target: molecular insights into eukaryotic RNA-interference machinery. *Nature structural & molecular biology*, 22(1).

Isola, A. & Chen, S. (2017) Exosomes: The Messengers of Health and Disease. *Current Neuropharmacology*, 15(1), 157.

JA, W., DCI, G., L, O. D., EI, B., C, B., B, B., H, C., D, D. V., TAP, D., U, E., JM, F.-P., QL, F., AF, H., M, L., SK, L., MG, M., S, M., A, M., R, N., ... & KW, W. (2024) Minimal information for studies of extracellular vesicles (MISEV2023): From basic to advanced approaches. *Journal of extracellular vesicles*, 13(2).

Jegerlehner, S., Bulliard, J., Aujesky, D., Rodondi, N., Germann, S., Konzelmann, I. & Chiolerio, A. (2017) Overdiagnosis and overtreatment of thyroid cancer: A population-based temporal trend study. *PLoS ONE*, 12(6).

- Jensen, C., Saucke, M., Francis, D., Voils, C. & Pitt, S. (2020) From Overdiagnosis to Overtreatment of Low-Risk Thyroid Cancer: A Thematic Analysis of Attitudes and Beliefs of Endocrinologists, Surgeons, and Patients. *Thyroid : official journal of the American Thyroid Association*, 30(5).
- Jeppesen, D., Zhang, Q., Franklin, J. & Coffey, R. (2023) Extracellular vesicles and nanoparticles: emerging complexities. *Trends in cell biology*, 33(8).
- Jiang, K., Li, G., Chen, W., Song, L., Wei, T., Li, Z., Gong, R., Lei, J., Shi, H. & Zhu, J. (2020) Plasma Exosomal miR-146b-5p and miR-222-3p are Potential Biomarkers for Lymph Node Metastasis in Papillary Thyroid Carcinomas. *OncoTargets and therapy*, 13.
- Jingwen, J., Jiayu, L., Xiumei, Z., Xueqin, Z., Biao, H. & Yuan, Q. (2022) Exosomes Regulate the Epithelial–Mesenchymal Transition in Cancer. *Frontiers in Oncology*, 12, 864980.
- Johannessen, J. & Sobrinho-Simões, M. (1980) The origin and significance of thyroid psammoma bodies. *Laboratory investigation; a journal of technical methods and pathology*, 43(3).
- Jung, C., Bychkov, A. & Kakudo, K. (2022) Update from the 2022 World Health Organization Classification of Thyroid Tumors: A Standardized Diagnostic Approach. *Endocrinology and metabolism (Seoul, Korea)*, 37(5).
- Kaliszewski, K., Diakowska, D., Miciak, M., Jurkiewicz, K., Kisiel, M., Makles, S., Dziekiewicz, A., Biernat, S., Ludwig, M., Ludwig, B., Sutkowska-Stępień, K., Sebastian, M., Domosławski, P., Sutkowski, K. & Wojtczak, B. (2023) The Incidence Trend and Management of Thyroid Cancer—What Has Changed in the Past Years: Own Experience and Literature Review. *Cancers*, 15(20), 4941.
- Kaliszewski, K., Diakowska, D., Wojtczak, B., Forkasiewicz, Z., Pupka, D., Nowak, Ł. & Rudnicki, J. (2019) Which papillary thyroid microcarcinoma should be treated as "true cancer" and which as "precancer"? *World journal of surgical oncology*, 17(1).
- Kalluri, R. & LeBleu, V. S. (2020) The biology, function, and biomedical applications of exosomes.
- Kanaoka, R., Iinuma, H., Dejima, H., Sakai, T., Uehara, H., Matsutani, N. & Kawamura, M. (2018) Usefulness of Plasma Exosomal MicroRNA-451a as a Noninvasive Biomarker for Early Prediction of Recurrence and Prognosis of Non-Small Cell Lung Cancer. *Oncology*, 94(5).
- Kennedy, R., Kuvshinov, D., Sdrolia, A., Kuvshinova, E., Hilton, K., Crank, S., Beavis, A., Green, V. & Greenman, J. (2019) A patient tumour-on-a-chip system for personalised investigation of radiotherapy based treatment regimens. *Scientific reports*, 9(1).
- Kilfoy, B., Zheng, T., Holford, T., Han, X., Ward, M., Sjodin, A., Zhang, Y., Bai, Y., Zhu, C., Guo, G., Rothman, N. & Zhang, Y. (2009) International patterns and trends in thyroid cancer incidence, 1973-2002. *Cancer causes & control : CCC*, 20(5).

- Kim, W., Park, J., Willingham, M. & Cheng, S. (2013) Diet-induced obesity increases tumor growth and promotes anaplastic change in thyroid cancer in a mouse model. *Endocrinology*, 154(8).
- Kitahara, C. & Sosa, J. (2016) The changing incidence of thyroid cancer. *Nature reviews. Endocrinology*, 12(11).
- Kobayashi, H., Shiba, T., Yoshida, T., Bolidong, D., Kato, K., Sato, Y., Mochizuki, M., Seto, T., Kawashiri, S. & Hanayama, R. (2024) Precise analysis of single small extracellular vesicles using flow cytometry. *Scientific reports*, 14(1).
- Köhrle, J. (2000) The deiodinase family: selenoenzymes regulating thyroid hormone availability and action. *Cellular and molecular life sciences : CMLS*, 57(13-14).
- Kopp, P. (2023) Iodine in the Therapy of Graves' Disease: A Century After Henry S. Plummer. *Thyroid*, 33(3), 273.
- Kotwal, A. & Stan, M. (2018) Thyrotropin Receptor Antibodies-An Overview. *Ophthalmic plastic and reconstructive surgery*, 34(4S Suppl 1).
- Kowal, E., Ter-Ovanesyan, D., Regev, A. & Church, G. (2017) Extracellular Vesicle Isolation and Analysis by Western Blotting. *Methods in molecular biology (Clifton, N.J.)*, 1660.
- Kowal, J., Arras, G., Colombo, M., Jouve, M., Morath, J., Primdal-Bengtson, B., Dingli, F., Loew, D., Tkach, M. & Théry, C. (2016) Proteomic comparison defines novel markers to characterize heterogeneous populations of extracellular vesicle subtypes. *Proceedings of the National Academy of Sciences of the United States of America*, 113(8).
- Krylova, S. & Feng, D. (2023) The Machinery of Exosomes: Biogenesis, Release, and Uptake. *International journal of molecular sciences*, 24(2).
- Kunjumon, D. (2016) Histopathological features of Papillary Thyroid Carcinoma wi... : Archives of Medicine and Health Sciences. *Archives of Medicine and Health Sciences*.
- La Vecchia, C., Malvezzi, M., Bosetti, C., Garavello, W., Bertuccio, P., Levi, F. & Negri, E. (2015) Thyroid cancer mortality and incidence: a global overview. *International journal of cancer*, 136(9).
- Lakhani, R., Rourke, T., Jefferis, A., Perry, L., Ghiacy, S. & Wood, S. (2011) Thy3 cytology: what to do next? *Annals of the Royal College of Surgeons of England*, 93(3).
- Lassalle, S., Zangari, J., Popa, A., Ilie, M., Hofman, V., Long, E., Patey, M., Tissier, F., Belléannée, G., Trouette, H., Catargi, B., Peyrottes, I., Sadoul, J., Bordone, O., Bonnetaud, C., Butori, C., Bozec, A., Guevara, N., Santini, J., Hénaoui, I., Lemaire, G., Blanck, O., Vielh, P., Barbry, P., Mari, B., Brest, P. & Hofman, P. (2016) MicroRNA-375/SEC23A as biomarkers of the in vitro efficacy of vandetanib. *Oncotarget*, 7(21).

Laukienė, R., Ambrozaityte, L., Cimbalistienė, L., Utkus, A. & Tamosiunas, A. (2022) Diagnostic Significance of FNAB miRNA Expression in Papillary Thyroid Carcinoma. *Diagnostics*, 12(6), 1384.

Laurberg, P., Cerqueira, C., Ovesen, L., Rasmussen, L., Perrild, H., Andersen, S., Pedersen, I. & Carlé, A. (2010) Iodine intake as a determinant of thyroid disorders in populations. *Best practice & research. Clinical endocrinology & metabolism*, 24(1).

Lawal, I., Nyakale, N., Harry, L., Lengana, T., Mokgoro, N., Vorster, M. & Sathekge, M. (2017) Higher preablative serum thyroid-stimulating hormone level predicts radioiodine ablation effectiveness in patients with differentiated thyroid carcinoma. *Nuclear medicine communications*, 38(3).

Lee, J., Zhao, J., Gundara, J., Serpell, J., Bach, L. & Sidhu, S. (2015) Papillary thyroid cancer-derived exosomes contain miRNA-146b and miRNA-222. *The Journal of surgical research*, 196(1).

Leung, C. M., de Haan, P., Ronaldson-Bouchard, K., Kim, G.-A., Ko, J., Rho, H. S., Chen, Z., Habibovic, P., Jeon, N. L., Takayama, S., Shuler, M. L., Vunjak-Novakovic, G., Frey, O., Verpoorte, E. & Toh, Y.-C. (2022) A guide to the organ-on-a-chip. *Nature Reviews Methods Primers*, 2(1), 1-29.

Li, J. (1988) Laminar and turbulent flow in the mammalian aorta: Reynolds number. *Journal of theoretical biology*, 135(3).

Liang, J., Zeng, W., Fang, F., Yu, T., Zhao, Y., Fan, X., Guo, N. & Gao, X. (2017) Clinical analysis of Hashimoto thyroiditis coexistent with papillary thyroid cancer in 1392 patients. *Acta otorhinolaryngologica Italica : organo ufficiale della Societa italiana di otorinolaringologia e chirurgia cervico-facciale*, 37(5).

Lim, H., Devesa, S., Sosa, J., Check, D. & Kitahara, C. (2017) Trends in Thyroid Cancer Incidence and Mortality in the United States, 1974-2013. *JAMA*, 317(13).

Los, M., Mozoluk, M., Ferrari, D., Stepczynska, A., Stroh, C., Herceg, Z. & Schulze-Osthoff, K. (2002) Activation and Caspase-mediated Inhibition of PARP: A Molecular Switch between Fibroblast Necrosis and Apoptosis in Death Receptor Signaling. *Molecular Biology of the Cell*, 13(3), 978.

Lötvall, J., Hill, A., Hochberg, F., Buzás, E., Di Vizio, D., Gardiner, C., Gho, Y., Kurochkin, I., Mathivanan, S., Quesenberry, P., Sahoo, S., Tahara, H., Wauben, M., Witwer, K. & Théry, C. (2014) Minimal experimental requirements for definition of extracellular vesicles and their functions: a position statement from the International Society for Extracellular Vesicles. *Journal of extracellular vesicles*, 3.

Ludwig, A. & Giebel, B. (2012) Exosomes: small vesicles participating in intercellular communication. *The international journal of biochemistry & cell biology*, 44(1).

- Lunn, M., Mouritzen, P., Faber, K. & Jacobsen, N. (2008) MicroRNA quantitation from a single cell by PCR using SYBR® Green detection and LNA-based primers. *Nature Methods*, 5(2).
- Ma, C., Peng, Y., Li, H. & Chen, W. (2021) Organ-on-a-Chip: A New Paradigm for Drug Development. *Trends in pharmacological sciences*, 42(2).
- Machens, A., Ukkat, J., Hauptmann, S. & Dralle, H. (2007) Abnormal carcinoembryonic antigen levels and medullary thyroid cancer progression: a multivariate analysis. *Archives of surgery (Chicago, Ill. : 1960)*, 142(3).
- MacKenna, B. (2019) *What are the most commonly prescribed medicines? Top 10 prescribed medicines in NHS England primary care for 2019*. Available online: <https://www.bennett.ox.ac.uk/blog/2020/03/what-are-the-most-commonly-prescribed-medicines-top-10-prescribed-medicines-in-nhs-england-primary-care-for-2019/> [Accessed 15th June].
- Mahoney, M., Lawvere, S., Falkner, K., Averkin, Y., Ostapenko, V., Michalek, A., Moysich, K. & McCarthy, P. (2004) Thyroid cancer incidence trends in Belarus: examining the impact of Chernobyl. *International journal of epidemiology*, 33(5).
- Majno, G. & Joris, I. (1995) Apoptosis, oncosis, and necrosis. An overview of cell death. *The American Journal of Pathology*, 146(1), 3.
- Manzella, L., Stella, S., Pennisi, M., Tirrò, E., Massimino, M., Romano, C., Puma, A., Tavarelli, M. & Vigneri, P. (2017) New Insights in Thyroid Cancer and p53 Family Proteins. *International journal of molecular sciences*, 18(6).
- Martinez-Tello, F., Martinez-Cabruja, R., Fernandez-Martin, J., Lasso-Oria, C. & Ballestin-Carcavilla, C. (1993) Occult carcinoma of the thyroid. A systematic autopsy study from Spain of two series performed with two different methods. *Cancer*, 71(12).
- Mastronikolis, N., Kyrodimos, E., Spyropoulou, D., Delides, A., Giotakis, E., Piperigkou, Z. & Karamanos, N. (2023) The Role of Exosomes in Epithelial-to-Mesenchymal Transition and Cell Functional Properties in Head and Neck Cancer. *Cancers*, 15(7).
- Mathivanan, S., Ji, H. & Simpson, R. (2010) Exosomes: extracellular organelles important in intercellular communication. *Journal of proteomics*, 73(10).
- McDermaid, A., Monier, B., Zhao, J., Liu, B. & Ma, Q. (2019) Interpretation of differential gene expression results of RNA-seq data: review and integration. *Briefings in bioinformatics*, 20(6).
- McDonald, J., Duffy, D., Anderson, J., Chiu, D., Wu, H., Schueller, O. & Whitesides, G. (2000) Fabrication of microfluidic systems in poly(dimethylsiloxane). *Electrophoresis*, 21(1).
- McLeod, D. & Cooper, D. (2012) The incidence and prevalence of thyroid autoimmunity. *Endocrine*, 42(2).

Meltzer, C., Hull, M., Sundang, A. & Adams, J. (2019) Association Between Annual Surgeon Total Thyroidectomy Volume and Transient and Permanent Complications. *JAMA Otolaryngology-- Head & Neck Surgery*, 145(9), 830.

Menck, K., Sivaloganathan, S., Bleckmann, A. & Binder, C. (2020) Microvesicles in Cancer: Small Size, Large Potential. *International journal of molecular sciences*, 21(15).

Mettler, F., Thomadsen, B., Bhargavan, M., Gilley, D., Gray, J., Lipoti, J., McCrohan, J., Yoshizumi, T. & Mahesh, M. (2008) Medical radiation exposure in the U.S. in 2006: preliminary results. *Health physics*, 95(5).

Mikoś, H., Mikoś, M., Obara-Moszyńska, M. & Niedziela, M. (2014) The role of the immune system and cytokines involved in the pathogenesis of autoimmune thyroid disease (AITD). *Endokrynologia Polska*, 65(2).

Mitchell, A., Gandhi, A., Scott-Coombes, D. & Perros, P. (2016) Management of thyroid cancer: United Kingdom National Multidisciplinary Guidelines. *The Journal of laryngology and otology*, 130(S2).

Mittendorf, E. & McHenry, C. (2001) Thyroidectomy for selected patients with thyrotoxicosis. *Archives of otolaryngology--head & neck surgery*, 127(1).

Mobarrez, F., Abraham-Nordling, M., Aguilera-Gatica, K., Friberg, I., Antovic, A., Pisetsky, D., Jörneskog, G. & Wallen, H. (2016) The expression of microvesicles in the blood of patients with Graves' disease and its relationship to treatment. *Clinical endocrinology*, 84(5).

Möller, A. & Lobb, R. (2020) The evolving translational potential of small extracellular vesicles in cancer. *Nature reviews. Cancer*, 20(12).

Morris, L., Sikora, A., Tosteson, T. & Davies, L. (2013) The increasing incidence of thyroid cancer: the influence of access to care. *Thyroid : official journal of the American Thyroid Association*, 23(7).

Mousavi, S., Ebrahimi, M., Vosough, M., Hosseindoost, S., Vousooghi, N., Javar, H., Larijani, B., Hadjighassem, M., Rahimian, N., Hamblin, M. & Mirzaei, H. (2022) Microfluidics for detection of exosomes and microRNAs in cancer: State of the art. *Molecular Therapy. Nucleic Acids*, 28, 758.

Musah, S., Mammoto, A., Ferrante, T., Jeanty, S., Hirano-Kobayashi, M., Mammoto, T., Roberts, K., Chung, S., Novak, R., Ingram, M., Fatanat-Didar, T., Koshy, S., Weaver, J., Church, G. & Ingber, D. (2017) Mature induced-pluripotent-stem-cell-derived human podocytes reconstitute kidney glomerular-capillary-wall function on a chip. *Nature biomedical engineering*, 1.

Nair, D., Kandiah, S., Rourke, T., Corbridge, R. & Nagala, S. (2021) Malignancy rates and initial management of Thy3 thyroid nodules in a district general hospital: The 'Reading' experience. *Endocrinology, Diabetes & Metabolism*, 4(3).

Niculescu, A., Chircov, C., Bîrcă, A. & Grumezescu, A. (2021) Fabrication and Applications of Microfluidic Devices: A Review. *International journal of molecular sciences*, 22(4).

Niederle, B., Sebag, F. & Brauckhoff, M. (2014) Timing and extent of thyroid surgery for gene carriers of hereditary C cell disease--a consensus statement of the European Society of Endocrine Surgeons (ESES). *Langenbeck's archives of surgery*, 399(2).

Noguchi, S., Yamashita, H., Uchino, S. & Watanabe, S. (2008) Papillary Microcarcinoma. *World Journal of Surgery*, 32(5), 747.

Nunez, E., Wallis, J. & Gershon, M. (1974) Secretory processes in follicular cells of the bat thyroid. 3. The occurrence of extracellular vesicles and colloid droplets during arousal from hibernation. *The American journal of anatomy*, 141(2).

O'Brien, J., Hayder, H., Zayed, Y. & Peng, C. (2018) Overview of MicroRNA Biogenesis, Mechanisms of Actions, and Circulation. *Frontiers in Endocrinology*, 9, 402.

Onyebuchi, O., Taylor, P. & Dayan, C. (2020) Should radioiodine now be first line treatment for Graves' disease? *Thyroid Research*, 13, 3.

Pacini, F., Vorontsova, T., Demidchik, E., Molinaro, E., Agate, L., Romei, C., Shavrova, E., Cherstvoy, E., Ivashkevitch, Y., Kuchinskaya, E., Schlumberger, M., Ronga, G., Filesi, M. & Pinchera, A. (1997) Post-Chernobyl thyroid carcinoma in Belarus children and adolescents: comparison with naturally occurring thyroid carcinoma in Italy and France. *The Journal of clinical endocrinology and metabolism*, 82(11).

Panalytical, M. (2015) *Using Nanoparticle Tracking Analysis to Characterize Carbon and Carbon Nanotubes*. Available online: <https://www.azonano.com/article.aspx?ArticleID=4063> [Accessed 02/02/2024].

Patel, R., West, J., Adah, D., Jiang, Y., Fogarty, E. & Grimson, A. (2020) Robust partitioning of microRNA targets from downstream regulatory changes. *Nucleic Acids Research*, 48(17), 9724.

Peeters, R. & Visser, T. J. (2017) Metabolism of Thyroid Hormone.

Peiris, A., Medlock, D. & Gavin, M. (2019) Thyroglobulin for Monitoring for Thyroid Cancer Recurrence. *JAMA*, 321(12), 1228-1228.

Perrier, N. D., Brierley, J. & Tuttle, R. M. (2019) Differentiated and Anaplastic Thyroid Carcinoma: Major Changes in the American Joint Committee on Cancer Cancer Staging Manual Eighth Edition. *CA: a cancer journal for clinicians*, 68(1), 55.

Peto, T., Affron, D., Agasu, A., Ainsworth, M., Allanson, A., Allen, K., Allen, C., Archer, L., Ashbridge, N., Aurfan, I., Avery, M., Badenoch, E., Bagga, P. & Balaji, R. (2021) COVID-19: Rapid antigen detection for SARS-CoV-2 by lateral flow assay: A national systematic evaluation of sensitivity and specificity for mass-testing. *eClinicalMedicine*, 36.

- Pirahanchi, Y., Toro, F. & Jialal, I. (2023) Physiology, Thyroid Stimulating Hormone.
- Pokhrel, B., Aiman, W. & Bhusal, K. (2022) Thyroid Storm.
- Poller, D. & Johnson, S. (2017) Recent Developments in the Pathology of Thyroid Cancer. *Clinical oncology (Royal College of Radiologists (Great Britain))*, 29(5).
- Ponmozhi, J., Dhinakaran, S., Varga-Medveczky, Z., Fónagy, K., Anna Bors, L., Iván, K. & Erdő, F. (2021) Development of Skin-On-A-Chip Platforms for Different Utilizations: Factors to Be Considered. *Micromachines*, 12(3), 294.
- Potla, P., Ali, S. & Kapoor, M. (2020) A bioinformatics approach to microRNA-sequencing analysis. *Osteoarthritis and cartilage open*, 3(1).
- Prete, A., Borges de Souza, P., Censi, S., Muzza, M., Nucci, N. & Sponziello, M. (2020) Update on Fundamental Mechanisms of Thyroid Cancer. *Frontiers in endocrinology*, 11.
- Pund, S., Chandak, R., Rajurkar, V., Kharat, N., Khalil, S., Shaikh, S., Parve, K., Kadam, M., Choudante, S., Pulate, C., Wakale, V. & Tare, H. (2022) A review on nanomedicines in treatment of thyroid and their applications in management of thyroid disorders. <https://sciencescholar.us/journal/index.php/ijhs>.
- Raju, D., Bathini, S., Badilescu, S., Ghosh, A. & Packirisamy, M. (2022) Microfluidic Platforms for the Isolation and Detection of Exosomes: A Brief Review. *Micromachines*, 13(5).
- Rana, S., Malinowska, K. & Zöller, M. (2013) Exosomal tumor microRNA modulates premetastatic organ cells. *Neoplasia (New York, N.Y.)*, 15(3).
- Reynolds, O. (1883) XXIX. An experimental investigation of the circumstances which determine whether the motion of water shall be direct or sinuous, and of the law of resistance in parallel channels.
- Richards, K., Zeleniak, A., Fishel, M., Wu, J., Littlepage, L. & Hill, R. (2017) Cancer-associated fibroblast exosomes regulate survival and proliferation of pancreatic cancer cells. *Oncogene*, 36(13).
- Riley, A., Green, V., Cheah, R., McKenzie, G., Karsai, L., England, J. & Greenman, J. (2019) A novel microfluidic device capable of maintaining functional thyroid carcinoma specimens ex vivo provides a new drug screening platform. *BMC Cancer*, 19(1), 1-13.
- Rinaldi, S., Plummer, M., Biessy, C., Tsilidis, K., Østergaard, J., Overvad, K., Tjønneland, A., Halkjaer, J., Boutron-Ruault, M., Clavel-Chapelon, F., Dossus, L., Kaaks, R., Lukanova, A., Boeing, H., Trichopoulou, A., Lagiou, P., Trichopoulos, D., Palli, D., Agnoli, C., Tumino, R., Vineis, P., Panico, S., Bueno-de-Mesquita, H., Peeters, P., Weiderpass, E., Lund, E., Quirós, J., Agudo, A., Molina, E., Larrañaga, N., Navarro, C., Ardanaz, E., Manjer, J., Almquist, M., Sandström, M., Hennings, J., Khaw, K., Schmidt, J., Travis, R., Byrnes, G., Scalbert, A., Romieu, I., Gunter, M., Riboli, E. & Franceschi, S. (2014) Thyroid-stimulating

hormone, thyroglobulin, and thyroid hormones and risk of differentiated thyroid carcinoma: the EPIC study. *Journal of the National Cancer Institute*, 106(6).

Ríos, A., Rodríguez, J., Canteras, M., Galindo, P., Tebar, F. & Parrilla, P. (2005) Surgical management of multinodular goiter with compression symptoms. *Archives of surgery (Chicago, Ill. : 1960)*, 140(1).

Rodríguez-Muñoz, A., Martínez-Hernández, R., Ramos-Leví, A., Serrano-Somavilla, A., González-Amaro, R., Sánchez-Madrid, F., de la Fuente, H. & Marazuela, M. (2015) Circulating Microvesicles Regulate Treg and Th17 Differentiation in Human Autoimmune Thyroid Disorders. *The Journal of clinical endocrinology and metabolism*, 100(12).

Romano, C., Martorana, F., Pennisi, M., Stella, S., Massimino, M., Tirrò, E., Vitale, S., Di Gregorio, S., Puma, A., Tomarchio, C. & Manzella, L. (2021) Opportunities and Challenges of Liquid Biopsy in Thyroid Cancer. *International journal of molecular sciences*, 22(14).

Romeo, P., Colombo, C., Granata, R., Calareso, G., Gualeni, A., Dugo, M., De Cecco, L., Rizzetti, M., Zanframundo, A., Aiello, A., Carcangiu, M., Gloghini, A., Ferrero, S., Licitra, L., Greco, A., Fugazzola, L., Locati, L. & Borrello, M. (2018) Circulating miR-375 as a novel prognostic marker for metastatic medullary thyroid cancer patients. *Endocrine-related cancer*, 25(3).

Ron, E. (2003) Cancer risks from medical radiation. *Health physics*, 85(1).

Rong-liang, S., Ning, Q., Tian, L., Wen-jun, W., Yu-Long, W. & Qing-hai, J. (2016) The Trend of Age-Group Effect on Prognosis in Differentiated Thyroid Cancer. *Scientific Reports*, 6, 27086.

Rossi, E., Pantanowitz, L. & Hornick, J. (2021) A worldwide journey of thyroid cancer incidence centred on tumour histology. *The lancet. Diabetes & endocrinology*, 9(4).

Roti, E., Rossi, R., Trasforini, G., Bertelli, F., Ambrosio, M., Busutti, L., Pearce, E., Braverman, L. & Degli Uberti, E. (2006) Clinical and histological characteristics of papillary thyroid microcarcinoma: results of a retrospective study in 243 patients. *The Journal of clinical endocrinology and metabolism*, 91(6).

Saiselet, M., Gacquer, D., Spinette, A., Craciun, L., Decaussin-Petrucci, M., Andry, G., Detours, V. & Maenhaut, C. (2015) New global analysis of the microRNA transcriptome of primary tumors and lymph node metastases of papillary thyroid cancer. *BMC genomics*, 16.

Saqr, K., Tupin, S., Rashad, S., Endo, T., Niizuma, K., Tominaga, T. & Ohta, M. (2020) Physiologic blood flow is turbulent. *Scientific reports*, 10(1).

Schlumberger, M., Brose, M., Elisei, R., Leboulleux, S., Luster, M., Pitoia, F. & Pacini, F. (2014) Definition and management of radioactive iodine-refractory differentiated thyroid cancer. *The lancet. Diabetes & endocrinology*, 2(5).

- Schmidt, A., Iglesias, L., Klain, M., Pitoia, F. & Schlumberger, M. (2017) Radioactive iodine-refractory differentiated thyroid cancer: an uncommon but challenging situation. *Archives of endocrinology and metabolism*, 61(1).
- Schumacher, K., Khong, Y., Chang, S., Ni, J., Sun, W. & Yu, H. (2007) Perfusion culture improves the maintenance of cultured liver tissue slices. *Tissue engineering*, 13(1).
- Seethala, R. R., Baloch, Z. W., Barletta, J. A., Khanafshar, E., Mete, O., Sadow, P. M., LiVolsi, V. A., Nikiforov, Y. E., Tallini, G. & Thompson, L. D. (2017) Noninvasive follicular thyroid neoplasm with papillary-like nuclear features: a review for pathologists. *Modern Pathology*, 31(1), 39-55.
- Seib, C. & Sosa, J. (2019) Evolving Understanding of the Epidemiology of Thyroid Cancer. *Endocrinology and metabolism clinics of North America*, 48(1).
- Selwyn, D., How-Hong, E., Tan, H. & England, R. (2023) Patient outcomes following thyroid surgery for thyrotoxicosis. *The Journal of laryngology and otology*, 137(3).
- Shahbaz, A., Aziz, K., Umair, M. & Sachmechi, I. (2018) Prolonged Duration of Hashitoxicosis in a Patient with Hashimoto's Thyroiditis: A Case Report and Review of Literature. *Cureus*, 10(6).
- Shenoda, B. & Ajit, S. (2016) Modulation of Immune Responses by Exosomes Derived from Antigen-Presenting Cells. *Clinical medicine insights. Pathology*, 9(Suppl 1).
- Shine, B., McKnight, R., Leaver, L. & Geddes, J. (2015) Long-term effects of lithium on renal, thyroid, and parathyroid function: a retrospective analysis of laboratory data. *Lancet (London, England)*, 386(9992).
- Silver, C., Owen, R., Rodrigo, J., Rinaldo, A., Devaney, K. & Ferlito, A. (2011) Aggressive variants of papillary thyroid carcinoma. *Head & neck*, 33(7).
- Singh, D., Mathur, A., Arora, S., S, R. & Mahindrooa, N. (2022) Journey of organ on a chip technology and its role in future healthcare scenario. *Applied Surface Sciences Advances*.
- Skotland, T., Sandvig, K. & Llorente, A. (2017) Lipids in exosomes: Current knowledge and the way forward. *Progress in lipid research*, 66.
- Smith, T. & Hegedüs, L. (2016) Graves' Disease. *The New England Journal of Medicine*, 375(16).
- Smithson, M., Asban, A., Miller, J. & Chen, H. (2019) Considerations for Thyroidectomy as Treatment for Graves Disease. *Clinical Medicine Insights. Endocrinology and Diabetes*, 12, 1179551419844523.
- Soares, A., Soares, J., Rodrigues, V., Follmann, H., Arantes, L., Carvalho, A., Melendez, M., Fregnani, J., Reis, R., Carvalho, A. & Oliveira, O. (2018) Microfluidic-Based Genosensor To Detect Human Papillomavirus (HPV16) for Head and Neck Cancer. *ACS applied materials & interfaces*, 10(43).

Soltani, S., Aghaee, A., Zakavi, S., Mottaghi, M., Emadzadeh, M. & Naeini, S. (2023) Effects of radioiodine therapy on fertility indicators among men with differentiated thyroid cancer: A cohort study. *International Journal of Reproductive Biomedicine*, 21(5), 387.

Staging, A. t. E. T. T. (2023) *Thyroid Cancer Stages | Staging Thyroid Cancer*. Available online: <https://www.cancer.org/cancer/types/thyroid-cancer/detection-diagnosis-staging/staging.html> [Accessed 24/11/2023].

Starenki, D. & Park, J. (2016) Pediatric Medullary Thyroid Carcinoma. *Journal of pediatric oncology*, 3(2), 29.

Tadokoro, H., Umezu, T., Ohyashiki, K., Hirano, T. & Ohyashiki, J. (2013) Exosomes derived from hypoxic leukemia cells enhance tube formation in endothelial cells. *The Journal of biological chemistry*, 288(48).

Taha, E., Ono, K. & Eguchi, T. (2019) Roles of Extracellular HSPs as Biomarkers in Immune Surveillance and Immune Evasion. *International journal of molecular sciences*, 20(18).

Théry, C., Amigorena, S., Raposo, G. & Clayton, A. (2006) Isolation and characterization of exosomes from cell culture supernatants and biological fluids. *Current protocols in cell biology*, Chapter 3.

Théry, C., Ostrowski, M. & Segura, E. (2009) Membrane vesicles as conveyors of immune responses. *Nature reviews. Immunology*, 9(8).

Théry, C., Witwer, K. W., Aikawa, E., Alcaraz, M. J., Anderson, J. D., Andriantsitohaina, R., Antoniou, A., Arab, T., Archer, F., Atkin-Smith, G. K., Ayre, D. C., Bach, J.-M., Bachurski, D., Baharvand, H., Balaj, L., Baldacchino, S., Bauer, N. N., Baxter, A. A., Bebawy, M., Beckham, C., Zavec, A. B., Benmoussa, A., Berardi, A. C., Bergese, P., Bielska, E., Blenkiron, C., Bobis-Wozowicz, S., Boilard, E., Boireau, W., Bongiovanni, A., Borràs, F. E., Bosch, S., Boulanger, C. M., Breakefield, X., Breglio, A. M., Brennan, M. Á., Brigstock, D. R., Brisson, A., Broekman, M. L., Bromberg, J. F., Bryl-Górecka, P., Buch, S., Buck, A. H., Burger, D., Busatto, S., Buschmann, D., Bussolati, B., Buzás, E. I., Byrd, J. B., Camussi, G., Carter, D. R., Caruso, S., Chamley, L. W., Chang, Y.-T., Chen, C., Chen, S., Cheng, L., Chin, A. R., Clayton, A., Clerici, S. P., Cocks, A., Cocucci, E., Coffey, R. J., Cordeiro-da-Silva, A., Couch, Y., Coumans, F. A., Coyle, B., Crescitelli, R., Criado, M. F., D'Souza-Schorey, C., Das, S., Chaudhuri, A. D., Candia, P. d., Junior, E. F. D. S., Wever, O. D., Portillo, H. A. d., Demaret, T., Deville, S., Devitt, A., Dhondt, B., Vizio, D. D., Dieterich, L. C., Dolo, V., Rubio, A. P. D., Dominici, M., Dourado, M. R., Driedonks, T. A., Duarte, F. V., Duncan, H. M., Eichenberger, R. M., Ekström, K., Andaloussi, S. E., Elie-Caille, C., Erdbrügger, U., Falcón-Pérez, J. M., Fatima, F., Fish, J. E., Flores-Bellver, M., Försonits, A., Frelet-Barrand, A., et al (2018) Minimal information for studies of extracellular vesicles 2018 (MISEV2018): a position statement of the International Society for Extracellular Vesicles and update of the MISEV2014 guidelines. <https://doi.org/10.1080/20013078.2018.1535750>.

Thiyagarajan, A., Platzbecker, K., Ittermann, T., Völzke, H. & Haug, U. (2022) Estimating Incidence and Case Fatality of Thyroid Storm in Germany Between 2007 and 2017: A

Claims Data Analysis. *Thyroid : official journal of the American Thyroid Association*, 32(11).

Tostões, R., Leite, S., Serra, M., Jensen, J., Björquist, P., Carrondo, M., Brito, C. & Alves, P. (2012) Human liver cell spheroids in extended perfusion bioreactor culture for repeated-dose drug testing. *Hepatology (Baltimore, Md.)*, 55(4).

Tuttle, M., Haugen, B. & Perrier, N. (2017) Updated American Joint Committee on Cancer/Tumor-Node-Metastasis Staging System for Differentiated and Anaplastic Thyroid Cancer (Eighth Edition): What Changed and Why? *Thyroid*, 27(6), 751.

University, N. K. (2024) *Thyroid Gland*. Available online: <https://www.nku.edu/~dempseyd/thyroid-slide.html> [Accessed 16/10/2023].

Uruba, V. (2019) Reynolds number in laminar flows and in turbulence | AIP Conference Proceedings | AIP Publishing. *HydroTermo*, 38th Meeting of Departments of Fluid Mechanics and Thermodynamics.

Vaira, V., Fedele, G., Pyne, S., Fasoli, E., Zadra, G., Bailey, D., Snyder, E., Favarsani, A., Coggi, G., Flavin, R., Bosari, S. & Loda, M. (2010) Preclinical model of organotypic culture for pharmacodynamic profiling of human tumors. *Proceedings of the National Academy of Sciences of the United States of America*, 107(18).

van der Pol, E., Welsh, J. & Nieuwland, R. (2022) Minimum information to report about a flow cytometry experiment on extracellular vesicles: Communication from the ISTH SSC subcommittee on vascular biology. *Journal of thrombosis and haemostasis : JTH*, 20(1).

Vander Poorten, V., Goedseels, N., Sanabria, A., Clement, P., Cohen, O., Golusinski, P., Guntinas-Lichius, O., Piazza, C., Randolph, G., Rinaldo, A., Cabanillas, M., Shaha, A., Teng, Y., Tufano, R., Williams, M., Zafereo, M. & Ferlito, A. (2022) Effectiveness of core needle biopsy in the diagnosis of thyroid lymphoma and anaplastic thyroid carcinoma: A systematic review and meta-analysis. *Frontiers in Endocrinology*, 13, 971249.

Vanderpump, M., Tunbridge, W., French, J., Appleton, D., Bates, D., Clark, F., Grimley Evans, J., Hasan, D., Rodgers, H. & Tunbridge, F. (1995) The incidence of thyroid disorders in the community: a twenty-year follow-up of the Wickham Survey. *Clinical endocrinology*, 43(1).

Vatine, G., Barrile, R., Workman, M., Sances, S., Barriga, B., Rahnama, M., Barthakur, S., Kasendra, M., Lucchesi, C., Kerns, J., Wen, N., Spivia, W., Chen, Z., Van Eyk, J. & Svendsen, C. (2019) Human iPSC-Derived Blood-Brain Barrier Chips Enable Disease Modeling and Personalized Medicine Applications. *Cell stem cell*, 24(6).

VectorLabs, V.-. (2024) *VECTABOND for Tissue Section Adhesion - VectorLabs*. Available online: <https://vectorlabs.com/products/vectabond-reagent-tissue-section-adhesion> [Accessed 08/10/2023].

Vidall, C., Barlow, H., Crowe, M., Harrison, I. & Young, A. (2011) Clinical nurse specialists: essential resource for an effective NHS. *British journal of nursing (Mark Allen Publishing)*, 20(17).

Viel, T., Manfra, L., Zupo, V., Libralato, G. & Costantini, M. (2023) Biodegradation of Plastics Induced by Marine Organisms: Future Perspectives for Bioremediation Approaches. *Polymers*, 15(12), 2673.

Vlasov, P., Doi, S. & Sellitti, D. (2016) FRTL-5 Rat Thyroid Cells Release Thyroglobulin Sequestered in Exosomes: A Possible Novel Mechanism for Thyroglobulin Processing in the Thyroid. *Journal of Thyroid Research*, 2016, 9276402.

Vu, M. (2024) *Thyroid Flashcards*. Available online: <https://quizlet.com/853955495/thyroid-flash-cards/> [Accessed 05/08/2023].

Wada, N., Duh, Q., Sugino, K., Iwasaki, H., Kameyama, K., Mimura, T., Ito, K., Takami, H. & Takanashi, Y. (2003) Lymph node metastasis from 259 papillary thyroid microcarcinomas: frequency, pattern of occurrence and recurrence, and optimal strategy for neck dissection. *Annals of surgery*, 237(3).

Wagner, E. (2013) Monitoring gene expression: quantitative real-time rt-PCR. *Methods in molecular biology (Clifton, N.J.)*, 1027.

Wang, C., Wu, Z., Lei, L., Dong, X., Cao, W., Luo, Z., Zheng, Y., Wang, F., Xu, Y., Zhao, L., Shi, J., Ren, J., Li, J., Zhang, Y., Chen, W. & Li, N. (2023a) Geographic disparities in trends of thyroid cancer incidence and mortality from 1990 to 2019 and a projection to 2030 across income-classified countries and territories. *Journal of global health*, 13.

Wang, H., Wang, L., Zhou, X., Luo, X., Liu, K., Jiang, E., Chen, Y., Shao, Z. & Shang, Z. (2020) OSCC Exosomes Regulate miR-210-3p Targeting EFNA3 to Promote Oral Cancer Angiogenesis through the PI3K/AKT Pathway. *BioMed research international*, 2020.

Wang, W., Zheng, Z. & Lei, J. (2023b) CTC, ctDNA, and Exosome in Thyroid Cancers: A Review. *International journal of molecular sciences*, 24(18).

Wang, X., Hang, Y., Liu, J., Hou, Y., Wang, N. & Wang, M. (2016) Over-expression of microRNA-375 inhibits papillary thyroid carcinoma cell proliferation and induces cell apoptosis by targeting ERBB2. *Journal of pharmacological sciences*, 130(2).

Wang, Z., Lv, J., Zou, X., Huang, Z., Zhang, H., Liu, Q., Jiang, L., Zhou, X. & Zhu, W. (2019) A three plasma microRNA signature for papillary thyroid carcinoma diagnosis in Chinese patients. *Gene*, 693.

Wei, Q., Wei, L., Zhang, J., Li, Z., Feng, H. & Ren, L. (2020) EphA2-enriched exosomes promote cell migration and are a potential diagnostic serum marker in pancreatic cancer. *Molecular medicine reports*, 22(4).

Weller, A., Sharif, B., Qarib, M., St Leger, D., De Silva, H. & Lingam, R. (2020) British Thyroid Association 2014 classification ultrasound scoring of thyroid nodules in

predicting malignancy: Diagnostic performance and inter-observer agreement. *Ultrasound (Leeds, England)*, 28(1).

Welsh, J., Goberdhan, D., O'Driscoll, L., Buzas, E., Blenkiron, C., Bussolati, B., Cai, H., Di Vizio, D., Driedonks, T., Erdbrügger, U., Falcon-Perez, J., Fu, Q., Hill, A., Lenassi, M., Lim, S., Mahoney, M., Mohanty, S., Möller, A., Nieuwland, R., Ochiya, T., Sahoo, S., Torrecilhas, A., Zheng, L., Zijlstra, A., Abuelreich, S., Bagabas, R., Bergese, P., Bridges, E., Brucale, M., Burger, D., Carney, R., Cocucci, E., Crescitelli, R., Hanser, E., Harris, A., Haughey, N., Hendrix, A., Ivanov, A., Jovanovic-Taliman, T., Kruh-Garcia, N., Ku'ulei-Lyn Faustino, V., Kyburz, D., Lässer, C., Lennon, K., Lötvall, J., Maddox, A., Martens-Uzunova, E., Mizenko, R., Newman, L., Ridolfi, A., Rohde, E., Rojalin, T., Rowland, A., Saftics, A., Sandau, U., Saugstad, J., Shekari, F., Swift, S., Ter-Ovanesyan, D., Tosar, J., Useckaite, Z., Valle, F., Varga, Z., van der Po, I. E., van Herwijnen, M., Wauben, M., Wehman, A., Williams, S., Zandrini, A., Zimmerman, A., Théry, C. & Witwer, K. (2024) Minimal information for studies of extracellular vesicles (MISEV2023): From basic to advanced approaches. *Journal of extracellular vesicles*, 13(2).

Whitesides, G. (2006) The origins and the future of microfluidics. *Nature*, 442(7101).

WHO (2016) 1986-2016: Chernobyl at 30.

Wilmer, M., Ng, C., Lanz, H., Vulto, P., Suter-Dick, L. & Masereeuw, R. (2016) Kidney-on-a-Chip Technology for Drug-Induced Nephrotoxicity Screening. *Trends in biotechnology*, 34(2).

Wise, P., Neviani, P., Riwaldt, S., Corydon, T., Wehland, M., Braun, M., Krüger, M., Infanger, M. & Grimm, D. (2021) Changes in Exosomal miRNA Composition in Thyroid Cancer Cells after Prolonged Exposure to Real Microgravity in Space. *International journal of molecular sciences*, 22(23).

Witczak, J. K., Ubaysekara, N., Ravindran, R., Rice, S., Yousef, Z. & Premawardhana, L. D. (2020) Significant cardiac disease complicating Graves' disease in previously healthy young adults. *Endocrinology, Diabetes & Metabolism Case Reports*, 2020, 19-0132.

Wolf, P. (1967) The nature and significance of platelet products in human plasma. *British journal of haematology*, 13(3).

Wong, K. T. & Ahuja, A. T. (2005) Ultrasound of thyroid cancer. *Cancer Imaging*, 5(1), 157.

Wufuer, M., Lee, G., Hur, W., Jeon, B., Kim, B., Choi, T. & Lee, S. (2016) Skin-on-a-chip model simulating inflammation, edema and drug-based treatment. *Scientific reports*, 6.

Xiang, Y., Wen, H., Yu, Y., Li, M., Fu, X. & Huang, S. (2020) Gut-on-chip: Recreating human intestine in vitro. *Journal of tissue engineering*, 11.

Xiaojie, H., Yuquan, C., Yiting, S., Rui, T., Yuqin, S. & Huafa, Q. (2022) Global prevalence and epidemiological trends of Hashimoto's thyroiditis in adults: A systematic review and meta-analysis. *Frontiers in Public Health*, 10, 1020709.

Xu, L., Wang, A., Li, X. & Oh, K. (2020) Passive micropumping in microfluidics for point-of-care testing. *Biomicrofluidics*, 14(3).

Xu, S., Zheng, L., Kang, L., Xu, H. & Gao, L. (2021) microRNA-let-7e in serum-derived exosomes inhibits the metastasis of non-small-cell lung cancer in a SUV39H2/LSD1/CDH1-dependent manner. *Cancer gene therapy*, 28(3-4).

Yamada, H., Itoh, M., Hiratsuka, I. & Hashimoto, S. (2014) Circulating microRNAs in autoimmune thyroid diseases. *Clinical endocrinology*, 81(2).

Yoshida, Y., Horiuchi, K. & Okamoto, T. (2020) Patients' View on the Management of Papillary Thyroid Microcarcinoma: Active Surveillance or Surgery. *Thyroid*, 30(5), 681.

Zabegina, L., Nazarova, I., Knyazeva, M., Nikiforova, N., Slyusarenko, M., Titov, S., Vasilyev, D., Sleptsov, I. & Malek, A. (2020) MiRNA let-7 from TPO(+) Extracellular Vesicles is a Potential Marker for a Differential Diagnosis of Follicular Thyroid Nodules. *Cells*, 9(8).

Zajkowska, K., Kopczyński, J., Góźdz, S. & Kowalska, A. (2020) Noninvasive follicular thyroid neoplasm with papillary-like nuclear features: a problematic entity. *Endocrine connections*, 9(3).

Zhan, L., Feng, H., Yu, X., Li, L., Song, J., Tu, Y., Yuan, J., Chen, C. & Sun, S. (2022) Clinical and prognosis value of the number of metastatic lymph nodes in patients with papillary thyroid carcinoma. *BMC Surgery*, 22, 235.

Zhang, Y., Chen, Y., Huang, H., Sandler, J., Dai, M., Ma, S. & Udelsman, R. (2015) Diagnostic radiography exposure increases the risk for thyroid microcarcinoma: a population-based case-control study. *European journal of cancer prevention : the official journal of the European Cancer Prevention Organisation (ECP)*, 24(5).

Zhao, H., Yang, L., Baddour, J., Achreja, A., Bernard, V., Moss, T., Marini, J., Tudawe, T., Seviour, E., San Lucas, F., Alvarez, H., Gupta, S., Maiti, S., Cooper, L., Peehl, D., Ram, P., Maitra, A. & Nagrath, D. (2016) Tumor microenvironment derived exosomes pleiotropically modulate cancer cell metabolism. *eLife*, 5.

Appendices

Appendix 1 – U Grading of Thyroid Nodules and AJCC – Thyroid Cancer Staging 8th Edition for Differentiated Thyroid Cancer

Appendix Table 1.1 - Classification of the ultrasound features (U) of thyroid nodules - U1 to U5 and the follow up and requirement for fine needle aspiration cytology (FNAC)

U Grading of Thyroid Nodules		
Classification	Ultrasound Scan Features	Follow Up
U1 – <i>Normal</i>	Normal - No nodules	No follow up required
U2 – <i>Benign</i>	Halo Iso-echoic or mildly hyper-echoic	No follow up required Unless high level of clinical suspicion of thyroid cancer
U3 – <i>Indeterminate</i>	Homogenous Hyper-echoic Solid, halo (follicular lesion) Cystic change Mixed/central vascularity	FNAC
U4 – <i>Suspicious</i>	Solid Hypo-echoic or very hypo-echoic Disrupted peripheral calcification Lobulated outline	FNAC
U5 – <i>Malignant</i>	Solid, hypoechoic, lobulated outline, microcalcification Medullary Thyroid Cancer – as above with globular calcification Intra-nodular vascularity Length greater than width Associated lymphadenopathy	FNAC

Appendix - Table 1.2 - AJCC – Thyroid Cancer Staging 8th Edition for Differentiated Thyroid Cancer. Taken from (Tuttle et al., 2017)

AJCC Stage	Age at diagnosis	Stage grouping	Differentiated Thyroid Cancer Stage Description
I	Younger than 55 years	Any T Any N M0	The cancer is any size (Any T) and might or might not have spread to nearby lymph nodes (Any N). It has not spread to distant sites (M0).
	OR		
	55 years or older	T1 N0 or NX M0	The cancer is no larger than 2 cm across and confined to the thyroid (T1). It has not spread to nearby lymph nodes (N0) or to distant sites (M0).
	OR		
	55 years or older	T2 N0 or NX M0	The cancer is larger than 2 cm across but no larger than 4 cm and confined to the thyroid (T2). It has not spread to nearby lymph nodes (N0) or to distant sites (M0).
II	Younger than 55 years	Any T Any N M1	The cancer can be any size (Any T). It might or might not have spread to nearby lymph nodes (Any N). It has spread to other parts of the body, such as distant lymph nodes, internal organs, bones, etc. (M1).
	OR		
	55 years or older	T1 N1 M0	The cancer is no larger than 2 cm [0.8 inches] across and confined to the thyroid (T1). It has spread to nearby lymph nodes (N1). It has not spread to distant sites (M0).
	OR		
	55 years or older	T2 N1 M0	The cancer is larger than 2 cm [0.8 inches] across but no larger than 4 cm and confined to the thyroid (T2). It has spread to nearby lymph nodes (N1). It has not spread to distant sites (M0).
OR			
	55 years or older	T3a or T3b Any N M0	The cancer is larger than 4 cm but confined to the thyroid (T3a) or it has grown into the strap muscles around the thyroid (T3b). It might or might not have spread to nearby lymph nodes (Any N). It has not spread to distant sites (M0).
III	55 years or older	T4a Any N M0	The cancer is any size and has grown extensively beyond the thyroid gland into nearby tissues of the neck, such as the larynx (voice box), trachea (windpipe), esophagus (tube connecting the throat to the stomach), or the nerve to the larynx (T4a).

			It might or might not have spread to nearby lymph nodes (Any N). It has not spread to distant sites (M0).
IVA	55 years or older	T4b Any N M0	The cancer is any size and has grown extensively beyond the thyroid gland back toward the spine or into nearby large blood vessels (T4b). It might or might not have spread to nearby lymph nodes (Any N). It has not spread to distant sites (M0).
IVB	55 years or older	Any T Any N M1	The cancer is any size (Any T) and might or might not have spread to nearby lymph nodes (Any N). It has spread to other parts of the body, such as distant lymph nodes, internal organs, bones, etc. (M1).

Appendix 2 – Buffers and Solutions

MES SDS Running Buffer: 50 mM MES, 50 mM Tris Base, 0.1% SDS, 1 mM EDTA, pH 7.3.

Recipe for 20X buffer stock:

MES 97.6 g
Tris Base 60.6 g
SDS 10 g
EDTA 3.0 g
Deionized water to 500 mL

Phosphate buffered saline with Tween 20 (PBST)

10X TBS 100 mL
Tween 20 1 mL
Deionized water to 1000 mL

20X Phosphate Buffered Saline (PBS)

NaCl 80 g
KCl 2 g
Na₂HPO₄ 14.4 g
NaH₂PO₄ 2.4 g
Deionized water 900 mL
pH to 7.0 with NaOH

5% nonfat milk

Nonfat dry milk 2.5 g
TBST or PBST Up to 50 mL

Stripping buffer

0.5 M Tris HCl, pH 6.8 12.5 mL
10% SDS 20 mL
2-mercaptoethanol 0.8 mL
Deionized water 67.5 mL

RIPA buffer: 25 mM Tris-HCl pH 7.6, 150 mM NaCl, 1% NP-40, 1% sodium deoxycholate, 0.1% SDS (100 mL)

NaCl 0.88 g
NP-40 1 g
Sodium deoxycholate 1 g
10% SDS 1 mL
1 M Tris-HCl, pH 7.6 2.5 mL
Deionized water to 100 mL
Protease Inhibitor Tablet (Cat. No. A32965) 2 tablets

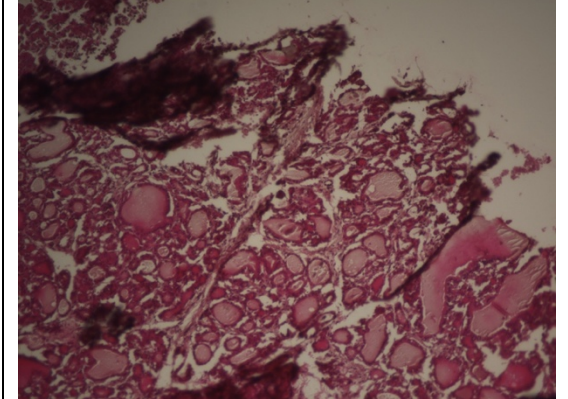
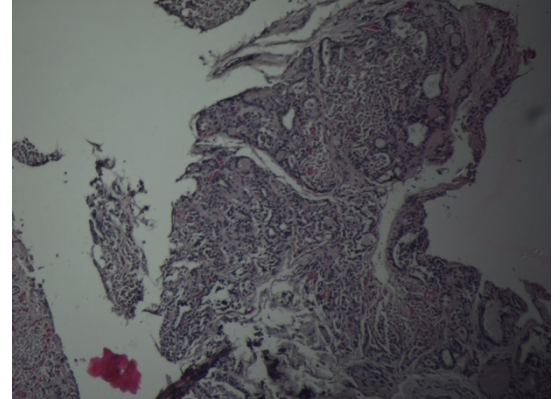
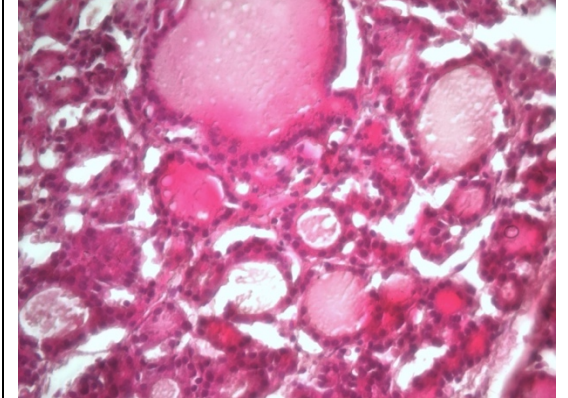
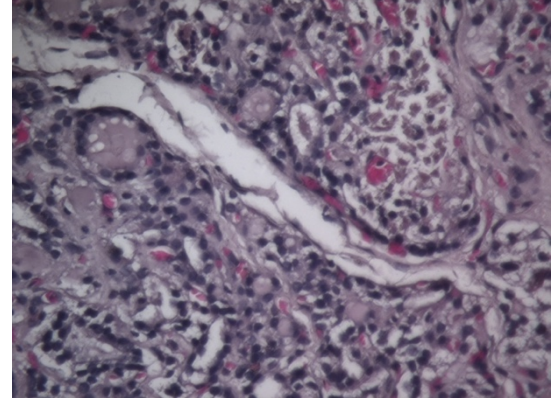
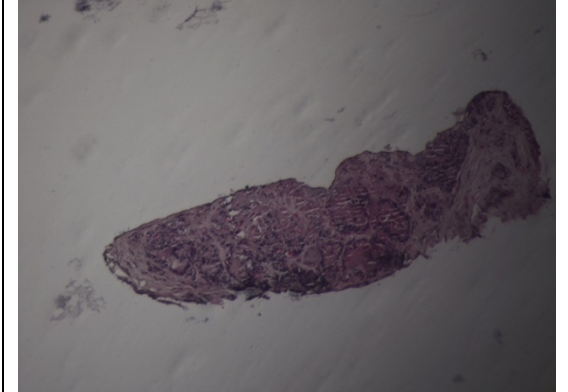
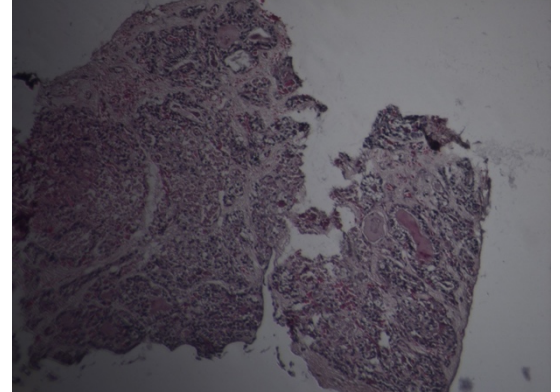
Taken from ThermoFisher Scientific Online

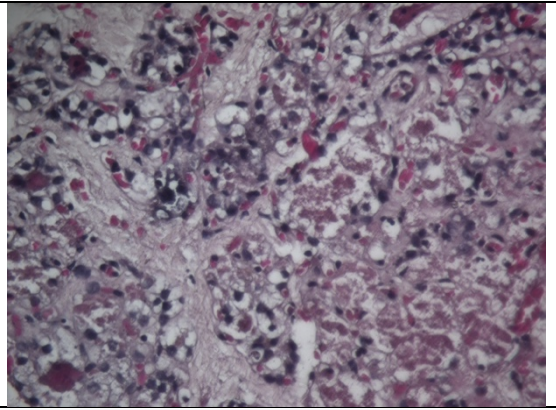
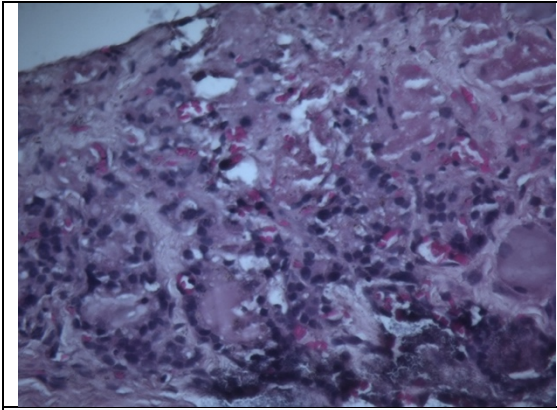
<https://www.thermofisher.com/uk/en/home/life-science/protein-biology/protein-biology-learning-center/protein-gel-electrophoresis-information/western-blot-protocols.html?open=tab3>. Accessed [02/06/24]

Appendix 3 - H&E Staining

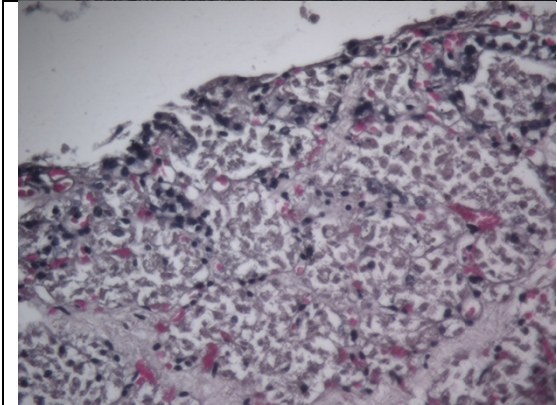
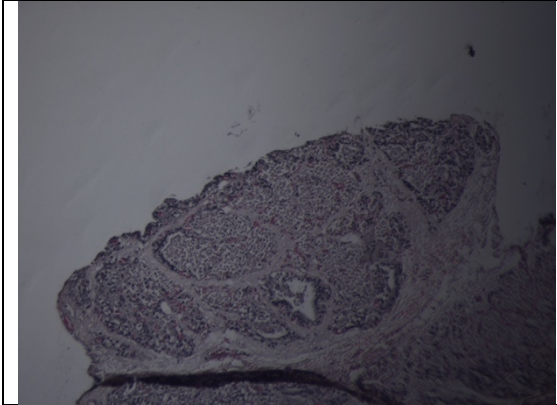
EMG

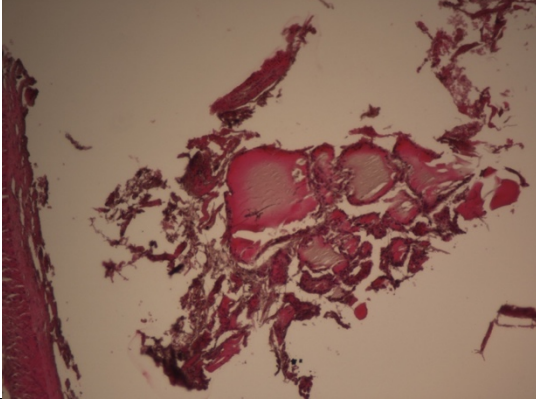
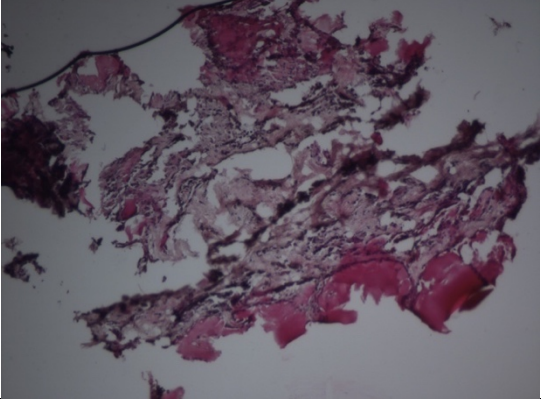
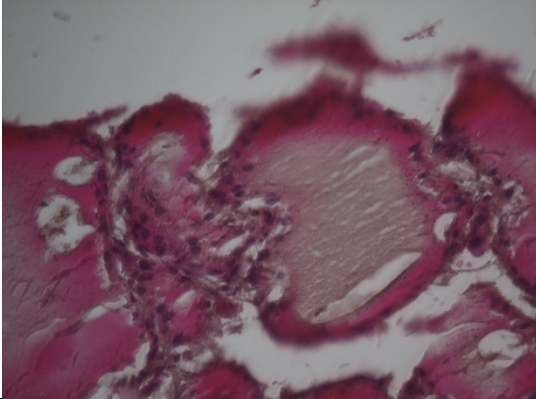
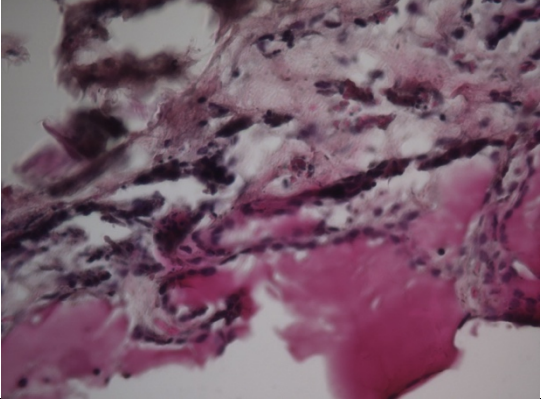
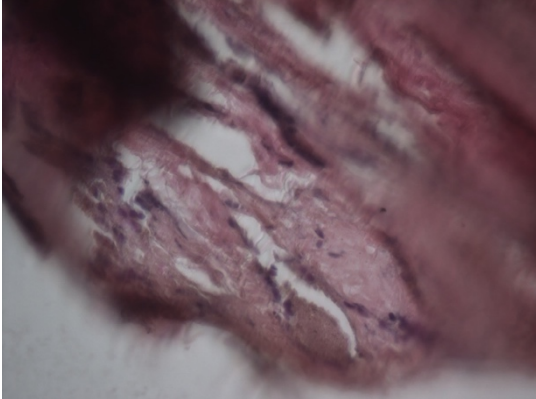
Appendix Table 3.1 – H&E Staining for EMG 1 to EMG 4 pre-culture and post-culture slides

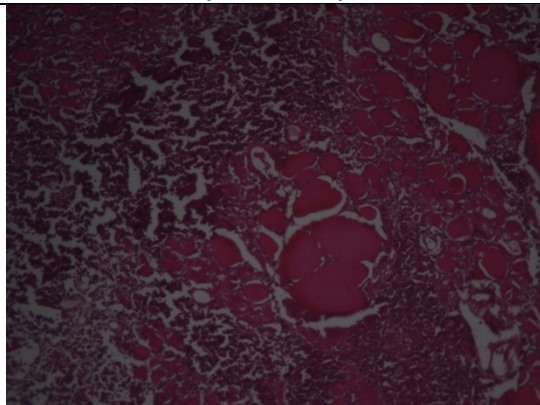
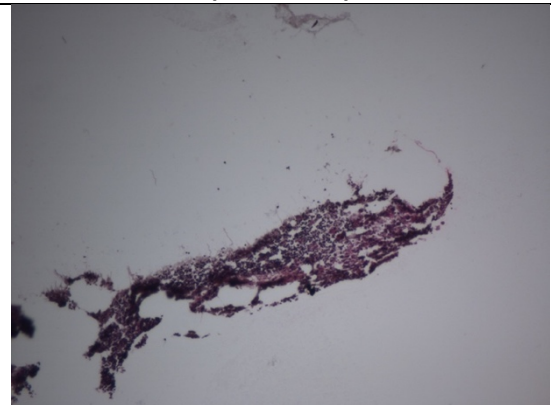
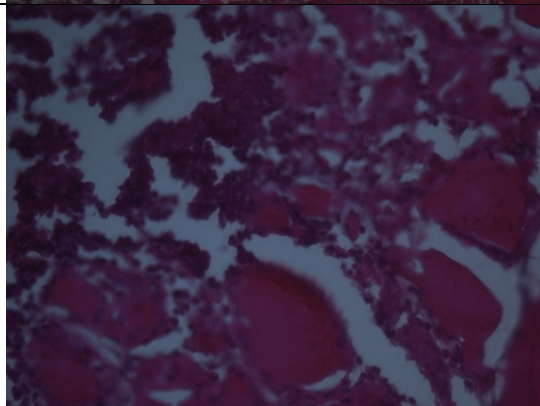
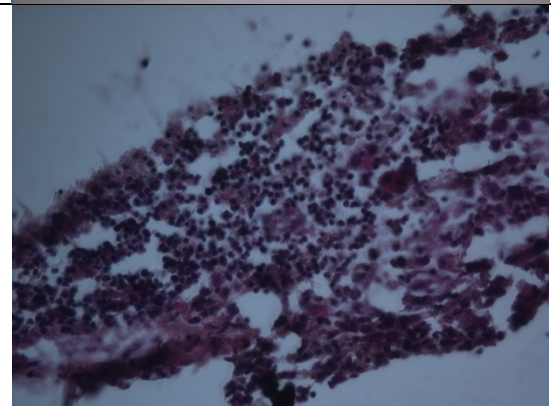
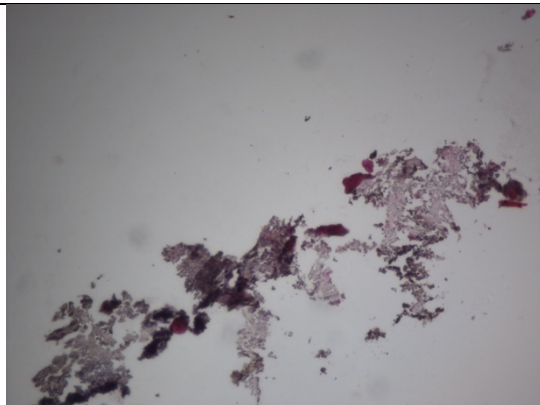
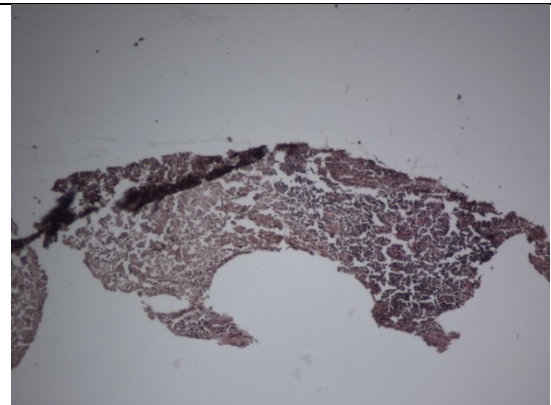
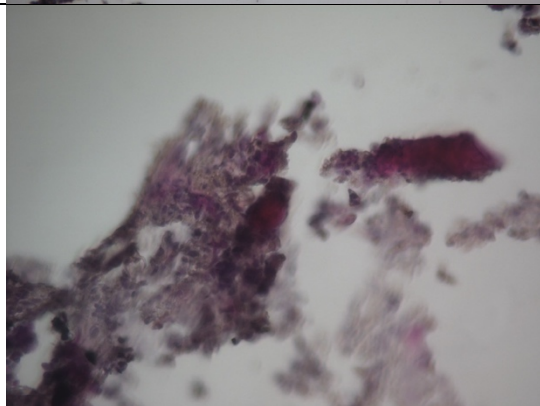
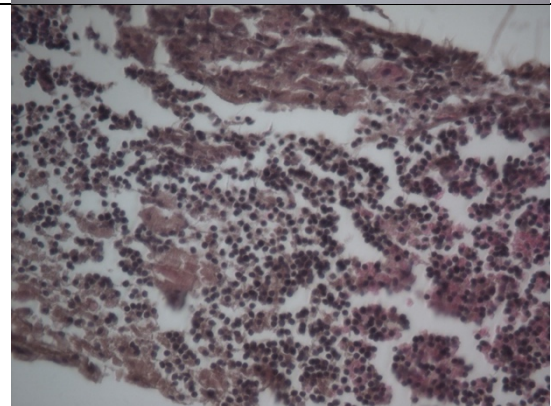
EMG 1 – Pre-culture (x10 + x40)	EMG 1 – Post-culture Device 3 - (x10 + x40)
	
	
EMG 1 – Post-culture - Device 4	EMG 1 – Post-culture - Device 5
	

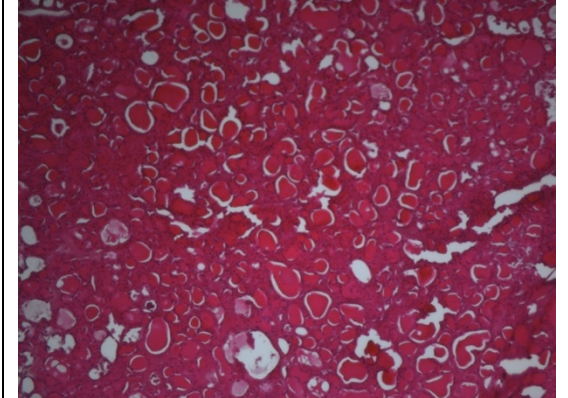
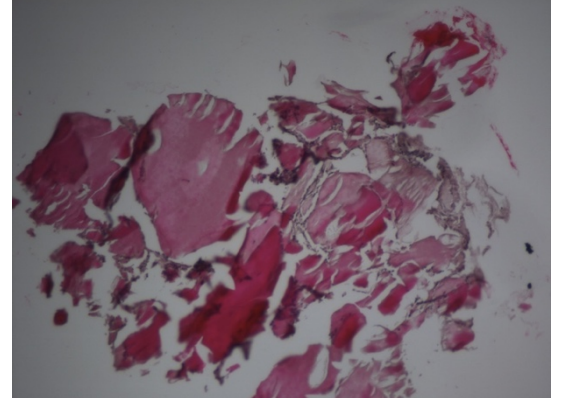
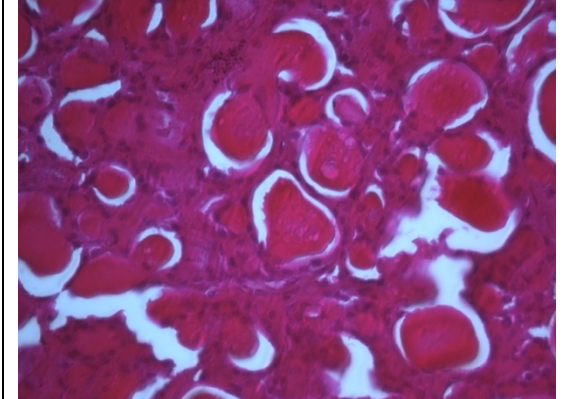
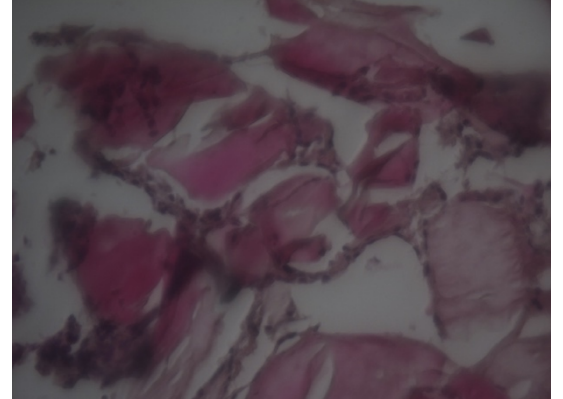
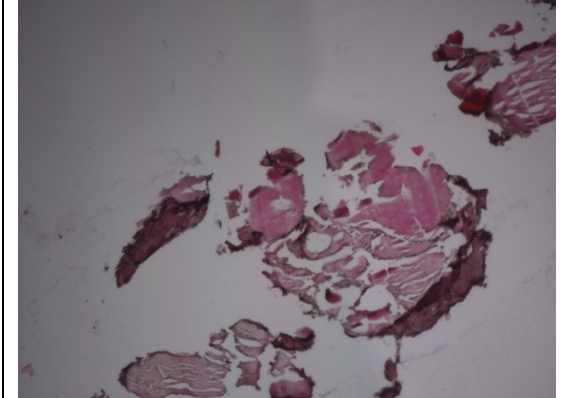
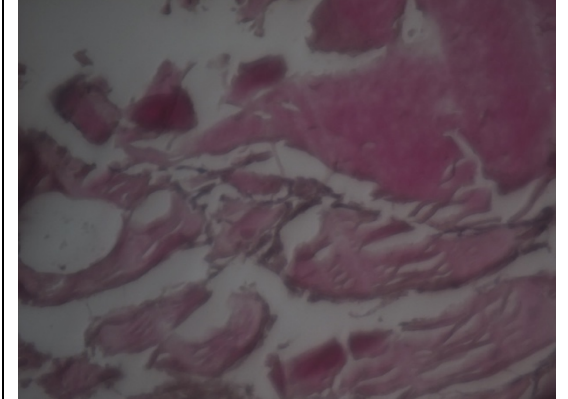
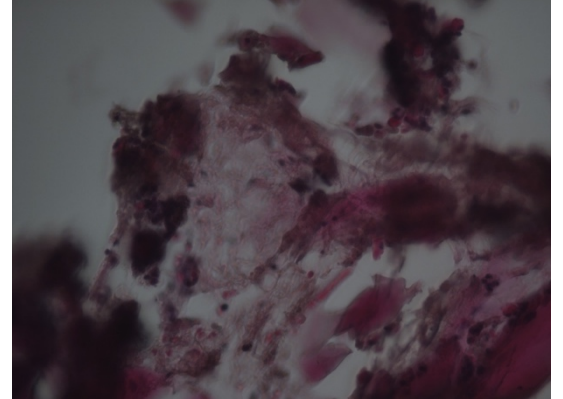


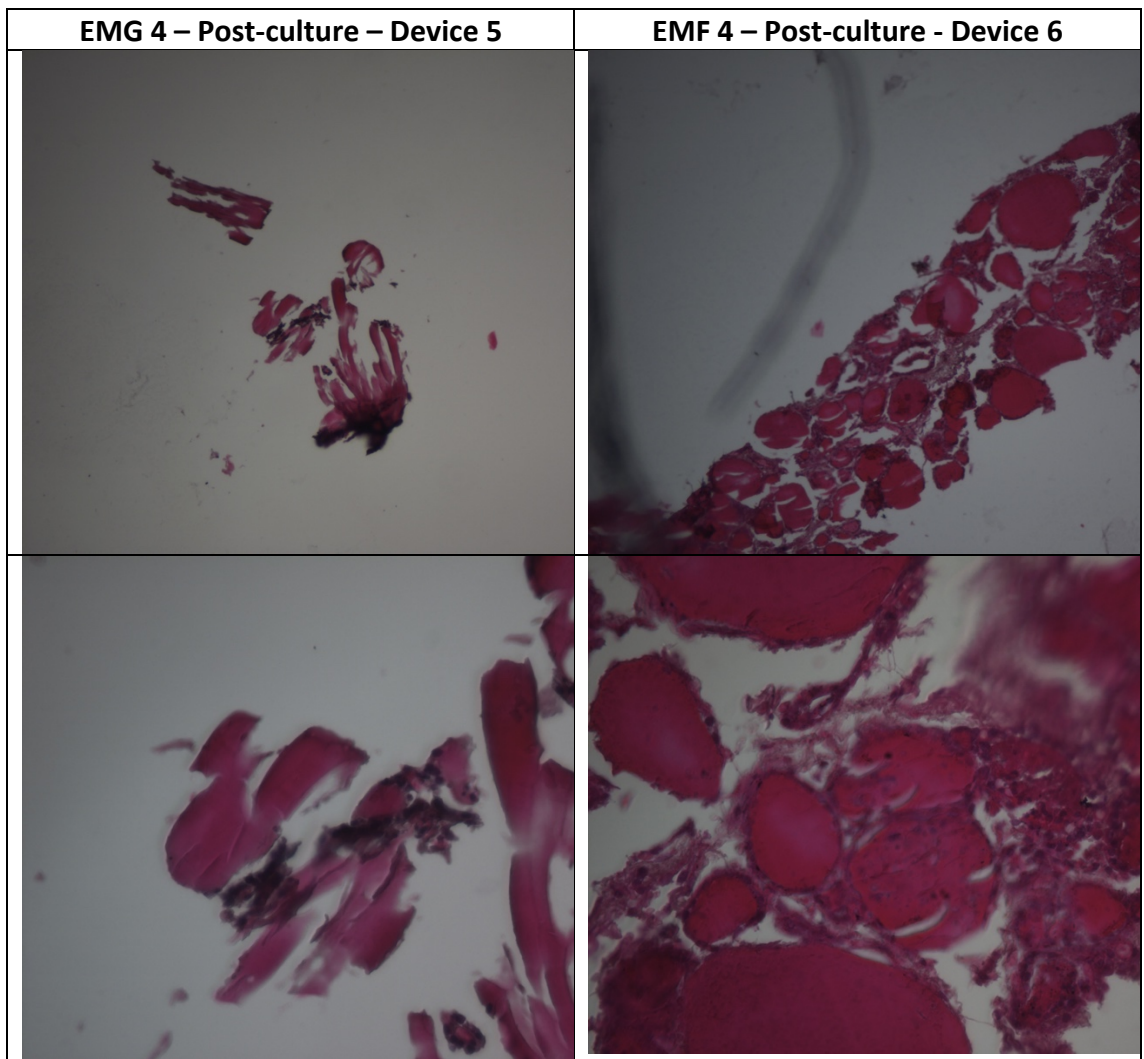
EMG 1 – Post-culture - Device 6



EMG 2 – Pre-culture (x10 + x40)	EMG 2 – Post-culture – Device 2 (x10 + x40)
	
	
EMG 2 – Post-culture – Device 5	
	
	

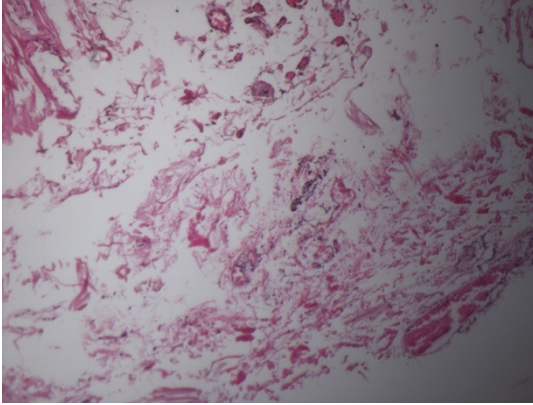
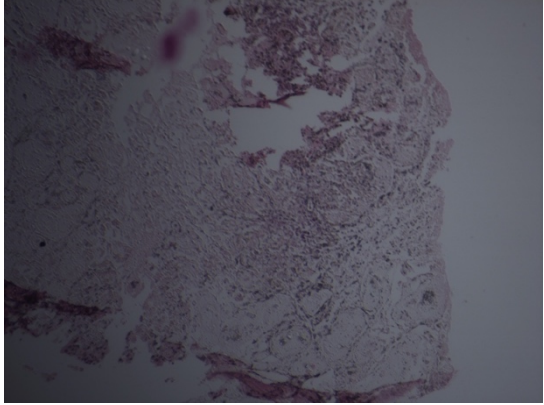
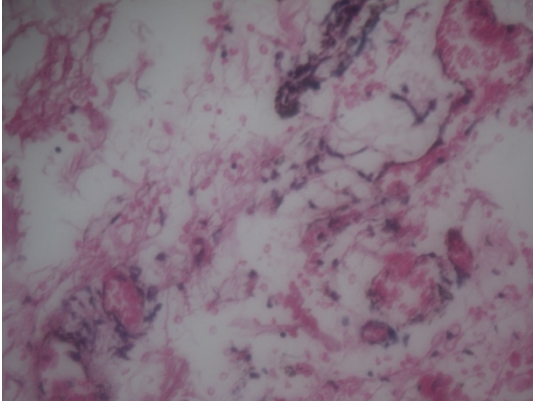
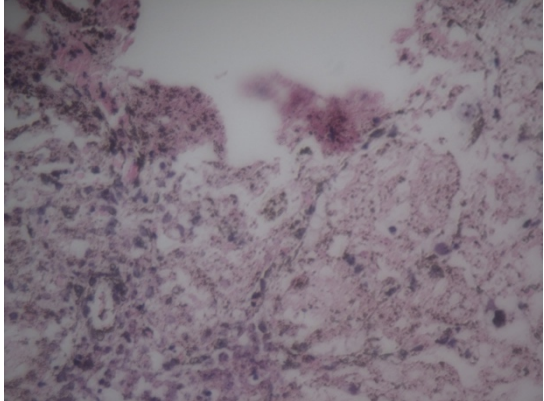
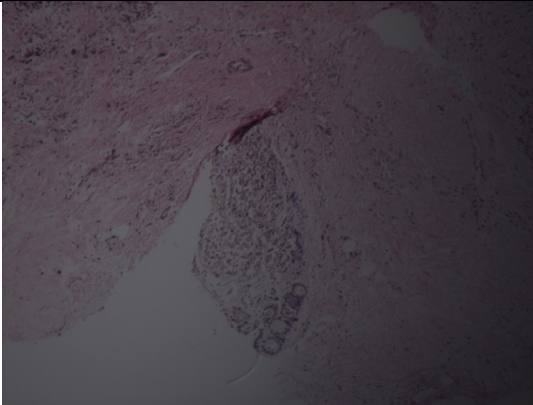
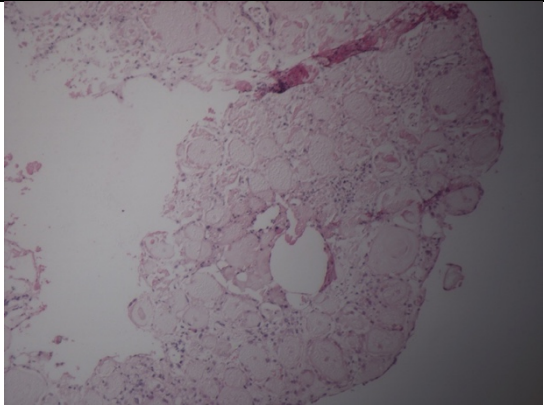
EMG 3 – Pre-culture (x10 + x40)	EMG 3 – Post-culture – Device 3 (x10 + x40)
	
	
EMG 3 – Post-culture - Device 4	EMG 3 – Post-culture - Device 5
	
	

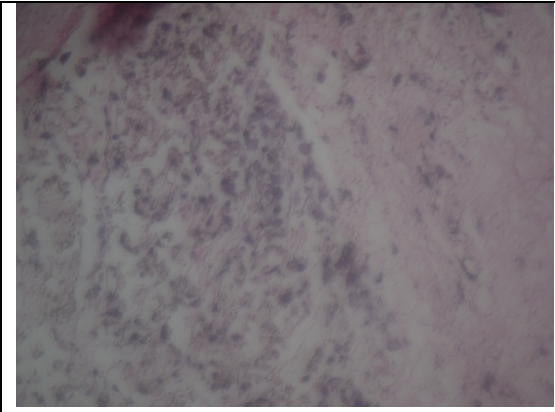
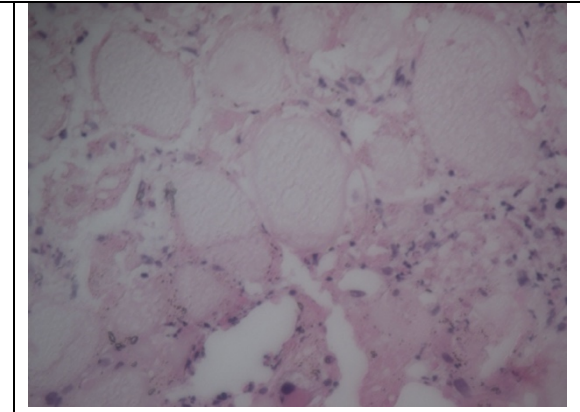
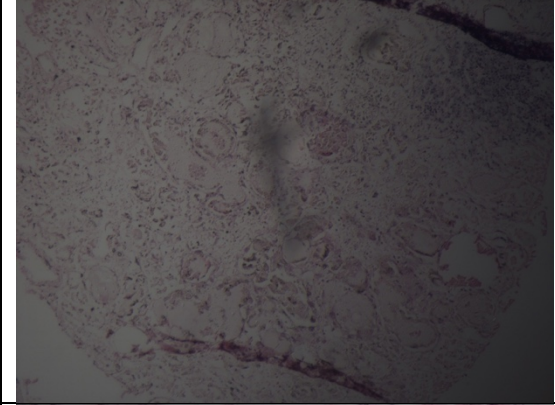
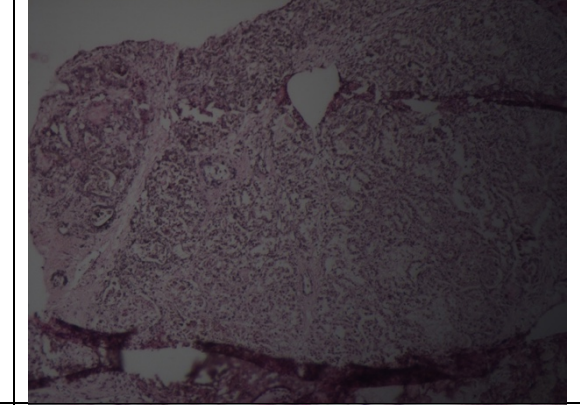
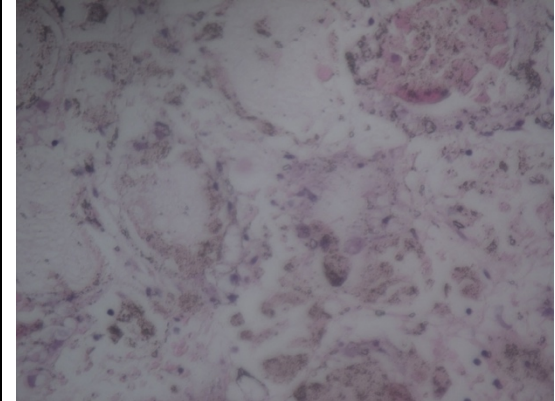
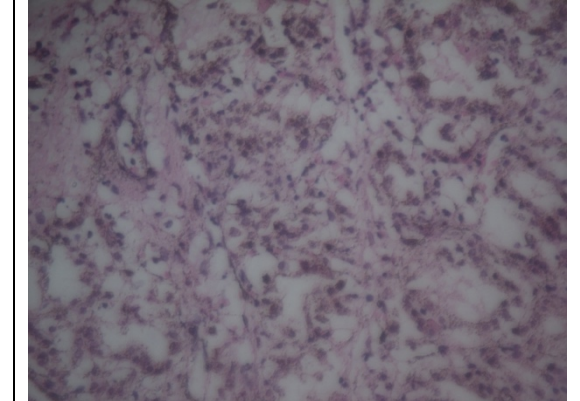
EMG 4 – Pre-culture (x10 + x40)	EMG 4 – Post-culture – Device 1 (x10 + x40)
	
	
EMG 4 – Post-culture - Device 2	EMG 4 – Post-culture - Device 4
	
	

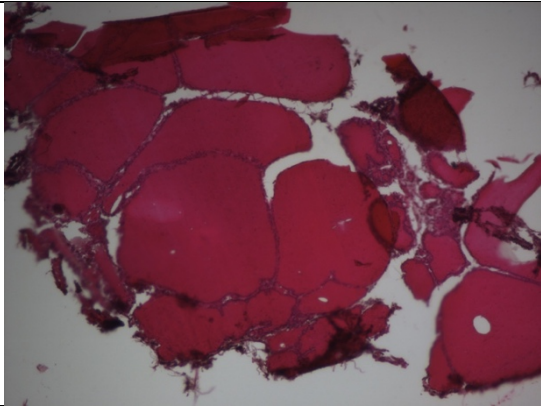
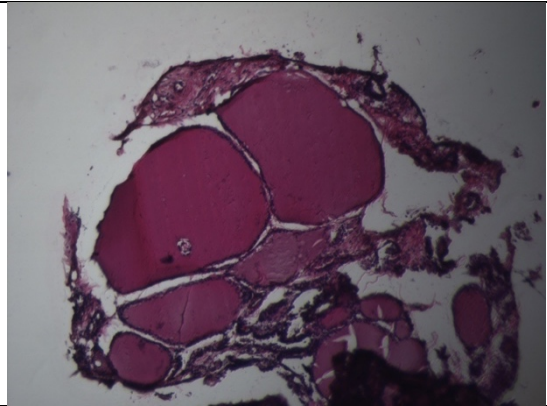
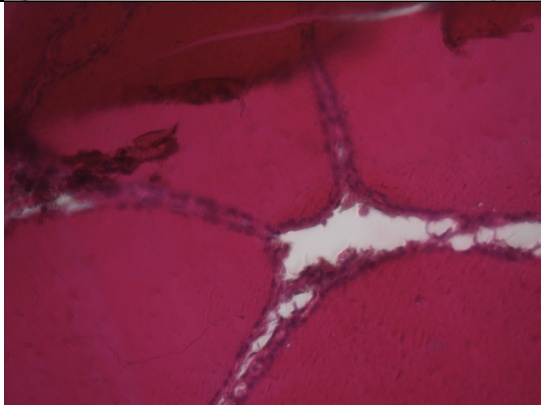
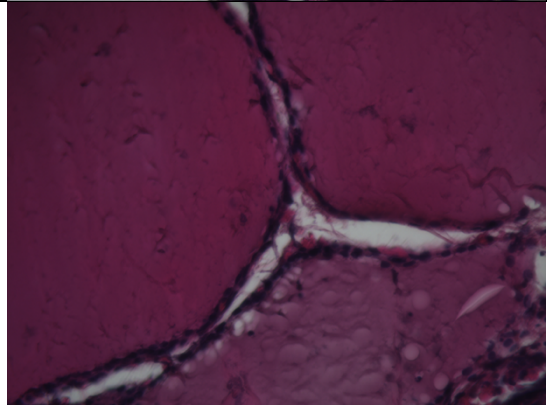
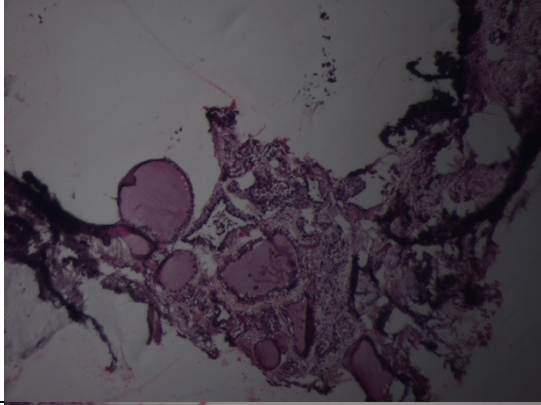
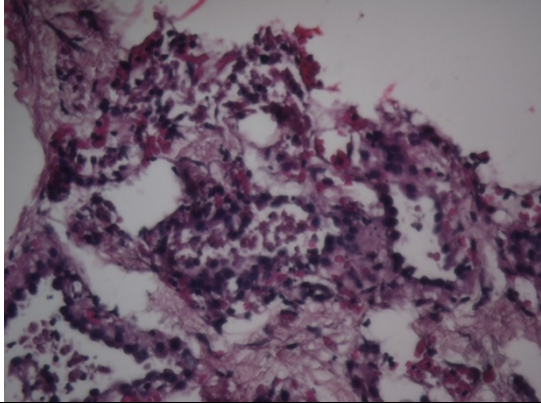


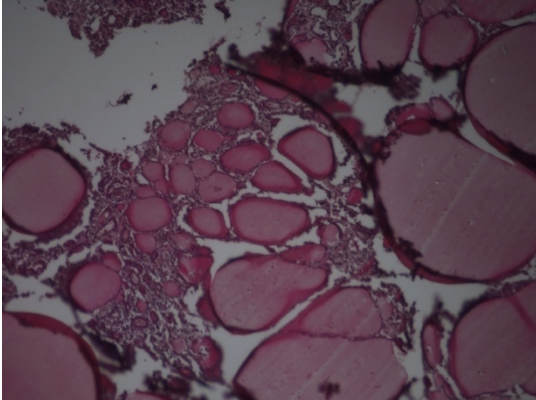
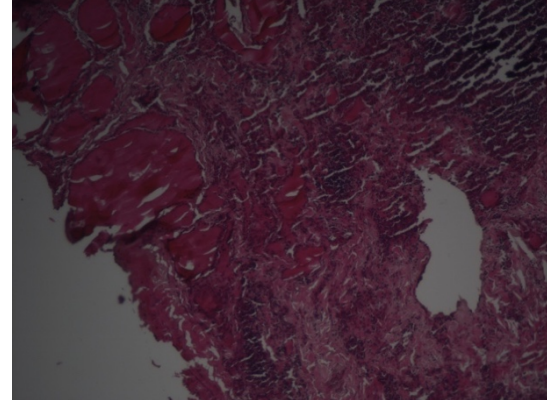
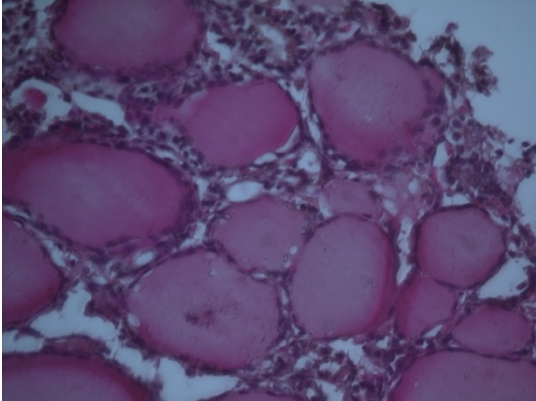
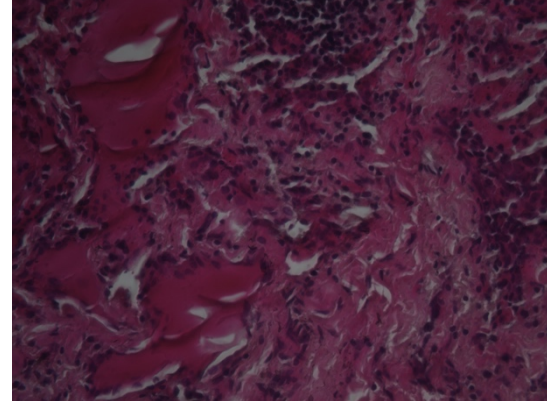
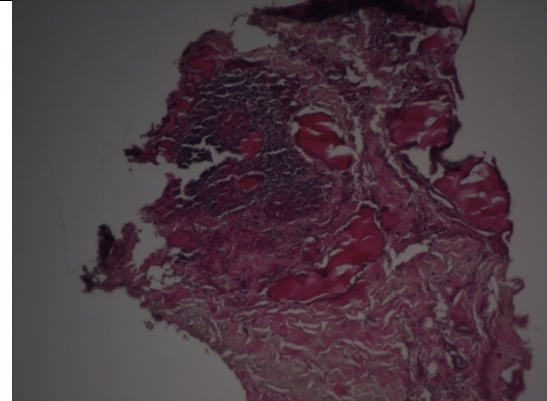
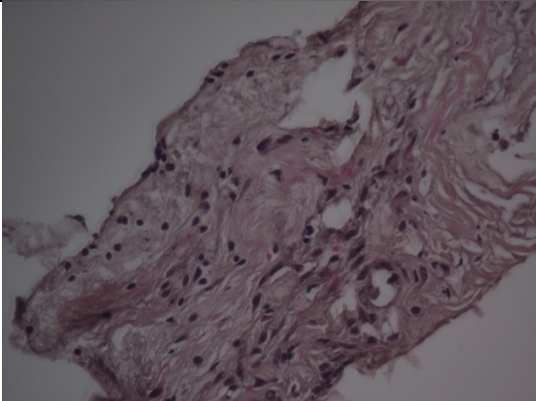
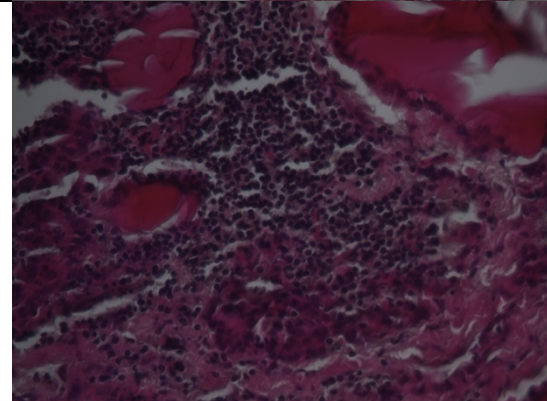
GD

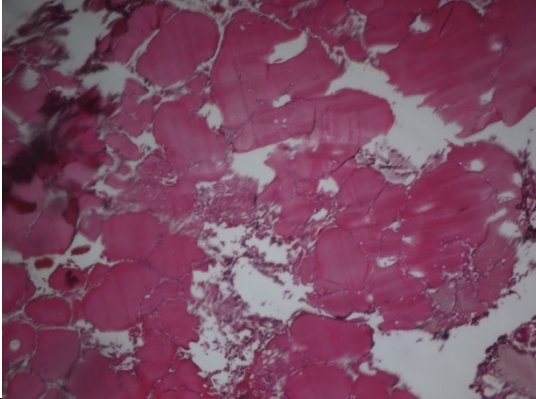
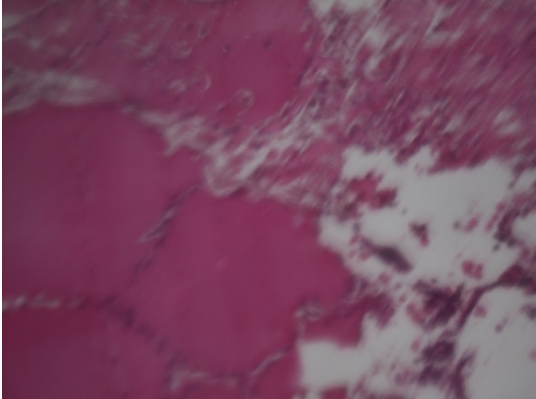
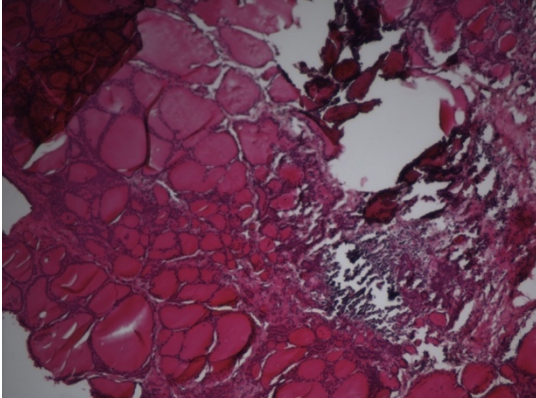
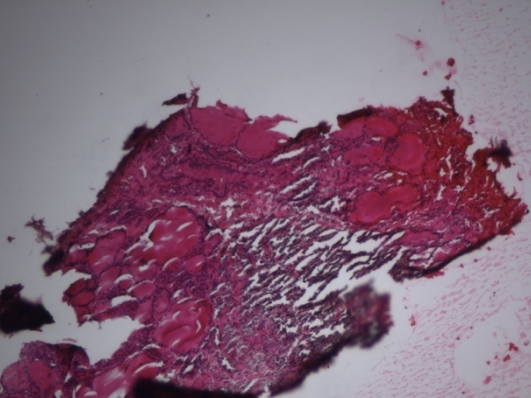
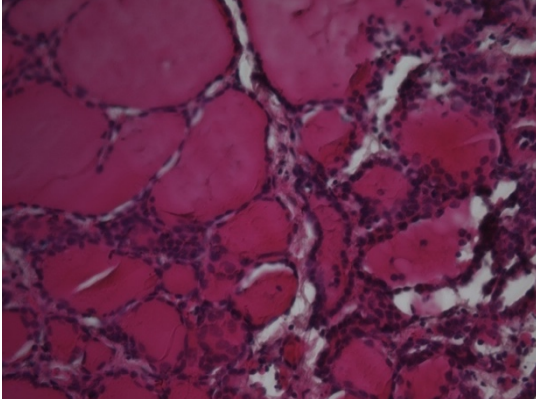
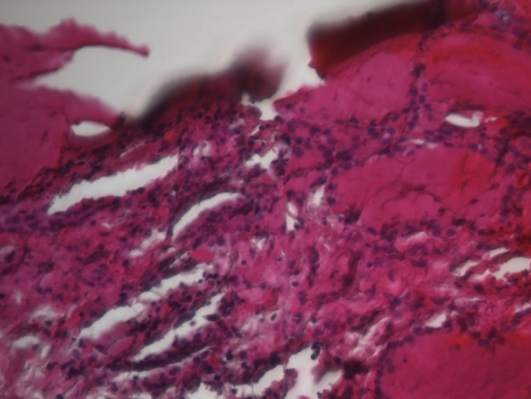
Appendix Table 3.2 – H&E Staining for GD 1 to GD 5 pre-culture and post-culture slides

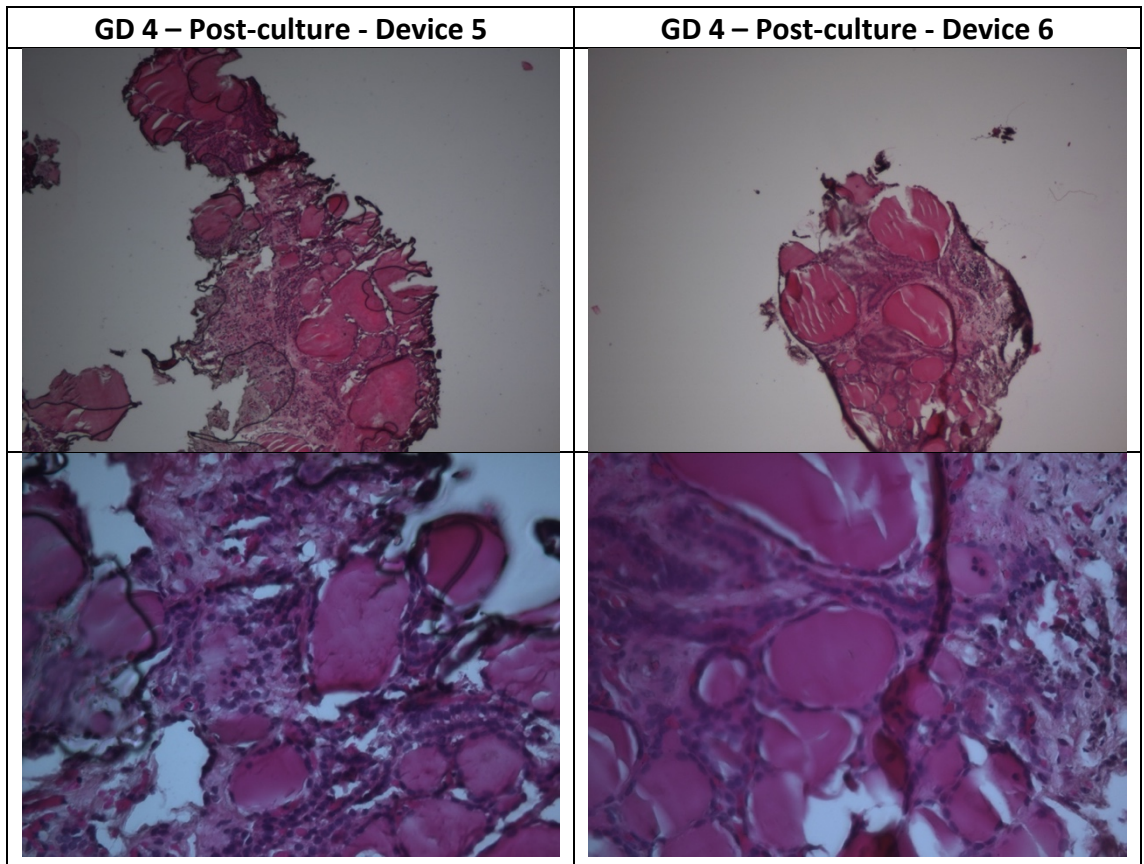
GD 1 – Pre-culture – (x10 + x40)	GD 1 – Post-Culture - Device 1 (x10 + x40)
	
	
GD 1 – Post-culture - Device 2	GD 1 – Post-culture - Device 3
	

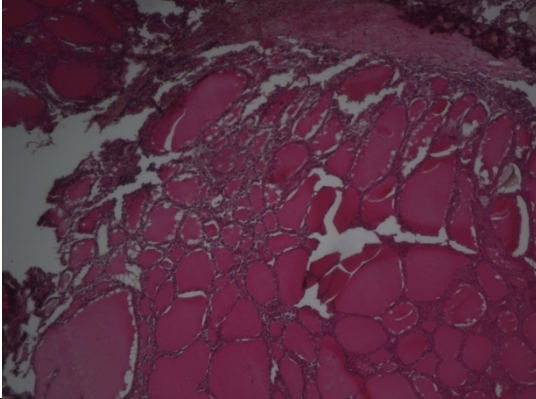
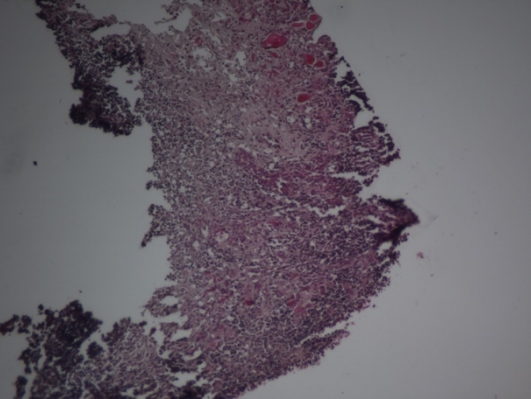
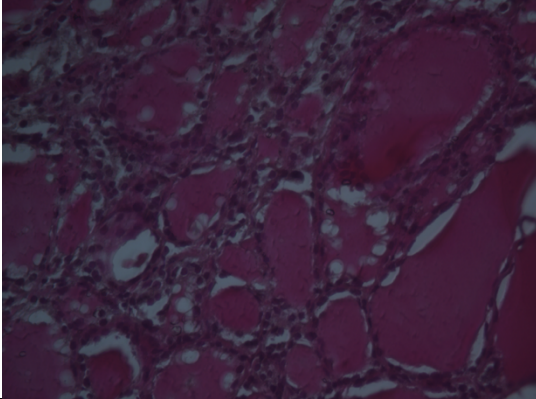
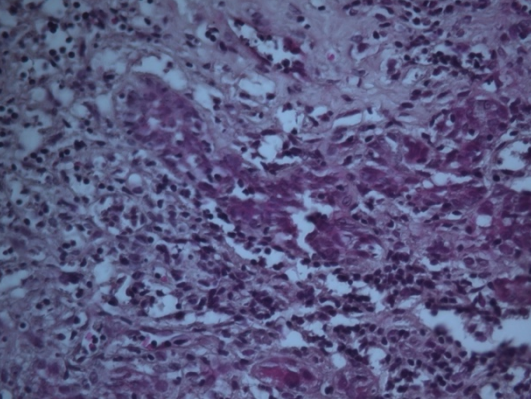
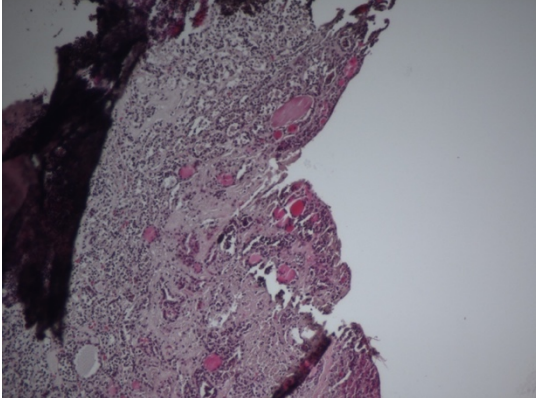
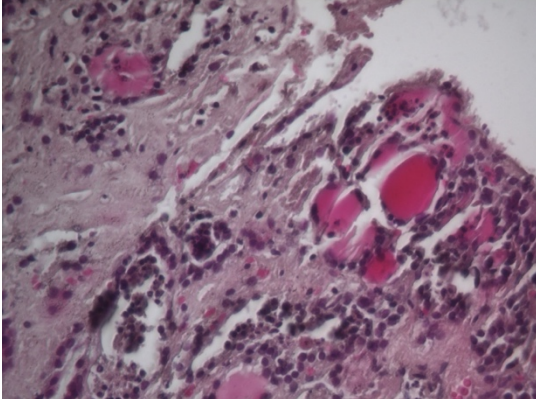
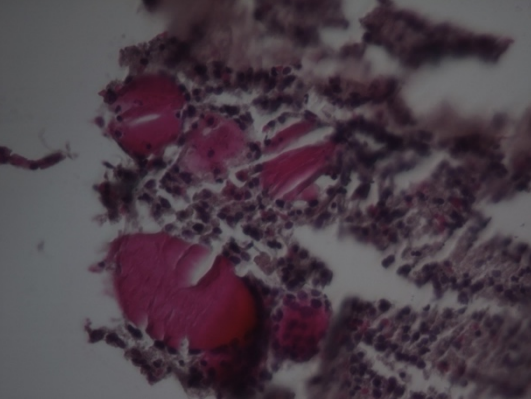
	
<p>GD 1 – Post-culture - Device 4</p>	<p>GD 1 – Post-culture - Device 5</p>
	
	

GD 2 – Pre-culture (x10 + x40)	GD 2 – Post-culture – Device 2 (x10 + x40)
	
	
GD 2 – Post-culture – Device 5	
	
	

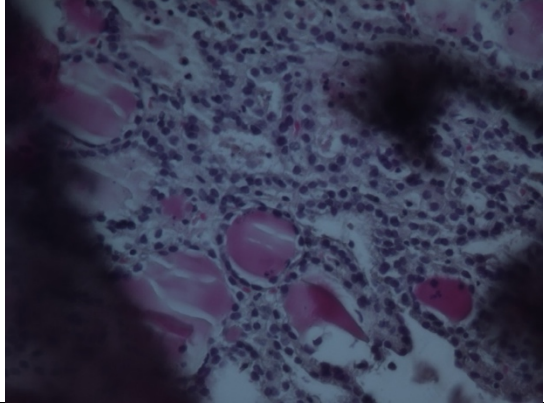
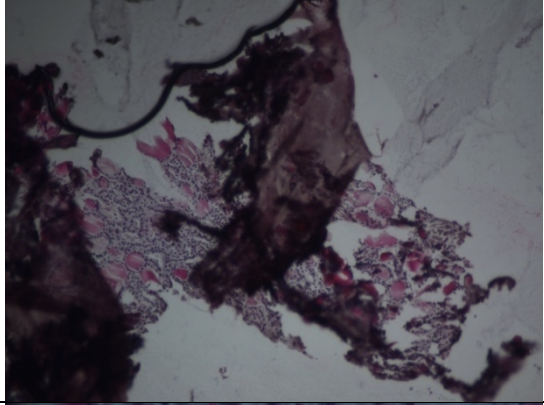
GD3 – Pre-culture (x10 + x40)	GD 3 – Post-culture – Device 1 (x10 + x40)
	
	
GD 3 – Post-culture – Device 2	GD3 – Post culture – Device 4
	
	

GD 4 – Pre-culture (x10 + x40)	GD 4 – Post-culture – Device 1 (x10 + x40)
	
	
GD 4 – Post-culture - Device 3	GD 4 – Post-culture - Device 4
	
	



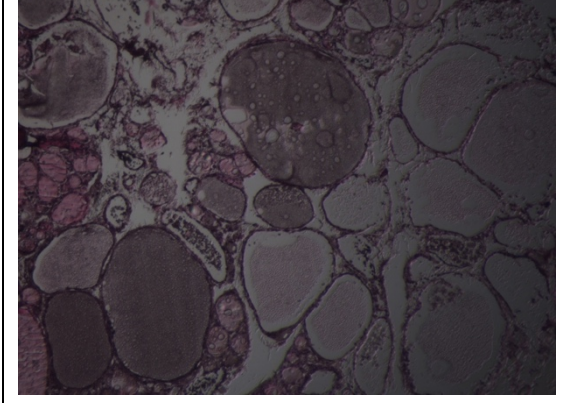
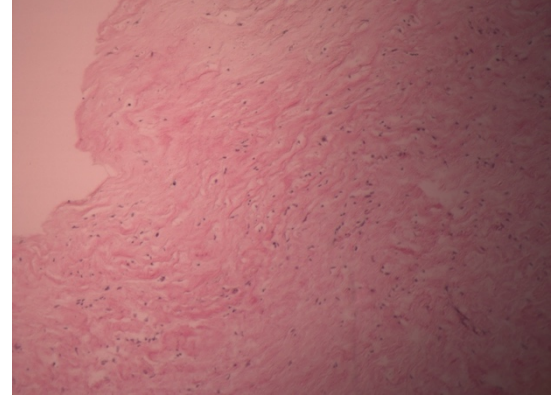
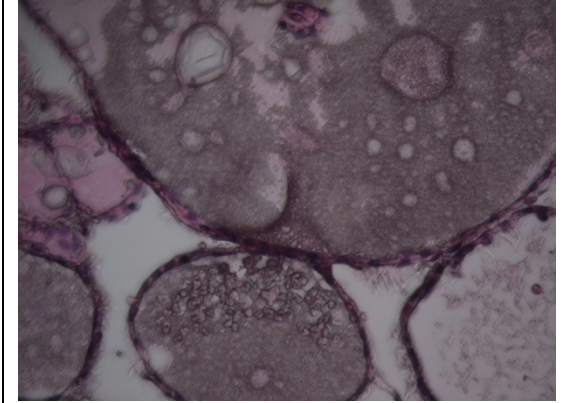
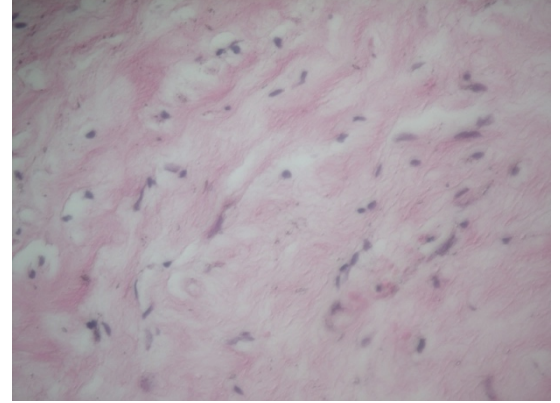
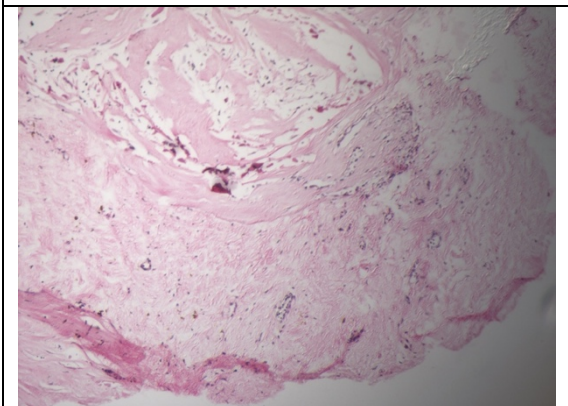
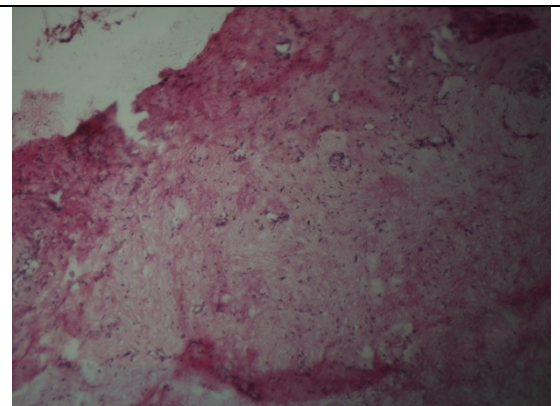
GD 5 – Pre-culture (x10 + x40)	GD 5 – Post-culture – Device 1 (x10 + x40)
	
	
GD 5 – Post-culture - Device 2	GD 5 – Post-culture - Device 3
	
	

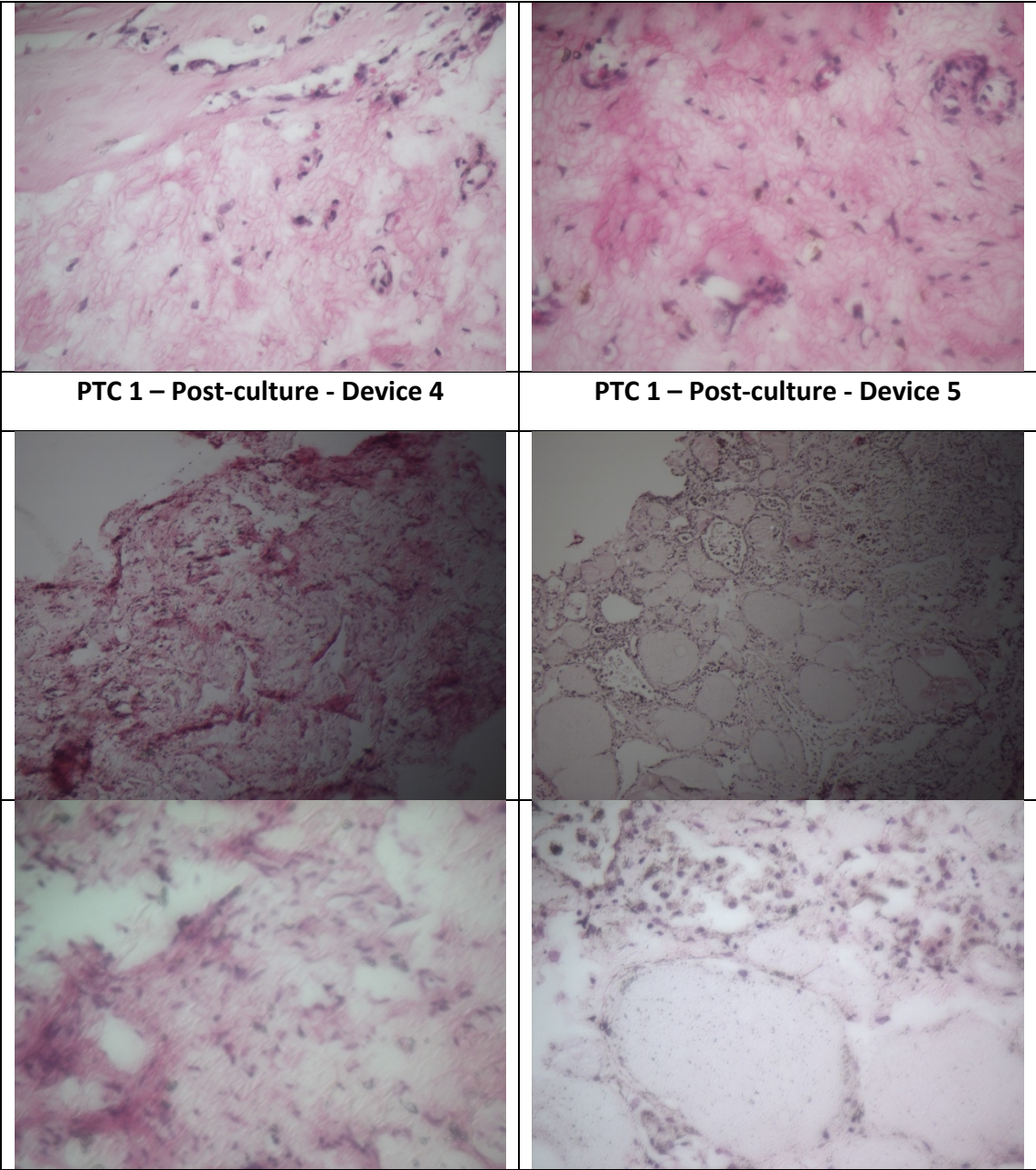
GD 6 – Post-culture - Device 6

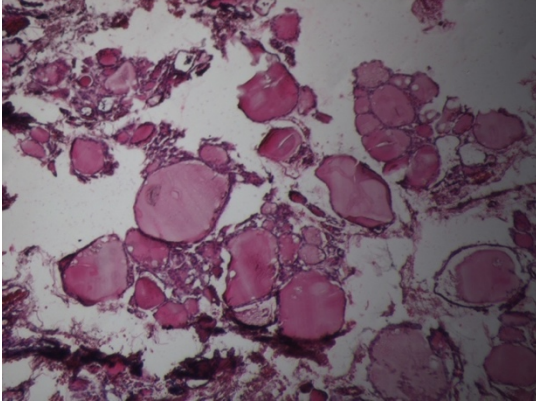
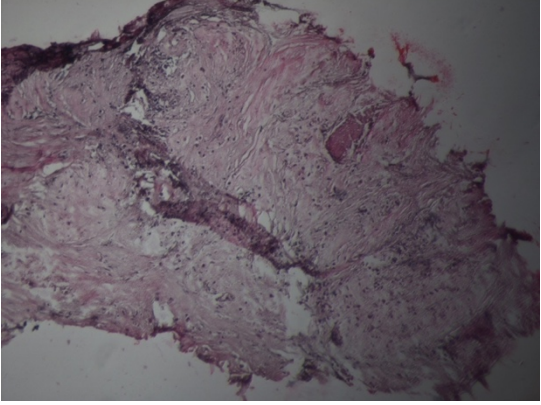
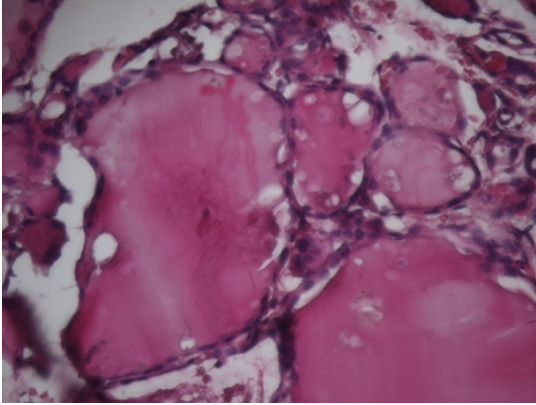
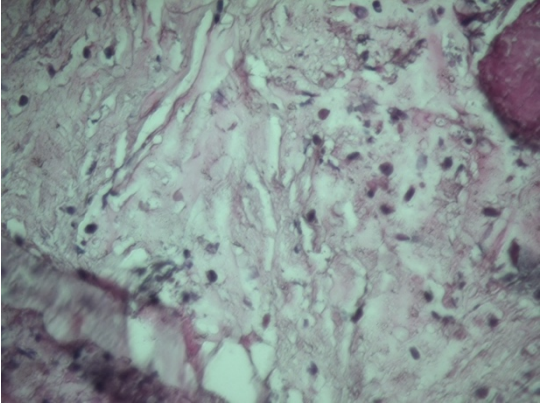
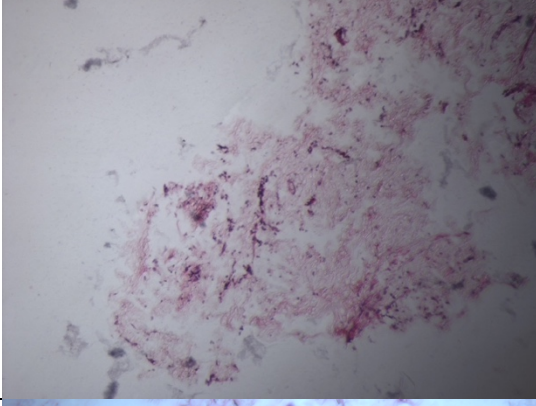
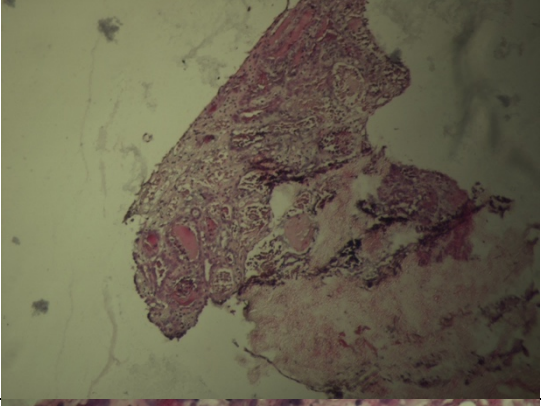
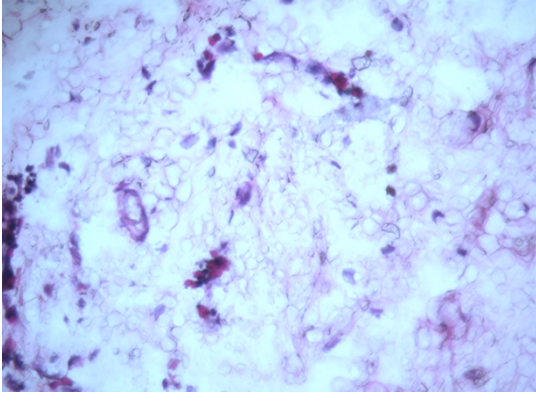
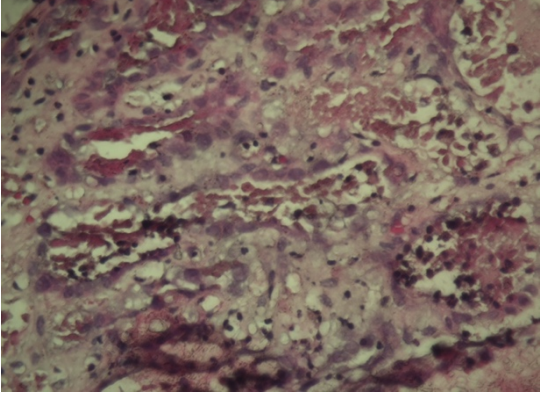


PTC

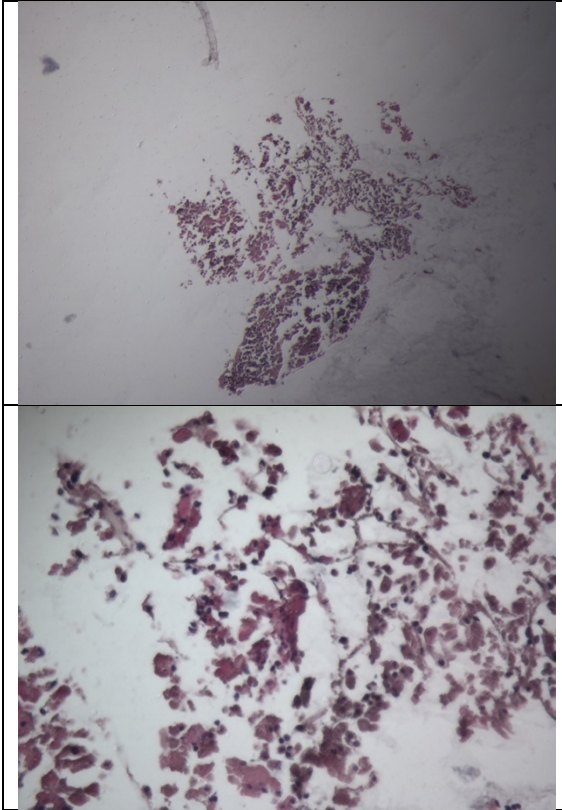
Appendix Table 3.3 – H&E Staining for PTC 1 to PTC 4 pre-culture and post-culture slides

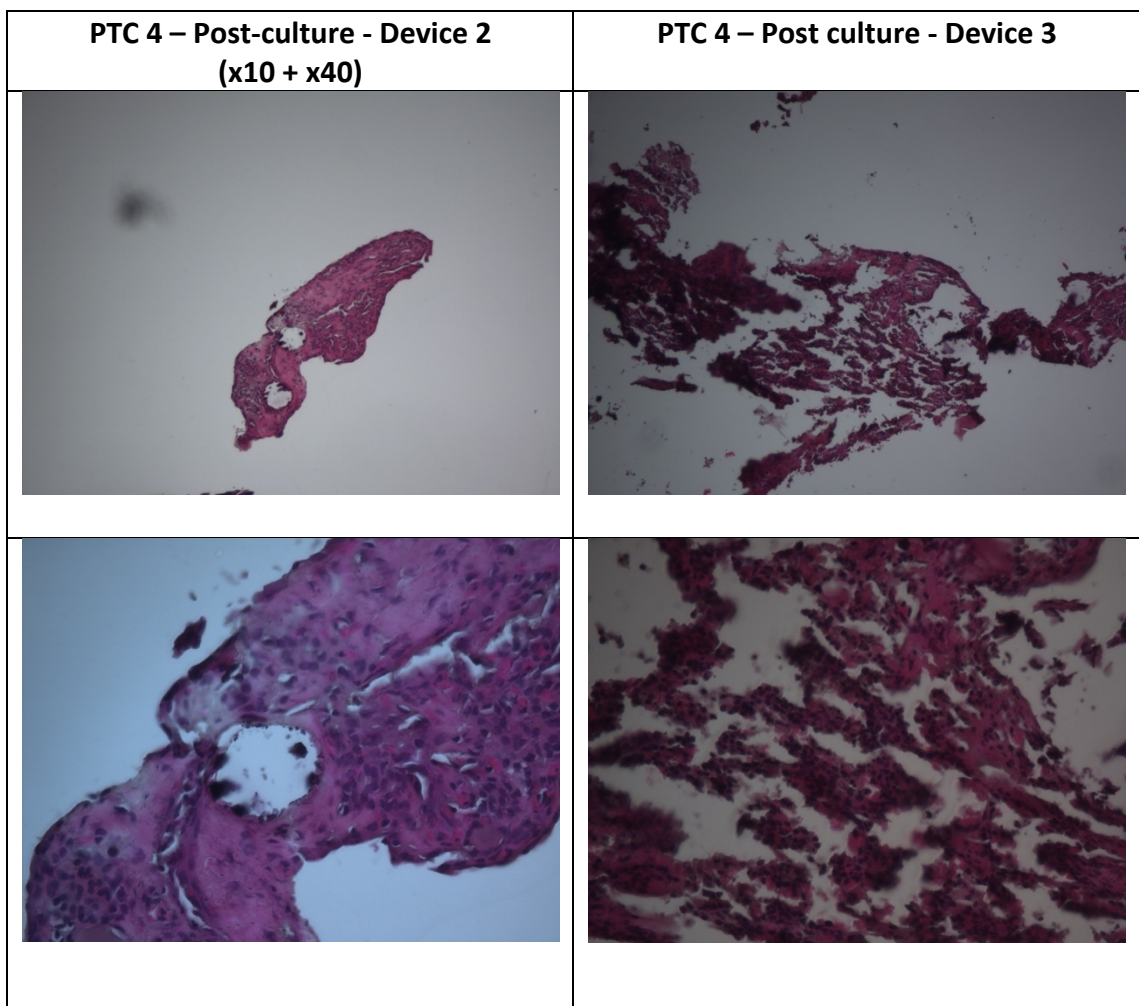
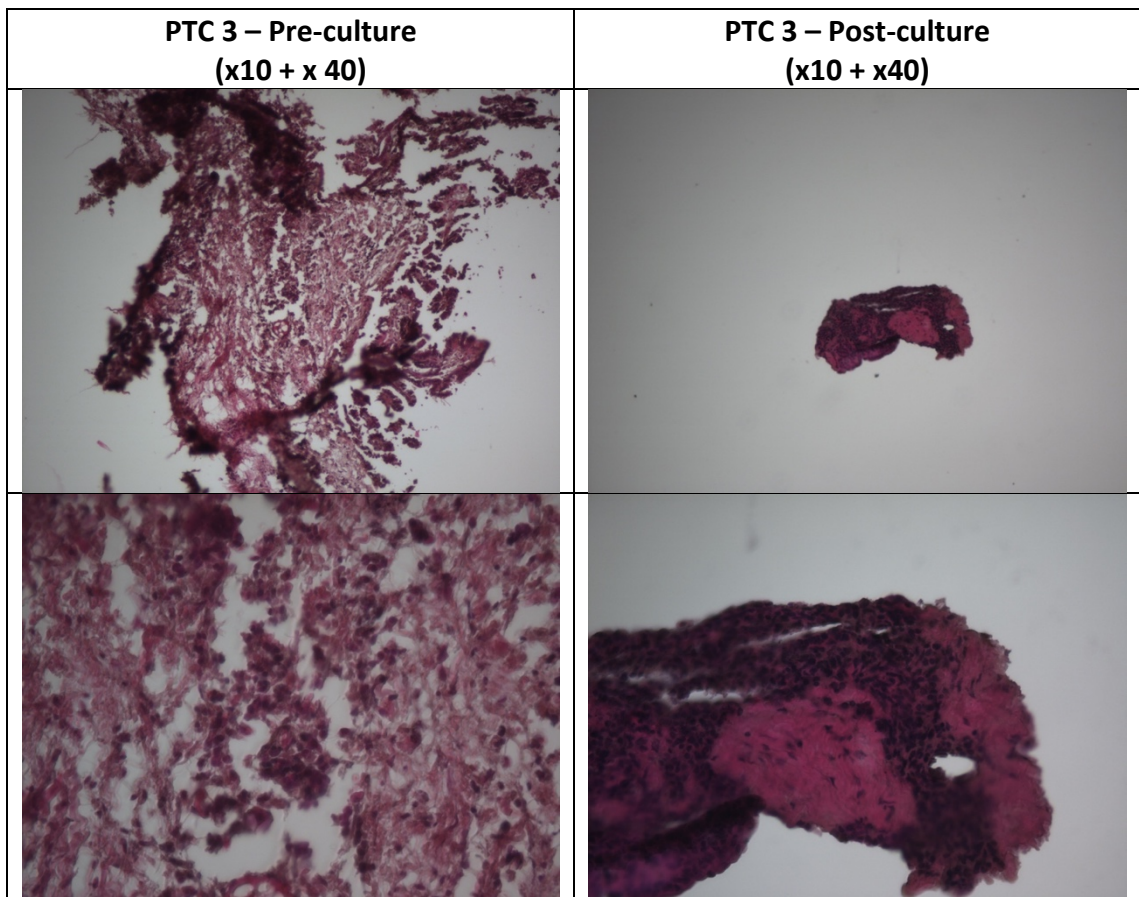
PTC 1 – Pre-culture (x10 + x40)	PTC 1 – Post-culture – Device 1 (x10 + x40)
	
	
PTC 1 – Post-culture - Device 2	PTC 1 – Post-culture - Device 3
	



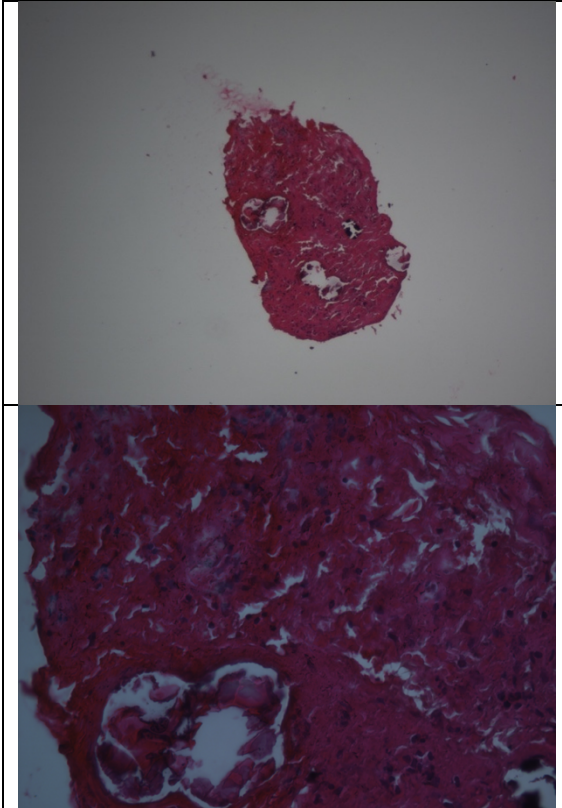
PTC 2 – Pre-culture – (x10 + x40)	PTC 2 – Post-culture – Device 3 (x10 + x40)
	
	
PTC 2 – Post-culture - Device 4	PTC 2 – Post-culture - Device 5
	
	

PTC 2 – Post-culture - Device 6





PTC 4 – Post-culture - Device 6



Appendix 4 – Nanoparticle Tracking Analysis

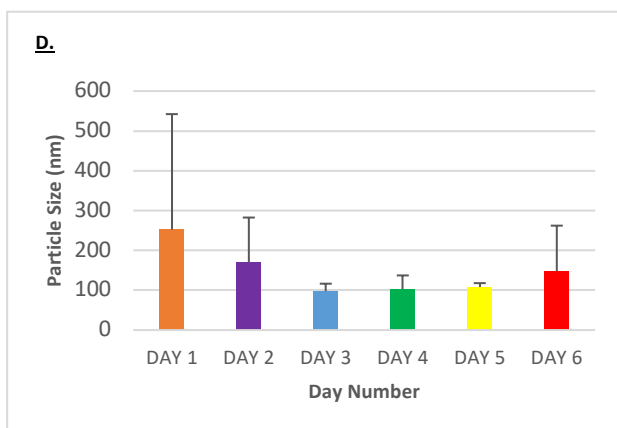
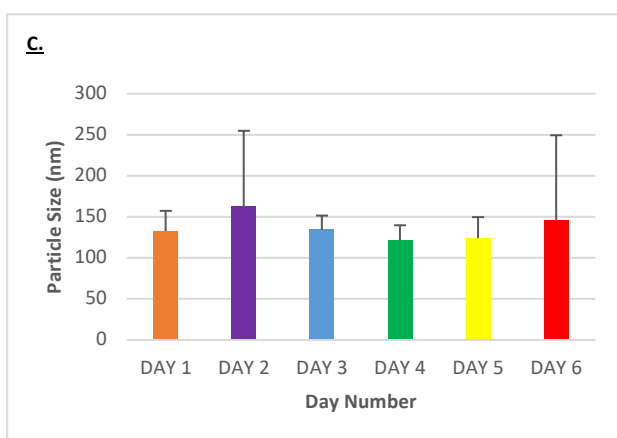
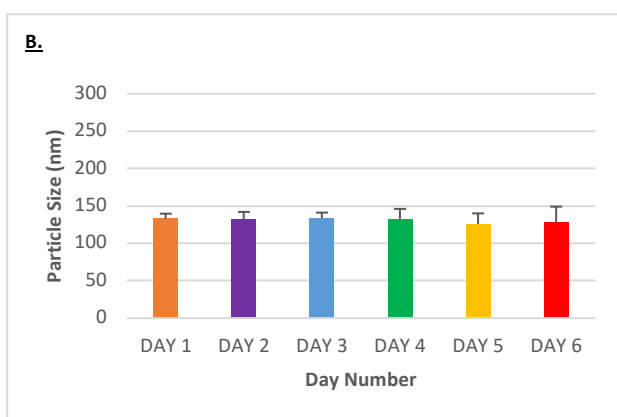
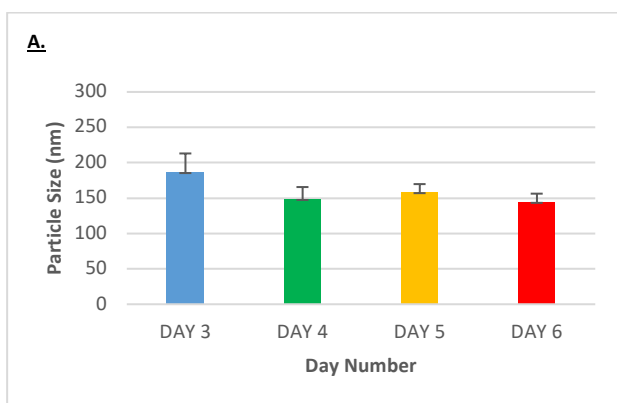
Appendix Table 4.1 - Thyroid 'Tissue-on-Chip' effluent samples subjected to NTA analysis

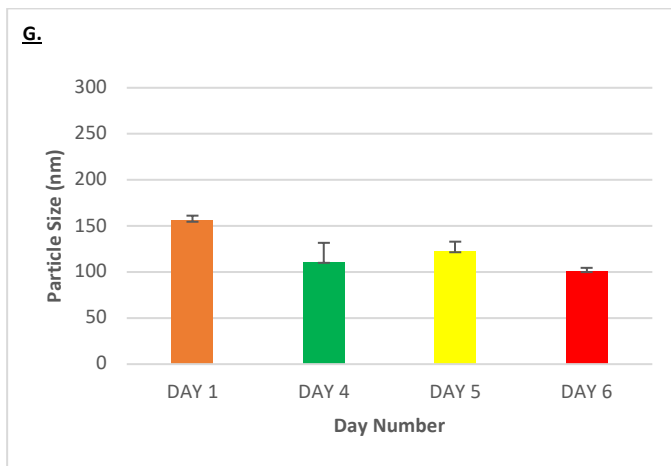
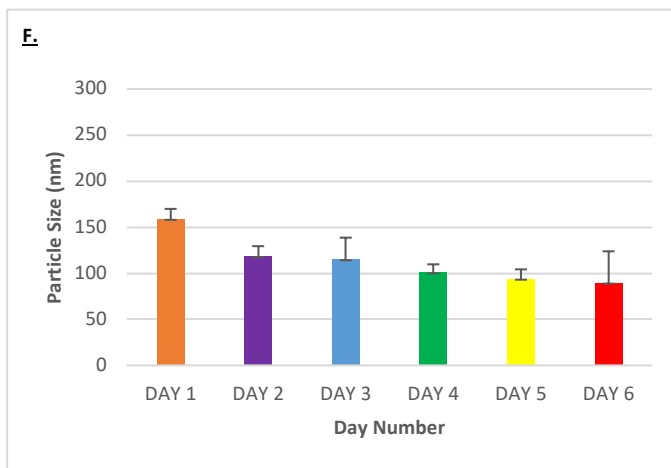
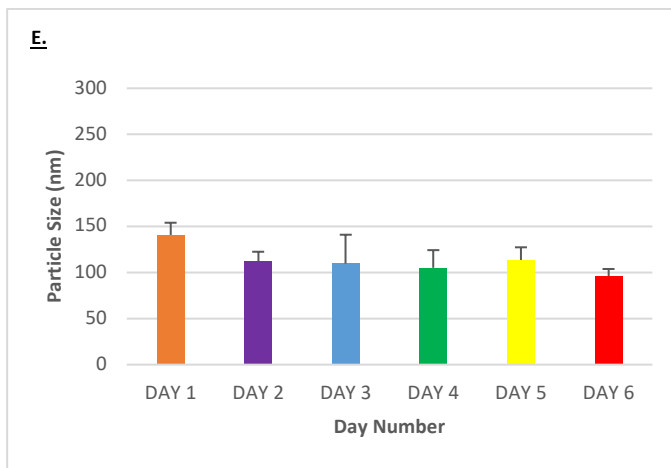
Displayed are sample pathology, demographic details (age and gender), the details of the collection of effluent and associated dilution factor

Sample	Age	Gender	Days of Effluent Collection and Effluent Dilution Factor
A. Hürthle cell carcinoma	60	F	Day 3 to Day 6 1:2 (in filtered 20nm PBS) <i>Optimisation run</i>
B. PTC	60	M	Day 1 to Day 6 1:8 dilution (in DMEM)
C. PTC	83	M	Day 1 to Day 6 1:8 dilution (in DMEM)
D. Hürthle cell carcinoma	74	M	Day 1 to Day 6 1:8 dilution (in DMEM)
E. PTC	50	F	Day 1 to Day 6 1:8 dilution (in DMEM)
F. FTC	52	F	Day 1 to Day 6 1:8 dilution (in DMEM)
G. PTC	61	M	Day 1, Day 4, Day 5 and Day 6 1:8 dilution (in DMEM)
H. GD	53	F	Day 3 to Day 6 1:4 (Filtered PBS) and 1:8 dilution (in DMEM) <i>Optimisation run</i>
I. GD	49	F	Day 1 to Day 6 1:8 dilution (in DMEM)
J. GD	42	M	Day 1 to Day 6 1:8 dilution (in DMEM)
K. EMG	59	F	Day 1 to Day 6 1:8 dilution (in DMEM)
L. EMG	51	F	Day 1 to Day 6 1:8 dilution (in DMEM)
M. EMG	75	F	Plastic Syringes – Day 1 to Day 6 Glass Syringes – Day 1 to Day 4 1:8 dilution (in DMEM)

PTC – papillary thyroid cancer; **FTC** – follicular thyroid cancer **GD** – Graves' disease; **EMG** – euthyroid multinodular goitre; **M** – Male; **F** - Female

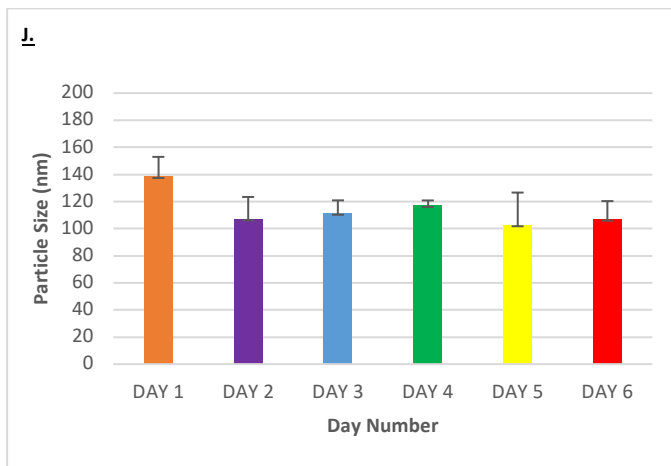
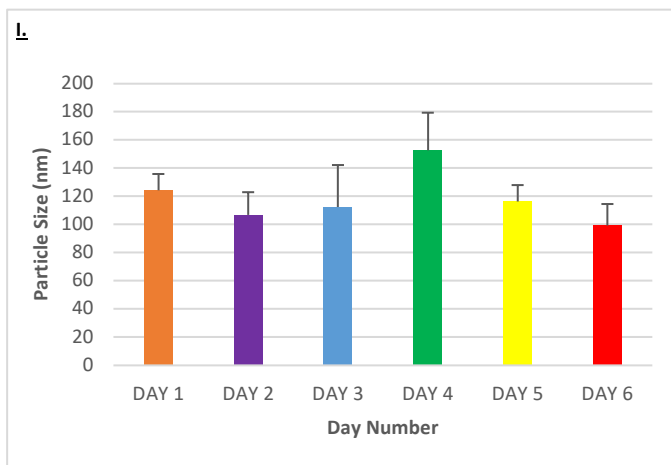
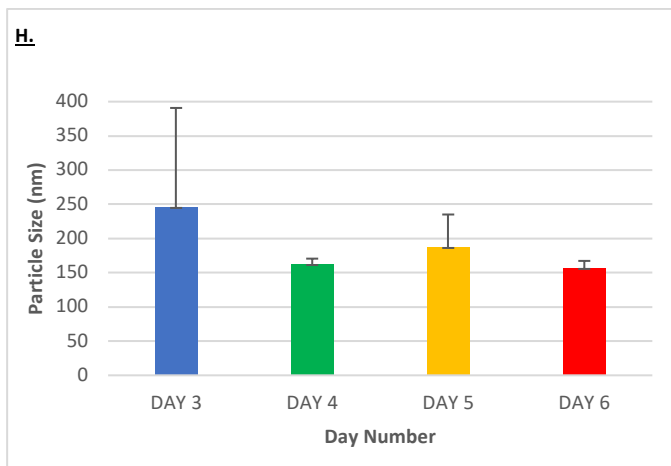
Particle Mean Size (nm)



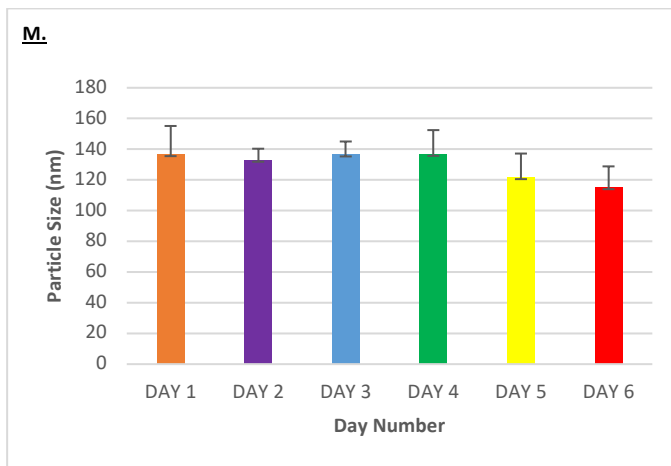
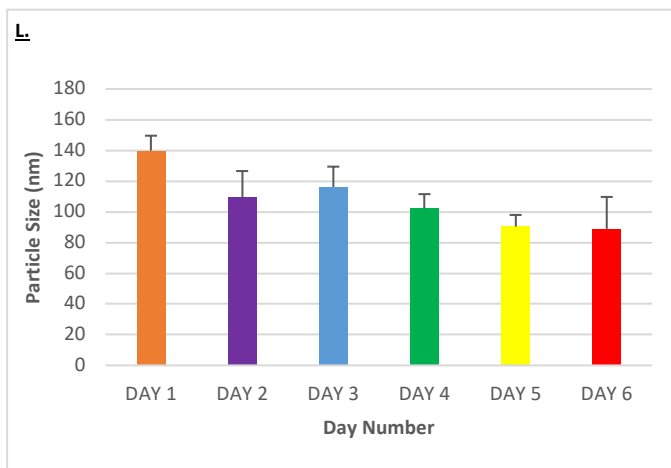
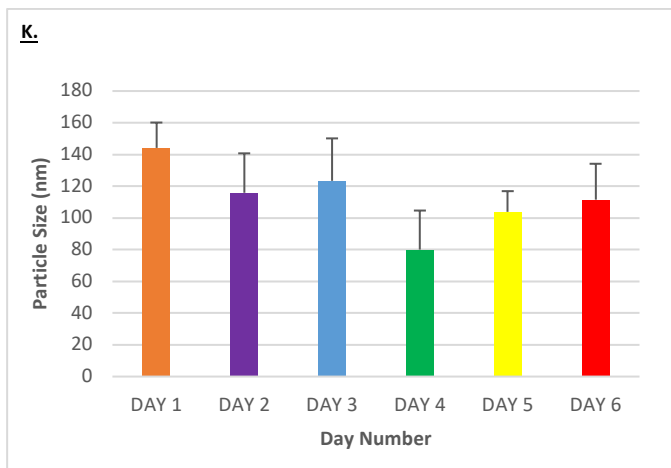


Appendix Figure 3.1 - TC Samples ($n=7$) particle mean size (nm) - day 1 to day 6 on tissue on chip device

A. - Hürthle cell carcinoma (*Optimisation study*), **B.** - PTC, **C.** - PTC, **D.** - Hürthle cell carcinoma, **E.** PTC, **F.** - FTC, **G.** - PTC

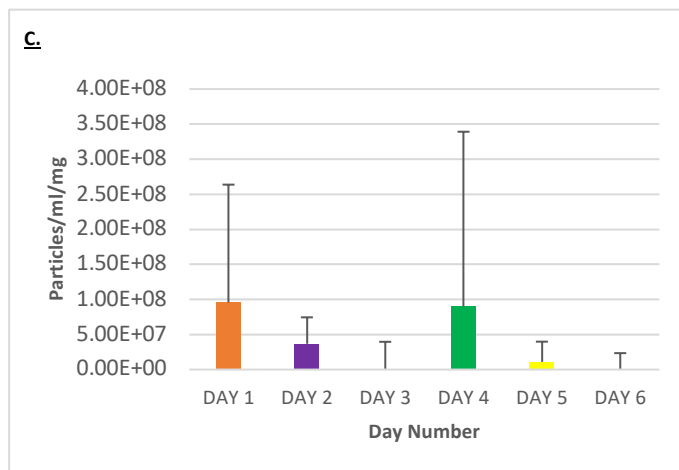
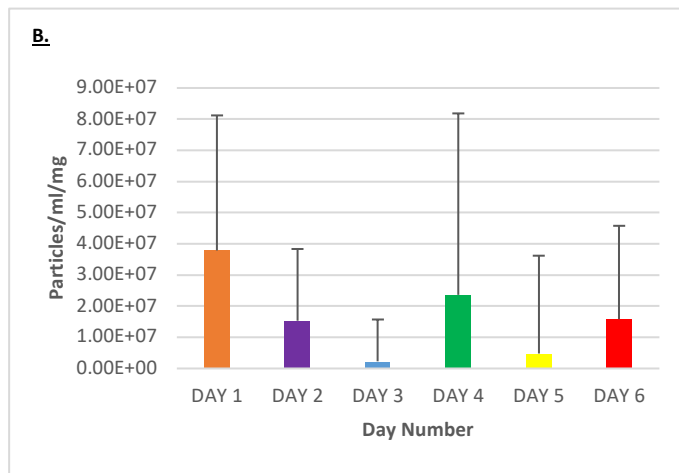
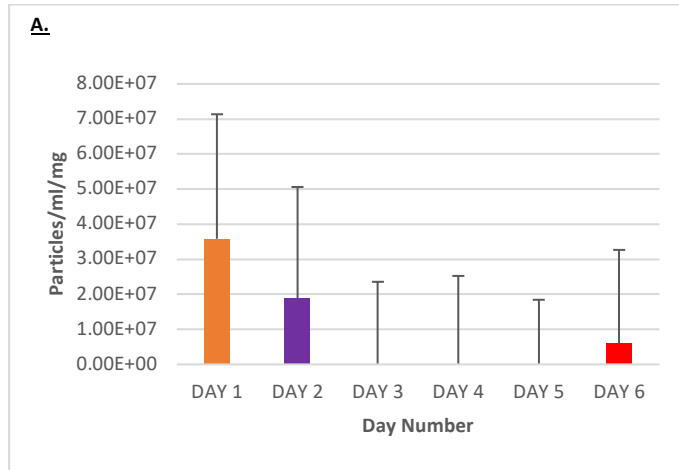


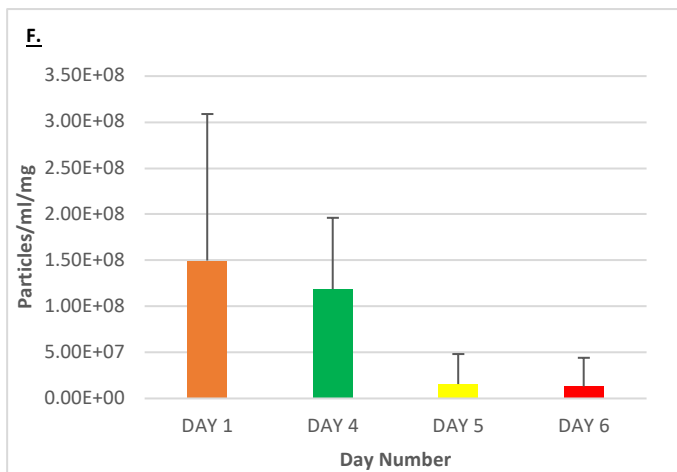
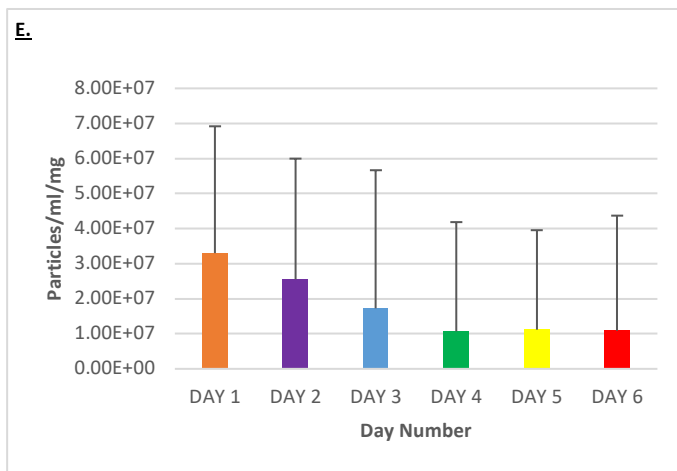
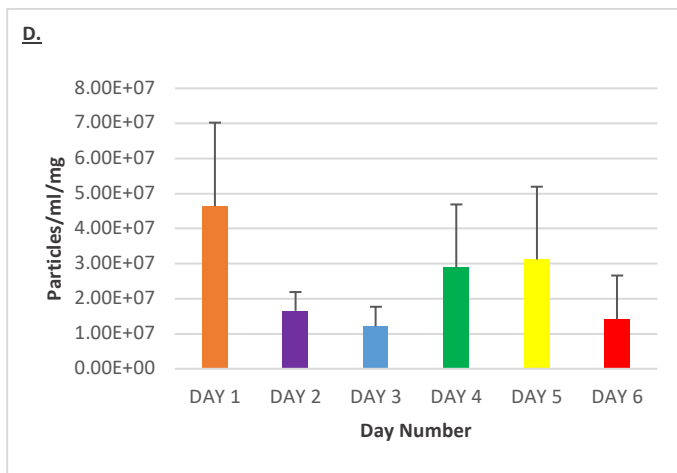
Appendix Figure 3.2 – GD Samples ($n=3$) particle mean size (nm) - day 1 to day 6 on tissue on chip device. **H.** - GD (*Optimisation study*)



Appendix Figure 3.3 – EMG ($n=3$) particle mean size (nm) - day 1 to day 6

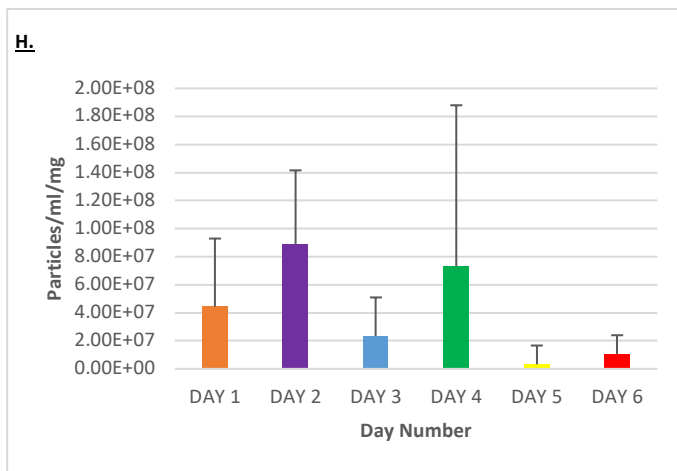
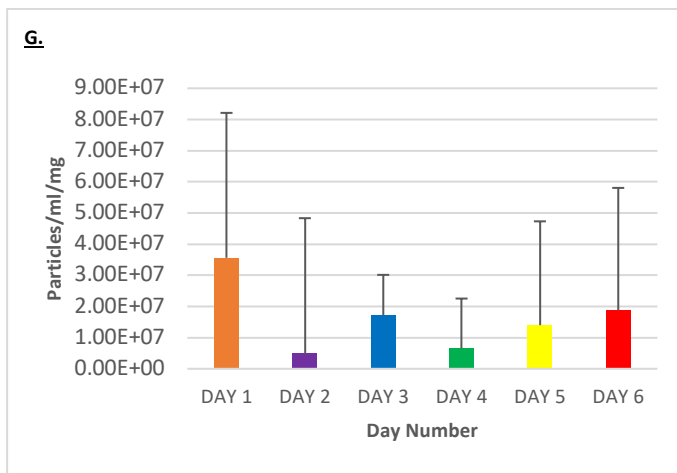
NTA - Particles/ml/mg



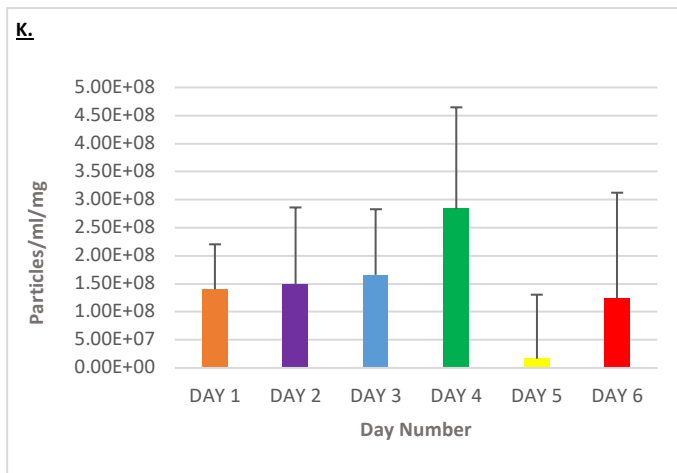
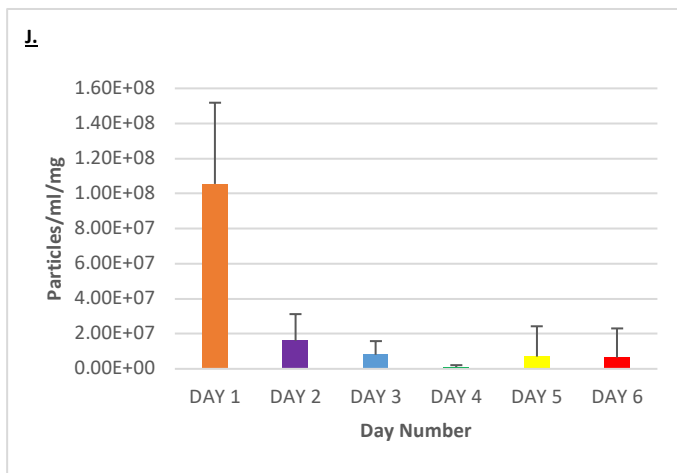
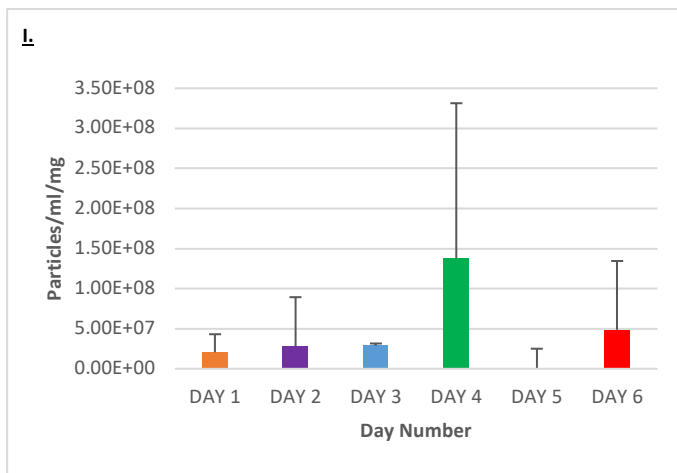


Appendix Figure 3.4 - TC Samples ($n=6$) particles/ml/mg - day 1 to day 6 on tissue on chip devices

A. – PTC, **B.** – PTC, **C.** – Hürthle cell carcinoma, **D.** – PTC, **E.** FTC, **F.** - PTC



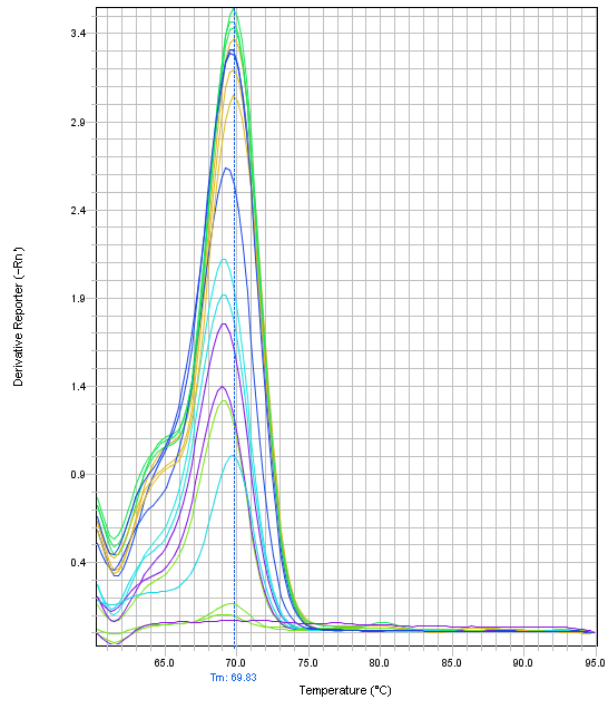
Appendix Figure 3.5 - GD Samples ($n=2$) particles/ml/mg - day 1 to day 6 on tissue on chip devices. **H.** - GD (*Optimisation study*)



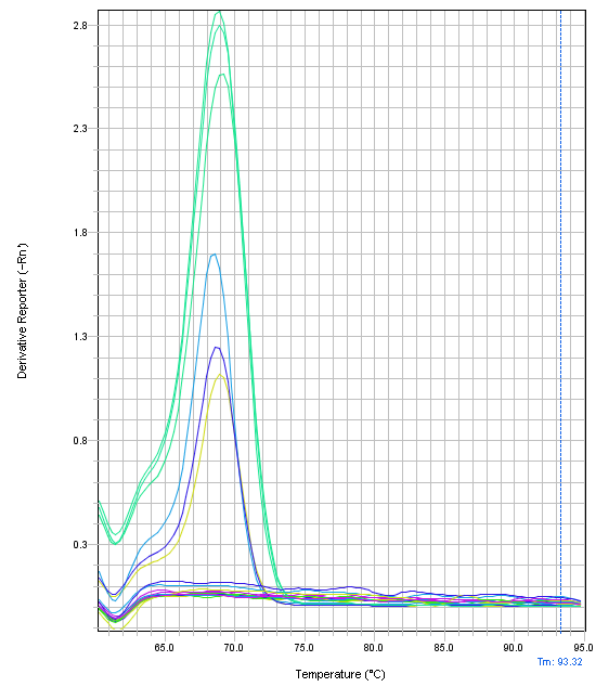
Appendix Figure 3.6 - EMG samples ($n=3$) particles/ml/mg - day 1 to day 6

Appendix 5 – RT-qPCR Melt Curves

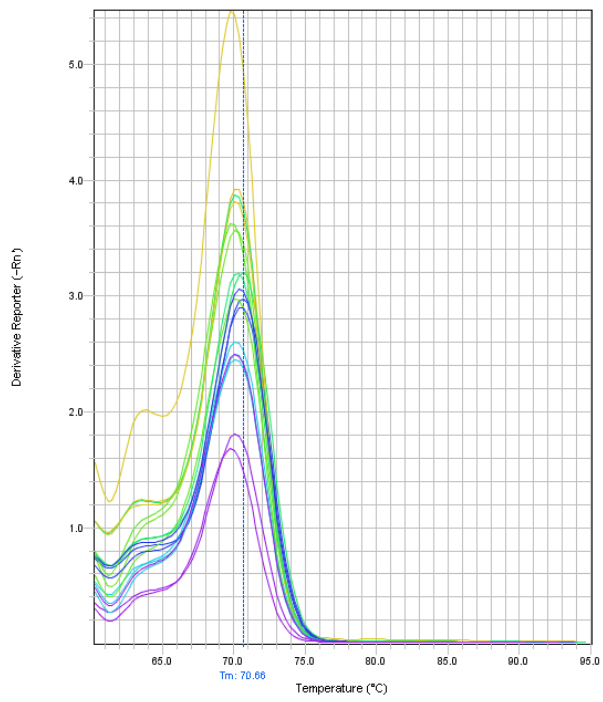
a. hsa-let-7c-5p



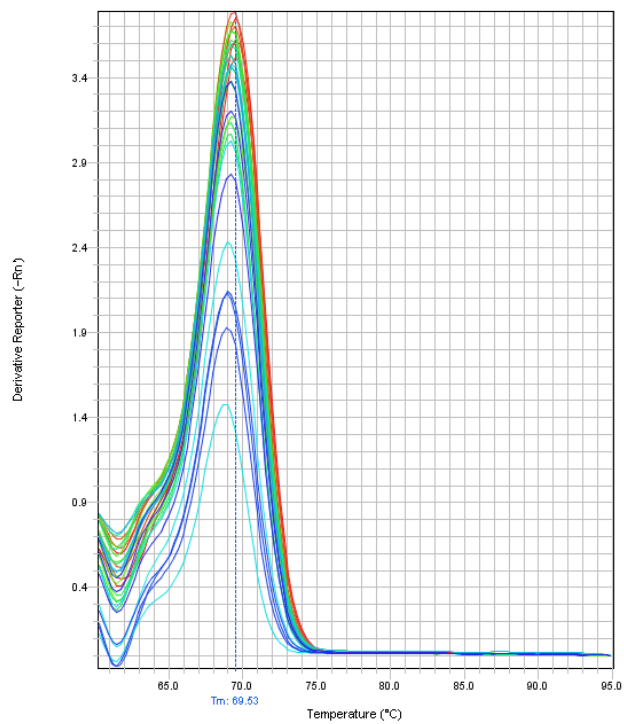
b. hsa-let-7e-5p



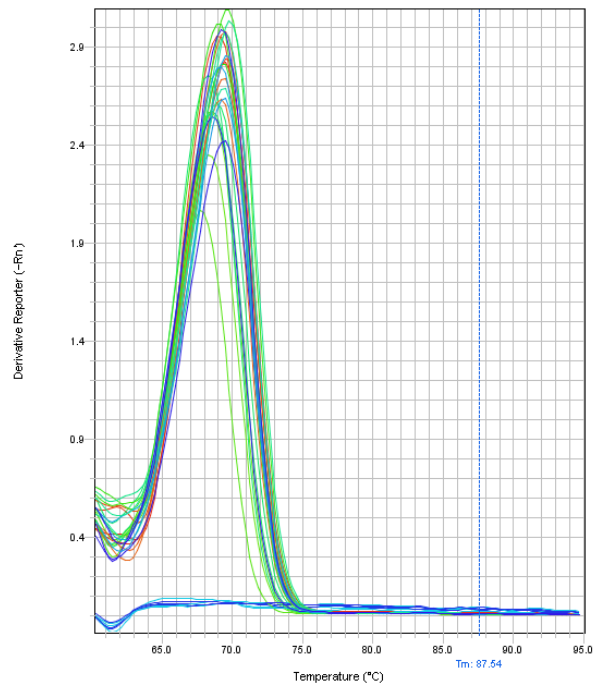
c. hsa-miR-16-5p



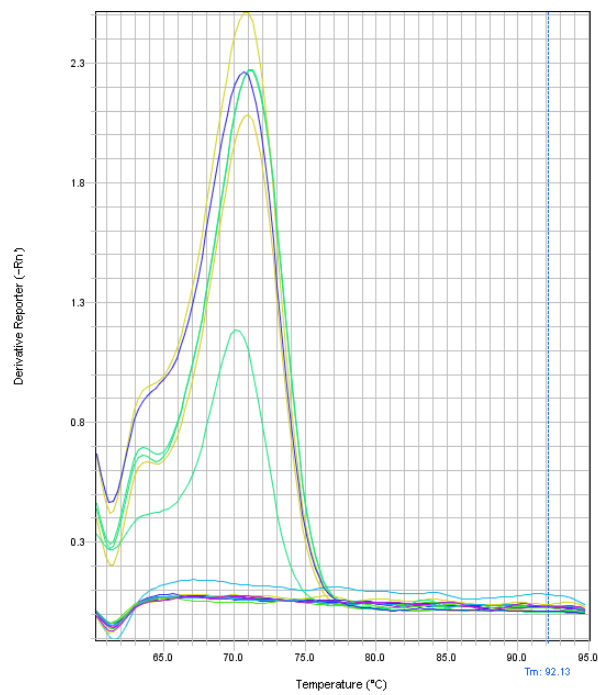
d. hsa-miR-320c



e. hsa-miR-191-5p



f. hsa-miR-191-5p



Appendix 6 – Research participant information sheet and study consent form

Research Participant Information Sheet

The use of microfluidic devices for the evaluation of thyroid tissue biology and treatment response and correlations with patient outcome

Invitation

We would like to invite you to take part in a research study. Before you decide you need to understand why the research is being done and what it would involve for you. Please take time to read the following information carefully. Talk to others about the study if you wish. Ask us if there is anything that is not clear, or you would like more information.

Purpose of the study

The University of Hull has developed a method to keep small pieces of tissue functioning for a number of days outside the body on a micro-chip. During this time substances secreted by the tissue will be identified and analysed along with changes in the tissue itself. The scientific study of what the tissue secretes and how the tissue changes in response to different treatment regimens applied whilst on-chip may lead to future developments in both the diagnosis and the personalised treatment of thyroid disease.

Why have I been chosen?

We are inviting you to take part in this study as you are undergoing a procedure in which your surgeon will take a biopsy of tissue as part of your operation. The tissue will be useful to us to study the responses to treatments described above outside of the body.

Do I have to take part?

It is up to you to decide. We will describe the study and go through this information sheet, which we will then give you to keep. If you decide to take part we will ask you to sign a consent form, to show you have agreed to take part.

Am I free to withdraw at anytime?

You are free to withdraw at any time without giving a reason for your withdrawal. This will not affect the standard of care you receive. Samples already collected will continue to be stored and any information gained from these used in this study. We would not access any information about your clinical progress.

What will happen to me if I take part?

If you agree to take part, some of the 'spare' tissue that is removed as part of your operation will be taken for our study ensuring that sufficient tissue is available for routine diagnostic testing. Along with that a teaspoon of blood (approximately 5ml) will be taken by the Anaesthetic team for further analysis in the laboratory. Once your samples are taken they will be only identifiable by a number: non-clinical laboratory staff will not have any access to your personal details. Information regarding your response to treatment and outcome (if applicable) will be accessed by the clinical staff involved with your treatment and possibly communicated with the research staff. You will not be contacted by the research team after today.

Expenses and Payment

You should not incur any expenses during participation. There will not be any financial benefit if this research leads to the development of a new treatment or test.

What are the possible risks of taking part?

There are no risks to you or your treatment if you take part.

What are the benefits of taking part?

There will be no direct benefit to you for taking part. The information we get from studying your sample will potentially help us with treatments for other patients in the future.

What do I do if I have a complaint?

Any complaint about the way you have been dealt with during the study can be addressed by Mr England, Consultant Surgeon on 01482 672498. Alternatively you can contact the Patient Advice and Liaison Service (PALS) on 01482 623065.

Will my taking part in the study be kept confidential?

Yes. We will follow ethical and legal practice and all information about you will be handled in confidence. Your sample will be identifiable only by a number that can only be linked back to personal details via your clinical care team (i.e. Mr England).

What will happen to the samples I give?

The samples will be taken to the research laboratory at Castle Hill Hospital where we will investigate the effect of treatments on them in terms of cell death and growth and changes in secretions. The blood samples will be frozen and investigated for similar secretions to those from the tissue. Following completion of the study excess samples will remain stored, securely and anonymously for possible use in future research for a similar project. In this instance further Research Ethical Approval will be sought.

What will happen to the results of the research study?

The results of the study maybe published in a scientific journal. At no time will you be identifiable to the reader. No feedback will be given to you unless specifically requested, in which instance the research team will be happy to discuss the general findings.

Who is organising and funding the research?

The Thyroid/Head and Neck Cancer research team from the University of Hull will be organising and conducting the research in the laboratories at Castle Hill Hospital. This research is partly funded by the Royal College of Surgeons of England.

Who has reviewed the study?

All research in the NHS is looked at by an independent group of people called a Research Ethics Committee to protect your interests.

Further information

If you require any further general or specific information on the research, advice on whether to take part, or if you are at all unhappy please contact Mr England on 01482 672498.

Thank you for taking the time to read this information sheet.

Consent

If you decide to take part in the study, we will provide you with a copy of the information sheet and ask you to sign a study Consent Form.

CONSENT FORM

Centre Number:

Study Number:

Patient Identification Number for this trial:

The use of microfluidic devices for the evaluation of thyroid tissue biology and treatment response and correlations with patient outcome

1. I confirm that I have read and understand the information sheet dated 10.10.21 (version 3) for the above study. I have had the opportunity to consider the information, ask questions and have had these answered satisfactorily.

2. I understand that my participation is voluntary and that I am free to withdraw at any time without giving a reason, without my medical care or legal rights being affected. If I do withdraw, samples already obtained may still be used

3. I understand that I am under no obligation to take part and that, if I agree to take part, I am free to change my mind at any time.

4. I understand that I will not benefit financially if this research leads to the development of a new treatment or test.

5. I give permission for a "spare" sample of the tissue taken during my operation to be used for this research.

6. I give permission for a vial of blood to be taken on insertion of the cannula used for the anaesthetic. I understand that the plasma extracted from this blood sample will be analysed in the laboratory.

7. I agree that any samples not used in this study may be stored and used in future research of a similar nature pending ethical approval.

8. I understand that these samples will be stored anonymously and I consent to the information derived from them to be analysed by a computer.

9. I understand that relevant sections of my medical notes and data collected during the study may be looked at by individuals from the University of Hull, from regulatory authorities, or from the NHS trust, where it is relevant to my taking part in this research. I give permission for these individuals to have access to my records.

10. I hereby freely give my consent to take part in this study.

Name of Volunteer

Date

Signature

Name of Person
taking consent

Date

Signature